MODELLING SPECTRAL AND BROADBAND UV-B (290-325 nm) IRRADIANCE FOR CANADA

BY

JACQUELINE BINYAMIN, M.Sc.

A Thesis

Submitted to the school of Graduate Studies

in Partial Fulfilment of the Requirements

for the Degree

Doctor of Philosophy

McMaster University

MODELLING UV-B IRRADIANCE FOR CANADA

DOCTOR OF PHILOSOPHY (2001) MCMASTER UNIVERSITY
(School of Geography and Geology) Hamilton, Ontario

TITLE: Modelling spectral and broadband UV-B (290-325 nm) irradiance for Canada

AUTHOR: Jacqueline Binyamin, B.Sc. (University of Mosul)
M.Sc. (Reading University)

SUPERVISOR Professor J. A. Davies

NUMBER OF PAGES: xvii, 206

ABSTRACT

This is a study concerning the modeling of UV-B irradiance at the earth's surface. It is timely because stratospheric ozone depletion has occurred globally as a result of increasing chlorofluorocarbons in the stratosphere. This reduction allows more UV-B irradiance (290-325 nm) to reach the earth's surface and cause detrimental biological effects. Presently there are few spectral UV-B radiation measurements. Therefore, irradiance models are useful tools for estimating UV-B irradiances in areas where measurements are not made. A numerical model to calculate spectral and broadband irradiances for all sky conditions is described and the results are validated with measurements for nine Canadian stations (Alert, Resolute Bay, Churchill, Edmonton, Regina, Winnipeg, Montreal, Halifax and Toronto). The model uses either the discrete ordinate radiative transfer (DISORT) or the delta-Eddington algorithms to solve the radiative transfer equation for a 49-layer, vertically inhomogeneous, plane-parallel atmosphere, with cloud inserted between the 2 and 3 km heights. Spectral calculations are made at 1 nm intervals. The model uses extraterrestrial spectral irradiance, spectral optical properties for each atmospheric layer for ozone, air molecules, and aerosol and surface albedo. Cloud optical depths τ_c were calculated separately for overcast irradiance measurements for nine stations from 26 years of data. The delta-Eddington method performed well for producing τ_c and overcast broadband irradiances. A fixed τ_c value of 18.7 was found to be accurate for calculating cloudy sky irradiances at all stations except in the arctic.

Twenty-six station years of irradiance measurements and model estimates are compared. Comparisons are made both for daily totals and for monthly averaged spectral and broadband irradiances. It is shown that the delta-Eddington method is not suitable for calculating spectral irradiances under clear skies, at short wavelengths (< 305 nm), where absorption by ozone is high, and at large solar zenith angles. The errors are smaller for overcast conditions. The method was found to be adequate for daily total spectral ($\geq$ 305 nm) and for broadband calculations for all sky conditions, although consistently overestimating the irradiances. There is a good agreement between broadband measurements and calculations for both daily totals and monthly averages with mean bias error (MBE) mainly less than 5% of the mean measured daily irradiance and root mean square error (RMSE) less than 26%, decreasing to below 15% for monthly averages. Agreement between mean monthly measured and calculated spectral irradiances is also good for wavelengths $\geq$ 305 nm. The accuracy of the Brewer instrument is questioned at wavelengths <305 nm at most stations.

Comparison of the model broadband irradiances with simultaneous satellite-based results and Brewer measurements at six stations shows that the model performs as well as the satellite model but with the advantage that it can provide irradiance estimates throughout the day and, therefore, daily totals.

ACKNOWLEDGEMENTS

It is probably difficult, if not impossible, for one to complete a doctoral program without the generous support and encouragement of others. Many people contributed to my work in a variety of ways and I wish to express my sincere appreciation to them.

First and foremost, I thank my supervisor, Dr. John Davies, who gave me the opportunity to work on a fascinating project, who taught me so much over the past several years, whose enlightened guidance, incredible patience, advice and support sustained me through many difficult times. He has always been there when I needed and has made my life so much better by teaching me his modeling and programming expertise. Thank you very much.

I am very grateful to Dr. Wayne Rouse, supervisory committee member, for his support, assistance, and from whom I have also learned a great deal throughout my time at McMaster. I am especially grateful for his time, invaluable editing and constructive suggestions. His encouragement is greatly appreciated.

I would also like to express my gratitude to Dr. Bruce McArthur, supervisory committee member, of the Meteorological Service of Canada (MSC) for his suggestions and ideas, for providing the UV-B and surface meteorological data needed for the study and finally for providing computing facilities.

Special thanks go to Dr. Howard Barker of MSC for illuminating conversations concerning cloud optical depths and gamma distributions and to Dr. Phurbu Tsering at the Canada Centre for Remote Sensing for providing the satellite data for the study.

I am indebted to Dr. Hoc Woo for his encouragement and along with Dr. Lee Liaw for their help with statistics, Dr. Alkiviadis Bais from the Aristotle University of Thessaloniki, Greece, for his helpful discussions regarding the Brewer cosine error, and Dr. John Frederick from the University of Chicago, USA, for his valuable points about clouds and wavelength independent scattering in the UV-B range.

I would also like to thank Drs. Tim Griffis, Mike Jerrett, and Mike Buzzelli, and my colleagues Joan Parker, Regina Bendig, Nancy Brand, Penny Kuhn, Susan Vajoczki,

Hanna Maoh and Talar Sahsuvaroglu for their valued friendship, assistance and continuous encouragement. Thanks to my office mates, Erin Mifflin and Amanda Bullen in BSB 305A and Claire Oswald and Devin Worth in GSB 325.

I give a special thank you to Clive Gibbons for being always ready to solve my computer problems, Hanna Maoh for drafting the map, and Vitali Fioletov and Edmund Wu of MSC for their prompt e-mails concerning the Brewer measurements.

Thanks also go to Nancy Brand, Janice Wade and Darlene Watson and the rest of the office staff for their generosity and assistance.

I would like to extend my greatest appreciation to McMaster University for providing me with financial assistance in the form of research scholarships and teaching assistantships, and to the Ontario Graduate Scholarship (OGS) program. This work was supported by a Natural Sciences and Engineering Research Council of Canada (NSERC) grant to Dr. Davies.

Finally, and most important, I am deeply grateful to my husband Ghassan, who supported me financially and encouraged me to enter the graduate program. I would like to thank Ghassan, my two children Marvin and Raman, my brother David and my sister Nadia for being so understanding during the preparation of this thesis. There is no way I could have progressed this far without them. Thank you for being patient.

TABLE OF CONTENTS

LIST OF FIGURES

Figure

LIST OF TABLES

CHAPTER 1

Introduction

1.1 The ozone problem

The magnitude of biologically active ultraviolet (UV-B) irradiance received at the earth's surface depends mainly on ozone concentrations in the stratosphere. Concerns about ozone depletion first started in 1970 when the possible destructive effects of the exhaust gases from supersonic transports were identified (Harrison, 1970; Johnston, 1971). The possibility of ozone break down due to reactions triggered by chlorine released from chlorofluorocarbons (CFCs) was first proposed by Molina and Rowland (1974). This possibility became reality with the discovery of the dramatic springtime ozone depletion in the Antarctic (Farman *et al.*, 1985; Stolarski *et al.*, 1986) and evidence for ozone decreases in middle and high latitudes in both hemispheres (Stolarski *et al.*, 1991, 1992; Gleason *et al.*, 1993; Chandra *et al.*, 1996; Herman *et al.*, 1996; Harris *et al.*, 1997; Staehelin *et al.*, 1998a, 1998b).

Ozone depletion has not been uniform over the planet. Depletion estimates for mid-latitudes range from 3% to 8% per decade, being less in the tropics and substantially greater in polar regions, especially in Antarctica (Liu *et al.*, 1991; Stolarski *et al.*, 1991; Stolarski *et al.*, 1992; Bojkov *et al.*, 1995a; Harris *et al.*, 1997). This is fortunate in

a way, because the ozone layer is naturally thickest over the poles and thinnest over low latitudes. The largest ozone depletion has been recorded at Halley in Antarctica (75° 31′ S, 26° 40′ W) where springtime levels in 1984 were reduced to 40% of 1975 values (Farman *et al.*, 1985), decreased further to 60 % in 1990 (Henderson *et al.*, 1991) and to 63% in 1994 (Jones and Shanklin, 1995). An average depletion of about 6% has been observed over most of southern Canada since the late 1970s (Kerr, 1991; Atmospheric Environment Service[1] (AES), 1999). Figure 1.1 shows annual averages from five Canadian monitoring stations (Toronto, Goose Bay, Edmonton, Churchill and Resolute Bay) measured from the ground by Brewer spectrophotometers, and global levels that were measured by TOMS (Total Ozone Mapping Spectrometer) on the Nimbus-7 (1979-92), Meteor-3 (1992-94), and Earth probe (1996-98) satellites and are averaged from 65° S to 65° N latitude. Both Canadian and global ozone levels show a decrease after 1982.

In Toronto (43° 47′ N, 79° 28′ W) Kerr and McElroy (1993) reported decreases in the ozone levels between 1989 and 1993 of 4.1% and 1.8% per year in winter and summer, respectively. Ozone depletion over North America is a strong function of season with greatest depletion occurring during the early spring (Stolarski *et al.*, 1992; Bojkov *et al.*, 1995a; Harris *et al.*, 1997; Staehelin *et al.*, 1998b). Over southern Canada, depletion averages about 8% to 12% during spring with maximum depletions reaching 20% for

[1] The name was changed to the Meteorological Service of Canada (MSC) in 2000.

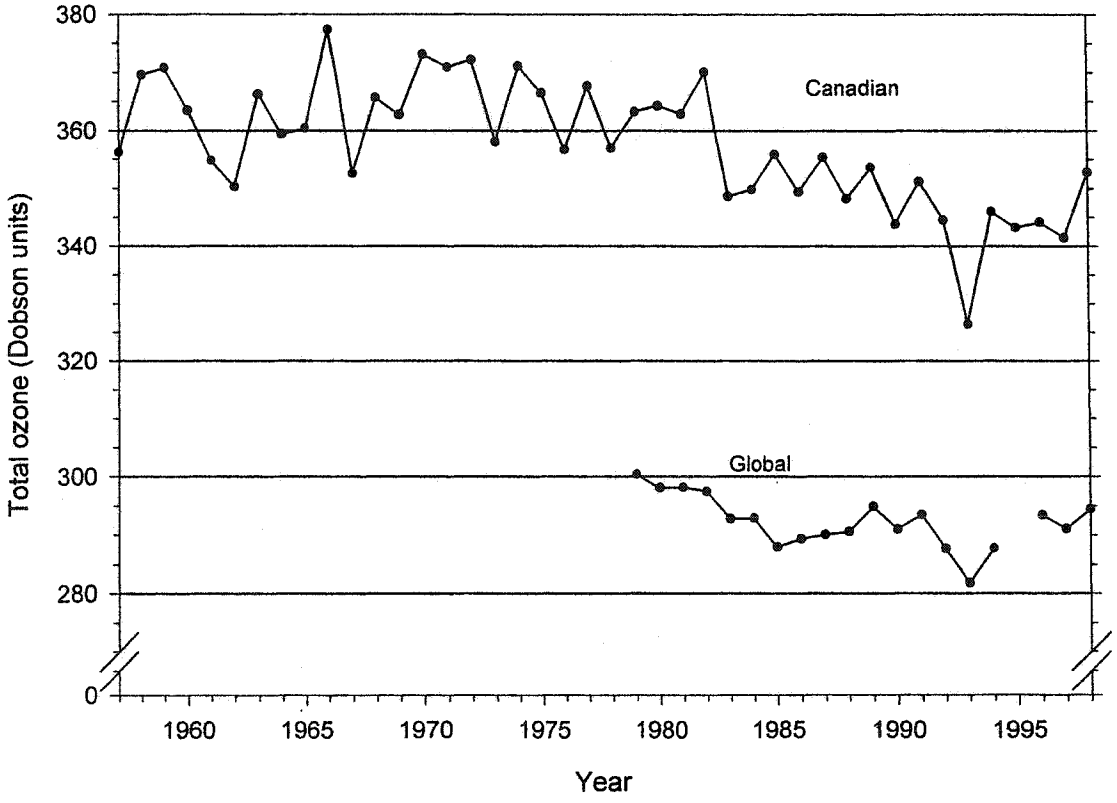

Figure 1.1. Annual average total ozone for five Canadian (Toronto, Goose Bay, Edmonton, Churchill and Resolute Bay) stations and the world (between 65° S and 65° N). Data from Canada's national environmental indicator series (AES, 1999).

short periods (MSC, 1999). Similar depletion rates were reported by Bojkov *et al.* (1995b) for 1994-95 over Europe and North America. Depletions as great as about 45% have been recorded in the high Arctic during the early spring (MSC, 1999).

Ozone is a greenhouse gas as well as a UV-B filter (Munro *et al.*, 1998). Therefore, stratospheric ozone depletion leads to a cooling of the stratosphere, making conditions even more favorable for ozone depletion (Kerr, 1998; Shindell *et al.*, 1998). Greenhouse gases warm the earth's surface but cool the stratosphere radiatively and such a cooling during long winter darkness could increase the formation of polar stratospheric clouds (Hofmann *et al.*, 1989; Solomon, 1999). These clouds are made up of frozen chemical particles, which can speed up the process of ozone depletion in the arctic stratosphere and combined with ozone-depleting substances, causing a hole to develop in the Antarctic stratosphere (Toon and Turco, 1991; Stolarski, 1992). UV-B irradiance inhibits plant growth. Reduced plant growth increases carbon dioxide gas, which is a major contributor to the greenhouse effect.

1.2 The ultraviolet irradiance problem

The most important consequence of ozone depletion is the increase in the amount of UV-B irradiance reaching the earth's surface (Madronich, 1992; Bais *et al.*, 1993; Klein and Furrer, 1994; Herman *et al.*, 1996). Most biological damage at the surface is caused by the UV-B band (280 to 325 nm) and, to a lesser extent, the UV-A band (325 to 400 nm). Although the irradiance in the UV-C band (200 to 280 nm) is potentially the most damaging to organisms, it is absorbed completely by the atmosphere so that negligible amounts reach the earth's surface. Irradiance in the UV-A band, which has

both beneficial and detrimental effects on organisms, is only slightly absorbed by ozone. UV-B irradiance in wavelengths between 280 and 290 nm is mainly absorbed by stratospheric ozone and does not reach the earth's surface, even after large reductions in atmospheric ozone such as occur over Antarctica in spring (Frederick *et al.*, 1993). For this reason, it is useful to adopt the spectral interval from 290 to 325 nm as the effective UV-B region. This is the wavelength range of Canadian spectrophotometer measurements. Even though the UV-B band is biologically important, it constitutes only 1.8% of the total solar radiation at the top of the atmosphere, and no more than 1% at the earth's surface (Frederick *et al.*, 1989).

UV-B irradiance exposure can cause skin erythema, pigmentation and cancer, eye cataracts and can weaken the immune system (McKinlay and Diffey, 1987; Madronich and deGruijl, 1993). Besides hazards to health, any depletion of the ozone layer may reduce crop yields and disrupt aquatic life (Biggs and Joyner, 1994; Caldwell and Flint, 1994). Since UV-B radiation can penetrate in water, it influences marine and freshwater ecosystems (Browman *et al.*, 2000). Also, high UV-B irradiance amounts can adversely affect animals in their early developmental stages (Tevini, 1993).

A 1% decrease in total column ozone is expected to cause an increase of 1.3% in erythemally active UV-B irradiance (McKinlay and Diffey, 1987; McKenzie *et al*, 1991; Herman *et al.*, 1996), 2% in wavelengths that can lead to DNA damage (United Nations Environmental Programme (UNEP), 1994) and 2% in those wavelengths implicated in non-melanoma skin cancer (Kelfkens *et al.*, 1990). Also, ozone depletion of 10% will induce about one million new cases of cataracts (UNEP, 1994). Bartlett and Webb (2000)

found that a 5.9% decrease in ozone between 1993 and 1997 produced a 4.3% increase in UV-B irradiance at Reading (51° 26′ N, 0° 56′ W), England.

Within the UV-B band the atmosphere becomes more transparent with increasing wavelength since ozone absorption decreases by two orders of magnitude as wavelength increases between 290-325 nm (Molina and Molina, 1986). Biological effects are not constant across the waveband. In general, the shorter the wavelength, the greater the biological effect (Lubin *et al.*, 1992). Therefore, spectral measurements are more useful.

The spectral distribution of UV-B irradiance reaching the earth's surface depends on both the spectral irradiance emitted by the sun and the spectral transmission properties of the atmospheric constituents namely ozone, clouds, dry air molecules and aerosols. Also other trace gases associated with urban pollution, mainly sulfur dioxide, nitrogen dioxide and tropospheric ozone can contribute to absorption in highly polluted areas.

1.3 Measurements and models

Normally, measurements in the UV-B are either broadband (spectrally integrated) or spectral. Broadband measurements provide total energy received across a given waveband, often weighted with an approximation to a biological action spectrum. The Robertson-Berger meter (Berger, 1976) is such an instrument with spectral response matching the McKinlay and Diffey (1987) erythemal action spectrum. Instruments such as the Brewer spectrophotometer measure spectral irradiance (Kerr *et al.*, 1985). Spectral measurements are easily adapted to a particular biological effect by applying appropriate spectral weighting.

Efforts have been made since 1990 to increase the number of ground-based monitoring sites, but the spectral UV-B irradiance measurements in Canada and internationally are few and have a short record duration. The record is too short to clearly show the effect of reduced ozone on UV-B irradiance. Therefore, radiation models are potentially very important tools to provide irradiance estimates for the past and for stations without any measurements. They also can be used to predict future irradiance changes for specified changes in ozone concentrations. Radiation models use either surface meteorological data, as in the present study, or satellite measurements.

Satellite-borne instruments measure reflected UV radiances at the top of the atmosphere. Wang *et al.* (2000) combined ozone and reflected radiance from the TOMS instrument on board the Russian Meteor 3 satellite and AVHRR (Advanced Very High Resolution Radiometer) on the NOAA (National Oceanographic and Atmospheric Adminstration) satellite with an algorithm developed by Li *et al.* (2000) to estimate broadband UV-B fluxes and erythemal weighted UV-B irradiances at the surface. This method provides global spatial coverage and is based on a single instrument (Eck *et al.*, 1995; Herman *et al.*, 1996). It is, however, indirect. The present TOMS on the NASA's Earth probe and the GOME (Global Ozone Monitoring Experiment) on the European ERS-2 (European Remote Sensing) satellites are characterized by relatively low spatial and temporal resolutions and need three days to map the entire globe. However, the original TOMS on Nimbus 7 satellite provided a global daily coverage with only one daily overpass which was most representative for mid-day irradiance for Toronto (Eck *et al.*, 1995). The Meteor 3 TOMS satellite is not sun synchronous and normally provides

only one measurement per day with a maximum of two (P. Tsering, private communication, 2001). Obtaining daily total irradiance from just one instantaneous measurements per day is a major drawback, as is the heavy computation involved in the processing of global satellite data (Li *et al.*, 2000).

Radiation models, which use surface data, apply algorithms which vary from simple approximations (Green *et al.*, 1974; Schippnick and Green, 1982) to rigorous solutions of the radiative transfer equation. Since they use local data, they represent point conditions more accurately than the large area estimates from satellite. The much larger historical record of surface meteorological data, compared with satellite measurements, makes it possible to establish a historical UV-B climatology.

The two most widely used radiative transfer solutions are the discrete ordinate radiative transfer (DISORT) model (Stamnes *et al.*, 1988; Liu *et al.*, 1991; Stamnes *et al.*, 1992; Wang and Lenoble, 1994; Zeng *et al.*, 1994; Forster *et al.*, 1995) and the delta-Eddington model (Joseph *et al.*, 1976; Madronich, 1992; Kuhn, 1996; Davies *et al.*, 2000). Both methods are known to be robust from comparisons with other detailed radiative transfer calculations (Joseph *et al.*, 1976; Wiscombe and Joseph, 1977; King and Harshvardhan, 1986; Harshvardhan and King, 1993) but have also limitations (e.g. parameterization of the sphericity of the atmosphere).

Validation studies that have compared model calculations with measurements are mostly restricted to data for just a few days and cloudless skies (Koskela *et al.*, 1993; Zeng *et al.*, 1994; Wang and Lenoble, 1994; Mayer *et al.*, 1997). There have been few studies where surface-based models have been validated for cloudy conditions

(Leontyeva and Stamnes, 1994; Forster, 1995; Forster *et al.*, 1995). This is the first comprehensive study for Canada. A pilot study was performed by Davies *et al.* (2000) at four Canadian stations (Bedford, Toronto, Winnipeg, Edmonton) using a small amount of data.

Surface models are generally hampered by sparse cloud information and the information that is available is of poor quality. In most model studies, clouds are usually defined as overcast plane parallel layers (Lubin and Frederick, 1991; Tsay *et al.*, 1983). The influence of partial cloud cover has been studied empirically by relating irradiance measurements to simultaneous observations of cloud properties (Ilyas, 1987, Frederick and Snell, 1990; Frederick *et al.*, 1993; Webb, 1992). Some studies have included a single cloud layer (Frederick and Lubin, 1988; Frederick and Snell, 1990), others multiple layers (Charache *et al.*, 1994). A major uncertainty concerns the optical depth of clouds, which is the most important optical parameter. There have been no determinations for the cloud optical depth for the UV-B band, other than an initial study with a small data set presented by Davies *et al.* (2000). On the other hand, a number of studies have determined cloud optical depth for the total solar radiation waveband (Leontyeva and Stamnes 1994; Leontieva *et al.*, 1994; Ricchiazzi and Gautier, 1995; Leontieva and Stamnes, 1996; Barker *et al.*, 1998).

1.4 Objectives and outline of the thesis

The general objectives of this thesis are:

1. to produce and evaluate a numerical model for UV-B irradiance for all sky conditions and to estimate cloud optical depth,

2. to validate spectral and broadband irradiances using Brewer spectrophotometer measurements and to assess the relative usefulness of the DISORT and delta-Eddington algorithms, and
3. to compare model results with those from a satellite model of the Canada Centre for Remote Sensing (CCRS), which is the first such comparison.

Chapter 2 describes the irradiance and ozone measurements, the model and the input parameters. Chapter 3 outlines the procedure for calculating cloud optical properties and presents the results. Chapter 4 presents the model validation results. Chapter 5 compares model results with those from the CCRS satellite model. Chapter 6 gives conclusions, emphasizes the contributions of this research and details some of the future research needs.

CHAPTER 2

The measurement and calculation of irradiance

2.1 Irradiance measurements

Spectral UV-B irradiance measurements in Canada began in March 1989 and are made at 13 locations with the Canadian designed single monochromator Brewer spectrophotometer. Nine of these locations, which have the necessary meteorological data for radiative transfer calculation, are used in this study (Figure 2.1). The Brewer instrument allows the calculation of daily ozone depth and measures spectral irradiance for wavelengths between 290 and 325 nm at a resolution of 0.5 nm. Each spectral measurement consists of the average of a forward and backward scan across the wavelength range, which takes about 8 minutes to complete (Kerr and McElroy, 1993). Measurements of the radiation intensity that falls on a horizontal diffusing surface are made once or twice each hour throughout the day from sunrise to sunset at irregular times in GMT. These spectral measurements were obtained from the World Ozone and Ultraviolet Radiation Data Centre (WOUDC).

The Brewer instruments have known uncertainties. They receive stray light from longer wavelengths adjacent to the one being measured (Bais *et al.*, 1996; Davies, 1996) which affects measurements below about 305 nm where the light intensity is very small.

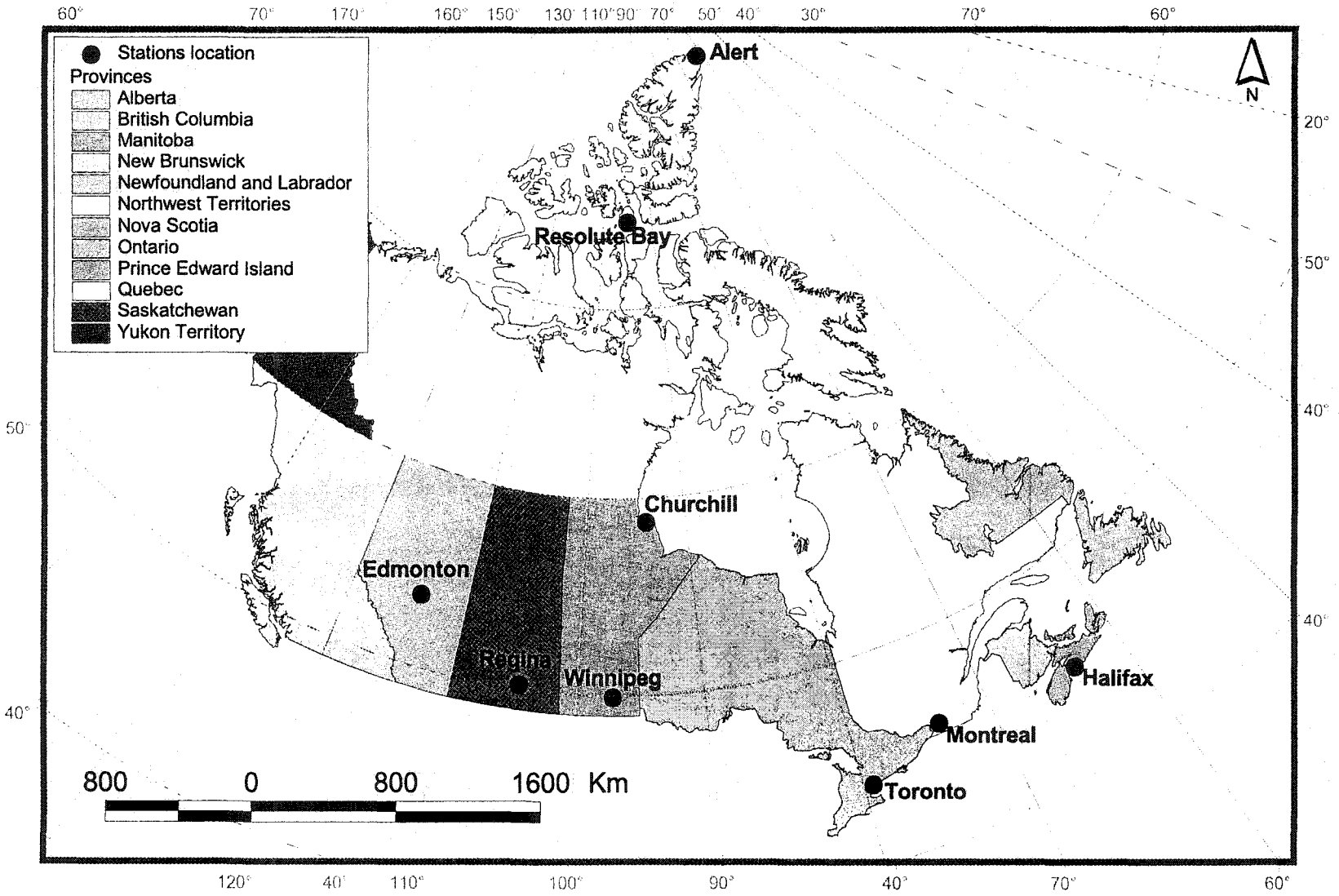

Figure 2.1 Location of Canadian stations used in this study

Also they are subject to cosine error[2] such that measurements usually underestimate the horizontal global irradiance by up to 8% depending on clouds, aerosols, and solar zenith angle[3] (Wardle and Kerr, 1999; Bais *et al.*, 1998). The cosine error for the Brewer instrument is due to the imperfection of a thin Teflon diffuser. Different instruments that have the same type of diffuser have roughly the same cosine response, but the orientation and vertical position of the diffuser may affect this response. Damage to the diffuser will also alter the directional responsivity of the instrument (L. J. B. McArthur, personal communication, 2000). Each instrument has its own cosine error, which can vary from 2% to 20% (e.g., Feister *et al.*, 1997; Bais *et al.*, 1998).

Calibration uncertainty for the Brewer instruments ranges from ±5 – 7% (Herman *et al.*, 1999; Wang *et al.*, 2000). The Brewer instrument is also affected by the ambient temperature and humidity variations (Bais *et al.*, 1996). It is provided with a temperature-stabilized enclosure but this does not totally eliminate the temperature variability. The temperature effect is greater at shorter wavelengths and can produce mean errors ranging from -2% to 2% in winter and summer, respectively over the Brewer spectral range (Wardle and Kerr, 1999). However, Cappellani and Kochler (1999) have found that for winter days (temperature range 9.8° to 21.7°C) and for summer days (temperature range 21.7° to 42°C), the Brewer values should be increased by 2% and 8%, respectively.

---

[2] The irradiance on a horizontal surface varies with the cosine of the angle of incidence. The cosine error is the deviation of the angular response of the instrument from the ideal response.

[3] Solar zenith angle is the vertical angle between the zenith and the sun's position.

Some quality control procedures are performed by the MSC. These include: calibration with 1000-watt standard lamps that are traceable to the US National Institute of Standards and Technology; daily radiometric stability that is maintained with an internal 20-watt quartz halogen lamp; a wavelength check is made several times per day using a mercury discharge lamp; and a correction for stray light (Wardle and Kerr, 1999). However, corrections for the effect of cosine error on the UV-B spectra and a wavelength-dependent temperature effect are not applied. In this study an increase of 6% was applied to the Brewer data to compensate for the cosine error effect on the basis of research by Krotkov *et al.* (1998) and Wang *et al.* (2000).

2.2 Other measurements

Daily total ozone column[4] measurements from the Brewer instrument were obtained from the WOUDC for the stations shown in Figure 2.1. Hourly (local standard time) measurements of total cloud opacity[5], surface temperature, pressure and relative humidity were provided by the MSC. Values were linearly interpolated for the irradiance measurement times in GMT. Solar zenith angles for each measurement time and the ratio of actual to mean Sun-Earth distance were calculated following Michalsky (1988). Daily snow depth measurements were provided by the MSC.

---

[4] Column ozone is the total amount of ozone in a column between the earth's surface and the top of the stratosphere expressed as Dobson Units (DU). One DU is equivalent to 10^{-5} m of pure ozone at standard temperature (0° C) and pressure (1013 mb) or = 2.69×10^{16} molecules/cm^2 (Frederick, 1990).

[5] Cloud opacity is the fraction of sky that is totally obscured by cloud.

2.3 McMaster Model description

Surface irradiance G is expressed as a cloudiness-scaled combination of cloudless sky irradiance G_0 and overcast sky irradiance $G_\otimes$:

$$G = (1-C)G_0 + CG_\otimes, \tag{2.1}$$

where C is the fraction of the sky that is cloud covered. G_0 and $G_\otimes$ are calculated spectrally at 1 nm intervals using either the DISORT (Stamnes *et al.*, 1988) or the delta-Eddington (Joseph *et al.*, 1976) solutions to the radiative transfer equation.

This model can be applied anywhere where there are daily measurements of column ozone and snow depth and hourly cloud cover observations. Radiative transfer calculations of G_0 and $G_\otimes$ require the following optical properties:

1. the optical depth τ which is defined as the integral of the extinction (absorption plus scattering) coefficient β_{ext} for each wavelength λ over the depth z of an atmospheric layer:

$$\tau_\lambda = \int_0^z \beta_{ext}(\lambda, z)dz; \tag{2.2}$$

2. single scattering albedo ω is the probability of a photon being scattered, which is equal to 1 for conservative scattering and is 0 when the extinction is by absorption only, and is defined as the ratio of the scattering to extinction coefficients:

$$\omega = \frac{\beta_{sca_\lambda}}{\beta_{ext_\lambda}}; \tag{2.3}$$

3. and the asymmetry factor g which is the average direction of scattering and is defined as

$$g = \frac{1}{2}\int_{-1}^{+1} p(\mu)\mu d\mu, \tag{2.4}$$

where $p(\mu)$ is the scattering phase function and μ is the cosine of the scattering angle. The asymmetry factor varies between –1 and +1 for complete scatter into the backward and forward directions and is 0 for isotropic scattering.

The atmosphere consists of a mixture of gases, aerosols and cloud particles with different spectral optical properties, which vary with altitude. In this study, the atmosphere is divided into 49 layers with constant scattering and absorbing properties within each. The layers are thin (1 km) in the lower atmosphere, intermediate (2.5 km) in the middle atmosphere and thick (5 km) in the upper atmosphere (Figure 2.2). Each layer is regarded as horizontally homogeneous and the curvature associated with sphericity of the earth is ignored. The cloud can be located at any level in the atmosphere (Leontyeva and Stamnes, 1994) and low clouds occur inside the lower 2 km (Schweiger and Key, 1992). Therefore, all cloud is placed in one layer (between 2 and 3 km) and in this plane-parallel atmosphere radiation transfer is considered only in the vertical. Incident irradiance has both direct beam and diffuse components. The direct beam spectral radiation $S_\lambda(\tau, \mu_0, \phi_0)$ at the ground is described by Beer's law:

$$S_\lambda(\tau, \mu_0, \phi_0) = \mu_0 \left[\frac{S_\lambda(0)}{(d/\bar{d})^2}\right] \exp(-\tau/\mu_0), \tag{2.5}$$

where λ is the wavelength, μ_0 the cosine of the solar zenith angle, ϕ_0 the solar azimuth

angle[6], $S_\lambda(0)$ is the extraterrestrial solar flux at Sun-Earth distance of 1 Astronomical Unit (AU)[7], d the actual daily Sun-Earth distance, $\bar{d}$ its average annual value and τ is the total optical depth for the atmosphere.

The diffuse irradiance is the downward component of atmospheric scattering. For a direction specified by μ and ϕ, the spectral radiance $I_\lambda(\tau,\mu,\phi)$ is given by:

$$\mu\frac{dI_\lambda}{d\tau_\lambda}(\tau_\lambda,\mu,\phi) = -I_\lambda(\tau_\lambda,\mu,\phi) + \frac{\omega_\lambda}{4\pi}\int_0^{2\pi}\int_{-1}^{+1} P(\mu,\phi;\mu',\phi')I_\lambda(\tau_\lambda,\mu',\phi')\,d\mu'd\phi' + \frac{\omega_\lambda}{4}S_{0\lambda}P_\lambda(\mu,\phi;\mu_0,\phi_0)e^{(-\tau_\lambda/\mu_0)}, \tag{2.6}$$

where $P_\lambda(\mu,\phi;\mu',\phi')$ is the scattering phase function that defines the light scattered from the direction μ',ϕ' into the direction μ,ϕ. The first term on the R.H.S. is the diffuse intensity attenuated by absorption and scattering, the second represents multiply scattered radiation from the direction μ',ϕ' into μ,ϕ, and the third represents scattering from the direct beam from μ_0,ϕ_0 into the direction μ,ϕ.

2.4 Radiative transfer solutions

Eq. (2.6) is an integro-differential equation, which, in general, cannot be solved analytically. The most accurate or exact methods include the discrete ordinates (Chandrasekhar, 1960), doubling (Hansen, 1971; Van de Hulst, 1980), and Monte Carlo (Plass and Kattawar, 1971) methods. These exact methods are computationally intensive. This makes them usually unsuitable for climatological purposes such as the calculation of

[6] Azimuth angle is the horizontal angle between the sun and a standard direction (north or south).
[7] AU is the average Sun-Earth distance (1.495×10^{11}m) and is assigned a value of 1.

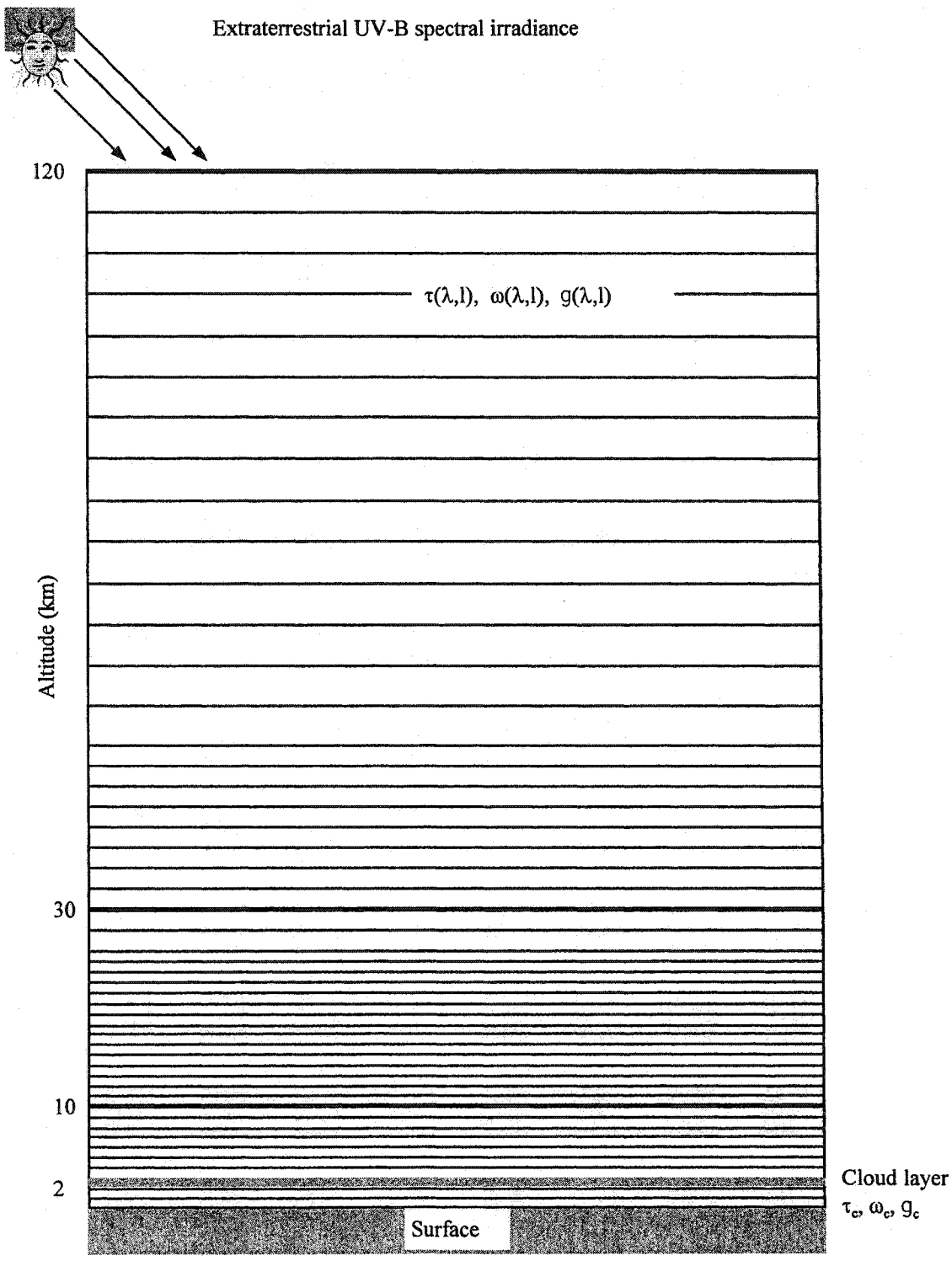

Figure 2.2. Model layers from the top of the atmosphere to the surface with cloud inserted between 2 and 3km above the surface. $\tau(\lambda,l)$, $\omega(\lambda,l)$, and $g(\lambda,l)$ are the spectral optical depth, single scattering albedo and asymmetry factor for each layer. τ_c, ω_c, and g_c are for the clould layer.

hourly irradiances over long time periods measured in years. They are invaluable, however, in providing the best possible estimates as standards against which calculations from simpler, less computationally-demanding methods can be compared. DISORT is used in this way in this study.

The simplest solutions are the two-stream (Frederick and Lubin, 1988; Lubin *et al.* 1989; Frederick and Snell, 1990; Lubin and Frederick, 1991) and the Eddington (Shettle and Weinman, 1970) approximations. All methods use τ, ω and g but the simple methods have a simplified scattering phase function. They lose accuracy when scattering is highly peaked in the forward direction which is the case for both cloud and aerosol particles (Wiscombe and Joseph, 1977). Joseph *et al.* (1976) modified the Eddington method using a delta function to handle the strong forward peak of the phase function. Their delta function has approximately the same second moment as the Henyey-Greenstein scattering phase function, which has a broad forward-scattering peak and is widely used to simulate asymmetric scattering (Wiscombe and Joseph, 1977). The delta-Eddington method is used in this study because it handles asymmetrical phase functions (which characterize aerosol and cloud particles) well, produces broadband irradiances similar to exact methods (Forster and Shine, 1995), and it is computationally fast which can be run on a personal computer.

The DISORT and delta-Eddington algorithms have been used to model irradiance under clear and cloudy skies (Chubarova, 1991; Liu *et al.*, 1991; Madronich, 1992; Tsay and Stamnes, 1992; Madronich, 1993; Davies and Runnalls, 1993; Wang and Lenoble, 1994; Zeng *et al.*, 1994; Forster, 1995; Forster *et al.*, 1995; Davies *et al.*, 2000).

Comparisons between the DISORT and delta-Eddington methods for theoretical model atmospheres for UV transmittance (290-400 nm) for various ozone amounts and aerosol and cloud optical depths and different solar zenith angles are given by Forster and Shine (1995). This is the first comparison of the two methods for a real atmosphere in the UV-B waveband in terms of daily total irradiances.

2.5 The delta-Eddington approximation

Eq. (2.6) is solved with the Wiscombe's (1977) delta-Eddington algorithm, which combines the Eddington approximation (Shettle and Weinman, 1970) with a Dirac delta function (Joseph *et al.*, 1976) to approximate the large forward peak in the phase function of asymmetric scattering. This is accomplished with scaled terms (τ', ω', g') of τ, ω and g where

$$\tau' = \left(1 - \omega g^2\right)\tau, \tag{2.7}$$

$$\omega' = \frac{\left(1 - g^2\right)\omega}{1 - \omega g^2}, \tag{2.8}$$

and

$$g' = \frac{g}{1 + g}. \tag{2.9}$$

Assuming that intensities and the phase function are independent of azimuth Eq. (2.6) reduces to

$$\mu \frac{dI}{d\tau'} = -I(\tau', \mu) + \frac{\omega'}{2} \int_{-1}^{+1} (1 + 3g'\mu\mu') I(\tau', \mu') d\mu'. \tag{2.10}$$

This is solved following Shettle and Weinman (1970) by assuming no downward diffuse irradiances at the top of the atmosphere and an upwelling flux at the ground, which is the product of surface albedo and the incident flux. The use of the scaled optical properties improves accuracy for highly anisotropic phase functions and for thin layers when absorption is large (Joseph *et al.*, 1976; Wiscombe and Joseph, 1977).

Joseph *et al.* (1976) tested the delta-Eddington fluxes against the doubling method (Wiscombe, 1976), which has an accuracy of 0.1%. The maximum delta-Eddington error for all flux computation did not exceed 2% of the incident flux and the average flux error was less than 0.5%. For flux ratios (transmissivity, reflectivity and absorptivity) accuracy is better than 0.02 for $\mu \geq 0.4$ over all values of optical depth (0.01-100) but errors increase with increasing solar zenith angles. Other studies also have compared the delta-Eddington approximation with doubling methods and concluded that it was very good for highly asymmetric phase functions and for a wide range of optical depths and single scattering albedos for a homogeneous layer calculation (Wiscombe and Joseph, 1977; King and Harshvardhan, 1986; Harshvardhan and King, 1993). Forster and Shine (1995) showed that the delta-Eddington is not suitable for spectral values for clear skies and at large solar zenith angles but for overcast skies the delta-Eddington errors were much smaller. For clear skies, the irradiance was overestimated by as much as 32% at 312 nm, for a solar zenith angle of 84.3°. For thick scattering layers, as is the case for cloud, the two-term expansion is enough because the multiple scattering is more dominant and the radiation field is smoother and not too sensitive to detailed phase function structure (Wiscombe and Joseph, 1977; Lenoble, 1993 p. 176). Erlick and

Frederick (1998) compared the delta-Eddington flux calculations with the 22-stream DISORT model for an isolated optically thick cloud layer ($\tau_c = 40$) at 290 nm with zero surface albedo. They found that transmission and reflection from these two methods were closely matched except for large zenith angles $\left(\geq 60^{\circ}\right)$ where the delta-Eddington transmissivity and reflectivity were systematically too high and too low (by 10%) respectively. Lubin *et al.* (1998) argued that the uncertainties in irradiance calculations using the delta-Eddington approximation instead of DISORT are less than the uncertainties involved in treating clouds as plane parallel layers. The delta-Eddington approximation may be adequate for modeling UV-B under all sky conditions.

2.6 The DISORT method

The discrete ordinate method was introduced originally by Chandrasekhar (1960) for radiative transfer applications in planetary atmospheres. Liou (1973) was the first to apply the method to compute radiation fields in aerosol and cloudy atmospheres. Numerical instabilities produced erroneous results such as small negative absorptions. A new formulation of the discrete ordinate method has overcome these difficulties by superior algorithms for faster calculation of eigenvalues and eigenvectors (Stamnes and Swanson, 1981). This algorithm is both efficient and accurate for calculating intensities and fluxes (Stamnes and Dale, 1981). Stamnes *et al.* (1988) made this algorithm (DISORT)[8] available to the scientific community through a computer code. DISORT is an exact solution of the radiative transfer equation since, in principle; it does not require

[8] The DISORT Fortran-77 code is available at:
http://climate.gsfc.nasa.gov/pub/wiscombe/multiple scat/

truncation of phase function expansion. In practice, the user does truncate and the method becomes an approximation.

After expanding I and P in Eq. (2.6) using Fourier cosine series and Legendre polynomials, and replacing the phase function integral with Gaussian quadrature, one achieves the following $2N$ first order differential equations

$$\mu_i \frac{dI(\tau,\mu_i)}{d\tau} = -I(\tau,\mu_i) + \frac{\omega}{2}\sum_{l=0}^{N}\omega_l P_l(\mu_i)\sum_{\substack{j=-N \\ j\neq 0}}^{N} a_j I(\tau,\mu_j) P_l(\mu_j) + \frac{\omega}{4} S_0 \left[\sum_{l=0}^{N}(-1)^l \omega_l P_l(\mu_i) P_l(\mu_0)\right] e^{-\tau/\mu_0}, \tag{2.11}$$

where i runs from $-n$ to n. For a vertically inhomogeneous atmosphere this equation constitutes a system of $2N$ coupled differential equations with nonconstant coefficients which is solved with the boundary conditions specified for the delta-Eddington solution. The accuracy of flux calculations depends on the number of discrete-ordinate streams (expansion terms) used. High accuracy flux calculations have been reported for 4-stream (Stamnes and Conklin, 1984; Curtis, 1996) and 8-stream forms (Stamnes and Dale, 1981; Stamnes and Swanson, 1981; Zeng *et al.*, 1994). Comparison between UV-B irradiance calculated by DISORT model and measurements have been presented by Wang and Lenoble (1994), Zeng *et al.* (1994) and Pachart *et al.* (2000) for clear sky conditions. Wang and Lenoble (1994) concluded that the variation of the ratio between measurement and model spectral results exceeds ±20%, but the agreement is better than ±6% when the ratio is averaged over intervals of 10 nm. Zeng *et al.* (1994) compared measured irradiances with DISORT (8-streams) results. They found that UV-B irradiances could be predicted to within 8% if the input parameters were well known.

These differences are due to calibration errors either in the instrument or in the extraterrestrial spectral irradiance.

2.7 Model inputs

2.7.1 Extraterrestrial spectral irradiance

The McMaster model uses solar spectral extraterrestrial irradiances from the Solar Ultraviolet Spectral Irradiance Monitor (SUSIM) instrument on board the third Atmospheric Laboratory for Applications and Science (ATLAS-3) space shuttle mission launched on Nov. 13, 1994 (D. Prinz, personal communication, 1998).

Since the Brewer instrument measures irradiance through a triangular filter (Figure 2.3) with a base of 1.1 nm (full width at half maximum of 0.55 nm), the high spectral resolution (full width at half maximum ~ 0.15 nm, sampled approximately every 0.05 nm) SUSIM data were averaged to mimic the Brewer. SUSIM measurements for average Sun–Earth distance were selected from the 289.45 and 326.55 nm wavelength range at a 0.05 nm interval, and averaged for each nanometer from 290 to 325 nm (Table 2.1). The average spectral irradiance $\overline{S_\lambda}$ for each nanometer was obtained from:

$$\overline{S_\lambda} = \frac{\sum w_\lambda S_\lambda}{\sum w_\lambda}, \tag{2.12}$$

where w_λ is the triangular filter weighting function with the value 1 at the centre of the filter and 0 at its two ends and S_λ is the extraterrestrial solar irradiance interpolated at every 0.05 nm. Weights were assigned at 0.05 nm intervals between the lower wavelengths limit of the filter and its midpoint using

$$w_\lambda = \frac{d}{0.55}, \tag{2.13}$$

where d is the difference between a particular wavelength and the starting wavelength of the triangular filter. The weights between the midpoint and the upper limit of the filter are mirror images of these. The triangularly averaged extraterrestrial solar irradiance is compared with the arithmetically averaged values in Figure 2.4. To show the difference more clearly the ratios between triangularly averaged and arithmetically averaged extraterrestrial spectral irradiance values are also shown. The ratios show some scatter and generally the differences are larger than 6%. The triangularly averaged irradiances are corrected for the departure of the Sun- Earth distance from the average value following Michalsky (1988).

2.7.2 Atmospheric optical properties

Since there are few measured atmospheric vertical profiles of ozone, temperature, pressure and humidity, standard model atmospheres containing these vertical profiles for 50 atmospheric levels from the surface to 120 km in LOWTRAN 7 (Kneizys *et al.*, 1988) were used for the model in this study. Summer and winter midlatitude and subarctic model atmospheres were used to calculate Rayleigh and ozone optical depths.

Radiative transfer calculations need spectral values of optical depth, single scattering albedo and asymmetry factor for each layer. These are calculated from their components, which are the result of ozone absorption, Rayleigh scattering and aerosol extinction indicated by the subscript $0, R$ and a using

$$\tau(\lambda,l) = \tau_0(\lambda,l) + \tau_R(\lambda,l) + \tau_a(\lambda,l), \tag{2.14}$$

$$\omega(\lambda,l)=\frac{\tau_R(\lambda,l)+\omega_a(\lambda,l)\tau_a(\lambda,l)}{\tau(\lambda,l)}, \tag{2.15}$$

and

$$g(\lambda,l)=\frac{g_a(\lambda,l)\omega_a(\lambda,l)\tau_a(\lambda,l)}{\tau(\lambda,l)\omega(\lambda,l)}. \tag{2.16}$$

In the calculation, cloud optical properties replace those calculated from Eqs. (2.14) - (2.16) for the layer between 2 and 3 km (Figure 2.2).

2.7.3 Rayleigh scattering

Since Rayleigh scattering by dry air molecules is proportional to λ^{-4}, it is strongest in the UV-B waveband. The spectral optical depth for Rayleigh scattering $\tau_R(\lambda,l)$ for an atmospheric layer is calculated as

$$\tau_R(\lambda,l)=\overline{\sigma_R(\lambda)}10^5\int_{z_t}^{z_b} n_R(z)\,dz, \tag{2.17}$$

where $\overline{\sigma_R(\lambda)}$ is the mean spectral Rayleigh scattering cross-section[9], $n_R(z)$ the molecular number density (number of molecules/cm^3) at height z and z_t and z_b are the heights of the top and bottom layer. Cross sections were calculated as weighted means (Table 2.1) from

$$\overline{\sigma_R(\lambda)}=\frac{\sum w_\lambda S_\lambda \sigma_R(\lambda)}{\sum w_\lambda S_\lambda}, \tag{2.18}$$

where $\sigma_R(\lambda)$ is the spectral Rayleigh scattering cross-section given by

[9] Scattering cross section is the area perpendicular to the light wave that receives the same amount of energy as the spherical particle scatters.

$$\sigma_R(\lambda) = \frac{8\pi^3 \left(m_r^2 - 1\right)^2}{3\lambda^4 n_s^2} \frac{6+3\delta}{6-7\delta}, \tag{2.19}$$

in which n_s is the molecular number density (2.547×10^{19} molecules/cm^3 at standard air[10]) (Elterman, 1968), δ the anisotropic factor which is set at 0.035 (Penndorf, 1957) and m_r, is the real part of the refractive index, which controls scattering and for standard air at 15° C temperature is given by

$$m_r = \left[6432.8 + \frac{2949810}{146 - \lambda^{-2}} + \frac{25540}{41 - \lambda^{-2}}\right] 10^{-8} + 1. \tag{2.20}$$

The imaginary part of the refractive index, which controls absorption, is insignificant for air molecules, therefore $\omega = 1$. $\sigma_R(\lambda)$ does not vary with temperature and pressure but $n_R(z)$ depends on both:

$$n_R(z) = n_s \left[\frac{p(z)}{p_0}\right]\left[\frac{T_0}{T(z)}\right]. \tag{2.21}$$

Here, p_0 and T_0 are the standard pressure (1013.25 mb) and standard temperature (273.15° K) at sea level, and $p(z)$ and $T(z)$ are the atmospheric pressure and temperature at height z. Then the final form of Eq. (2.17) can be approximated by

$$\tau_R(\lambda, l) = \overline{\sigma_R(\lambda)} 10^5 n_s \left[\frac{p(z_t)}{T(z_t)} + \frac{p(z_b)}{T(z_b)}\right]\left(\frac{T_0}{p_0}\right)(z_t - z_b)/2. \tag{2.22}$$

[10] Standard air is defined as dry air containing 0.03% CO_2 by volume at normal pressure (1013.25 mb) and having an air temperature of 15° C.

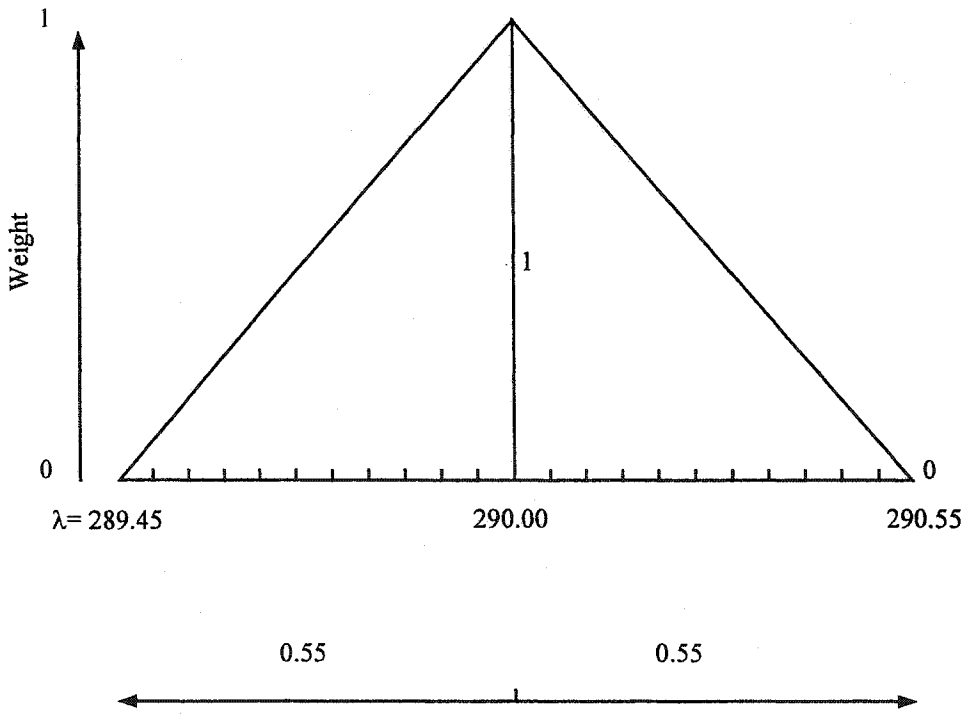

Figure 2.3. The weighting factors applied to the extraterrestrial solar spectral irradiance, Rayleigh scattering and ozone absorption cross sections to mimic the Brewer filter.

Table 2.1. Triangularly averaged extraterrestrial spectral irradiances and Rayleigh scattering optical cross section $\overline{\sigma_R(\lambda)}$ used in the model.

Wavelength (nm)	Flux (mw m^{-2} nm^{-1})	$\overline{\sigma_R(\lambda)}$ (cm^2)
290	592.32	6.5674×10^{-26}
291	605.73	6.4721×10^{-26}
292	568.57	6.3771×10^{-26}
293	536.78	6.2812×10^{-26}
294	501.15	6.1916×10^{-26}
295	506.52	6.1014×10^{-26}
296	607.94	6.0135×10^{-26}
297	417.03	5.9267×10^{-26}
298	596.11	5.8462×10^{-26}
299	544.51	5.7565×10^{-26}
300	450.32	5.6813×10^{-26}
301	487.27	5.5958×10^{-26}
302	397.48	5.5197×10^{-26}
303	668.10	5.4393×10^{-26}
304	588.83	5.3647×10^{-26}
305	660.80	5.2880×10^{-26}
306	530.88	5.2139×10^{-26}
307	625.43	5.1416×10^{-26}
308	663.84	5.0727×10^{-26}
309	604.18	5.0052×10^{-26}
310	483.83	4.9353×10^{-26}
311	824.53	4.8666×10^{-26}
312	657.76	4.8012×10^{-26}
313	715.97	4.7354×10^{-26}
314	805.91	4.6716×10^{-26}
315	726.37	4.6073×10^{-26}
316	531.16	4.5475×10^{-26}
317	784.77	4.4845×10^{-26}
318	684.16	4.4288×10^{-26}
319	767.22	4.3682×10^{-26}
320	817.19	4.3092×10^{-26}
321	768.81	4.2553×10^{-26}
322	805.39	4.1970×10^{-26}
323	6.39.57	4.1421×10^{-26}
324	761.06	4.0875×10^{-26}
325	790.42	4.0356×10^{-26}

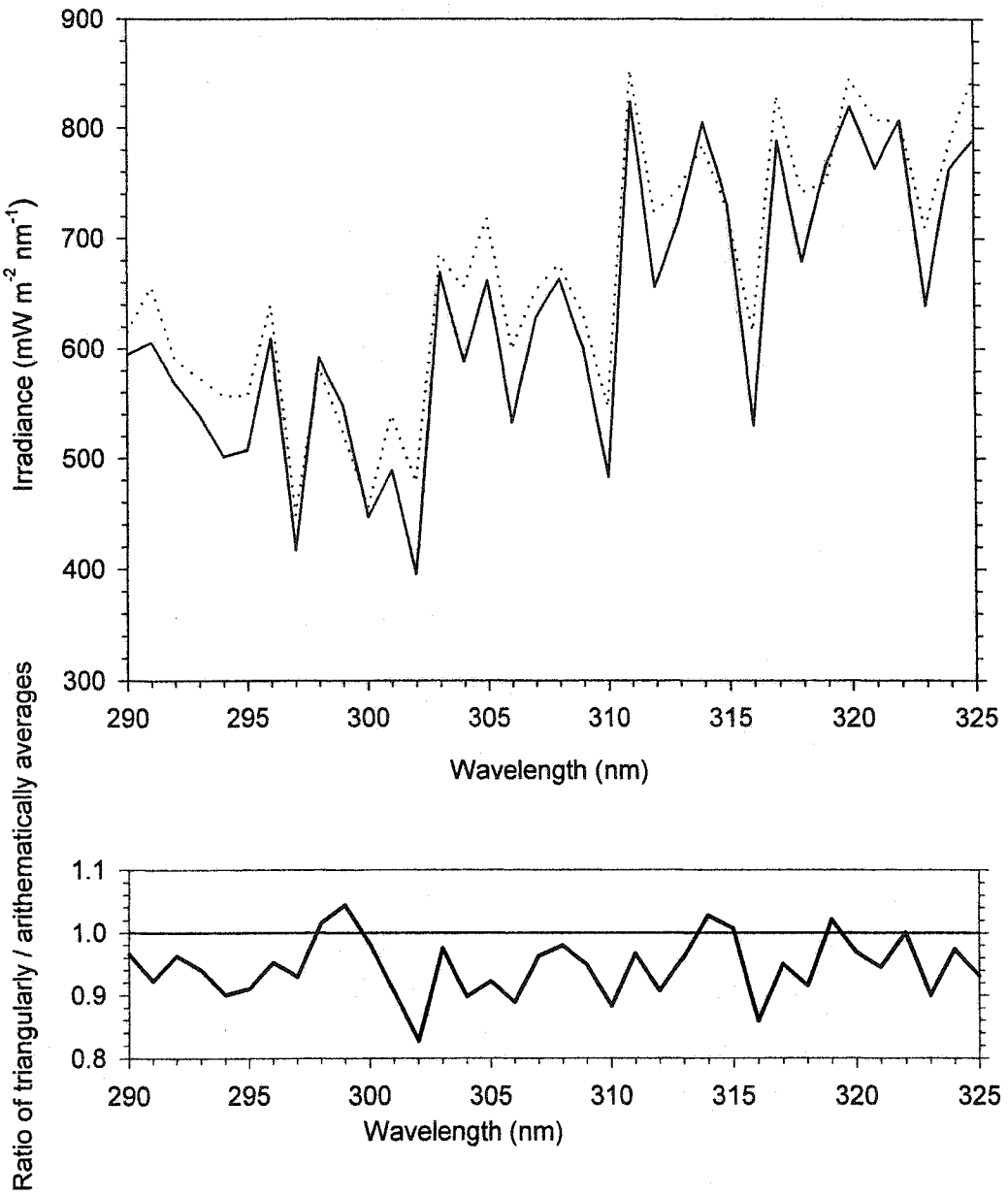

Figure 2.4. Triangularly averaged (Brewer-like) (solid line) and arithmetically averaged (dotted line) extraterrestrial UV-B solar irradiance from ATLAS-3. The thick solid curve in the lower graph represents the ratio of the two averages.

2.7.4 Ozone absorption

Ozone spectral optical depth for each atmospheric layer $\tau_o(\lambda,l)$ is calculated from the mean spectral ozone absorption cross-section $\overline{\sigma_o(\lambda,z)}$, and the ozone molecular number density $N_o(z)$ at height z:

$$\tau_o(\lambda,l)=\int_{z_t}^{z_b}\overline{\sigma_o(\lambda,z)}N_o(z)dz, \tag{2.23}$$

where $\overline{\sigma_o(\lambda,z)}$ is calculated as weighted means in a similar manner to Eq. (2.18),

$$\overline{\sigma_o(\lambda,z)}=\frac{\sum w_\lambda S_\lambda \sigma_o(\lambda,z)}{\sum w_\lambda S_\lambda}, \tag{2.24}$$

where, following Paur and Bass (1985),

$$\sigma_o(\lambda,z)=C_0(\lambda)+C_1(\lambda)T(z)+C_2(\lambda)T(z)^2, \tag{2.25}$$

in which C_0, C_1 and C_2 are temperature-dependent ozone absorption coefficients and T is the temperature in degrees Celsius.

Ozone molecular number density $N_o(z)$ is the product of the number of ozone molecules in each gram n_o and ozone density $O_3(z)$,

$$N_o(z)=O_3(z)n_o, \tag{2.26}$$

where

$$n_o=\frac{6.022045\times10^{23}}{M_o}=1.25467\times10^{22}, \tag{2.27}$$

in which the numerator is Avogadro's number and M_o is the molecular weight of ozone (47.9982 g mol^{-1}). $O_3(z)$ values in ppmv were converted to density (gm^{-3}) by the ideal gas equation:

$$O_3(z) = \frac{O_3(z)'}{10^6}\left[\frac{p(z)}{T(z)}\frac{10^5}{R}\right]\frac{M_o}{M_a}, \tag{2.28}$$

where $O_3(z)'$ is the ozone concentration at height z in ppmv scaled by the ratio of measured daily column ozone amount by Brewer instrument to the model atmospheres value, M_a is the molecular weight of dry air (28.966 g mol^{-1}), p is pressure (Pa), T is temperature in Kelvin and R is the gas constant (287.053 J kg^{-1} K^{-1}). The ozone spectral optical depths for each layer $\tau_o(\lambda, l)$ were calculated from

$$\tau_o(\lambda, l) = \left[\overline{\sigma_o(\lambda, z_t)}N_o(z_t) + \overline{\sigma_o(\lambda, z_b)}N_o(z_b)\right](z_t - z_b)/2. \tag{2.29}$$

2.7.5 Aerosol optical properties

There are no aerosol data for the UV-B band for Canada. Therefore, values were extracted from the Shettle and Fenn (1979) data tabulated in LOWTRAN 7. Weighted means of optical cross-sections are not used for aerosol parameters for the reason that LOWTRAN 7 provides low-resolution aerosol spectral values and aerosol optical properties vary slowly with wavelength in the UV-B band.

Aerosol spectral optical depth for each layer is defined by

$$\tau_a(\lambda, l) = \int_{z_t}^{z_b} \beta_{ext}(\lambda, z)dz, \tag{2.30}$$

where the aerosol extinction coefficient $\beta_{ext}(\lambda, z)$ is determined from

$$\beta_{ext}(\lambda, z) = \beta_a \times \beta_{asf}, \tag{2.31}$$

where β_a is the normalized (divided by the extinction at $\lambda = 0.55\mu m$) aerosol spectral extinction and β_{asf} is the aerosol scaling factor extinction coefficient at $\lambda = 0.55\mu m$. The atmosphere is divided into four layers of different aerosol shown in Figure 2.2: the boundary layer (0 to 2 km), the troposphere (>2 to 10 km), the stratosphere (>10 to 30 km) and the upper atmosphere (>30 km).

Aerosol extinction data β_a were interpolated for each wavelength from the low-resolution spectral values of Shettle and Fenn (1979). Their data provide extinction and absorption coefficients and asymmetry factors for 15 wavelengths between $0.200\mu m$ and 4.5 μm for the four atmospheric layers. For the boundary layer these optical properties are provided for rural, urban and maritime aerosol types. Aerosol optical properties for the first 10 km from the surface (i.e., the boundary layer and troposphere) are humidity dependent, because with increasing relative humidity water vapor condenses onto the atmospheric particulates, thereby increasing their sizes and changing their composition and optical properties.

The aerosol scaling factors β_{asf} are provided for 33 heights from LOWTRAN 7 (Kneizys *et al.*, 1988) and were interpolated to match this model's 50 atmospheric levels. These aerosol profile data are classified according to visibility in the boundary layer, season and visibility in the troposphere, and season and volcanic aerosol in the stratosphere. Table 2.2 summarizes the aerosol model components.

Table 2.2. Aerosol model components for four layers: Boundary layer, troposphere, stratosphere and upper atmosphere. Aerosol types are also shown for the boundary layer and stratosphere.

Boundary layer	**Troposphere**	**Stratosphere**
1= 50 km 2= 23 km 3= 10 km 4= 5 km 5= 2 km 6= 36.5 km (average of 1 and 2)	1= Fall-Winter 50 km 2= Fall-Winter 23 km 3= Spring-Summer 50 km 4= Spring-Summer 23 km	1= Background F-W 2= Moderate Volcanic F-W 3= High Volcanic F-W 4= Extreme Volcanic F-W 5= Background S-S 6= Moderate Volcanic S-S 7= High Volcanic S-S 8= Extreme Volcanic S-S
Upper Atmosphere	**Boundary layer Aerosols**	**Stratospheric Aerosols**
1= Normal Upper Atmosphere 2= Volcanic to Normal 3= Volcanic to Extreme 4= Extreme Upper Atmosphere	1= Rural 2= Urban 3= Maritime	1= Background Stratosphere 2= Aged Volcanic 3= Fresh Volcanic

Rural (with 50 km visibility) and urban aerosols (for 50 km and 36.5 km visibilities, the later is the average of 23 km and 50 km) were used in the boundary layer as appropriate. For the troposphere 50 km visibility aerosol was selected. Background aerosol and normal aerosol for the stratosphere and upper atmosphere, respectively, for all stations.

The aerosol extinction coefficient β_{ext}, single scattering albedo ω_a and asymmetry factor g_a were interpolated linearly at each level and for each nanometer. Layer aerosol optical depth was calculated from

$$\tau_a(\lambda,l)=\left[\beta_a(\lambda,z_t)\beta_{asf}(z_t)+\beta_a(\lambda,z_b)\beta_{asf}(z_b)\right](z_t-z_b)/2. \qquad (2.32)$$

Single scattering albedos were calculated from interpolated absorption and extinction coefficients:

$$\omega_a(\lambda,z)=1-\frac{abs(\lambda,z)}{\beta_a(\lambda,z)}. \qquad (2.33)$$

Layer values of single scattering albedos and asymmetry factors were calculated as layer averages.

2.7.6 Surface albedo

Surface albedo measurements for the UV-B band are not available in Canada. Albedo was calculated following Davies *et al.* (2000) as a linear function of daily snow depth measurement sd between $\alpha_l = 0.05$ for a snow free ground (Bowker *et el.*, 1985) and $\alpha_h = 0.75$ for a snow cover of 30 cm or greater:

$$\alpha = \alpha_l + \frac{sd}{30}(\alpha_h - \alpha_l). \tag{2.34}$$

The value of 0.75 was determined from Stony Plain data (approximately 37 km west of Edmonton) where measurements were made with extensive snow cover. Albedo is independent of wavelength and the effects of melting and snow contamination are ignored.

CHAPTER 3

The role of clouds in modeling UV-B radiation

This Chapter addresses the cloud amount and cloud optical properties for nine stations. All cloud types and heights are incorporated into calculating mean cloud amount. Cloud types and heights are broken down separately to investigate their effects when calculating cloud optical properties. Some sensitivity analyses are presented to show the influence of cloud optical properties on the transmitted broadband irradiances.

Stations with concurrent measurements of UV-B irradiance and meteorological data for radiation calculations are listed in Table 3.1. They include two arctic (Alert and Resolute), one sub-arctic (Churchill) and six midlatitude stations. They provide 26 years of data in total. All the datasets used are from the period between 1993 to 1996 because ozone data were only available for that period.

3.1 Cloud amount

Cloud amount is the most important determinant of solar irradiance in cloudy skies because it controls the partitioning between direct beam and diffuse radiation (Eq. 2.1). Visual estimates of hourly cloud amount (tenths) have been made by the MSC at airports. Since ground based observers see sides of clouds as well as bases, their estimates normally overestimate true cloud cover. The MSC does not correct for this

Table 3.1. Stations used in the study.

Station	Latitude, °N	Longitude, °W	Elevation, m	Years of data
Alert (NWT)	82° 30′	62° 18′	62	1995
Resolute Bay (NWT)	74° 43′	94° 59′	64	1993-1996
Churchill (Man.)	58° 45′	94° 04′	35	1993-1996
Edmonton (Alta.)	53° 33′	114° 06′	766	1993-1996
Regina (Sask.)	50° 13′	104° 40′	592	1994-1995
Winnipeg (Man.)	49° 55′	97° 14′	239	1993
Montreal (Que.)	45° 28′	73° 45′	24	1993-1994
Halifax (NS)	44° 44′	63° 40′	31	1993-1996
Toronto (Ont.)	43° 47′	79° 23′	198	1993-1996

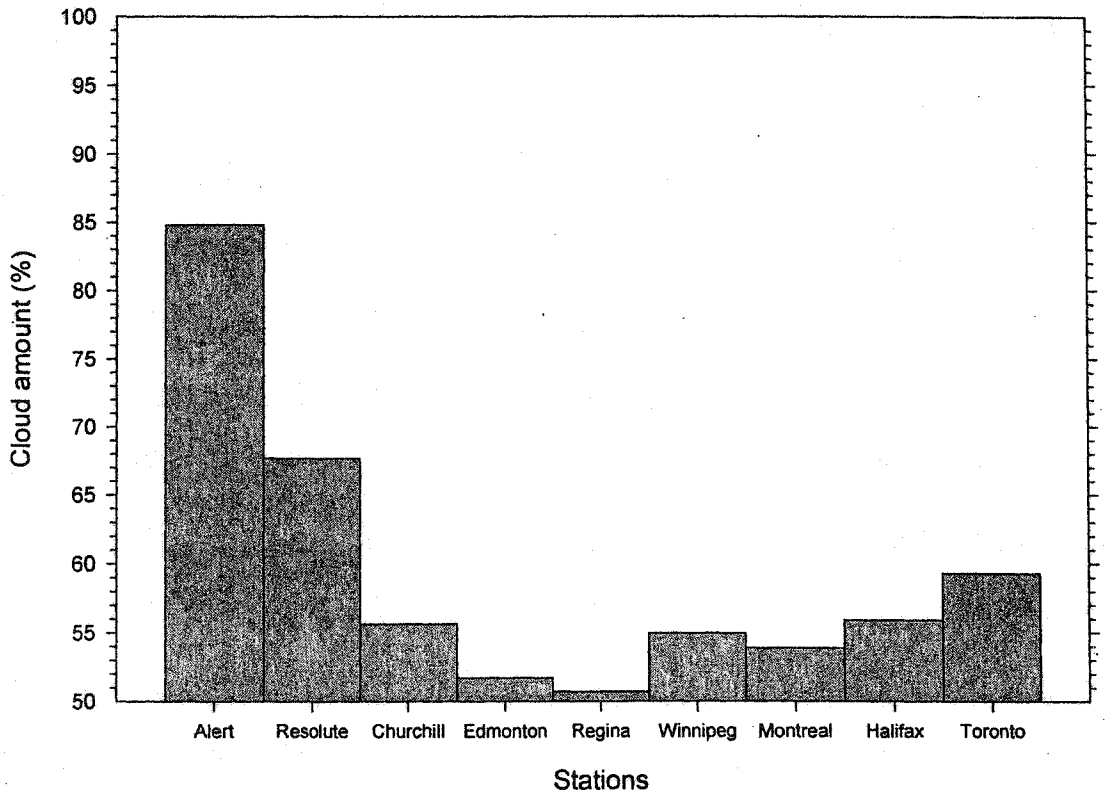

Figure 3.1. Mean total cloudiness at each station (all years). Total cloud amounts are based on daytime observations.

systematic error but, based on the work of Davies and McKay (1982), an effective approximation can be made using observations of total cloud opacity instead of cloud amount. Therefore this study uses cloud opacity and henceforth, the term cloud amount will be used to designate cloud opacity. Figure 3.1 shows that daytime mean total cloud exceeds 50% for all stations, reaching 85% at Alert.

Cloud amount frequencies for all years are shown in Figure 3.2. With the exception of Alert, all cloud amounts are well represented in these distributions. Consequently, error in specifying cloud amount is an important component of the error in calculating radiation from Eq. 2.1. Alert shows a distinct J-shaped distribution with overcast skies for about 60% of the year. Here, error in cloud amount will have the least effect since it is expected to be small for overcast skies. The southern stations have U-shaped distributions that are characteristic of most midlatitude-stations (Essenwanger, 1976). Resolute Bay seems to have a combination of J-U shaped distributions.

Cloud type is potentially important in determining variation in optical depth. Surface observations provided by the MSC contain cloud amounts, opacities and types for up to four cloud layers. Observing cloud types from surface observations is difficult because overcast low clouds obscure higher-level clouds, therefore only low level cloud types are recorded reliably. Table 3.2 shows the frequency of occurrence of different cloud types for overcast cases. Stratocumulus is the most common type at all stations. Additionally there is significant representation of stratofractus and altocumulus types. Fog is significant at coastal locations.

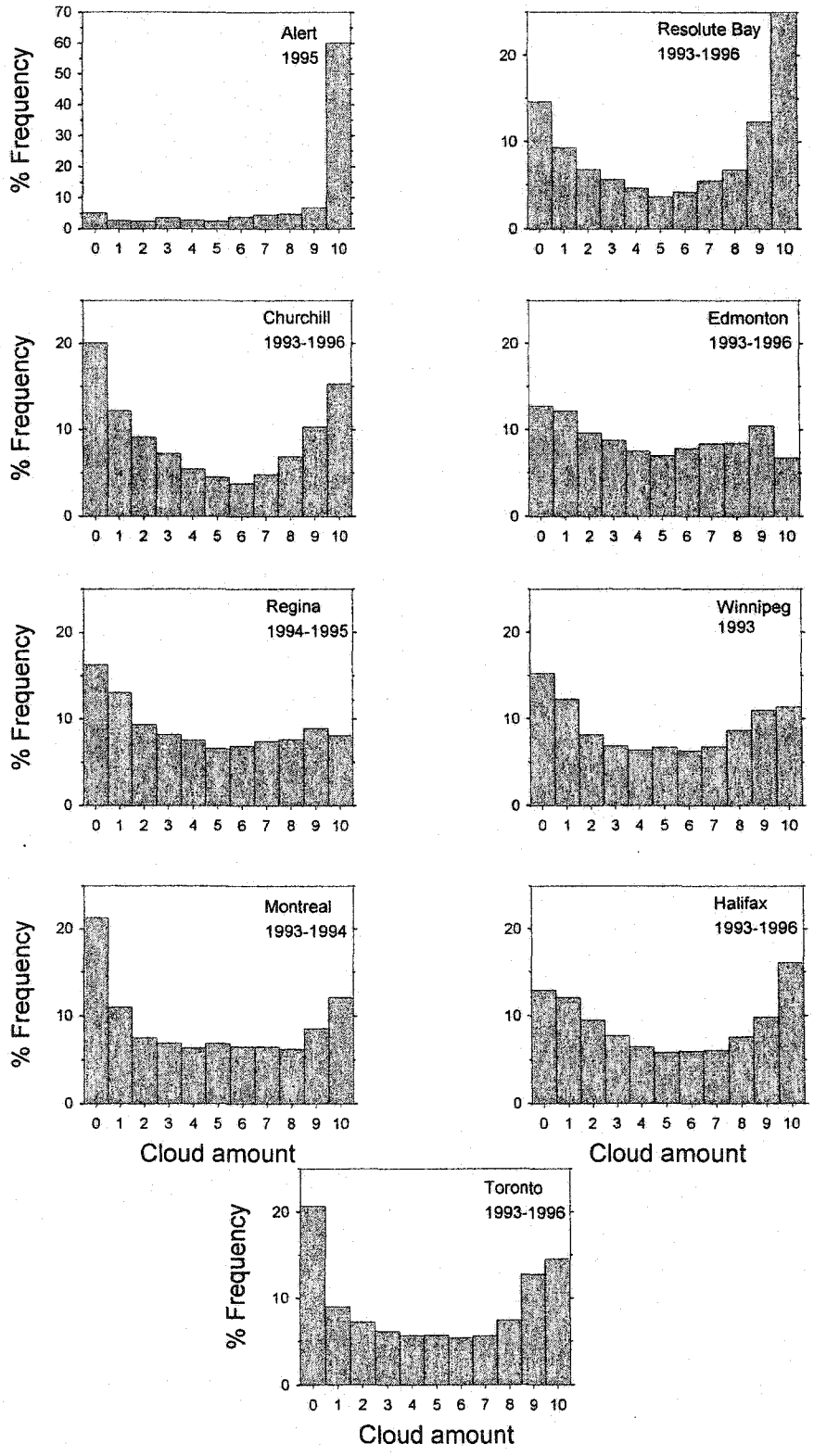

Figure 3.2. Percent frequency distributions of cloud amount for Alert, Resolute Bay, Churchill, Edmonton, Regina, Winnipeg, Montreal, Halifax and Toronto.

Table 3.2. Percentage frequency distributions of cloud type for overcast skies. The shaded and bold numbers indicate the first and second most common cloud types, respectively.

	Resolute	Churchill	Edmonton	Regina	Winnipeg	Montreal	Halifax	Toronto
Type				% Frequency				
Altocumulus	8.8	18.4	12.6	15.2	**25.9**	**18.3**	12.6	**24.1**
Altocumulus Castellanus	0	0.12	0.4	4.3	1.7	0	0	0.0
Altostratus	0.9	0.9	3.3	4.6	2.7	4.9	2	3.3
Cirrocumulus	0	0	0	0	0	0	0	0
Cirrostratus	0.6	0.1	1	0	5.4	1.1	1.1	1.5
Cirrus	0.5	1.7	3.1	7.5	5.1	0.6	3.7	2.4
Cumulonimbus	0	0.3	0.3	0.2	0.6	0.8	0.1	0.3
Cumulus	0.1	1.8	8.0	5.9	8.8	2.6	1.7	2.5
CumulusFractus	0	0.2	4.7	1.5	1.7	1.7	0.6	4
Stratus Fractus	**25.1**	**18.8**	**13.3**	**21.9**	6	8.5	**28.8**	4.9
Towering Cumulus	0	0	1.6	1.3	1.1	0	0.2	0.4
Nimbostratus	0	0	0.2	0	0	0	1.4	0.3
Stratocumulus	44.3	36.1	48.4	33.3	39.0	58.2	31.2	49.7
Stratus	5.3	5.5	1.2	0.7	1.5	1.8	2.5	1.8
Fog	13.6	11.9	0.7	2.1	0.7	1.2	13.3	3.6
Obstruction other than Fog	0.9	4.2	1.2	1.5	0	0.4	0.9	1.1
				Number of observations				
Cloudy	2855	2059	1647	676	851	1063	5177	7539
Clear	3285	2949	1013	852	829	1223	6551	6042
Total	6140	5008	2660	1528	1680	2286	11728	13581

3.2 Cloud optical properties

The cloud optical properties needed for radiative transfer calculations are the optical depth τ_c, the single scattering albedo ω_c and the asymmetry factor g_c. These dimensionless properties are not measured and must be estimated from Mie theory, assuming that clouds are composed of spherical droplets of virtually pure water of known radii (Stephens, 1984).

Optical depth is the most important property and is given by the integral of the extinction cross section[11] over all droplet radii over the depth of a horizontally homogeneous cloud:

$$\tau_c(\lambda) = \int_{z_b}^{z_t} \int_0^\infty n(r) Q_{ext}(x, m_\lambda) \pi r^2 dr dz, \tag{3.1}$$

where $n(r)$ is the number of particles per unit volume with radius between r and $r + dr$, $Q_{ext}(x, m_\lambda)$ is the extinction efficiency factor defined as the ratio of extinction to geometrical cross sections:

$$Q_{ext}(x, m_\lambda) = \frac{C_{ext}}{\pi r^2}, \tag{3.2}$$

in which C_{ext} is the extinction cross section for a cloud particle of radius r, x is the Mie size parameter defined as the ratio of sphere circumference to incident wavelength ($x = 2\pi r/\lambda$) and m is the complex refractive index of the sphere relative to the surrounding medium and is composed of a real part m_r and an imaginary part m_i, such

[11] Extinction cross section is the area perpendicular to the light wave that receives the same amount of energy as the spherical particle absorbs and scatters (Liou, 1980).

that $m(\lambda) = m_r(\lambda) - m_i(\lambda)$. Efficiencies are calculated from Mie theory (Dave, 1968) as a function of particle radius, wavelength of the incident ray and refractive index. Following standard practice in radiation climatology computations over a particle size distribution are replaced with a single computation for the equivalent radius of a spherical droplet:

$$r_e = \frac{\int_0^\infty r^3 n(r) dr}{\int_0^\infty r^2 n(r) dr}. \tag{3.3}$$

Mie calculations for the UV-B band wavelengths show that Q_{ext} for a given equivalent radius of cloud drops is approximately constant and approaches an asymptotic value of 2 (Hansen and Travis, 1974). Figure 3.3 shows that $Q_{ext} \simeq 2$ for the range of x values (135-209) that is appropriate for the UV-B band. This range was determined for equivalent radii of $7\mu m$ and $10\mu m$. The equivalent radius was specified as $10\mu m$ for the midlatitude and subarctic stations clouds, which is close to the global mean value for liquid water clouds $\approx 11\mu m$ (Han *et al.*, 1994), and $7\mu m$ for the arctic stations following studies presented by Herman and Curry (1984) and Leontyeva and Stamnes (1994).

Assuming that Q_{ext} does not vary spectrally, it follows from equation (3.1) that τ_c is independent of wavelength and can be treated as a broadband cloud optical depth throughout the UV-B range. In reality, τ_c changes due to variations in equivalent radius of its droplets (Slingo and Schrecker, 1982; Slingo, 1989, Hu and Stamnes, 1993). Observations show that the drop size distribution varies with height within the cloud (Slingo, 1989). However, the variation of $n(r)$ with height is unknown for Canadian

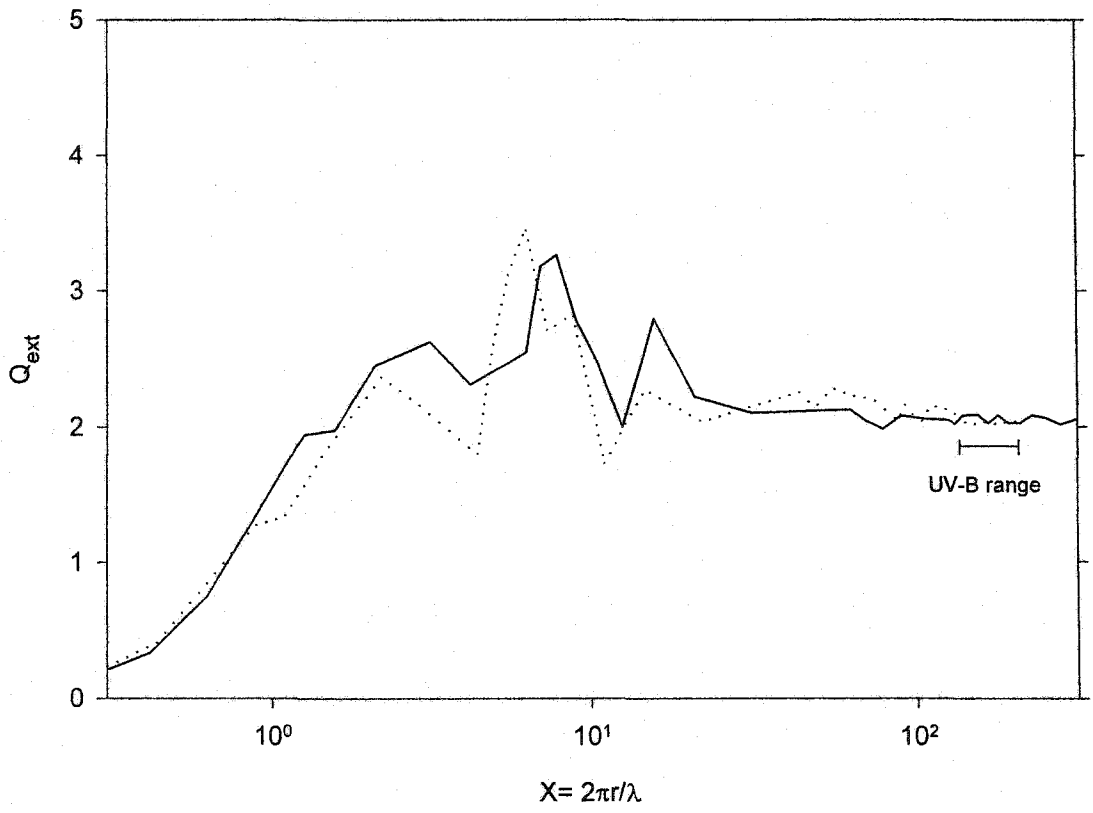

Figure 3.3. Extinction efficiency factor Q_{ext} as a function of the Mie size parameter x for two equivalent radii, 7μm (dotted line) and 10μm (solid line).

conditions and, for this study, an iterative approach (Brent method, from Press et al., 1992) is adopted to calculate a broadband τ_c from overcast irradiance measurements (Stamnes *et al.*, 1990; Stamnes *et al.*, 1991; Leontyeva and Stamnes 1994; Leontieva *et al.*,1994; Davies *et al.*, 2000). This procedure amounts to iterating the cloud optical depth in the model until computed and measured spectrally integrated irradiances agree to within 1×10^{-6} Wm^{-2}. Only days with at least two overcast measurements were selected. Times with snow on the ground were avoided since snow albedo in the UV-B band, which is not measured, can vary greatly with surface contamination and state of the snow (Wiscombe and Warren, 1980; Warren and Wiscombe, 1980). By restricting overcast data to snow free conditions, this eliminates about 50-55% of total overcast conditions for the arctic and subarctic stations and 15% for the midlatitude stations.

For clouds g_c lies between 0.75 and 0.9 (Liou, 1992; Min and Harrison, 1996) and an average value of about 0.85-0.87 has often been used (Hansen and Travis, 1974; Slingo and Schrecker, 1982; Hu and Stamnes, 1993). Figure 3.4 shows g_c as a function of x. For small particles g_c approaches zero, the value for Rayleigh scattering. For large x, g_c approaches 0.87. ω_c is also shown as a function of x in Figure 3.5. For the UV-B band ω_c and g_c vary little with wavelength and variation in the equivalent radius have little effect in this narrow range (Slingo and Schrecker, 1982). Also, their variations have small effect on transmissivity as compared with those resulting from changes in τ_c (Leontyeva and Stamnes, 1994).

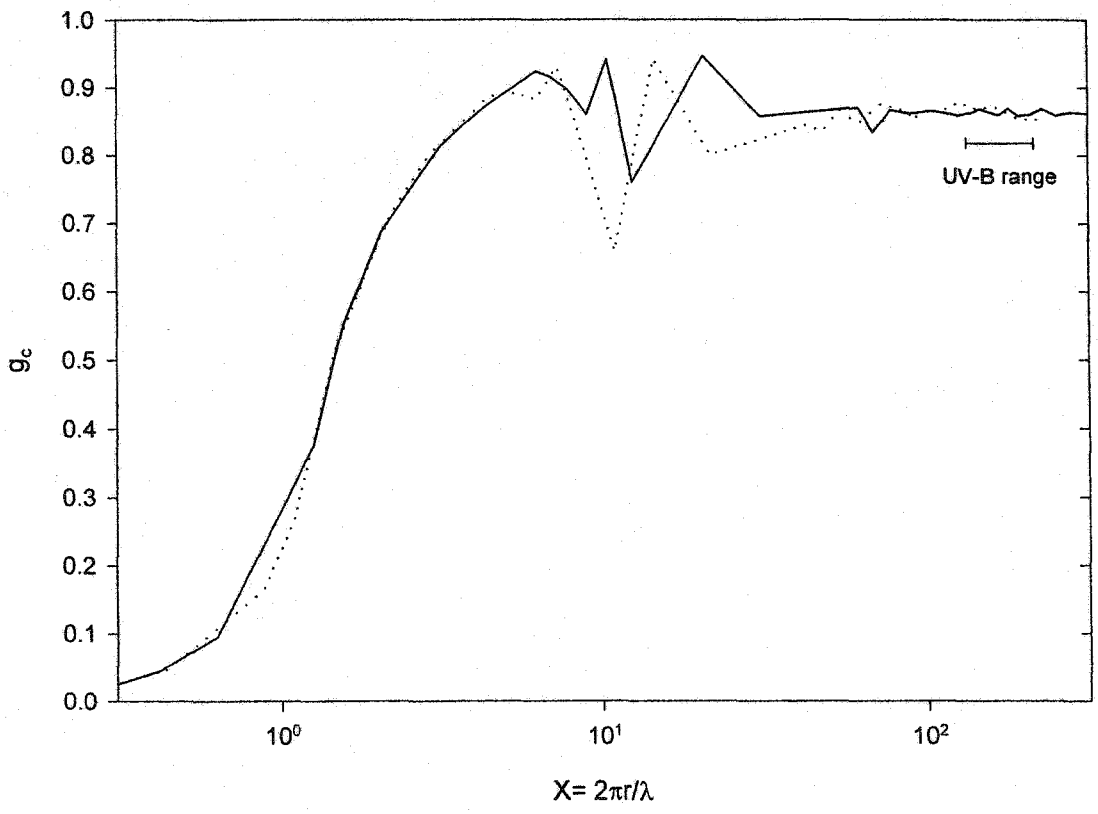

Figure 3.4. Cloud asymmetry factor g_c as a function of Mie size parameter x for two equivalent radii, 7μm (dotted line) and 10μm (solid line).

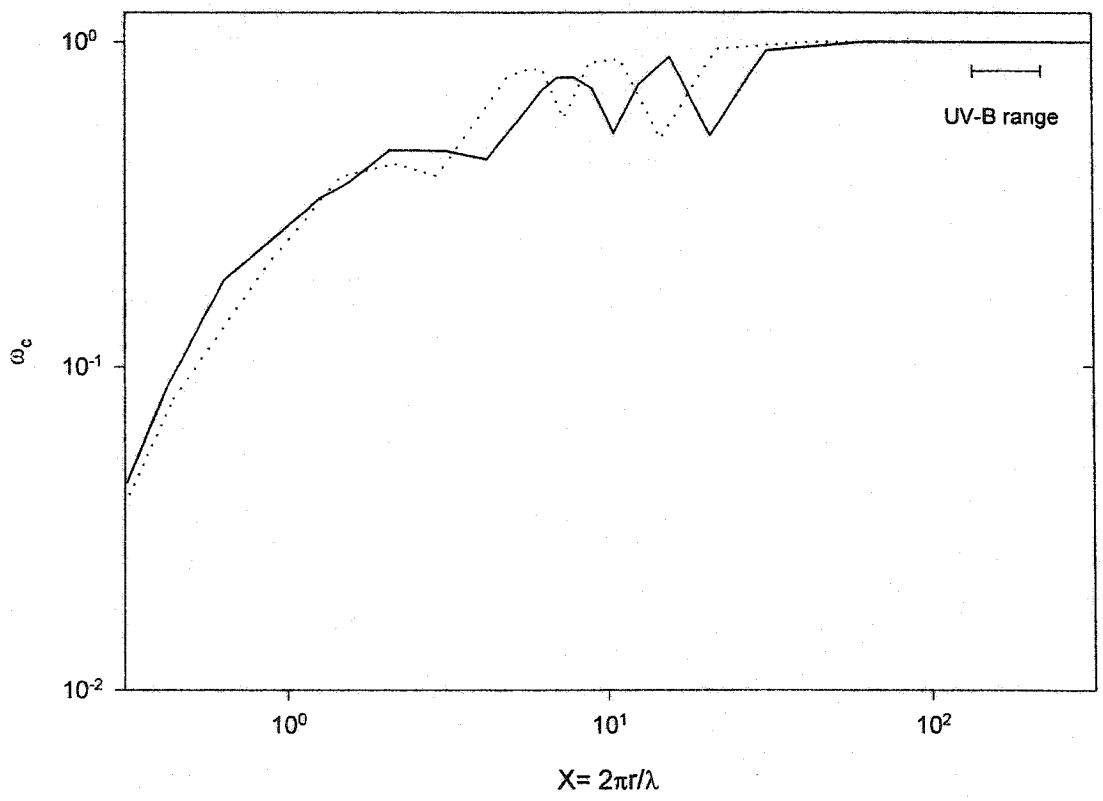

Figure 3.5. Cloud single scattering albedo ω_c as a function of Mie size parameter x for two equivalent radii, 7μm (dotted line) and 10μm (solid line).

Table 3.3. Co-albedo $(1-\omega_c)$ and asymmetry factor (g_c) values for two different equivalent radii (r_e) obtained from Mie calculation and the two parameterizations.

Method	$(1-\omega_c)$	g_c
$r_e = 10\mu m$		
Mie theory (present study)	5×10^{-6}	0.8587
Slingo and Schrecker (1982)	4×10^{-6}	0.8578
Hu and Stamnes (1994)	6×10^{-6}	0.8685
$r_e = 7\mu m$		
Mie theory (present study)	3×10^{-6}	0.8709
Slingo and Schrecker (1982)	3×10^{-6}	0.8528
Hu and Stamnes (1994)	5×10^{-6}	0.8641

In this study ω_c and g_c were calculated from Mie theory for wavelengths of 300 and 325 nm using the complex refractive index data of Hale and Querry (1973). The ice crystal and mixed-phase clouds were neglected because ω_c and g_c for these clouds are roughly equal to those for liquid clouds (Tsay and Stamnes, 1992; Forster, 1995; Barker *et al.*, 1998). The averages of co-albedo[12] $(1-\omega_c)$ and g_c for 300 and 325 nm wavelengths are presented in Table 3.3 along with cloud properties obtained as functions of equivalent radius by Slingo and Schrecker (1982) and Hu and Stamnes (1993).

Slingo and Schrecker (1982) developed simple linear relationships for $(1-\omega_c)$ and g_c as functions of equivalent radius r_e:

$$1-\omega_c = -6.5\times10^{-7} + 4.33\times10^{-7}\,r_e, \tag{3.4}$$

$$g_c = 0.841 + 1.680\times10^{-3}\,r_e, \tag{3.5}$$

where the coefficients apply to the 300-325 nm waveband and were obtained from least squares fitting of these functions to the data (Slingo, 1989). Following Ackerman and Stephens (1987), Hu and Stamnes (1993) arrived at nonlinear fittings of the droplet absorption and g_c for solar wavelengths:

$$1-\omega_c = \left[\left(1.42\times10^{-6}\,r_e^{0.766}\right) + \left(-2.33\times10^{-5}\,r_e^{-0.232}\right)\right]/2 + 9.24\times10^{-6}, \tag{3.6}$$

$$g_c = \left[\left(0.111\,r_e^{0.094}\right) + \left(-0.0806\,r_e^{-0.762}\right)\right]/2 + 0.8065, \tag{3.7}$$

where the coefficients apply to the 290-314 nm wavelengths and were derived by least squares. Table 3.3 summarizes $(1-\omega_c)$ and g_c values obtained from the above

[12] Co-albedo is the fraction of the incident radiation absorbed by the particle.

parameterizations and by the Mie theory used in this study. This shows that the Mie values of $(1-\omega_c)$ and g_c for $r_e = 10\mu m$ lie between the values obtained from the two parameterizations. For $r_e = 7\mu m$, the Mie values are slightly larger. In general, the Mie results are similar to the results from both parameterizations. These values will be used in all future radiation flux calculations.

3.3 Results

3.3.1 Delta-Eddington-DISORT comparisons

The DISORT model was used to calculate τ_c for five years at four stations to validate the delta-Eddington model results. These four stations were selected rather than all stations to reduce the amount of computation with DISORT. Alert was excluded because it had little data. The 8-stream (8 degrees of expansion of the phase function) DISORT algorithm was chosen to achieve high accuracy. Min and Harrison (1996) reported that the uncertainty in inferring τ_c using DISORT with 8 streams is only 1%.

Cloud optical depths derived from the two models are compared in Figures 3.6 and 3.7 for 50 km visibility aerosol. Figure 3.6 shows that the agreement is excellent for all five cases and indicates no bias. This is evident in the scatter plots for Resolute in 1993 and 1995, Churchill in 1993, Winnipeg in 1993, and Toronto in 1993 with slopes 1.03, 1.013, 0.986, 0.986, and 1.009. Differences between median cloud optical depths for the two models are always less than one. Percentage frequency distributions of τ_c (Figure 3.7) calculated by the two models for the same years are positively skewed with the most frequent τ_c values in the class interval of $10 < \tau_c \leq 20$ for all five years.

Resolute has quite distinctive distribution with most frequent τ_c (over 60%) is between 5 and 15. This illustrates that a high percentage of overcast conditions at high latitudes are optically thin. Churchill and Winnipeg have similar τ_c distributions with the highest frequency (over 30%) occurring between 10 and 20. However, Winnipeg has lower frequency (less than 10%) for τ_c between 5 and 10. Toronto shows broad distributions with fairly large number of observations in the higher optical depth ranges. These broad distributions with many large values of τ_c are what contribute to high mean and median values at Toronto.

Table 3.4 summarizes the results of τ_c calculated by both models and indicates mean, median and number of observations for each year for the nine stations. Mean values exceed median values by 3 to 36 optical depth. Median values are smaller for arctic and sub-arctic stations (5-15) and between 17 and 28 for the rest. At Bergen, Norway Leontieva *et al.* (1994) obtained much larger median values between 33 and 55. However, Leontiyeva and Stamnes (1994), Ricchiazzi and Gautier (1995) and Barker *et al.* (1998) did not present median τ_c but only the mean values, and they are similar to those obtained by this study.

3.3.2 Optical depths

Cloud optical depths were calculated for all stations with the delta-Eddington model. Overcast sky is the sum of all clouds in four layers. This sum is inserted within one model layer located between 2 and 3 km. Urban aerosol optical depths with 50 and 36.5 km visibilities were selected for the boundary layer for both Toronto and Montreal

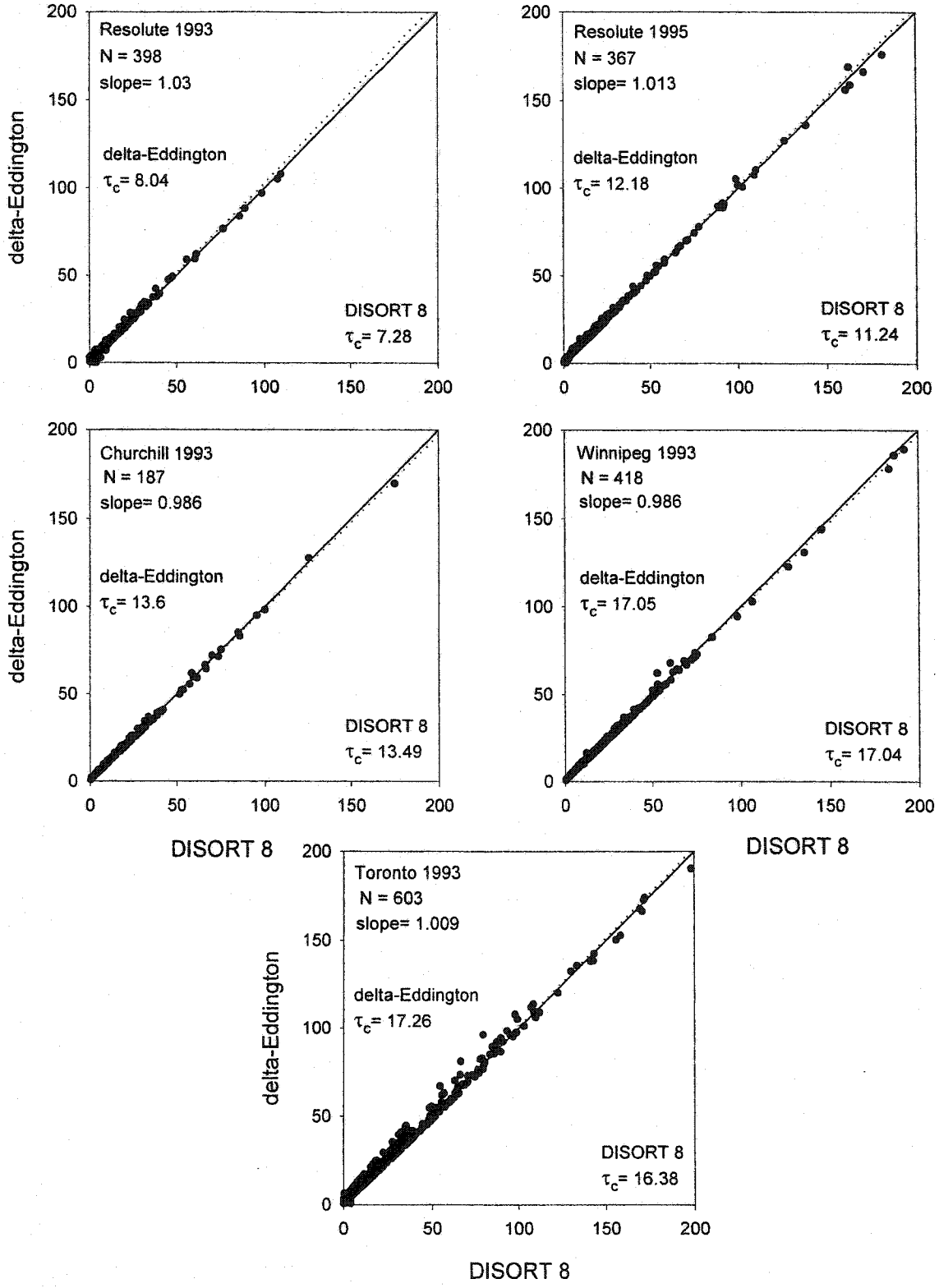

Figure 3.6. Correlation between cloud optical depths calculated by delta-Eddington and Disort 8 models for Resolute Bay, Churchill, Winnipeg, and Toronto. N is the number of data points.

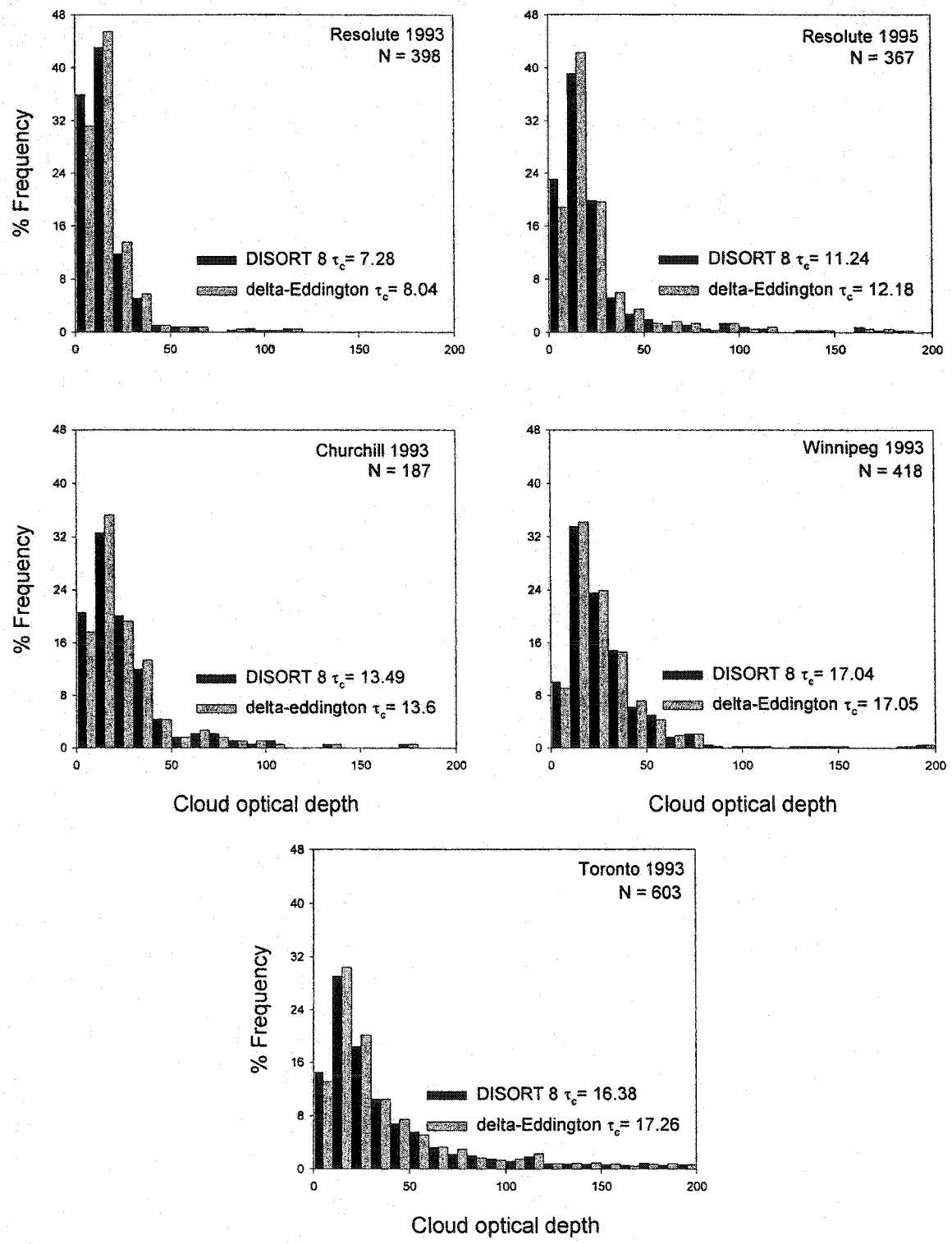

Figure 3.7. Comparison of cloud optical depth calculated by delta-Eddington and DISORT 8 models at Resolute Bay, Churchill, Winnipeg, and Toronto. N is the number of data points.

Table 3.4. Characteristics of the inferred cloud optical depth for the nine Canadian datasets. N is the number of data points.

Station	Year	Aerosol type	Mean and Median cloud optical depth				
			δ -Eddington		DISORT 8		
			Mean	Median	Mean	Median	N
Alert (NWT)	1995	Rural+50km	7.88	4.98			224
Resolute (NWT)	1993	Rural+50km	11.9	8.04	11.43	7.28	398
	1994		12.77	8.76			371
	1995		22.68	12.18	21.99	11.24	367
	1996		15.63	7.79			361
	Station		17.04	10.18			1497
Churchill (Man.)	1993	Rural+50km	21.85	13.6	21.9	13.49	187
	1994		54.07	18.26			234
	1995		35.39	14.07			228
	1996		20.15	11.8			585
	Station		31.38	14.99			1234
Edmonton (Alta.)	1993	Rural+50km	25.34	17.28			120
	1994		29.09	21.91			138
	1995		39.54	24.52			159
	1996		23.93	16.9			245
	Station		29.62	19.62			662
Regina (Sask.)	1994	Rural+50km	29.23	17.22			245
	1995		38.46	17.49			134
	Station		32.48	17.4			379
Winnipeg (Man.)	1993	Rural+50km	24.8	17.05	24.85	17.04	420
Montreal (Que.)	1993	Urban+50km	37.74	21.89			281
	1994		39.89	20.77			231
	Station		38.71	20.84			512
	1993	Urban+36.5km	34.46	17.23			220
	1994		32.59	19.98			265
Halifax (NS)	1993	Rural+50km	30.81	19.42			623
	1994		25.93	17.03			672
	1995		25.65	16.55			751
	1996		21.53	14.82			823
	Station		25.65	16.6			2869
Toronto (Ont.)	1993	Urban+50km	31.65	17.26	30.29	16.38	603
	1994		35.11	22.95			919
	1995		38.47	20.95			716
	1996		42.84	27.69			1103
	Station		37.76	22.98			3341
	1993	Urban+36.5km	26.69	14.07			590
	1995		33.93	17.19			705

as being the heaviest aerosol loading places in Canada to find the effect of aerosol on τ_c (Table 3.4) and then on the fluxes in Chapter 4. The selection was made after Davies *et al.* (2000) who found, for cloudless skies, that best results were obtained at different times with either a 23 km visibility urban atmosphere or the average for a 23 km and 50 km visibilities atmosphere. However, rural aerosol with 50 km visibility was used for all other stations. Aerosol for 50 km visibility was selected for the whole year (spring-summer and fall-winter) in the troposphere and background and normal aerosols were selected for the stratosphere and upper atmosphere layers respectively (Table 2.2).

Since cloud optical depth was calculated from surface irradiance measurements, which have been attenuated by aerosol, aerosol optical depth within the 2-3 km layer is implicitly included within the cloud optical depths. However, this aerosol contribution ($\tau_{a_\lambda} < 0.5$) is a very small part of the total optical depth (Davies *et al.*, 2000).

The frequency distributions of cloud optical depth for the nine stations using 50 km visibility aerosol are presented in Figure 3.8. All distributions are strongly positively skewed with maximum frequencies between 10 and 20. The shapes are similar to those shown in the studies of Leontyeva and Stamnes (1994), Curtis (1996) and Barker *et al.* (1998), but are very unlike the distribution presented by Leontieva *et al.*, (1994) for the whole spectrum at Bergen, Norway. Thus, the median was adopted as the best measure of central tendency. Arctic stations show smaller spread and stronger mode. Clouds at Alert are optically thinner than those at all other stations with a maximum frequency of 50% occurring at $\tau_c \leq 10$. At Resolute, 45% of the cases occur at $\tau_c \leq 20$. At southern locations distributions become wider with more optically thick clouds. High percentages

of completely overcast conditions at the arctic stations are in keeping with the frequent occurrence of thin low clouds and fog. Figures A1, A2, A3, A4, A5, and A6 (Appendix A) show yearly frequency distributions of τ_c for seven stations. The general patterns of the histograms are consistent with that for the two and four years period (Figure 3.8) but with little yearly variation.

Barker *et al.* (1998) found that the observed distributions of hourly overcast τ_c across Canada followed the gamma distribution, which is defined by

$$P_{\Gamma}(\tau_c) = \frac{1}{\Gamma(\nu)}\left(\frac{\nu}{\overline{\tau}_c}\right)^{\nu} {\tau_c}^{\nu-1} e^{-\nu\tau_c/\overline{\tau}_c}; \quad \{\tau_c > 0; \nu > 0\}, \tag{3.8}$$

where $\Gamma(\nu)$ is the gamma function and ν is the variance-related parameter and is determined either by the method of moments (mom) $\nu_{mom} = (\overline{\tau}_c/\sigma)^2$, or the maximum likelihood estimation (mle) $\psi(\nu_{mle}) + \ln(\overline{\tau}_c/\nu_{mle}) - \overline{\ln \tau_c} = 0$, where $\overline{\tau}_c$ and σ are the mean and standard deviation of τ_c and $\psi(\nu) = \frac{d}{d\nu}\ln\Gamma(\nu)$. $\overline{\tau}_c$ as well as ν values (Table 3.5) are computed using only τ_c values less than 150 for each station to avoid extreme values of τ_c that affect the mean (H. W. Barker, private communication, 2000). Also the average transmittance for all sun angles at $\tau_c = 150$ is equal to 0.05 and a further increase in τ_c has no effect on surface fluxes (Figure 3.9) Figure 3.10 shows the gamma distributions. Both methods provide an excellent fit to the observed histograms. The best fits of these two methods to the observations are at Toronto and Montreal and the worst are at Resolute and Churchill. This is because for sites with large $\overline{\tau}_c$ values, the

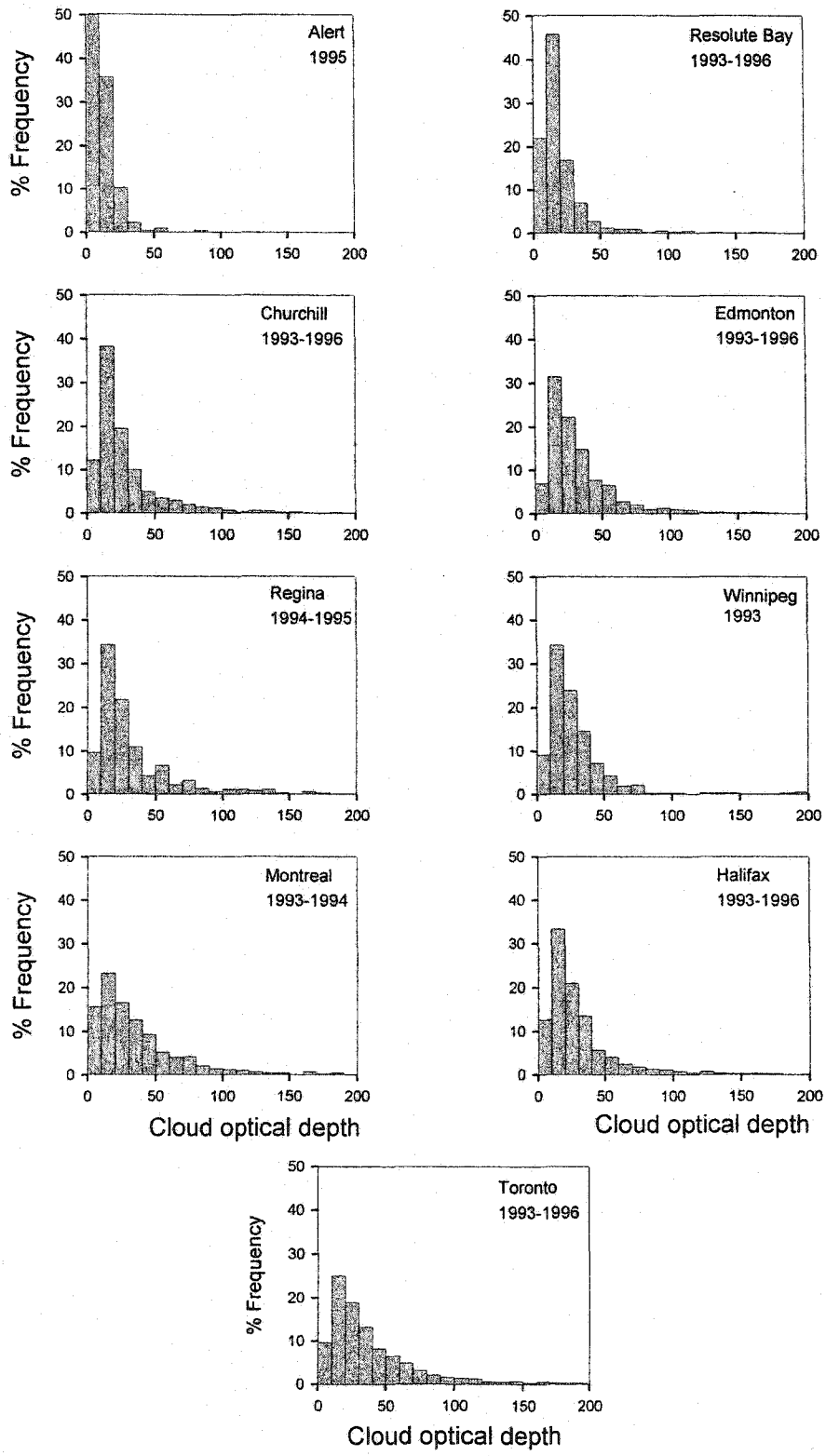

Figure 3.8. Frequency distributions of cloud optical depths calculated by delta-Eddington at Alert, Resolute, Churchill, Edmonton, Regina, Winnipeg, Montreal, Halifax and Toronto.

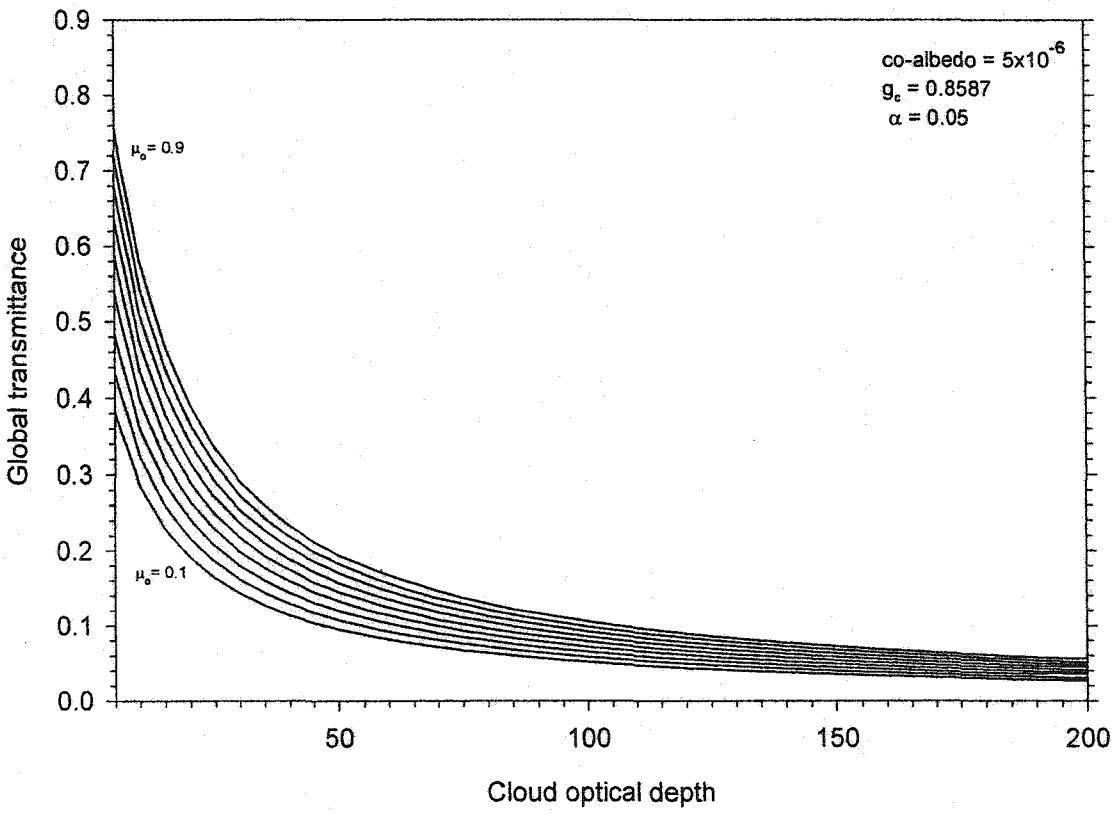

Figure 3.9. The sensitivity of global (direct +diffuse) transmittance calculated by delta-Eddington to cloud optical depth and cosine of the sun angle (μ_0). g_c is the cloud asymmetry factor and α is the surface albedo.

slopes of the lines are less steep and the differences between ν_{mom} and ν_{mle} are actually small (Table 3.5).

Halifax and Toronto are the only stations with enough observations to show any seasonal variations in τ_c. In general, arctic and subarctic stations only have observations from May to October and midlatitude stations have few observations from December to March. Figure 3.11 shows monthly median values of τ_c and number of days included in each month. Although there is some seasonal variability at Toronto there is little at Halifax. Toronto has optically thinner overcast conditions in the winter and maximum τ_c values occur in October and April. Clouds are optically thick in summer months due to warmer conditions, which lead to large evaporation and to more water in the atmosphere forming more stratocumulus clouds.

3.3.3 Cloud type

Although cloud optical depth is expected to vary with cloud type (Stamnes *et al.*, 1991), there have been few studies on this. Table 3.6 contains median τ_c values for low cloud types, incorporating only data with more than 30 observations. Values are quite similar and do not indicate clear differences in τ_c between cloud types.

3.3.4 Cloud height

Min and Harrison (1996) positioned the cloud layer in a radiative transfer model at different heights from 1-2 km to 5-6 km to see the effect of cloud altitude in the inferred τ_c. They found no significant effect. Here, this is further examined by placing

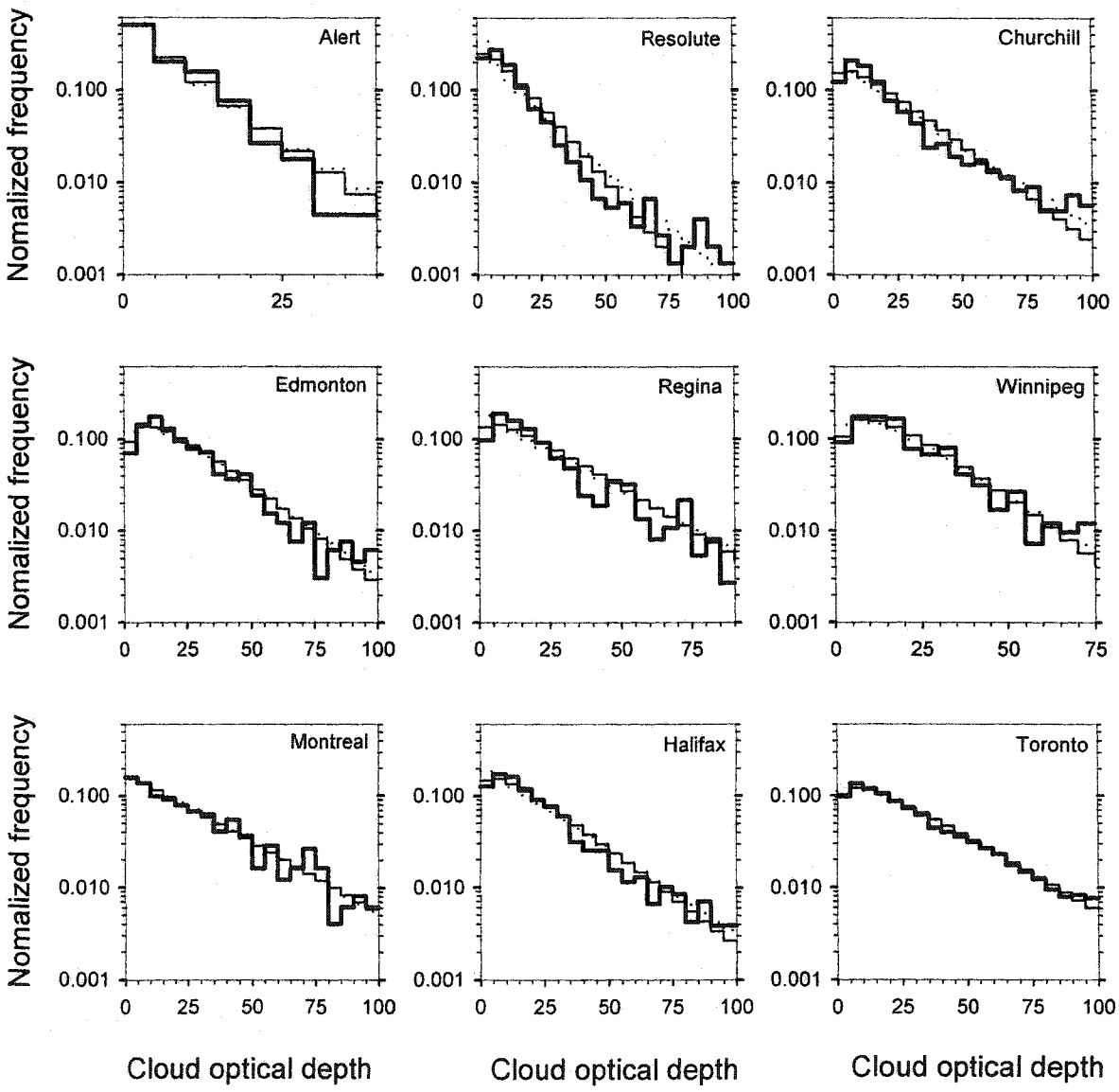

Figure 3.10. Normalized frequency distributions of observed cloud optical depths for the nine stations (thick line) and Gamma function fits based on the method of moments (dotted line) and maximum likelihood method (thin line).

Table 3.5. Mean cloud optical depths ($\overline{\tau}_c$) and variance-related parameters determined by the method of moments (ν_{mom}) and maximum likelihood estimate (ν_{mle}). The value N is the number of overcast cloud optical depth observations for each station.

Station	$\overline{\tau}_c$	ν_{mle}	ν_{mom}	N
Alert (NWT)	7.88	0.81	0.71	224
Resolute Bay (NWT)	15.13	1.19	0.78	1487
Churchill (Man.)	23.26	1.23	0.9	1234
Edmonton (Alta.)	26.42	1.53	1.31	655
Regina (Sask.)	26.19	1.22	0.97	370
Winnipeg (Man.)	22.19	1.64	1.35	413
Montreal (Que.)	28.76	1.04	1.12	493
Halifax (NS)	23.67	1.23	1.01	2838
Toronto (Ont.)	30.83	1.28	1.22	3254

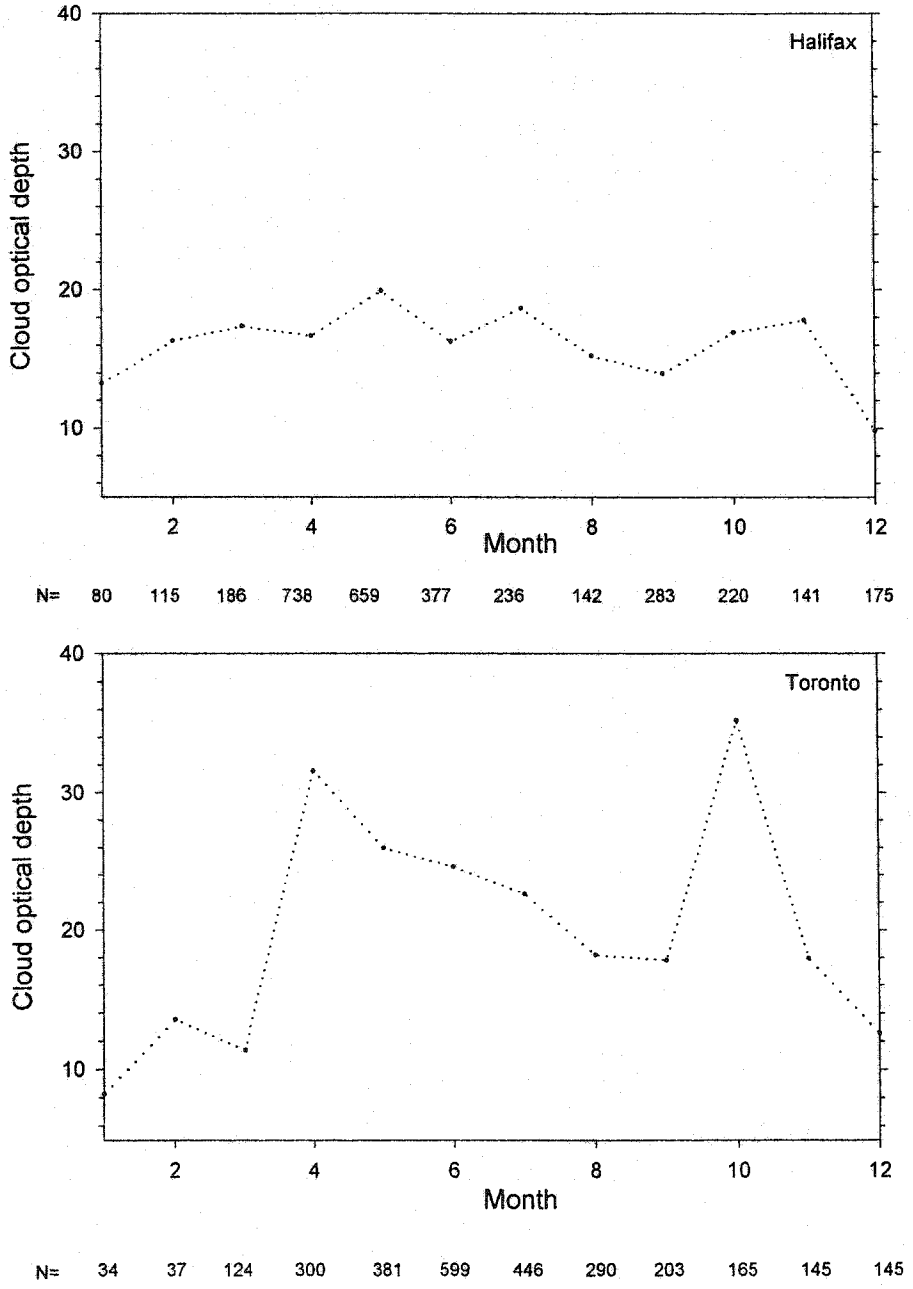

Figure 3.11. Annual monthly median values of cloud optical depth at Halifax and Toronto during 1993-1996. N is the number of data points.

the cloud layer at five different heights (between 1-2 km, 2-3 km, 4-5 km, 5-6 km and 6-7 km). Table 3.7 shows that median τ_c values decrease slightly with increasing cloud height but overall differences are slight. Thus, positioning cloud in the 2-3 km layer will not introduce significant systematic error in retrieving τ_c. Median τ_c values (Table 3.4) will be used to calculate irradiances because there is no variation with cloud type, height and season.

3.3.5 Sensitivity analyses

3.3.5.1 Sensitivity to cloud optical depth

The influence of τ_c on direct and diffuse transmitted broadband irradiances from both the delta-Eddington and DISORT models is shown in Figure 3.12. This shows model calculations of transmitted irradiance through a single layer of variable optical depth irradiated from above solely by direct beam radiation of quantity τ_c. Both models show that the direct beam irradiance at the surface becomes smaller with increasing τ_c. It also shows that when τ_c is greater than 3 or 10 for the DISORT and delta-Eddington models, respectively, the direct beam drops to virtually zero and the surface irradiance is diffuse. Also, there is no further increase in surface diffuse component beyond this point at any wavelength and sun angle (Bodeker and McKenzie, 1996). There are also discrepancies in the direct and diffuse components between the two models at smaller τ_c and higher sun angles. This is because the delta-Eddington model uses the scaled optical depth in calculating the direct beam, which makes the direct irradiance larger than the

Table 3.6. Median cloud optical depths for different cloud types, values in the brackets indicate number of observations.

Station	Cloud type			
	Stratus Fractus	Stratocumulus	Stratus	Fog
Resolute Bay	11.1 (77)	8.8 (126)		12.7 (178)
Churchill	16.1 (104)	11.5 (118)	10 (65)	14.7 (135)
Regina	17.4 (37)	11.7 (63)		
Winnipeg		19.7 (69)		
Montreal		19.4 (68)		
Halifax	20.4 (274)	11.6 (208)	15.2 (62)	14.7 (332)
Toronto		18.5 (251)		

Table 3.7. Median cloud optical depths calculated by delta-Eddington model for different cloud heights.

Station and year	Cloud height				
	1-2 km	2-3 km	4-5 km	5-6 km	6-7 km
Edmonton 1993	17.91	17.28	16.41	16.3	16.16
Winnipeg 1993	17.77	17.05	16.03	15.81	15.52
Montreal 1993	22.59	21.89	21.2	20.73	20.67
Toronto 1993	17.95	17.26	16.62	16.52	16.48

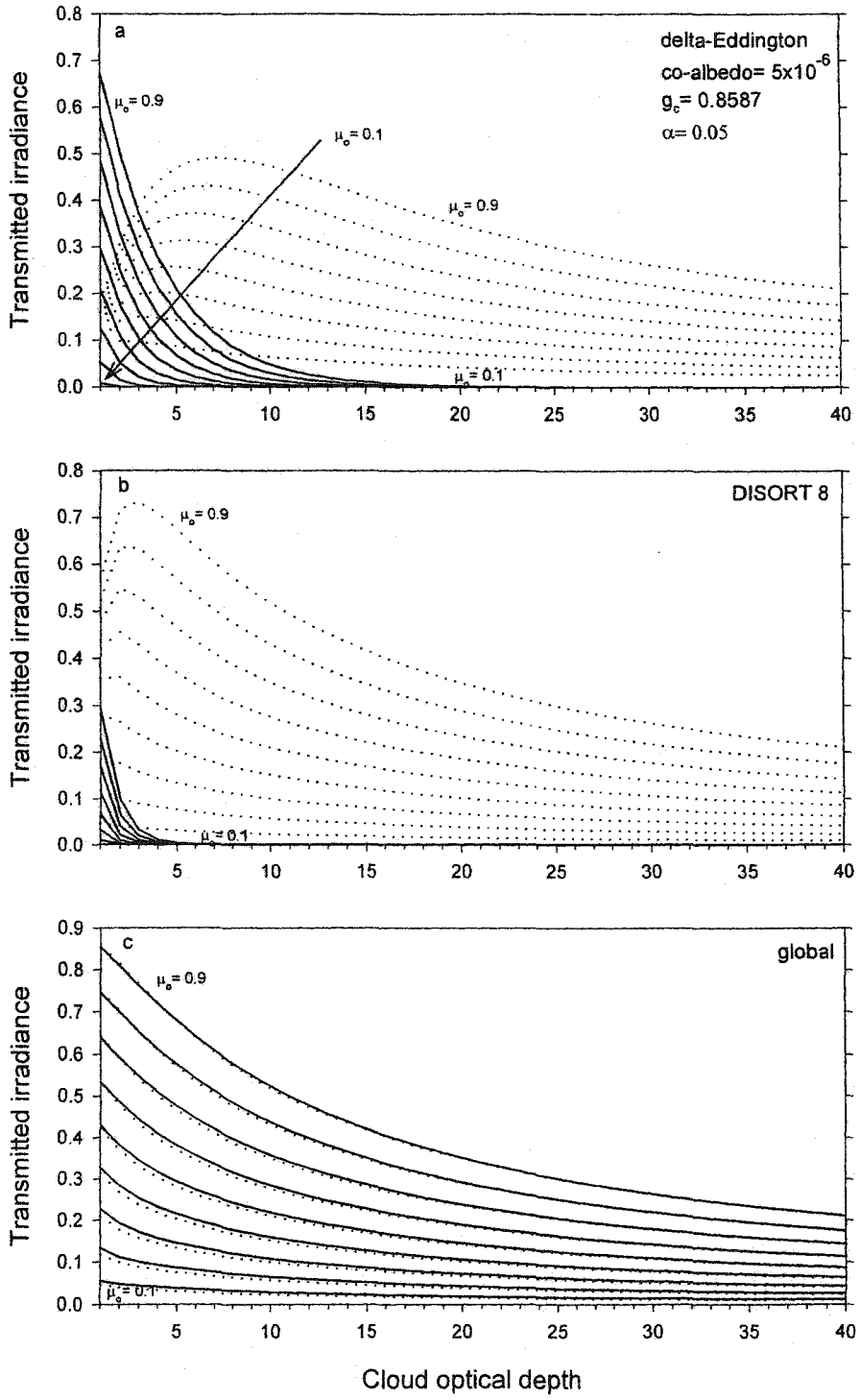

Figure 3.12. The variation of direct beam (solid line) and diffuse (dotted line) transmitted irradiance with cloud optical depth and cosine of the sun angle (μ_0). (a) calculated by delta-Eddington and (b) by DISORT 8. Figure c shows the global (direct+diffuse) transmitted irradiance calculated by delta-Eddington (solid line) and DISORT 8 (dotted line). g_c is the cloud asymmetry factor and α is the surface albedo.

actual direct irradiance (Joseph *et al.*, 1976). Also the direct beam includes diffuse radiation that travels in the same direction as the direct beam resulting in overestimation of the direct beam and underestimation of diffuse irradiance. This is evidently not a problem in the calculation of global fluxes. To confirm this, the globally (direct + diffuse) transmitted irradiance is plotted against τ_c in Figure 3.12c and shows that the delta-Eddington values compare well with that of DISORT at low τ_c and higher sun angles. Thus, the delta-Eddington model is accurate when calculating the global fluxes anywhere, although it overestimates by an average of 6%.

The variation of the transmitted diffuse irradiance with τ_c calculated by both delta-Eddington and DISORT models is presented in Figure 3.13 (Davies *et al.*, 2000). The disagreement between the two models for $\mu_o \geq 0.6$ and when $\tau_c < 10$ is apparent. However, both models show that transmitted irradiance changes little with τ_c for larger solar zenith angles. Therefore, the above comparisons suggest that the delta-Eddington model is not suitable for calculating direct and diffuse components separately but is suitable for calculating diffuse irradiances for cloudy conditions for two cases only at northern latitudes where solar zenith angles are large and at southern Canada where τ_c values are always greater than 10.

3.3.5.2 Sensitivity to equivalent radius

The sensitivity of total irradiance and cloud optical depth to different equivalent radii and sun angles is shown in Figure 3.14. For smaller droplet sizes $r_e = 7\mu m$ the

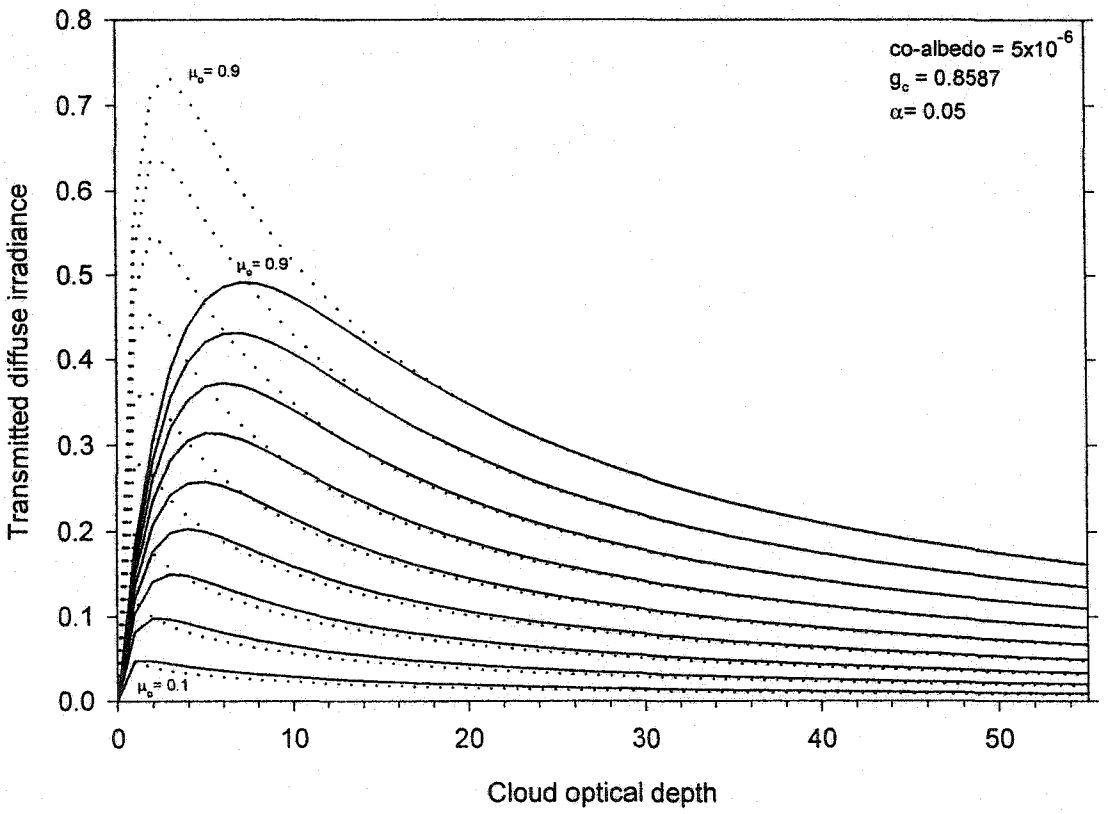

Figure 3.13. The sensitivity of diffuse UV-B irradiance calculated by delta-Eddington (solid line) and DISORT 8 (dotted line) to cloud optical depth and cosine of the sun angle (μ_0). g_c is the cloud asymmetry factor and α is the surface albedo.

transmitted flux increases with the larger values of ω_c and g_c and τ_c is about 10% smaller than that for $r_e = 10\mu m$. Leontieva *et al.* (1994) found that the variations in r_e from $5\mu m$ to $15\mu m$ can produce an uncertainty of about 15% in retrieved τ_c for the whole solar irradiance. r_e has varying impact on irradiances. Rawlins and Foot (1990) stated that increasing the value of r_e results in greater forward scattering by the cloud layer and an increase in transmitted irradiance. This is true only for low surface albedo but for larger albedo ≥ 0.8 the transmitted irradiance at the surface is larger with smaller r_e (Leontyeva and Stamnes, 1994). However, this study shows that the total UV-B transmitted irradiance is always larger with smaller r_e for both cases of low ($\alpha = 0.05$) and high ($\alpha = 0.75$) albedos (Figure 3.14). The effect of surface albedo is more obvious in Figure 3.15 where transmitted diffuse irradiance is shown for one sun angle and two different r_e values. Multiple reflections between the snow surface (i.e., α = 0.75) and cloud base can double the surface radiation.

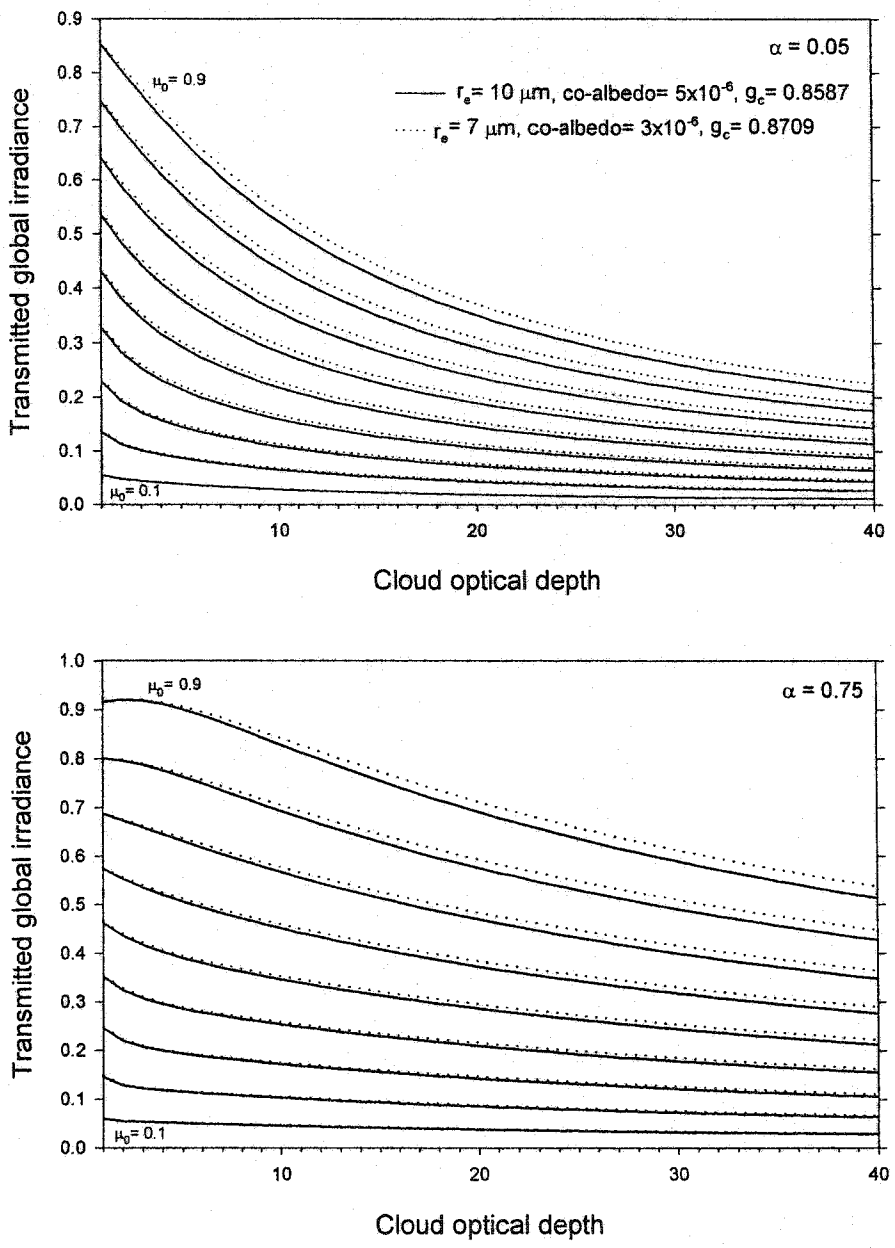

Figure 3.14. The sensitivity of global trasmitted UV-B irradiance to cloud optical depth for different equivalent radii (r_e), sun angle cosines (μ_o) and surface albedos (α), calculated by the delta-Eddington algorithm. g_c is the cloud asymmetry factor.

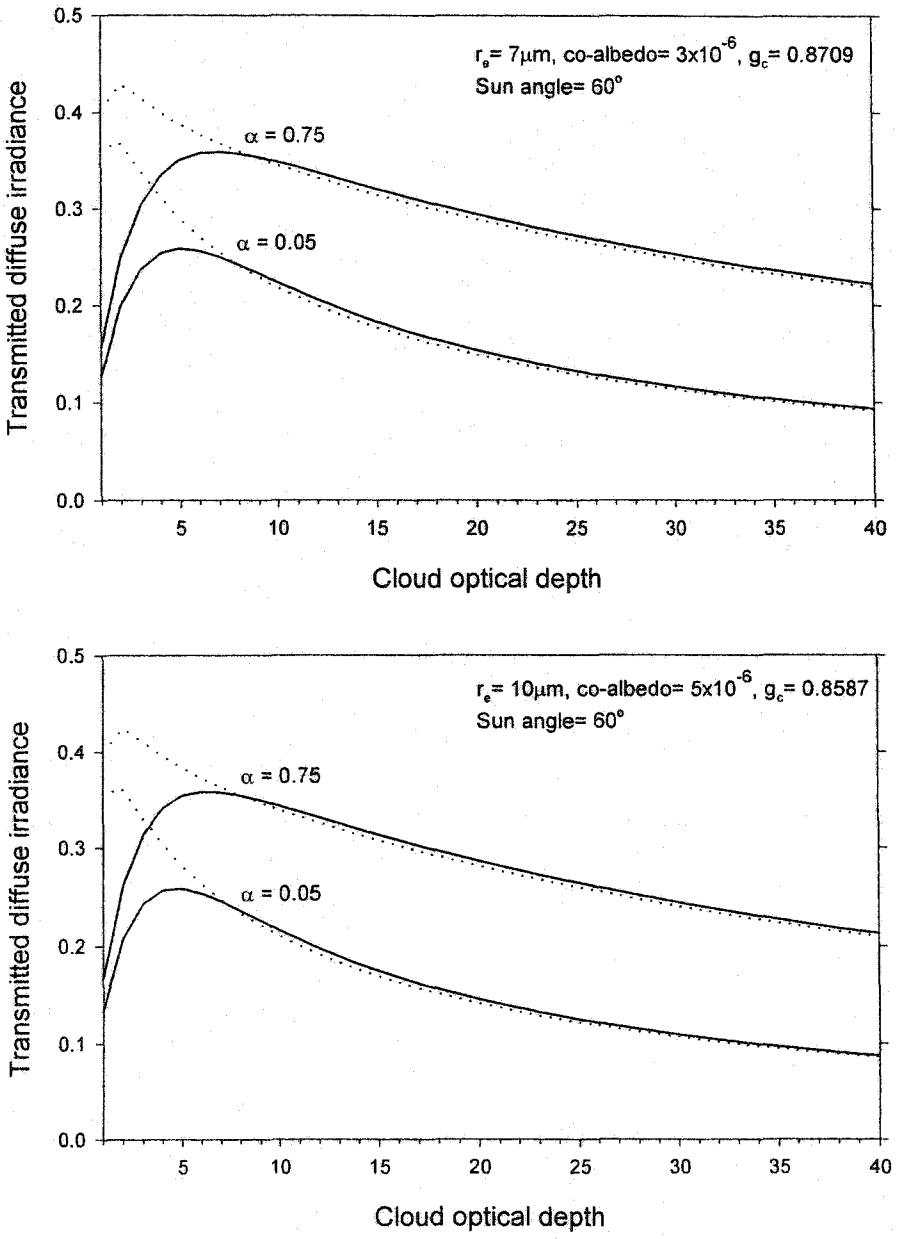

Figure 3.15. The sensitivity of diffuse transmitted irradiance to cloud optical depth at various surface albedos (α) and equivalent radii (r_e), computed by delta-Eddington (solid line) and DISORT (dotted line) methods. g_c is the cloud asymmetry factor.

CHAPTER 4

Validation of model irradiances

4.1 Introduction

This chapter assesses the model's performance in calculating spectral and broadband irradiances using the extraterrestrial solar spectrum, the calculated optical parameters as described in Chapter 2, and the broadband cloud optical depths given in Chapter 3. Although the results in Chapter 3 showed that the DISORT 8 and delta-Eddington algorithms yielded very similar cloud optical depths for all stations in the study it is also important to examine how well irradiances from the two methods compare since the delta-Eddington method is an approximate solution of the radiative transfer equation whereas the DISORT 8 method is close to an exact solution.

4.2 Performance measures

Model performance is assessed using the mean bias error (MBE), which measures systematic error, and the root mean square error (RMSE), which includes both systematic and non-systematic error (Hay and Wardle, 1982). When MBE is small the RMSE measures mainly the non-systematic error. If d_i is the difference between calculated and measured irradiances (daily or monthly), MBE and RMSE are defined from the variance

of d

$$\sigma_d^2 = \frac{\sum d_i^2}{N} - \left(\frac{\sum d_i}{N} \right)^2 = (RMSE)^2 - (MBE)^2, \qquad (4.1)$$

where N is the number of data points. Both measures are calculated for spectral and broadband irradiances for both daily totals and monthly averages. Irradiances are in $J\ m^{-2} day^{-1} nm^{-1}$ for spectral irradiance and in $kJ\ m^{-2} day^{-1}$ for broadband values. The performance measures are given both in these radiation units and also as percentages of the mean measured irradiance for the relevant period. RMSE is also shown for different averaging periods. This is useful since it indicates the length of averaging period that is needed to obtain a desired level of accuracy. This is not necessary for the MBE because it does not vary with averaging period.

The main source of random error stems from the cloud cover data. Since cloud cover is only reported once an hour, cloudiness variations between hours are missed. Linear interpolation of cloud cover for the Brewer instrument's measurement time only improves the validity of cloud estimates if the real variation of cloudiness between hourly observations is linear. Intuitively, errors arising from interpolation are expected to be random although initial errors in observer cloud estimates are probably systematic since observers tend to overestimate cloud cover because the earth curvature leads to an impression of greater cloudiness toward the horizon in non-overcast sky conditions (Hughes, 1984).

4.3 Comparisons of irradiances from the delta-Eddington and DISORT methods

Delta-Eddington values are compared with DISORT 8 values of spectral and broadband irradiances for both daily totals and monthly averages for all sky conditions using annual values of cloud optical depth for each station (Table 3.4).

Seven wavelengths (295, 300, 305, 310, 315, 320 and 325 nm) were selected to demonstrate model spectral performance for one arctic (Resolute in 1993 and 1995), one sub-arctic (Churchill in 1993) and two mid-latitudes (Winnipeg in 1993 and Toronto in 1993) stations. Figures 4.1 shows spectral performance for two distinctive wavelengths (295 nm and 305 nm). Five other wavelengths are shown in Appendix B. The spectral irradiances in Resolute are much smaller than the other stations; this is a consequence of greater cloudiness and larger solar zenith angles.

MBE, RMSE statistics and slope (the ratio of two means of calculated irradiances, which is the slope of the regression line constrained to pass through the origin) are presented in Table 4.1. In general the relative MBE shows that the delta-Eddington method values are systematically larger than DISORT's values with the exception of Resolute at 295 nm. The delta-Eddington estimates are larger by 2-11% (mostly between 3-7%) and relative RMSE values are mainly within 5-11% of the mean measured daily value. These differences are, however, within the uncertainty of the Brewer instrument ($\sim \pm 10\%$) and are much smaller than the differences between irradiances measured with various instruments (Gardiner *et al.*, 1993; McKenzie *et al.*, 1993; Seckmeyer *et al.*, 1994; Wang and Lenoble, 1994; Bais *et al.*, 2001).

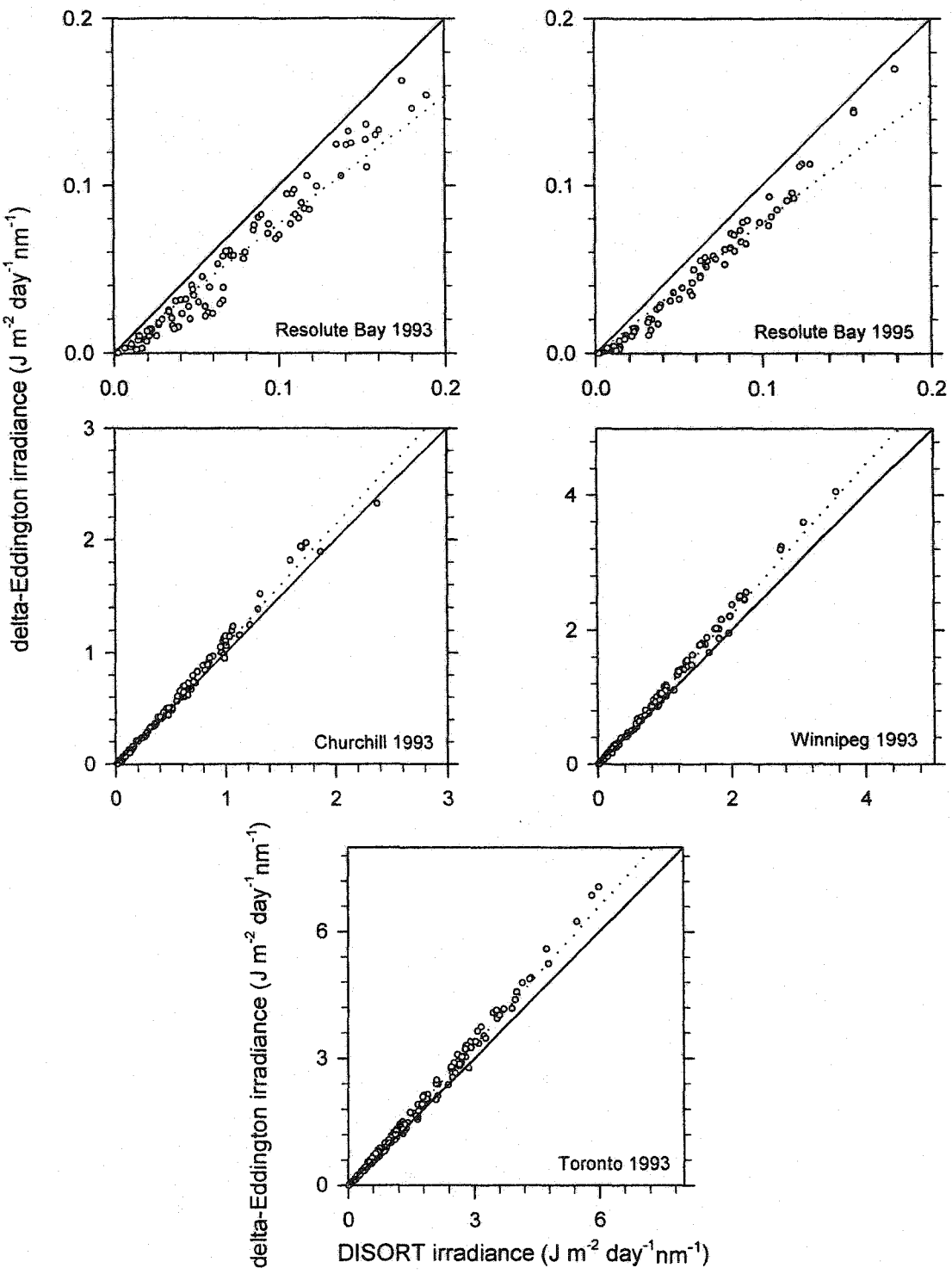

Figure 4.1a. Comparison of DISORT and delta-Eddington daily total spectral irradiances calculated using annual values of cloud optical depth for each station (Table 3.4) for 295 nm. The dotted lines represent linear regressions constrained to pass through the origin.

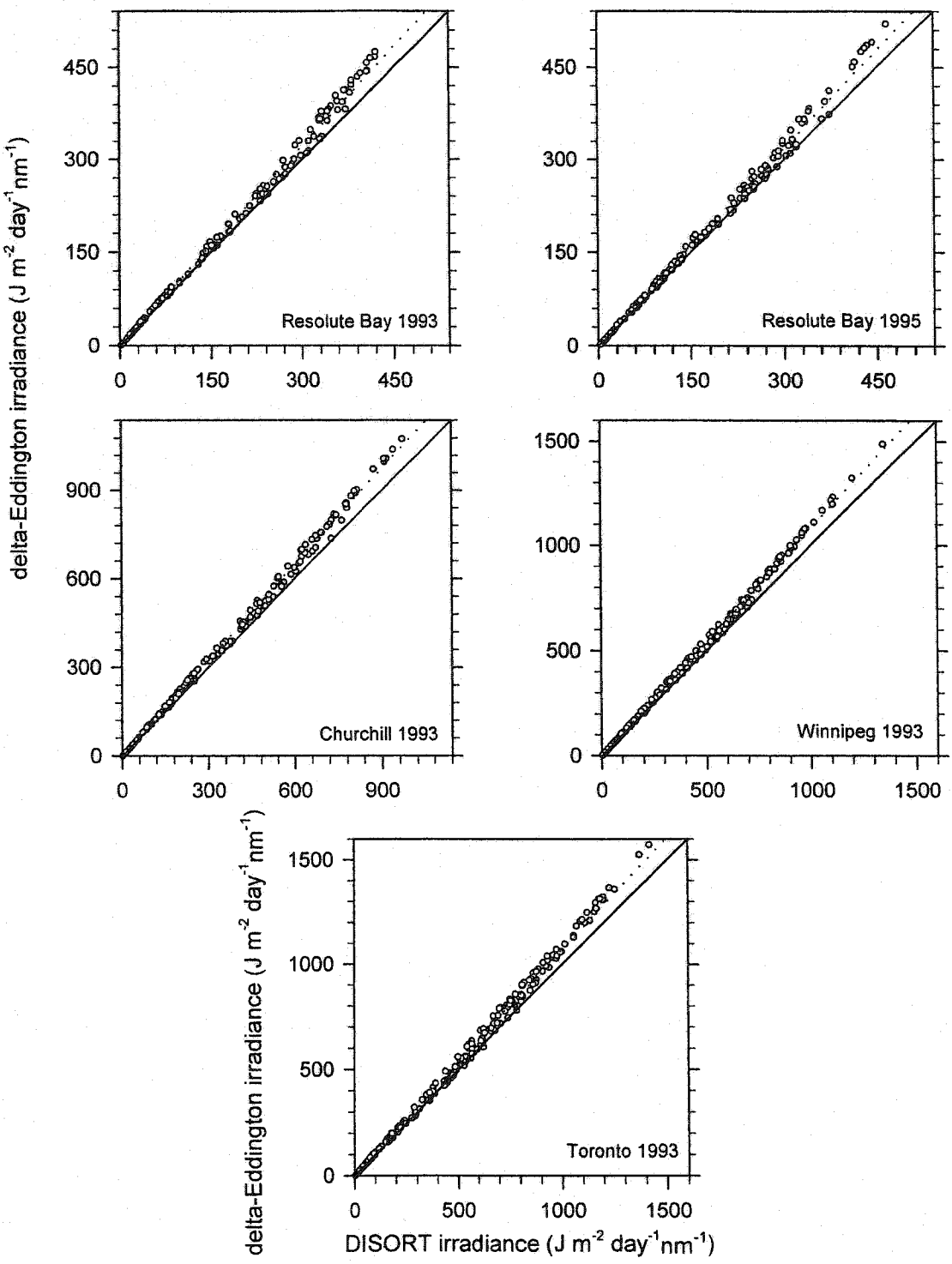

Figure 4.1b. same as Figure 4.1a but for 305 nm.

Table 4.1. Comparison of daily spectral irradiances from the delta-Eddington and DISORT 8 methods for the period indicated for each station. N is the number of data points and $\bar{M}$ is the mean annual daily spectral irradiance calculated by DISORT ($J\ m^{-2}day^{-1}nm^{-1}$). Values of MBE and RMSE are given both in $J\ m^{-2}day^{-1}nm^{-1}$ and in percentages (italic) of $\bar{M}$. Positive MBE values indicate delta-Eddington overestimation.

Wavelength	Resolute Bay 1993	Resolute Bay 1995	Churchill 1993	Winnipeg 1993	Toronto 1993
295 nm					
N	89	80	136	136	192
$\bar{M}$	0.07	0.06	0.46	0.83	1.37
MBE	- 0.02	- 0.01	0.03	0.09	0.13
%MBE	*- 23.00*	*- 22.50*	*6.54*	*10.96*	*9.88*
RMSE	0.02	0.02	0.07	0.16	0.26
%RMSE	*26.91*	*25.87*	*14.64*	*19.35*	*19.15*
Slope	0.770	0.774	1.066	1.109	1.099
300 nm					
N	141	154	178	228	250
$\bar{M}$	6.63	5.89	21.88	26.03	39.86
MBE	0.26	0.12	1.84	2.75	3.73
%MBE	*3.95*	*1.96*	*8.41*	*10.56*	*9.36*
RMSE	0.77	0.61	3.08	4.71	6.46
%RMSE	*11.55*	*10.35*	*14.09*	*18.11*	*16.20*
Slope	1.039	1.020	1.084	1.106	1.094
305 nm					
$\bar{M}$	180.45	167.91	347.49	370.41	474.93
MBE	13.36	10.14	28.73	30.06	33.28
%MBE	*7.40*	*6.04*	*8.27*	*8.12*	*7.01*
RMSE	20.04	16.39	38.98	43.84	51.56
%RMSE	*11.11*	*9.76*	*11.22*	*11.84*	*10.86*
Slope	1.074	1.060	1.083	1.081	1.070

Table 4.1 (Contd).

Wavelength	Resolute Bay 1993	Resolute Bay 1995	Churchill 1993	Winnipeg 1993	Toronto 1993
310 nm					
$\bar{M}$	655.41	641.52	932.35	928.91	1071.97
MBE	48.05	38.03	66.36	64.39	66.35
%MBE	*7.33*	*5.93*	*7.12*	*6.93*	*6.19*
RMSE	61.80	51.34	82.03	85.58	94.73
%RMSE	*9.43*	*8.00*	*8.80*	*9.21*	*8.84*
Slope	1.073	1.059	1.071	1.069	1.062
315 nm					
$\bar{M}$	2463.48	2488.15	2929.36	2786.79	3051.05
MBE	135.87	101.07	178.86	139.80	141.32
%MBE	*5.52*	*4.06*	*6.11*	*5.02*	*4.63*
RMSE	169.97	135.04	211.98	181.17	201.52
%RMSE	*6.90*	*5.43*	*7.24*	*6.50*	*6.61*
Slope	1.055	1.041	1.061	1.050	1.046
320 nm					
$\bar{M}$	4015.38	4102.07	4431.48	4124.11	4442.47
MBE	204.32	149.48	246.88	192.13	196.63
%MBE	*5.09*	*3.64*	*5.57*	*4.66*	*4.43*
RMSE	250.73	195.05	287.73	243.91	273.40
%RMSE	*6.24*	*4.75*	*6.49*	*5.91*	*6.15*
Slope	1.051	1.036	1.056	1.047	1.044
325 nm					
$\bar{M}$	5220.08	5381.33	5409.77	4932.72	5263.36
MBE	258.20	191.75	278.24	228.40	237.35
%MBE	*4.95*	*3.65*	*5.14*	*4.63*	*4.51*
RMSE	309.51	240.28	319.43	283.20	318.19
%RMSE	*5.93*	*4.47*	*5.90*	*5.74*	*6.05*
Slope	1.049	1.036	1.051	1.046	1.045

Although systematic overestimation by the delta-Eddington method was not reported in the original study of Joseph *et al.* (1976) it became apparent in the numerical experiments by Forster and Shine (1995). Here, their analysis has been repeated. UV-B irradiances were calculated for June 24, 1993 at Toronto using the actual atmosphere calculations but for three simulated cloudiness states: cloudless, overcast and 50% cloud cover. Results are summarized in Figures 4.2 and 4.3.

Figure 4.2 shows ratios of spectral UV-B irradiances calculated by both the delta-Eddington and DISORT (using 4 and 8 streams) methods to irradiances calculated by a 16-stream DISORT method for a solar zenith angle of 64.4°, as used by Forster and Shine (1995). The DISORT ratios are close to one at wavelengths greater than 300 nm for all the three cloud cases. Below 300 nm DISORT 4 values decrease rapidly. This decrease is not apparent for DISORT 8. The delta-Eddington model agrees to within 1% with DISORT 4 and 8 for the overcast case at wavelengths greater than 303 nm but the error increases to 12% and 17% for the 50% cloudy and clear sky cases, respectively, at 305 nm. Also delta-Eddington values fall off sharply for wavelengths below 303 nm (overcast) or 300 nm (cloudless) like the DISORT 4 values although at longer wavelengths.

Figure 4.3 compares the delta-Eddington and DISORT 8 irradiances at six solar zenith angles, for simulated clear and overcast skies. The delta-Eddington values generally overestimate spectral irradiances in the clear sky case model (Figure 4.3a). Underestimations only occur at wavelengths below 305 nm at larger solar zenith angles. In the overcast case model (Figure 4.3b) delta-Eddington estimates are closer to

DISORT 8 values except at smaller wavelengths at larger solar zenith angles. Also the irradiance decrease increases for larger solar zenith angles and with overcast sky case. For example with a solar zenith angle of 60° and 71°, the delta-Eddington irradiances decrease rapidly at about 295 nm and 300 nm, respectively for the clear sky conditions, whereas for the overcast conditions, it fall off sharply at 297 nm and 301 nm.

The simulation results in Figures 4.2 and 4.3 show clearly that the delta-Eddington method will overestimate spectral irradiances at most wavelengths. For all sky conditions, Figure 4.1 also suggests that the overestimation, as measured by the slope statistics, increases as wavelength decreases. The Resolute results are an exception.

At 295 nm at Resolute the delta-Eddington approximation underestimates UV-B irradiance by 23% and the relative RMSE is increased to 27%. Resolute is more cloudy than other subarctic and midlatitude stations (Figure 3.1). Forster and Shine (1995) found that the delta-Eddington method underestimates the multiple scattering of cloud by up to 14%. The underestimation of irradiances by the delta-Eddington method at Resolute is exacerbated by the rapid decrease in irradiance at the large sun angles encountered at Resolute (Figure 4.3b). This is confirmed by examining cloudy data (total cloud amount $\geq$ 0.8) for one year of Resolute, Winnipeg and Toronto (Figure 4.4). It shows clearly that the delta-Eddington method underestimates irradiances at 295 nm by 34% for Resolute. Figure 4.3 shows that this stems from the larger solar zenith angles at Resolute where the mean zenith angle is about 69°. This is not apparent for the lower latitude stations where sun angles are higher with the mean solar zenith angles being 50° and 59° for Winnipeg and Toronto, respectively.

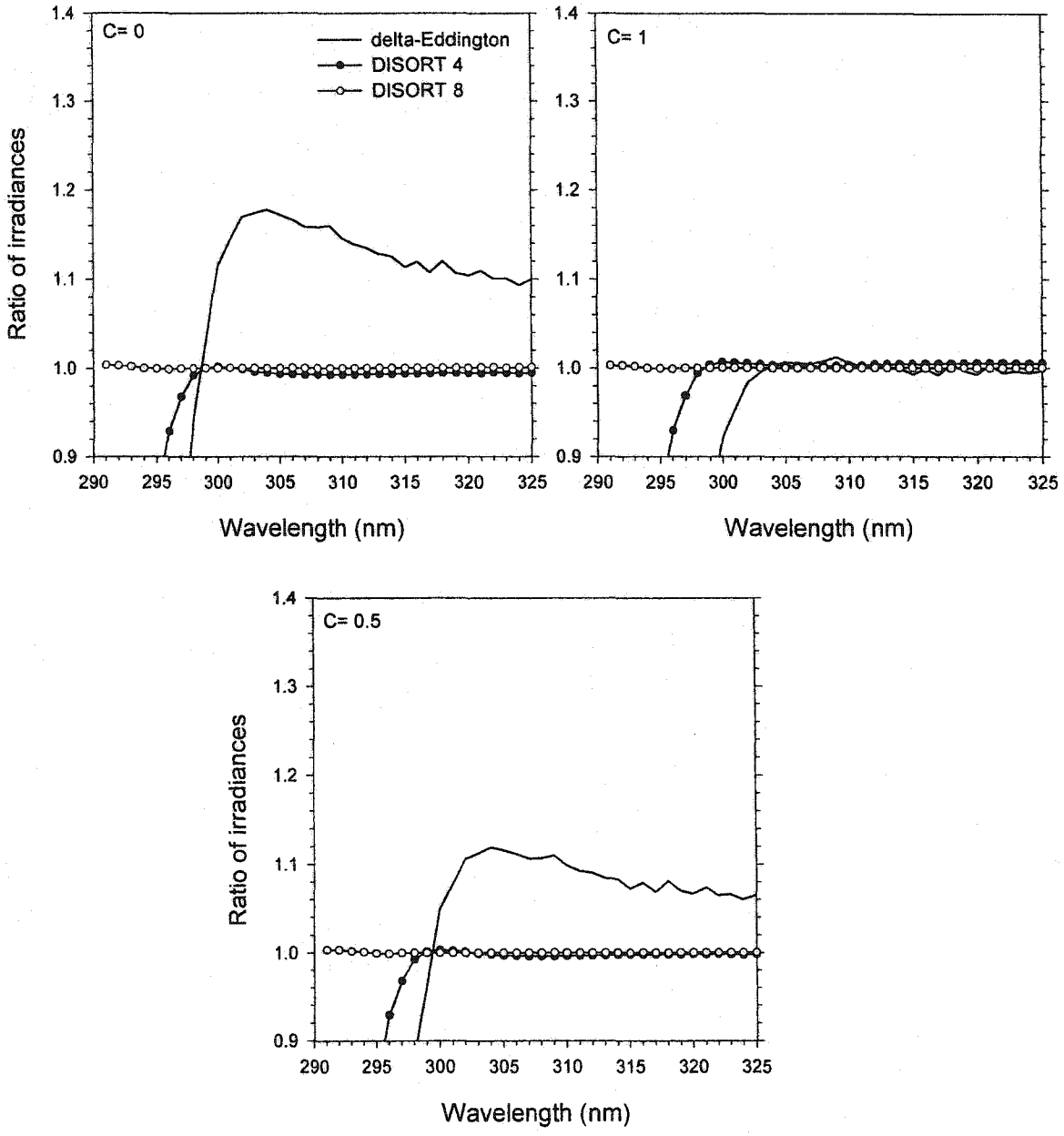

Figure 4.2. Ratio of irradiance calculated by delta-Eddington, DISORT 4 and DISORT 8 methods to that of DISORT 16 method for solar zenith angle of 64.4° for clear (C= 0), 50% clouds (C= 0.5) and overcast (C= 1) sky conditions for Toronto on June 24, 1993 with 302 DU total ozone column and a surface albedo of 0.05.

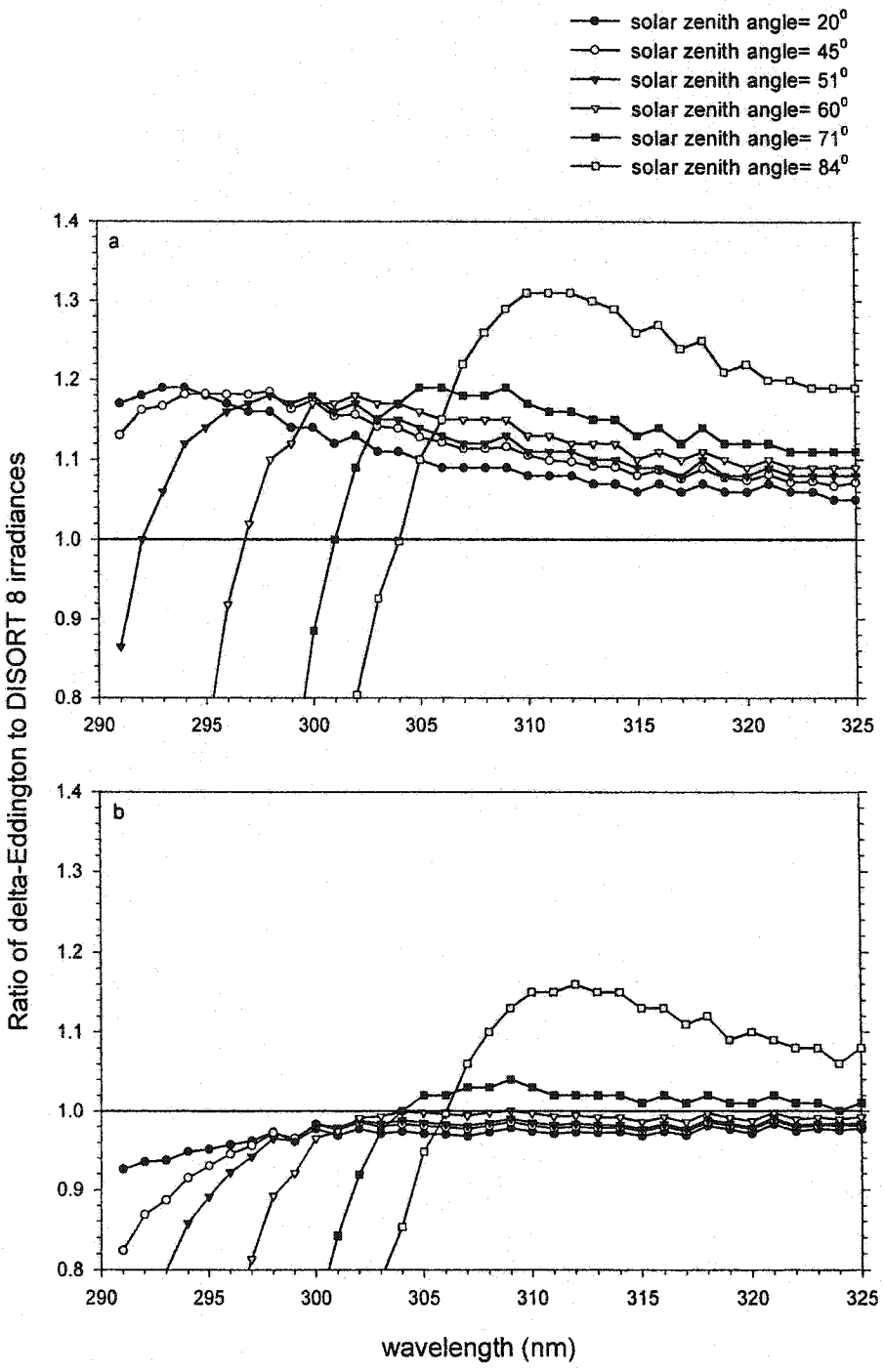

Figure 4.3. Ratio of irradiances calculated by delta-Eddington approximation to DISORT 8 method for clear sky (a) and for overcast sky conditions (b) for different solar zenith angles for Toronto (June 24, 1993) with 302 DU total column ozone and a surface albedo of 0.05.

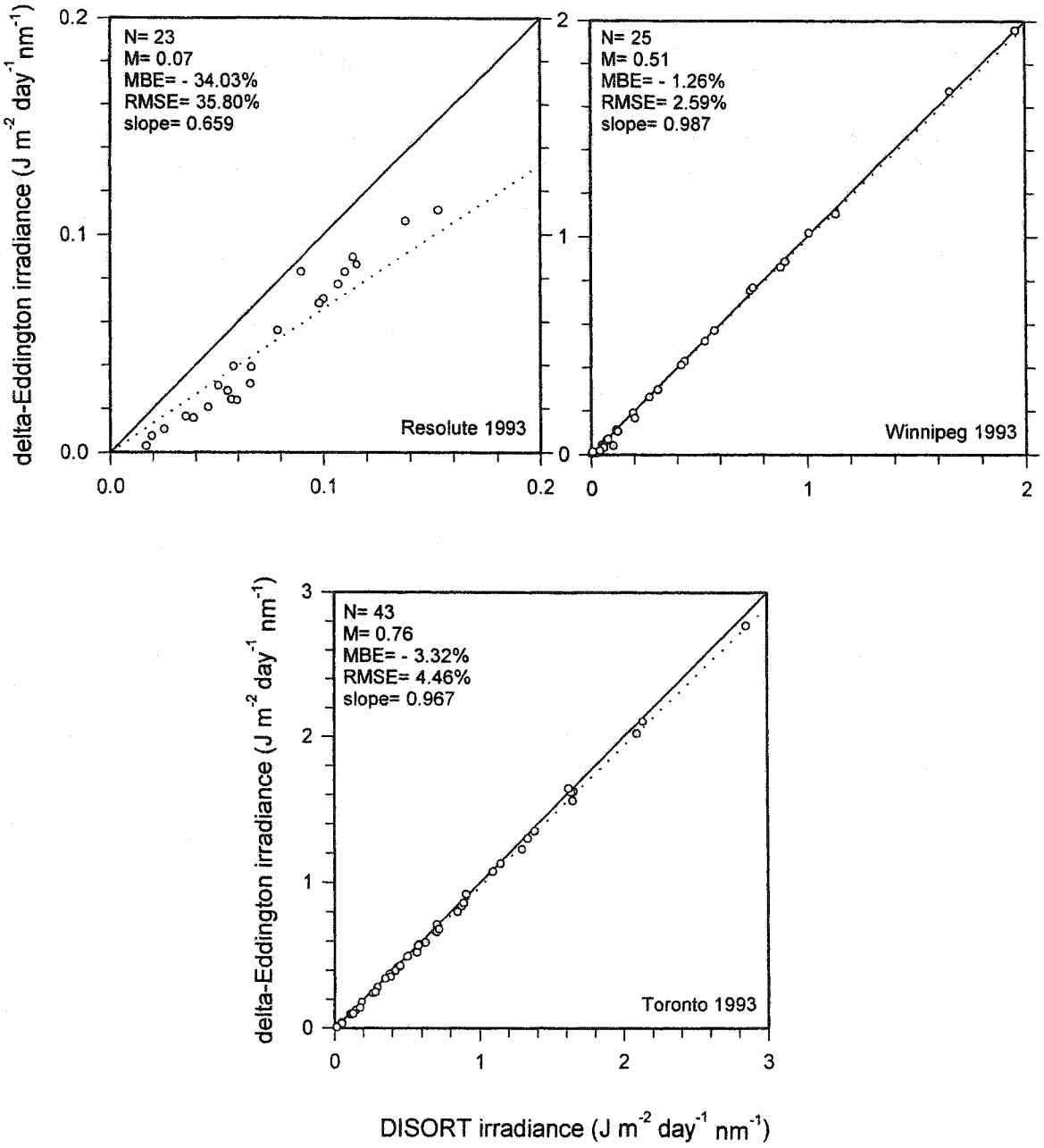

Figure 4.4. Correlation between DISORT and delta-Eddington algorithms for daily total spectral irradiances at 295 nm for cloudy sky conditions (cloud amount >= 0.8) for Resolute, Winnipeg and Toronto. N is the number of days, M is the mean daily measured irradiance.

Delta-Eddington and DISORT mean monthly spectra are compared in Figure 4.5. The agreement in irradiances is good for these months at all four stations except at wavelengths ≤ 300 nm at months with larger mean zenith angles where the delta-Eddington method always underestimates spectral irradiances. This confirms the effect of a rapid decrease in irradiance at shorter wavelengths and at larger sun angles in the delta-Eddington method.

All the above comparisons showed that for large solar zenith angles and at shorter wavelengths (less than 305 nm) where ozone absorption is high, the delta-Eddington method did not perform well because of the truncation of the phase function to two terms. Although the amount of irradiance is very small, short wavelengths are nevertheless important because the biological sensitivities are maximum for many processes. Therefore, DISORT 8 method is superior for spectral irradiances. Figure 4.6 shows the ratio of irradiances of the delta-Eddington and DISORT 8 methods as a function of total column ozone and solar zenith angle for two simulated cases (cloudless and overcast) and for two wavelengths (295 nm and 305 nm). At a wavelength of 295 nm (Figure 4.6 a) the delta-Eddington error depends strongly on the ozone amount. Increases in the amount of ozone generally increase the delta-Eddington error especially at larger solar zenith angles. For example, at a solar zenith angle of 71° and a small ozone amount (200 DU), the delta-Eddington underestimates irradiances by 36%, but the underestimation is much larger (a factor of 3) with increasing ozone amount up to 500 DU. At 305 nm (Figure 4.6 b) the delta-Eddington error depends slightly on ozone but the error increases with increasing solar zenith angles up to 83°. Therefore, for wavelength ≥ 305, and when considering

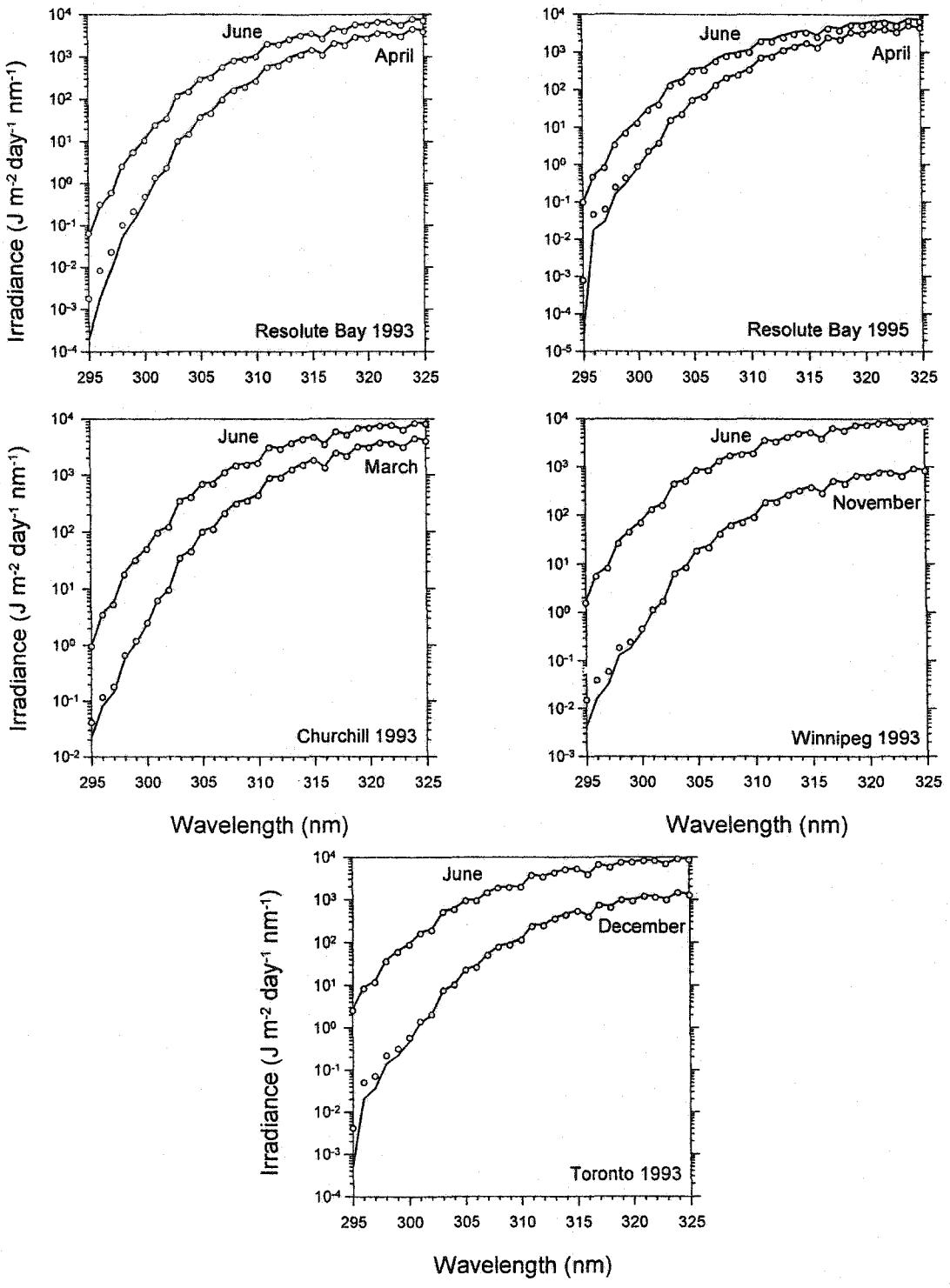

Figure 4.5. Mean monthly spectral irradiances calculated by the delta-Eddington (solid lines) and DISORT (white circles) algorithms.

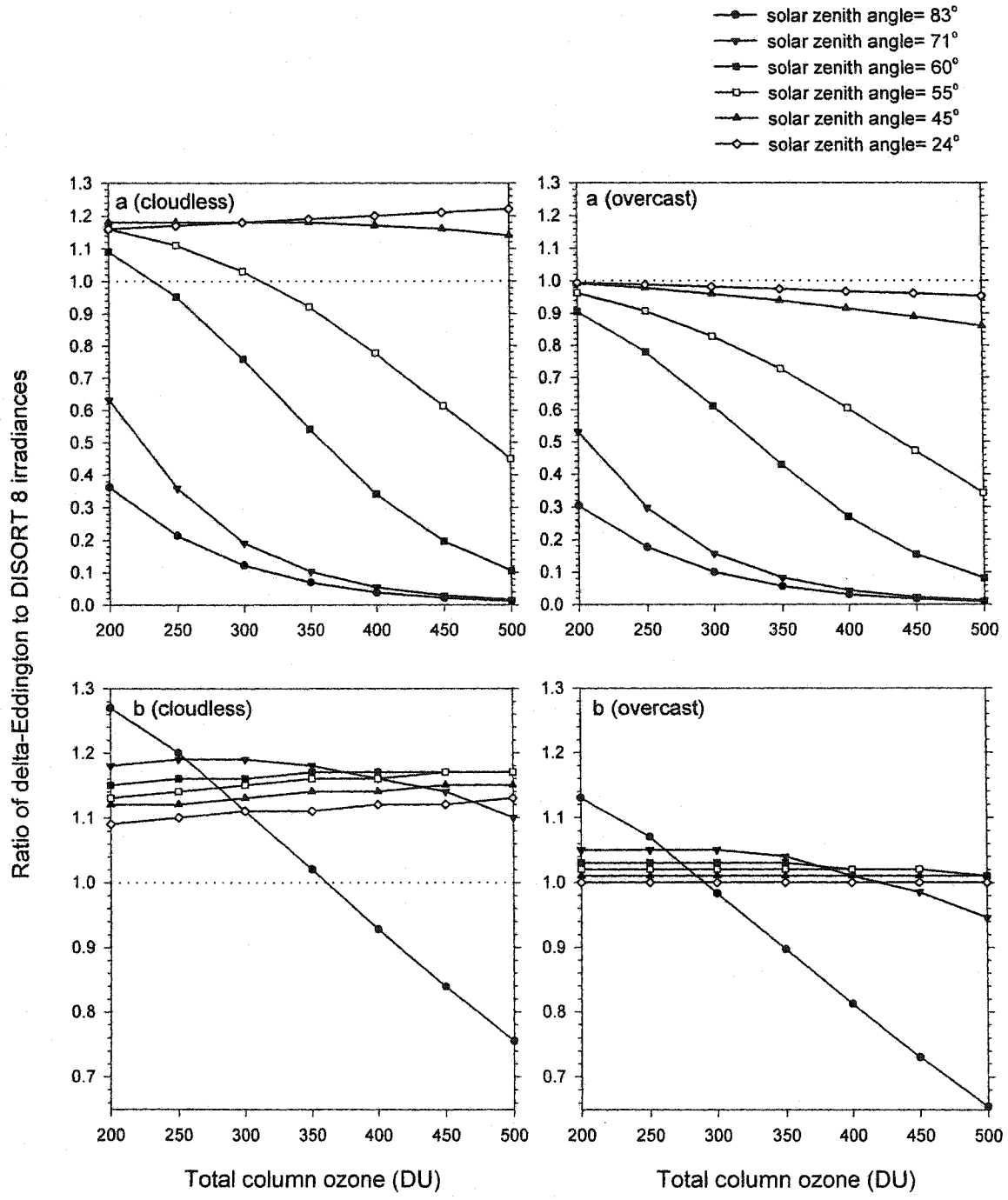

Figure 4.6. Ratio of irradiances calculated by delta-Eddington method to DISORT 8 method as a function of total column ozone and solar zenith angle for a wavelength of 295 nm (a) and 305 nm (b) for Toronto on June 24, 1993 for cloudless and overcast sky conditions with a surface albedo of 0.05.

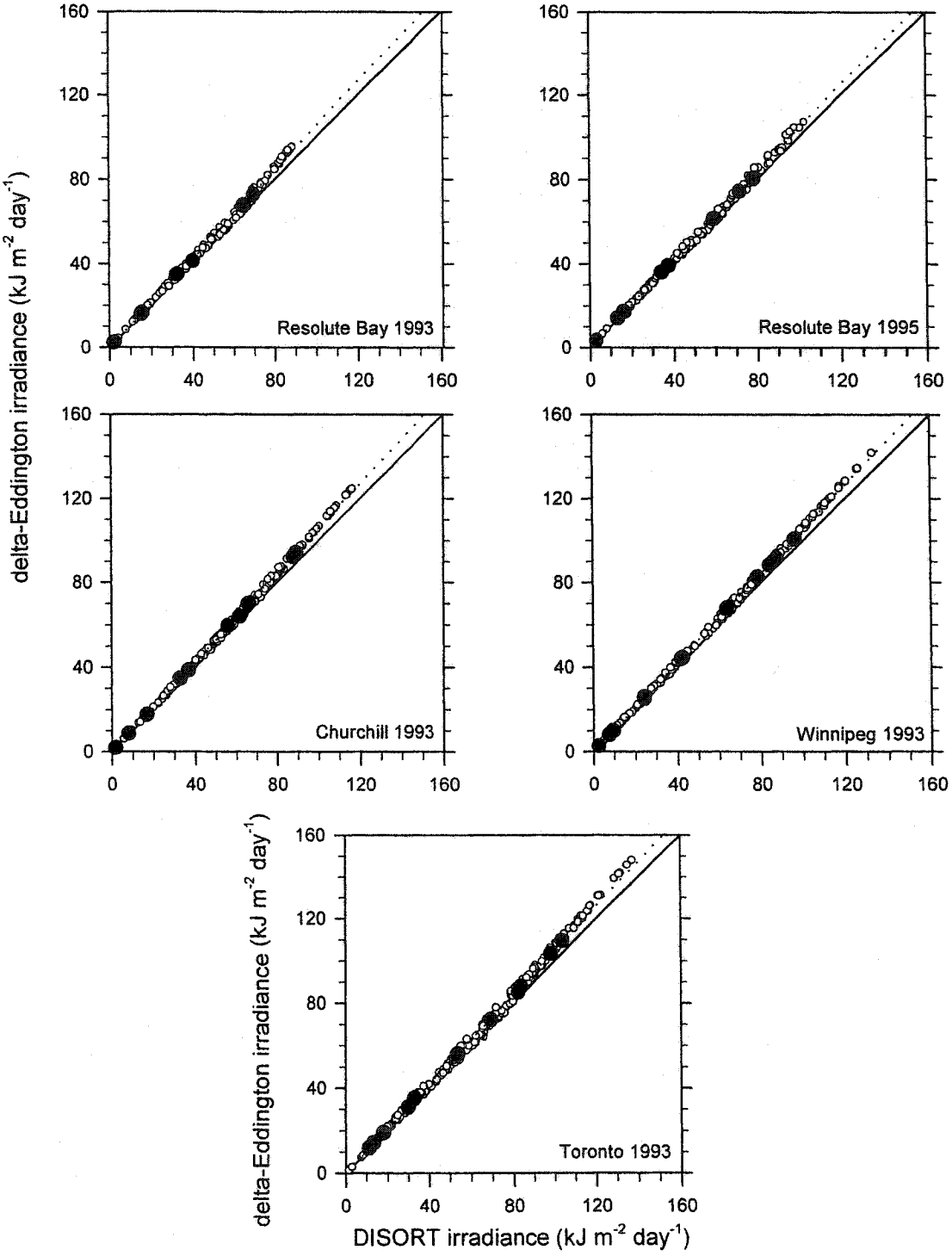

Figure 4.7. Comparison of DISORT and delta-Eddington daily totals (white circles) and monthly averages (black circles) broadband irradiances using annual values of cloud optical depth for each station (Table 3.4) at Resolute Bay, Churchill, Winnipeg and Toronto. The dotted lines represent linear regressions constrained to pass through the origin.

Table 4.2. Comparison of daily total and monthly average broadband irradiances from the delta-Eddington and DISORT 8 methods for the period indicated for each station. N is the number of data points and $\bar{M}$ is the mean annual daily broadband irradiance calculated by DISORT ($kJ\ m^{-2}day^{-1}$). Values of MBE and RMSE are given both in $kJ\ m^{-2}day^{-1}$ and in percentages (italic) of $\bar{M}$. Positive MBE values indicate delta-Eddington overestimation.

Irradiance	Resolute Bay 1993	Resolute Bay 1995	Churchill 1993	Winnipeg 1993	Toronto 1993
Daily total					
N	141	154	178	228	250
$\bar{M}$	49.90	50.82	56.74	53.32	58.37
MBE	2.77	2.09	3.30	2.84	2.94
%MBE	*5.55*	*4.12*	*5.82*	*5.33*	*5.03*
RMSE	3.38	2.70	3.89	3.63	4.06
%RMSE	*6.78*	*5.30*	*6.86*	*6.81*	*6.95*
Slope	1.055	1.041	1.058	1.053	1.050
Monthly average					
N	8	8	10	12	12
$\bar{M}$	37.88	39.16	45.50	46.84	55.81
MBE	2.15	1.72	2.68	2.51	0.99
%MBE	*5.69*	*4.38*	*5.89*	*5.36*	*1.77*
RMSE	2.44	1.91	3.13	3.01	2.72
%RMSE	*6.45*	*4.86*	*6.88*	*6.43*	*4.88*
Slope	1.056	1.043	1.059	1.054	1.018

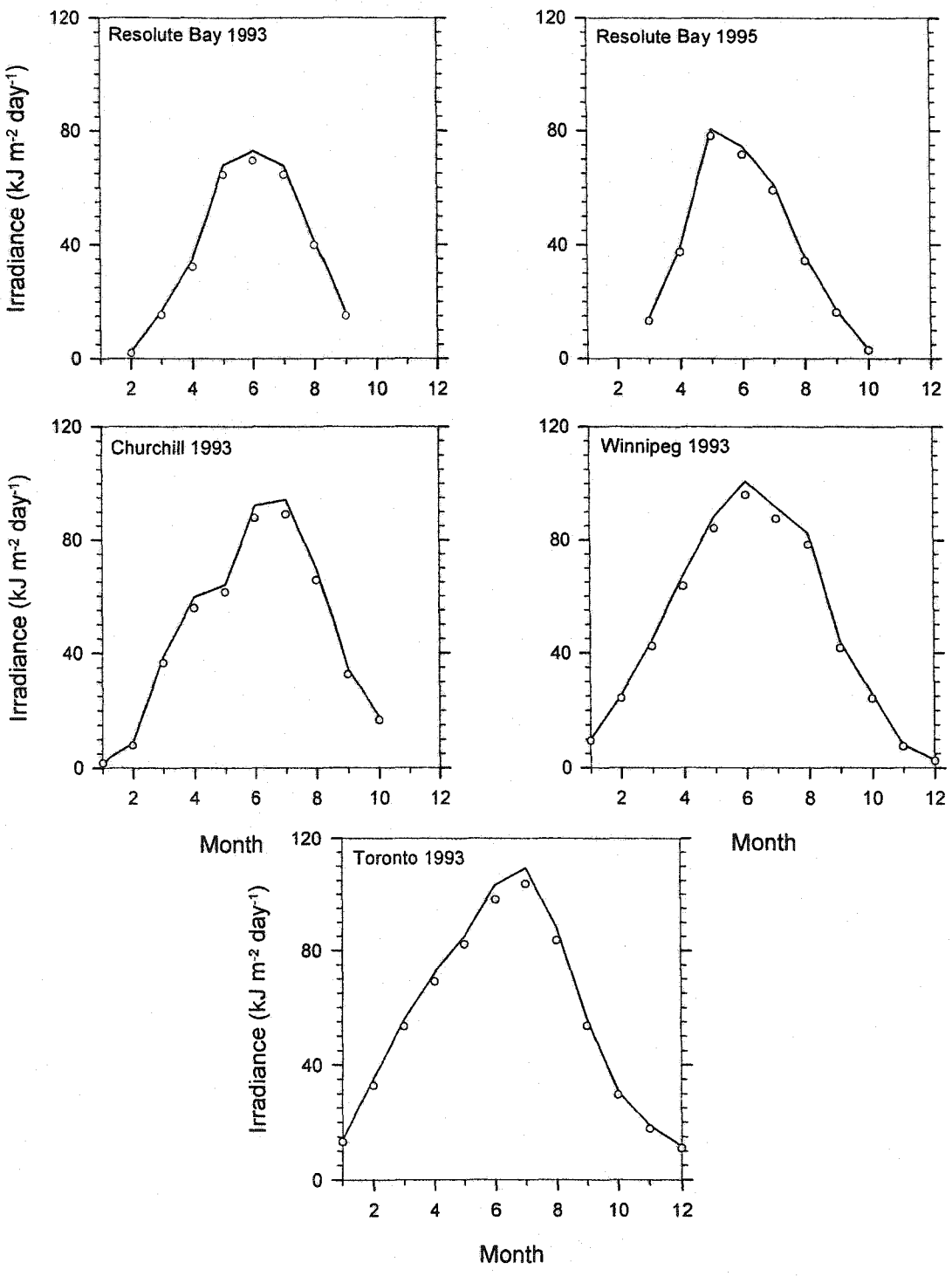

Figure 4.8. Monthly averaged broadband irradiances calculated by the delta-Eddington (solid lines) and DISORT (white circles) algorithms.

daily total spectral irradiances, errors produced with the delta-Eddington approximation are less important. This is because the times of day with smaller solar zenith angles contribute most to the total irradiances.

Model estimates of daily total and monthly averaged broadband irradiances are compared in Figure 4.7. Agreement is good for both daily total and monthly averages. This is also indicated by the statistics in Table 4.2 where both MBE and RMSE values are less than 7%. This is consistent with the findings of Forster and Shine (1995), which indicate that the average delta-Eddington transmittance for the broadband UV-B exceeds DISORT 16-stream model estimates by 5% at sun angle of 60°. Plots of the mean monthly calculated broadband irradiances (Figure 4.8) show that both sets of model estimates agree well with each other with delta-Eddington consistently overestimating.

4.4 Comparisons of the delta-Eddington and DISORT model calculations with measurements

This section compares model estimates with Brewer spectral and broadband irradiances for both daily totals and monthly averages for all sky conditions using annual values of cloud optical depth for each station (Table 3.4).

4.4.1 Spectral results

4.4.1.1 Daily spectral irradiance

Daily spectral irradiances from the delta-Eddington and DISORT 8 methods are compared with measurements in Figures 4.9 and 4.10 for two wavelengths (295 nm and 305 nm). Other wavelengths (300, 310, 315, 320 and 325 nm) are presented in Appendixes C and D. The performance statistics for the seven wavelengths are given in

Table 4.3. With the exception of the 295 and 300 nm plots the scatter in the data points are quite evenly distributed around the 1:1 line and the corresponding relative MBE values are small. For wavelengths ≥ 305 nm the relative MBE for the two methods is mainly within 5% of the mean measured irradiance. This is well within the uncertainty of the Brewer instrument.

Table 4.3 shows that there are systematic biases for delta-Eddington but most MBE values for DISORT are negative, indicating underestimation by the model. This finding is consistent with the results of section 4.3 which showed that the delta-Eddington, generally, produces larger spectral irradiances than DISORT 8. DISORT estimates are closer to measurements at shorter wavelengths (≤ 300 nm) than the delta-Eddington estimates. This is the result of the rapid decrease in delta-Eddington irradiances at those wavelengths. The better MBE for delta-Eddington at longer wavelengths may suggest systematic overestimation by Brewer instruments. This may indicate that the 6% increase due to cosine error may be too large. Otherwise, it is difficult to see why an inferior model performs better than DISORT 8.

The larger relative MBE values at 295 and 300 nm at most stations in both the delta-Eddington and DISORT estimates may be attributed to the difficulty in measuring this spectral region. In the wavelength range (290-304 nm) there are very low light levels and increased stray light scattering that increase the instrumental uncertainty (E. Wu, personal communication, 2001).

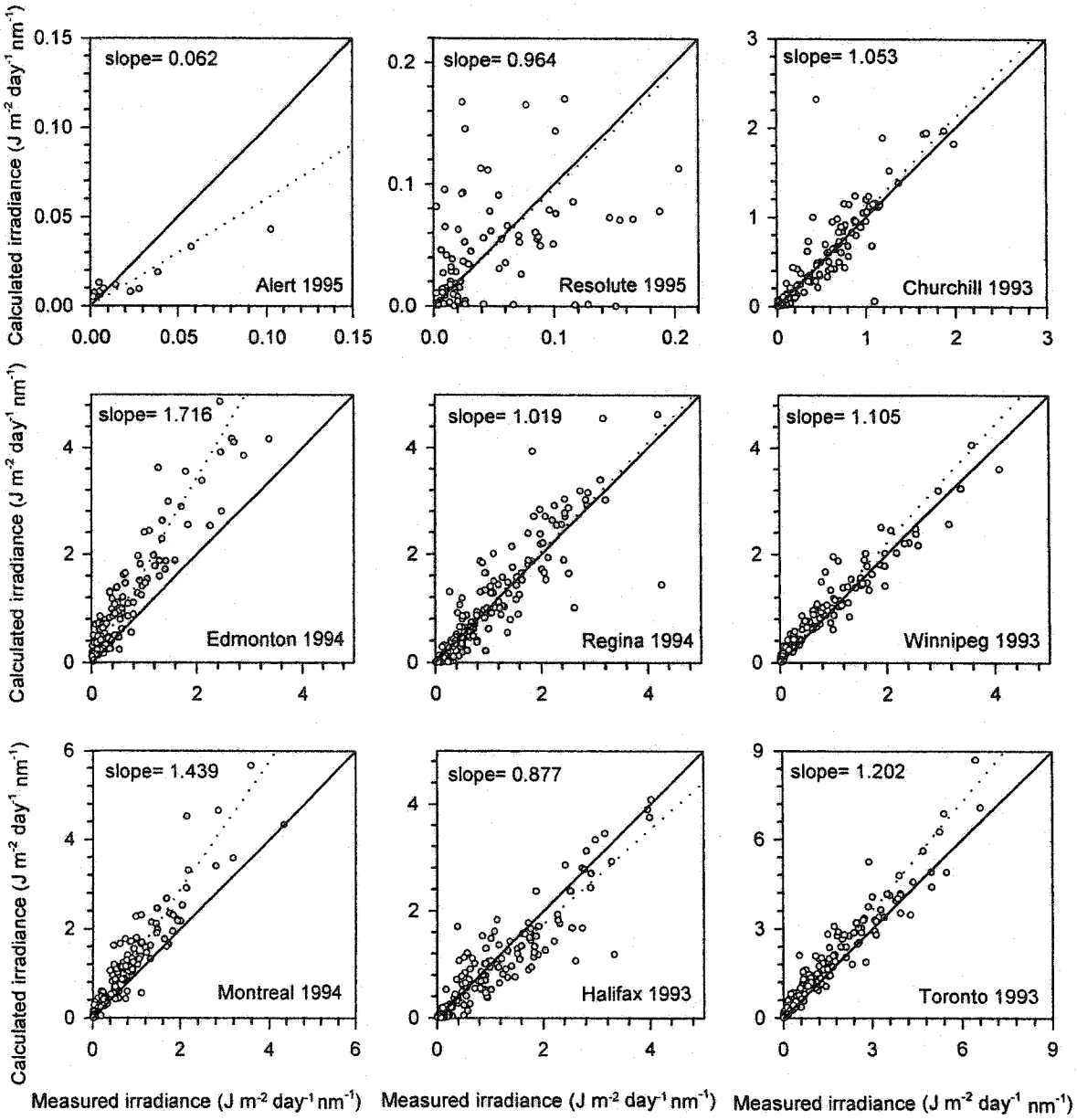

Figure 4.9a. Comparison of measured and calculated (delta-Eddington) daily total spectral irradiances using annual values of cloud optical depth for each station (Table 3.4) for 295 nm. The dotted lines represent linear regressions constrained to pass through the origin.

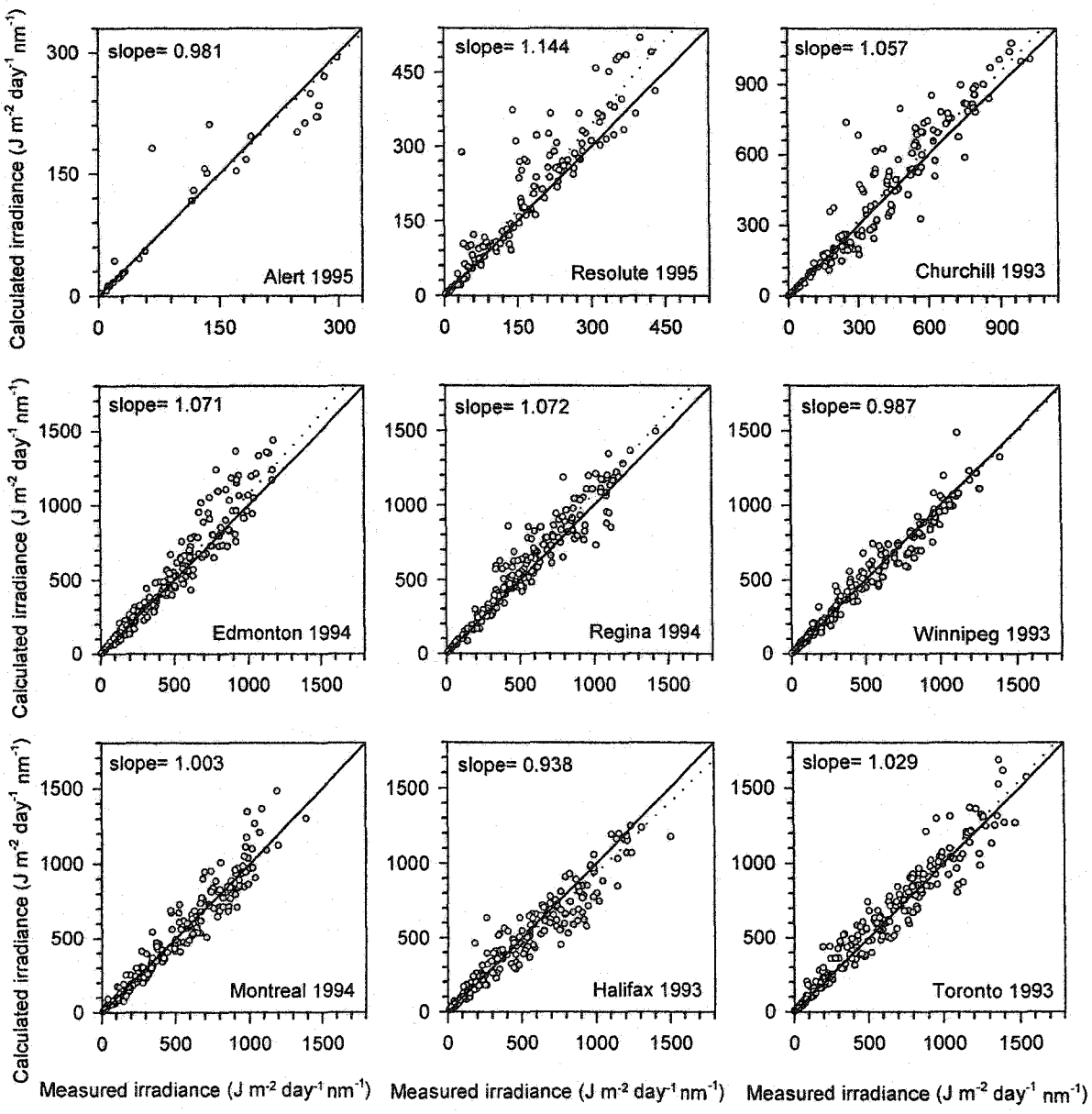

Figure 4.9b. same as Figure 4.9a but for 305 nm.

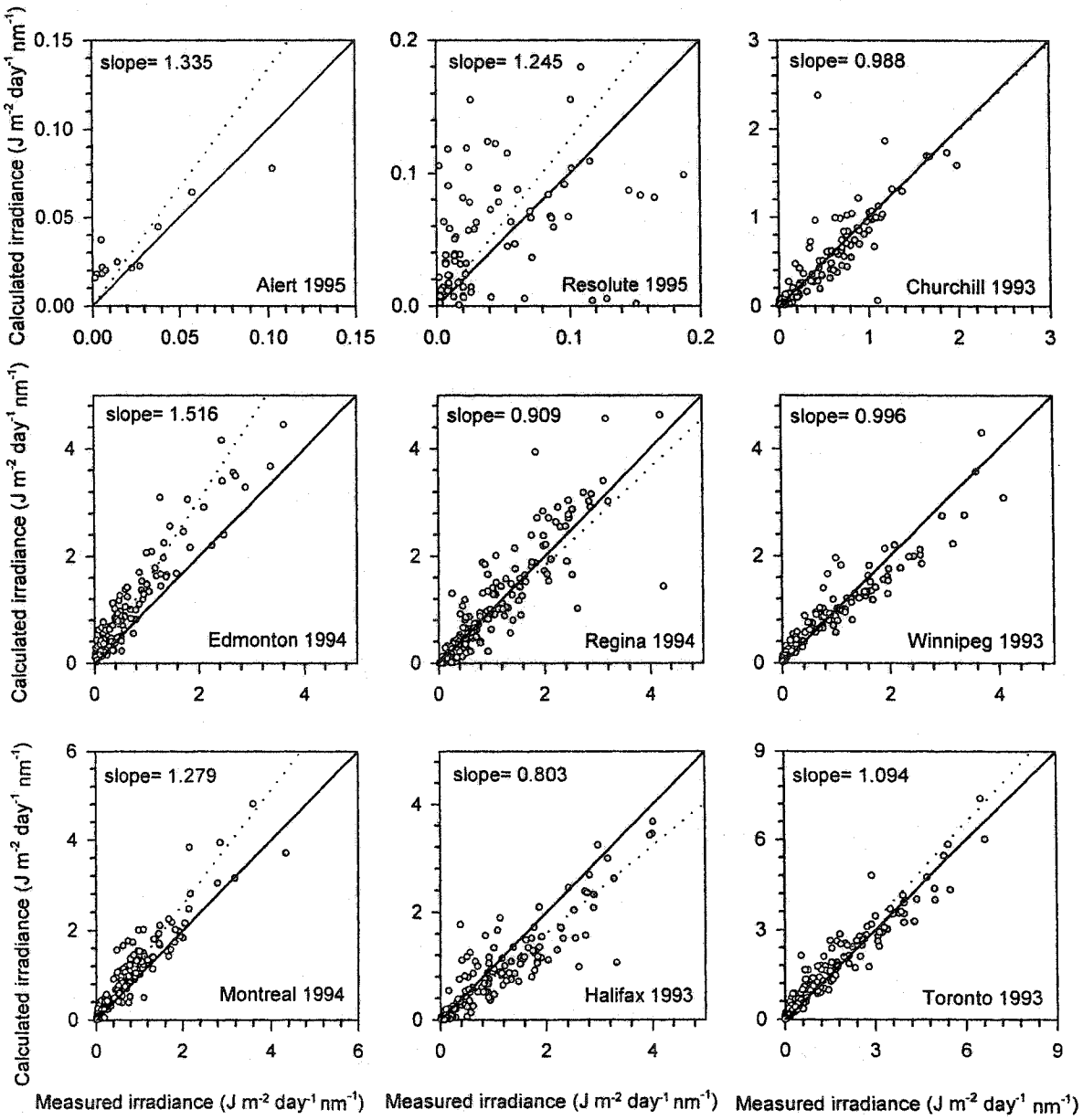

Figure 4.10. Comparison of measured and calculated (DISORT) daily total spectral irradiances using annual values of cloud optical depth for each station (Table 3.4) for 295 nm. The dotted lines represent linear regressions constrained to pass through the origin.

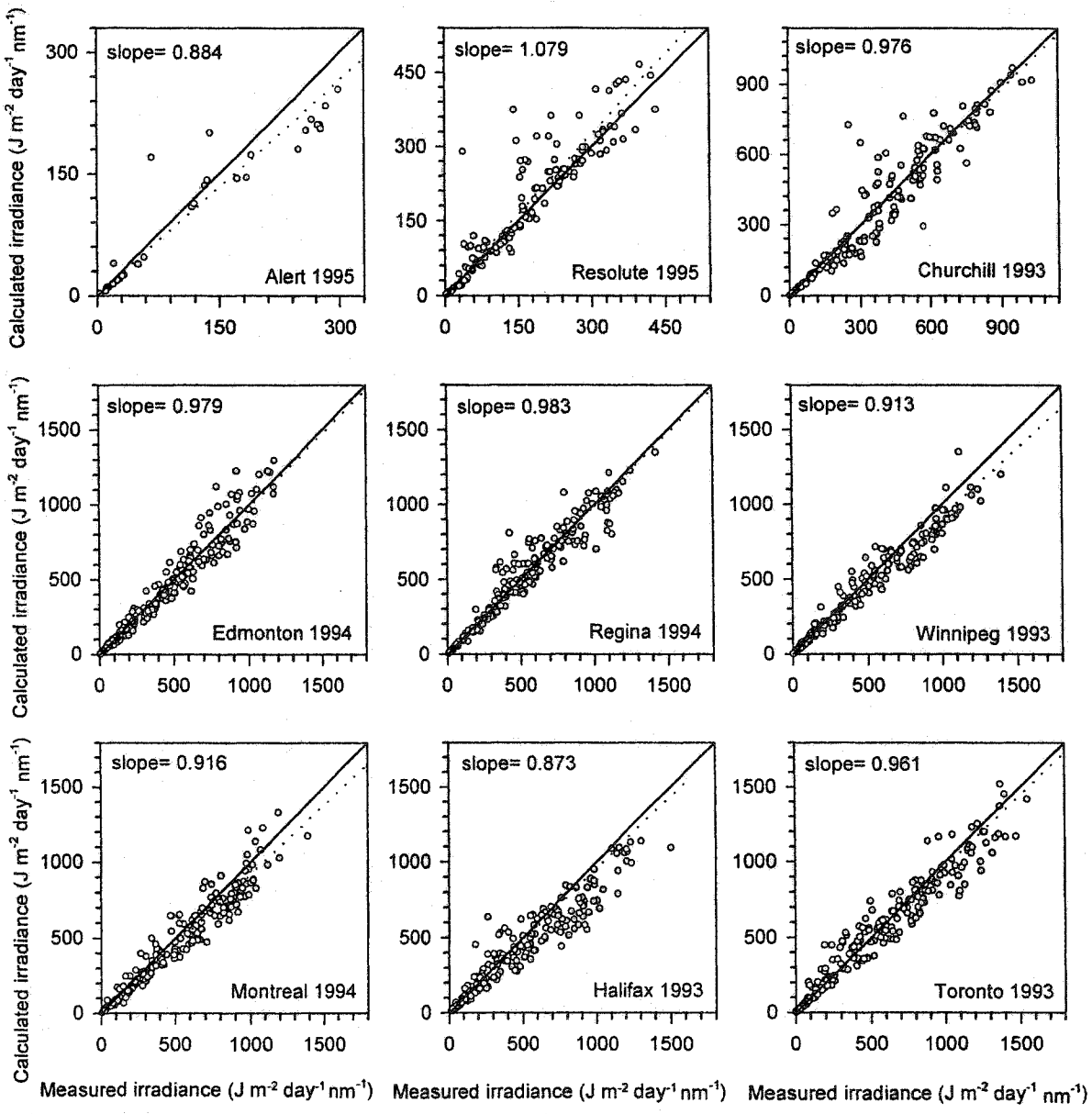

Figure 4.10b. same as Figure 4.10a but for 305 nm.

Table 4.3. Comparison of daily spectral irradiances from the delta-Eddington (DE) and DISORT 8 (D8) methods against measurements for the period indicated for each station. N is the number of data points and $\bar{M}$ is the mean annual measured daily spectral irradiance ($J\ m^{-2} day^{-1} nm^{-1}$). Values of MBE and RMSE are given as percentages (italic) of $\bar{M}$. Positive MBE values indicate model overestimation.

Wavelength	Alert 1995	Resolute 1995	Churchill 1993	Edmonton 1994	Regina 1994	Winnipeg 1993	Montreal 1994	Halifax 1993	Toronto 1993
295 nm									
N	12	80	136	135	204	136	154	206	192
$\bar{M}$	0.02	0.05	0.46	0.62	0.84	0.84	0.72	0.80	1.25
%MBE (DE)	*-39.93*	*-3.54*	*5.25*	*71.62*	*1.99*	*10.50*	*43.94*	*-12.31*	*20.22*
%MBE (D8)	*33.46*	*24.46*	*-1.21*	*51.60*	*-9.06*	*-0.42*	*27.90*	*-19.67*	*9.41*
%RMSE (DE)	*85.71*	*107.09*	*51.14*	*105.31*	*49.19*	*32.28*	*70.22*	*45.18*	*38.84*
%RMSE (D8)	*64.40*	*117.81*	*51.47*	*75.81*	*45.56*	*34.21*	*51.34*	*51.89*	*32.08*
300 nm									
N	31	154	178	274	211	228	212	231	250
$\bar{M}$	3.06	4.63	18.50	20.94	30.19	26.08	29.83	27.95	35.82
%MBE (DE)	*-2.13*	*29.91*	*28.24*	*30.73*	*32.94*	*10.33*	*19.94*	*6.98*	*21.69*
%MBE (D8)	*-2.05*	*27.42*	*18.29*	*17.60*	*21.08*	*-0.20*	*9.09*	*-1.49*	*11.27*
%RMSE (DE)	*29.47*	*71.56*	*56.42*	*61.85*	*49.71*	*27.50*	*38.16*	*29.67*	*37.66*
%RMSE (D8)	*31.19*	*67.42*	*45.97*	*40.91*	*36.11*	*23.47*	*27.20*	*29.33*	*26.68*
305 nm									
$\bar{M}$	121.09	155.68	355.85	340.43	497.54	405.60	475.38	425.44	494.14
%MBE (DE)	*-1.88*	*14.37*	*5.72*	*7.07*	*7.23*	*-1.26*	*0.28*	*-6.15*	*2.85*
%MBE (D8)	*-11.58*	*7.85*	*-2.35*	*-2.15*	*-1.73*	*-8.68*	*-8.39*	*-12.68*	*-3.89*
%RMSE (DE)	*26.69*	*33.50*	*25.11*	*26.18*	*20.13*	*16.18*	*17.82*	*23.56*	*18.43*
%RMSE (D8)	*31.50*	*30.30*	*23.28*	*20.18*	*17.77*	*20.40*	*19.14*	*27.95*	*19.15*

Table 4.3 (Contd).

Wavelength	Alert 1995	Resolute 1995	Churchill 1993	Edmonton 1994	Regina 1994	Winnipeg 1993	Montreal 1994	Halifax 1993	Toronto 1993
310 nm									
$\bar{M}$	475.94	606.14	954.10	827.71	1155.39	962.63	1131.6	980.79	1068.12
%MBE (DE)	*3.51*	*12.11*	*4.68*	*9.59*	*7.70*	*3.19*	*-0.38*	*-1.85*	*6.57*
%MBE (D8)	*-5.86*	*5.84*	*-2.28*	*1.83*	*0.82*	*-3.50*	*-7.21*	*-7.46*	*0.36*
%RMSE (DE)	*24.55*	*22.88*	*21.38*	*24.55*	*18.35*	*14.18*	*15.73*	*19.26*	*18.10*
%RMSE (D8)	*26.35*	*19.94*	*20.06*	*18.35*	*15.39*	*14.41*	*16.50*	*21.19*	*15.77*
315 nm									
$\bar{M}$	1974.4	2533.37	3221.14	2635.63	3491.34	2934.00	3419.93	2941.86	3250.50
%MBE (DE)	*-4.26*	*2.20*	*-3.51*	*2.86*	*1.51*	*-0.25*	*-4.87*	*-3.72*	*-1.79*
%MBE (D8)	*-11.64*	*-1.78*	*-9.06*	*-3.29*	*-4.58*	*-5.02*	*-11.10*	*-8.39*	*-6.14*
%RMSE (DE)	*24.93*	*13.82*	*18.09*	*18.00*	*14.98*	*12.71*	*14.77*	*18.49*	*14.81*
%RMSE (D8)	*28.72*	*14.46*	*19.99*	*16.06*	*15.09*	*14.03*	*17.63*	*20.43*	*16.14*
320 nm									
$\bar{M}$	3216.68	4181.29	4910.39	3894.57	5015.57	4278.33	4867.78	4268.91	4668.61
%MBE (DE)	*-4.20*	*1.68*	*-4.73*	*3.65*	*2.23*	*0.89*	*-2.62*	*-2.43*	*-0.63*
%MBE (D8)	*-10.92*	*-1.89*	*-9.75*	*-1.97*	*-3.22*	*-3.60*	*-8.40*	*-6.75*	*-4.84*
%RMSE (DE)	*24.42*	*12.70*	*17.81*	*17.64*	*14.52*	*12.41*	*14.02*	*17.61*	*14.28*
%RMSE (D8)	*27.69*	*13.29*	*19.83*	*15.40*	*14.10*	*12.94*	*15.59*	*18.99*	*15.02*
325 nm									
$\bar{M}$	3999.21	5548.12	5810.78	4679.64	5710.72	4943.37	5715.44	4932.53	5422.23
%MBE (DE)	*-0.20*	*0.45*	*- 2.11*	*4.17*	*5.51*	*4.41*	*-1.97*	*0.67*	*1.45*
%MBE (D8)	*-6.63*	*-3.01*	*-6.90*	*-1.03*	*0.63*	*-0.2*	*-7.14*	*-3.49*	*-2.93*
%RMSE (DE)	*22.60*	*11.87*	*16.97*	*17.59*	*15.75*	*13.12*	*13.95*	*16.98*	*14.06*
%RMSE (D8)	*24.59*	*12.74*	*18.13*	*15.33*	*13.89*	*11.85*	*14.94*	*17.38*	*13.97*

Delta-Eddington's rapid decrease in irradiance at 295 nm is only detectable at the arctic stations as a result of the greater cloudiness (Figure 3.1) and solar zenith angles. At the other stations except Halifax, delta-Eddington's MBE values are positive. This is attributed to the effect of greater flux overestimation in cloudless skies that are more common than in the arctic. At Halifax, the negative MBE for both models suggests a systematic error in the Brewer instrument.

Relative RMSE values for wavelengths greater than 300 nm are mainly within 12% to 25%. RMSE decreases similarly with length of averaging period for both models. An example is shown for Toronto (1993-1996) in Figure 4.11. For wavelengths greater than 300 nm, RMSE values are between 17 and 20% for individual days and decrease to between 6 and 8% for 30-day averaging periods. Davies and McKay (1982) showed a similar decrease for radiation estimates over the broadband solar spectrum. The larger values of RMSE at 300 nm are due to larger MBE values.

4.4.1.2 Monthly averaged spectral irradiance

Mean monthly measured and calculated spectral irradiances are plotted for four stations (one arctic, one subarctic and two midlatitudes) in Figure 4.12 and performance statistics for the two models are shown in Table 4.4. Figure 4.12 illustrates the annual variation of spectral irradiance at four stations. Both model estimates follow measurements well except for Churchill in April at wavelength ≥ 310 nm. This is because the snow depth at Churchill is small and the station is very close to Hudson Bay, which is covered with ice during that time of the year (W. Rouse, personal communication, 2001). Consequently, the model is underestimating the effect of multiple

scattering from the ice and producing less irradiance than the measured values. At wavelengths ≤ 300 nm the delta-Eddington method is consistently overestimating the irradiances at the four stations.

Table 4.4 shows that for 295-310 nm the magnitude of the relative MBE is smaller for DISORT 8 than delta-Eddington but for larger wavelengths MBE is smaller for delta-Eddington. The larger magnitude of biases at 295 nm for delta-Eddington (- 49% to 71%) follows from the results shown in Figures 4.2 and 4.3. However, similar magnitude for DISORT 8 biases (- 30% to 51%) require a different explanation since DISORT 8 is a good approximation to an exact discrete ordinates solution of the radiative transfer equation. Delta-Eddington overestimates on average for 19 of the 24 cases while DISORT 8 underestimates for 15. Larger delta-Eddington irradiances were anticipated on the basis of the findings in Figure 4.3.

Figure 4.13 shows the annual variation of measured and modeled spectral irradiances for Toronto 1993. The systematic errors at 295 and 300 nm are visually more obvious on a logarithmic scale. The Table below Figure 4.13 also indicates largest MBE (22% for the delta-Eddington method and 11% for the DISORT method) and RMSE (31% for the delta-Eddington method and 18% for the DISORT method). However, the model performs very well at wavelengths 305 nm and above with MBE less than 7% and RMSE between 4-8%.

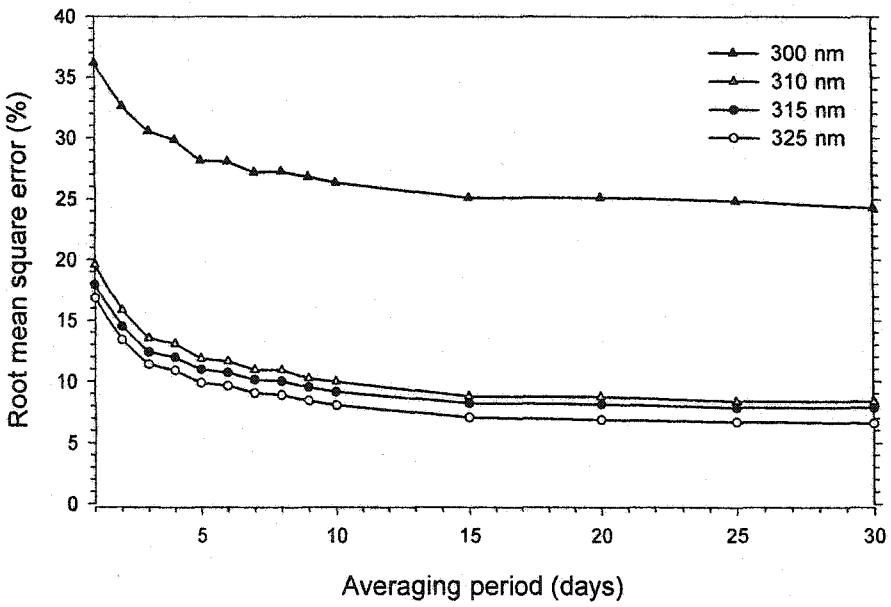

Figure 4.11. The relative root mean square error between delta-Eddington and measured daily total spectral irradiances for different averaging periods for Toronto 1993-1996.

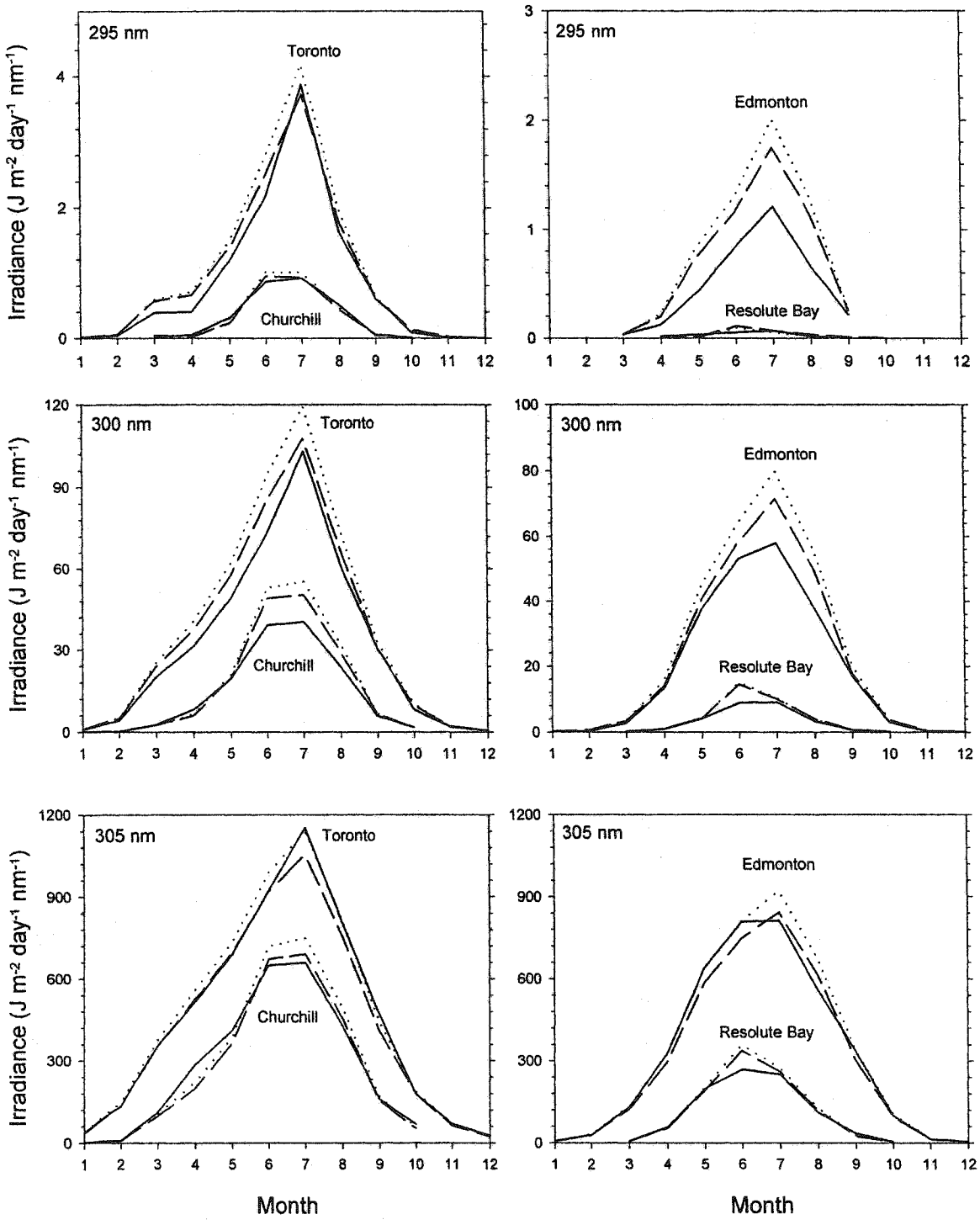

Figure 4.12a. Mean monthly measured (solid lines) and calculated by delta-Eddington (dotted lines) and DISORT (dash lines) methods spectral irradiance at 295, 300, 305 nm using annual values of cloud optical depth for each station (Table 3.4) for Toronto in 1993, Churchill in 1993, Edmonton in 1994 and Resolute Bay in 1995.

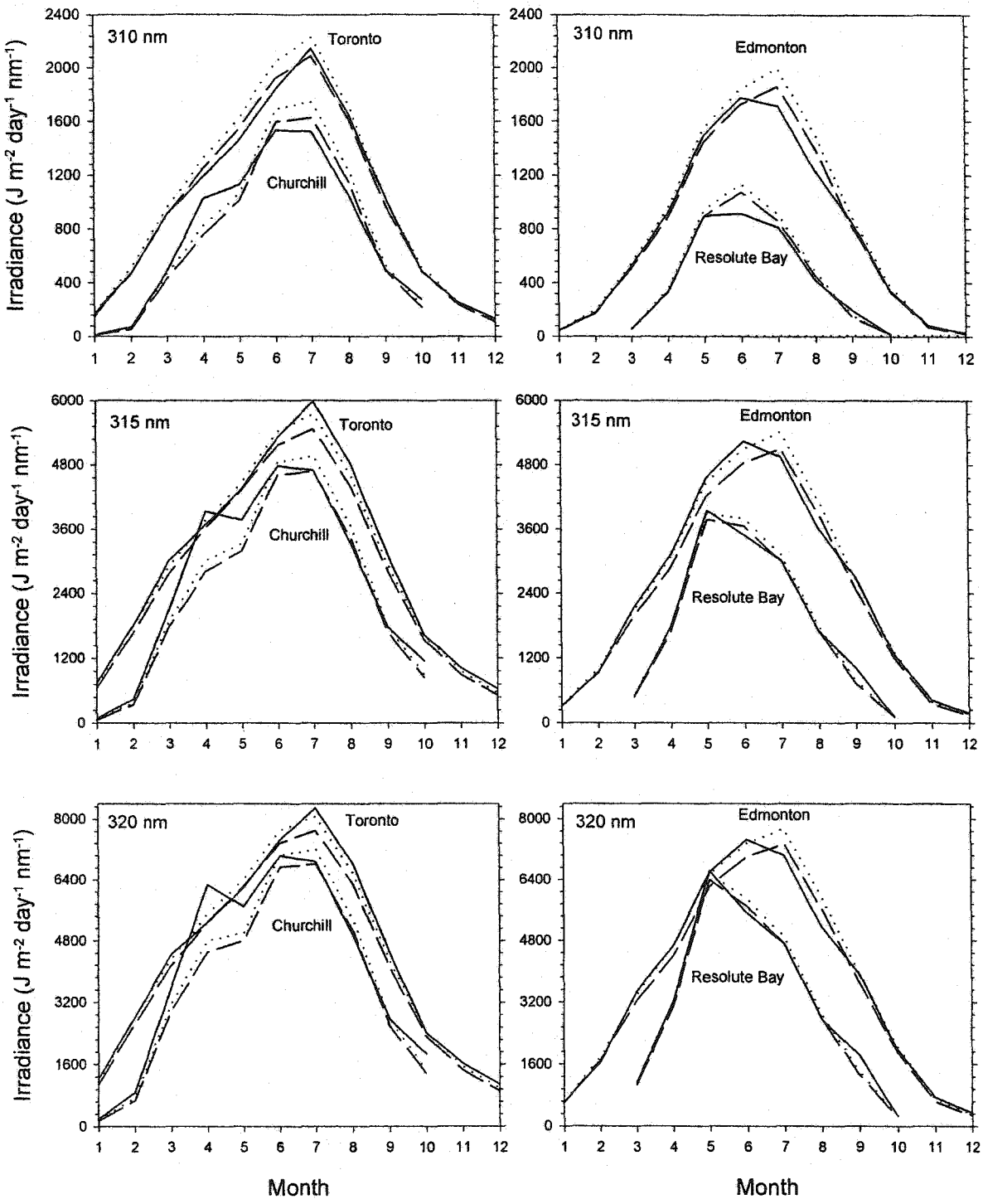

Figure 4.12b. same as Figure 4.12a but for 310, 315 and 320 nm.

Table 4.4. Summary of delta-Eddington (DE) and DISORT 8 (D8) performance measures against measurements for mean monthly spectral irradiances for the period indicated for each station. N is the number of data points and $\bar{M}$ is the mean monthly measured spectral irradiance ($J\,m^{-2}day^{-1}nm^{-1}$). Values of MBE and RMSE are given as percentages (italic) of $\bar{M}$. Positive MBE values indicate model overestimation.

Wavelength	Resolute 1995	Churchill 1993	Edmonton 1994	Toronto 1993
295 nm				
N	7	8	7	12
$\bar{M}$	0.05	0.34	0.50	0.87
%MBE (DE)	*-49.12*	*3.64*	*70.75*	*20.70*
%MBE (D8)	*-29.96*	*-1.56*	*51.24*	*10.29*
%RMSE (DE)	*123.73*	*20.97*	*90.70*	*30.39*
%RMSE (D8)	*126.19*	*14.71*	*65.06*	*18.47*
300 nm				
N	8	10	12	12
$\bar{M}$	3.37	14.09	18.58	31.96
%MBE (DE)	*29.65*	*26.93*	*29.62*	*21.85*
%MBE (D8)	*27.98*	*17.36*	*16.77*	*11.45*
%RMSE (DE)	*67.53*	*50.22*	*49.25*	*30.90*
%RMSE (D8)	*60.38*	*34.96*	*29.82*	*16.50*
305 nm				
$\bar{M}$	115.54	278.03	313.71	446.02
%MBE (DE)	*14.04*	*4.75*	*6.33*	*2.97*
%MBE (D8)	*7.61*	*-3.22*	*-2.75*	*-3.83*
%RMSE (DE)	*29.42*	*17.22*	*14.67*	*6.56*
%RMSE (D8)	*22.24*	*12.54*	*10.42*	*8.02*

Table 4.4 (Contd).

Wavelength	Resolute 1995	Churchill 1993	Edmonton 1994	Toronto 1993
310 nm				
$\bar{M}$	456.06	760.33	765.23	978.16
%MBE (DE)	*11.54*	*3.48*	*9.02*	*6.52*
%MBE (D8)	*5.11*	*-3.44*	*-1.32*	*0.20*
%RMSE (DE)	*19.90*	*16.53*	*15.41*	*9.52*
%RMSE (D8)	*13.76*	*14.32*	*9.04*	*4.99*
315 nm				
$\bar{M}$	1946.21	2606.23	2451.69	3008.96
%MBE (DE)	*1.49*	*-4.70*	*2.42*	*-1.89*
%MBE (D8)	*-2.73*	*-10.26*	*-3.69*	*-6.34*
%RMSE (DE)	*7.56*	*14.02*	*8.70*	*4.33*
%RMSE (D8)	*7.00*	*16.64*	*8.57*	*8.02*
320 nm				
$\bar{M}$	3257.42	4005.02	3636.02	4341.95
%MBE (DE)	*0.80*	*-6.02*	*3.25*	*-0.74*
%MBE (D8)	*-3.02*	*-11.05*	*-2.34*	*-5.06*
%RMSE (DE)	*6.64*	*14.34*	*8.64*	*4.01*
%RMSE (D8)	*6.53*	*17.14*	*7.46*	*6.72*

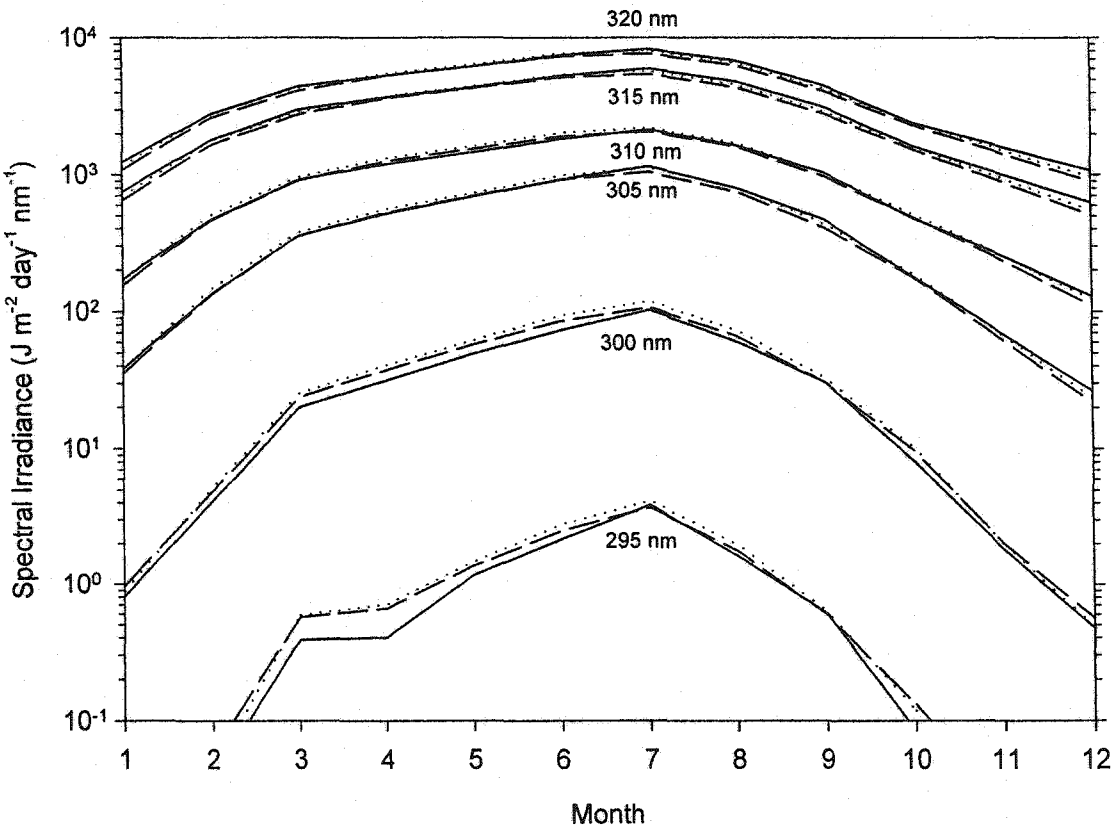

		Delta-Eddington			DISORT 8		
Wavelength	*M*	Slope	MBE%	RMSE%	Slope	MBE%	RMSE%
295 nm	0.87	1.207	20.70	30.39	1.103	10.29	18.47
300 nm	31.96	1.219	21.85	30.90	1.115	11.45	16.50
305 nm	446.02	1.030	2.97	6.56	0.962	- 3.83	8.02
310 nm	978.16	1.065	6.52	9.52	1.002	0.20	4.99
315 nm	3008.96	0.981	- 1.89	4.33	0.934	- 6.34	8.02
320 nm	4341.95	0.993	- 0.74	4.01	0.949	- 5.06	6.72

Figure 4.13. Mean monthly measured (solid lines) spectral irradiances and calculated by the delta-Eddington (dotted lines) and DISORT (dash lines) models for various wavelengths for Toronto 1993. Table gives relative MBE and RMSE values with positive MBE indicating model overestimation. *M* is the mean monthly measured Irradiance.

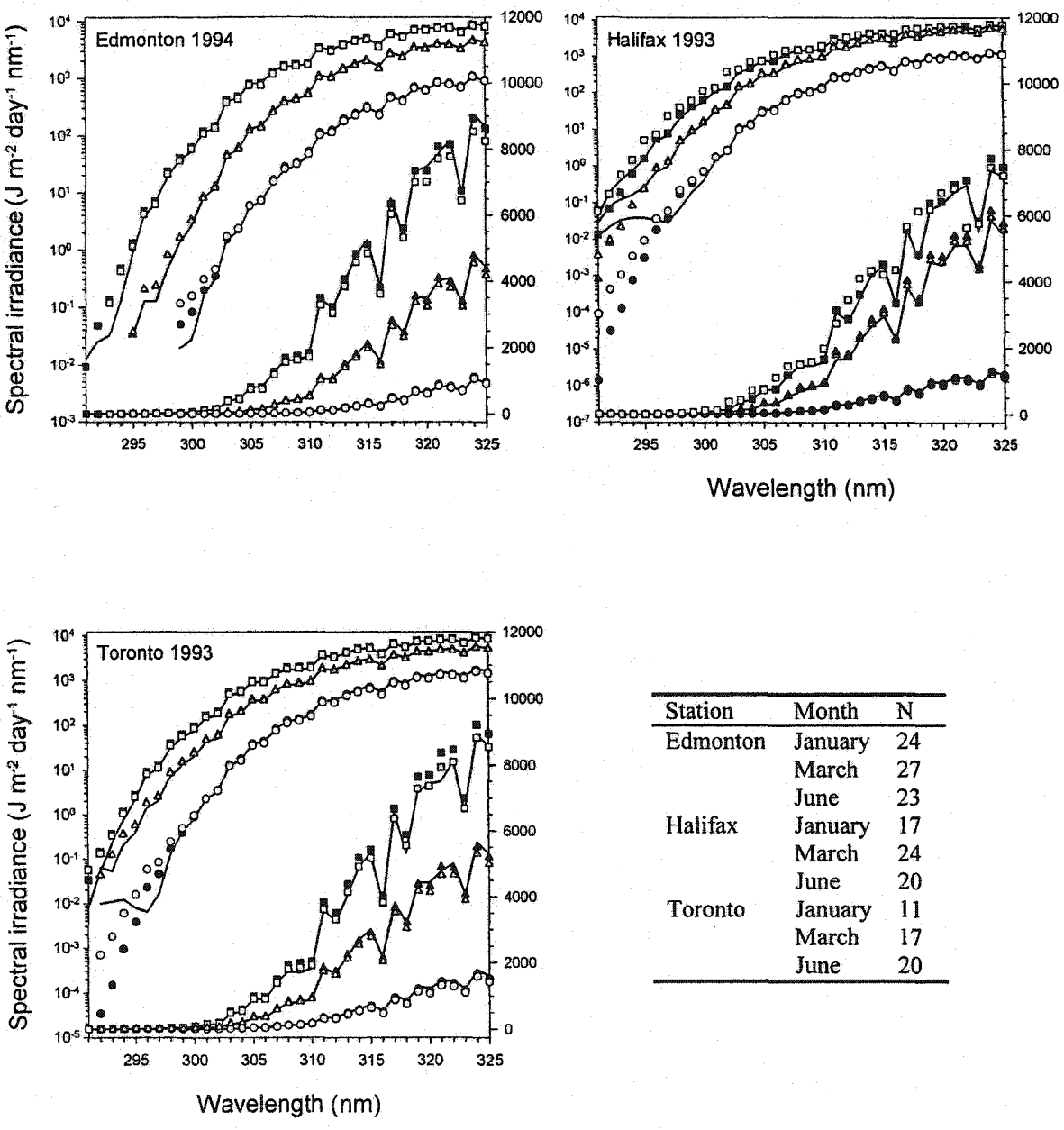

Station	Month	N
Edmonton	January	24
	March	27
	June	23
Halifax	January	17
	March	24
	June	20
Toronto	January	11
	March	17
	June	20

Figure 4.14. Mean monthly measured (solid lines) and calculated by delta-Eddington (black circles, triangles and squares) and DISORT (white circles, triangles and squares) spectral irradiance on a logarithmic (upper lines, left axis) and linear (lower lines, right axis) scale for January (circles), March (triangles) and June (squares) for Edmonton in 1994, Halifax in 1993 and Toronto in 1993. Table gives N which is the number of days used for each month.

Figure 4.14 shows mean monthly measured spectral irradiance and corresponding DISORT and delta-Eddington values with both linear and logarithmic plots for three months (January, March and June) for Edmonton in 1994, Halifax in 1993 and Toronto in 1993. The linear plot illustrates more clearly the agreement of measured and calculated irradiances at higher wavelengths while the logarithmic plot is better for showing the agreement at smaller wavelengths. Model values follow measurements well except at shorter wavelengths (≤ 300 nm). This may be attributable as stated earlier to the difficulty of measuring such low irradiance levels and to the light leakage problem even though a correction has been applied to irradiances for wavelengths less than 305 nm (Wardle and Kerr, 1999). Model calculations show the same spectral variation as the Brewer measurements at wavelengths greater than 295-298 nm. The Halifax and Toronto data indicate that there is still evidence of stray light leakage in the corrected Brewer measurements.

4.4.2 Broadband irradiance results

4.4.2.1 Daily total irradiance

In this section, daily total and monthly averaged broadband irradiances estimated from delta-Eddington and DISORT methods are compared with measurements (Figures 4.15 and 4.16). Performance statistics are given in Table 4.5. In general the delta-Eddington method performs very well for broadband calculations with relative MBE less than 6.5% and RMSE less than 23.5%, which is similar to values obtained from comparisons for global irradiance (Davies and McKay, 1989) and the preliminary UV-B irradiance study for Canadian stations by Davies *et al.* (2000). The delta-Eddington

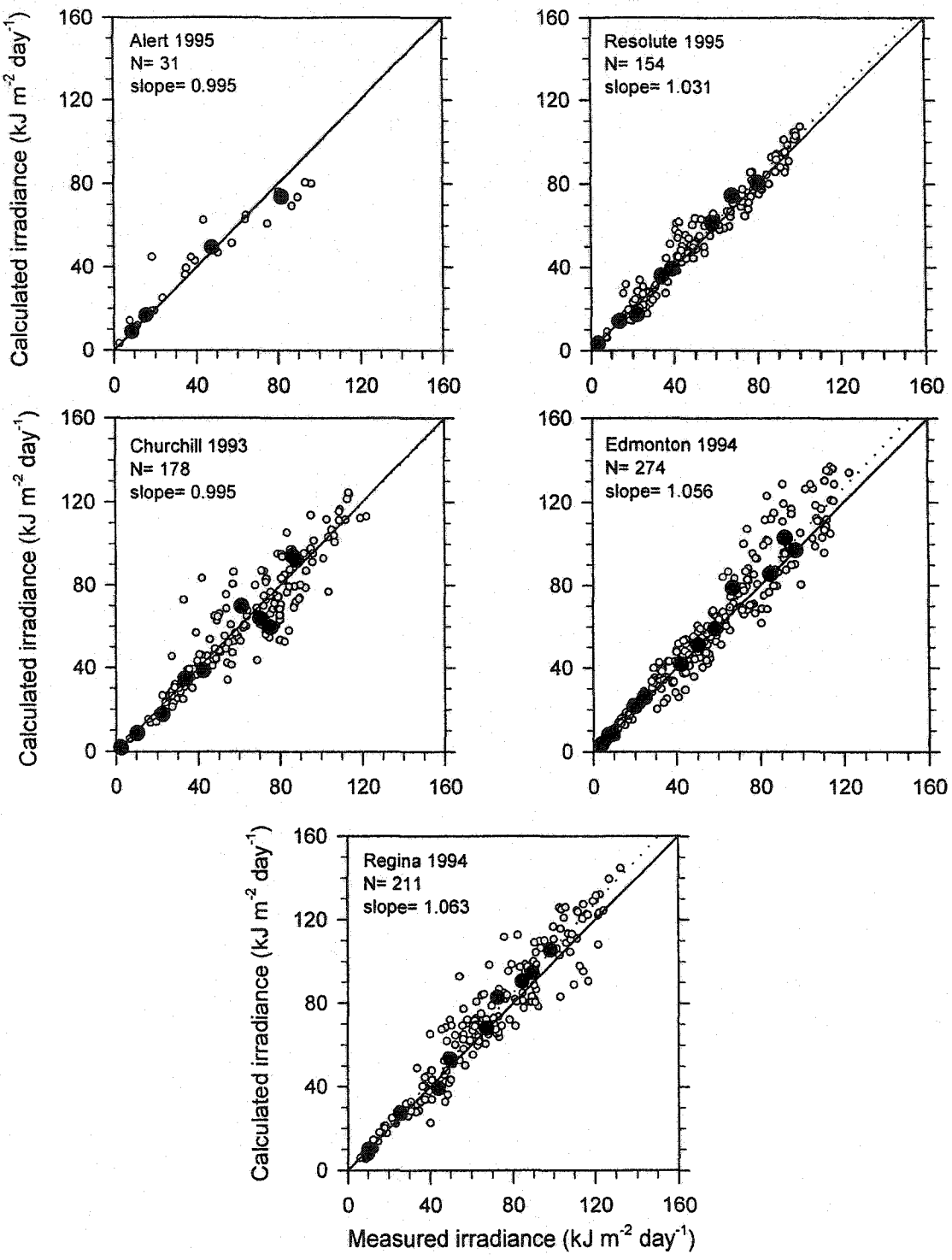

Figure 4.15a. Comparison of measured and calculated (delta-Eddington) daily totals (white circles) and monthly averaged (black circles) irradiances at Alert, Resolute, Churchill, Edmonton and Regina, using annual values of cloud optical depth for each station. N is the number of days. The dotted lines represent linear regressions constrained to pass through the origin.

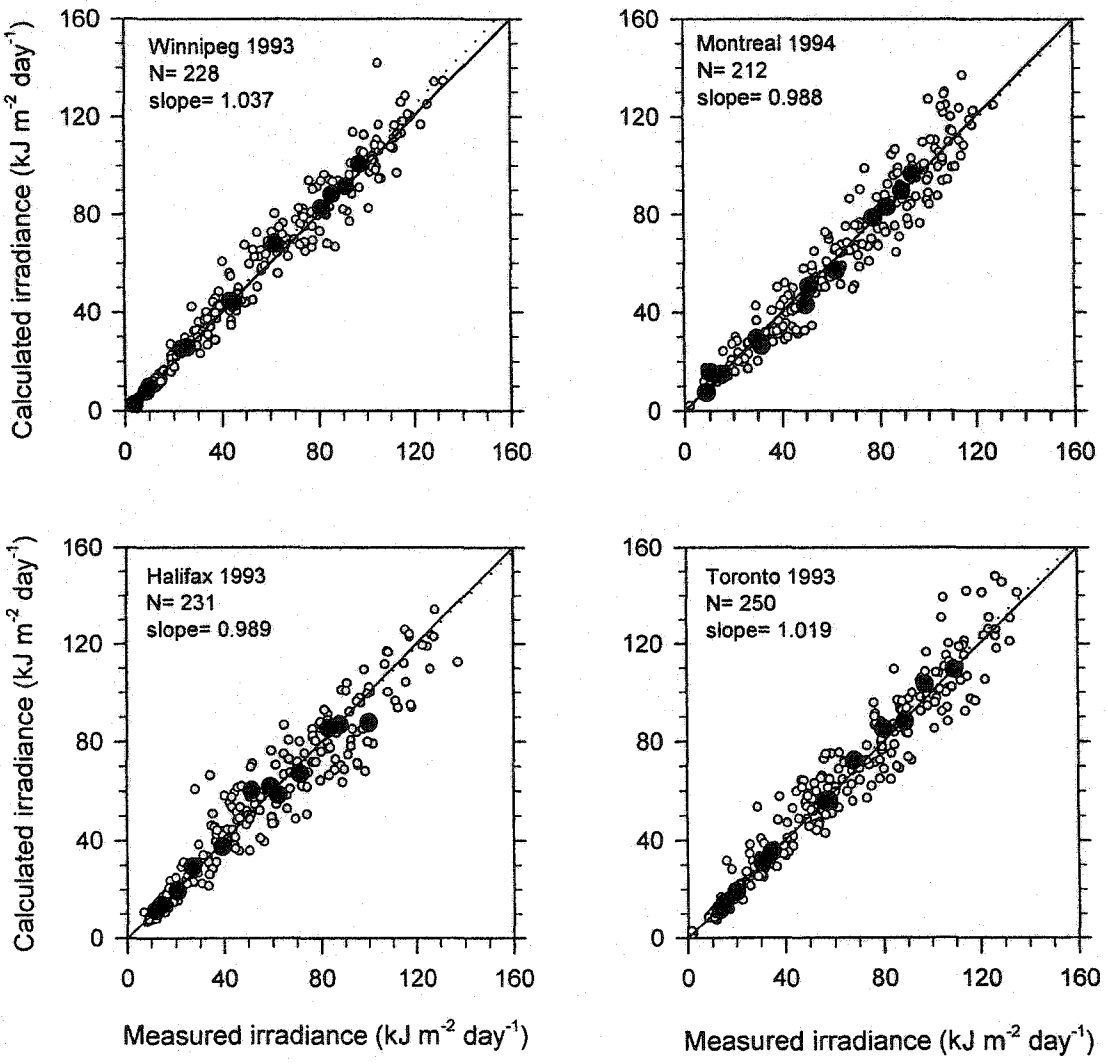

Figure 4.15b. same as Figure 4.15a but for Winnipeg, Montreal, Halifax and Toronto.

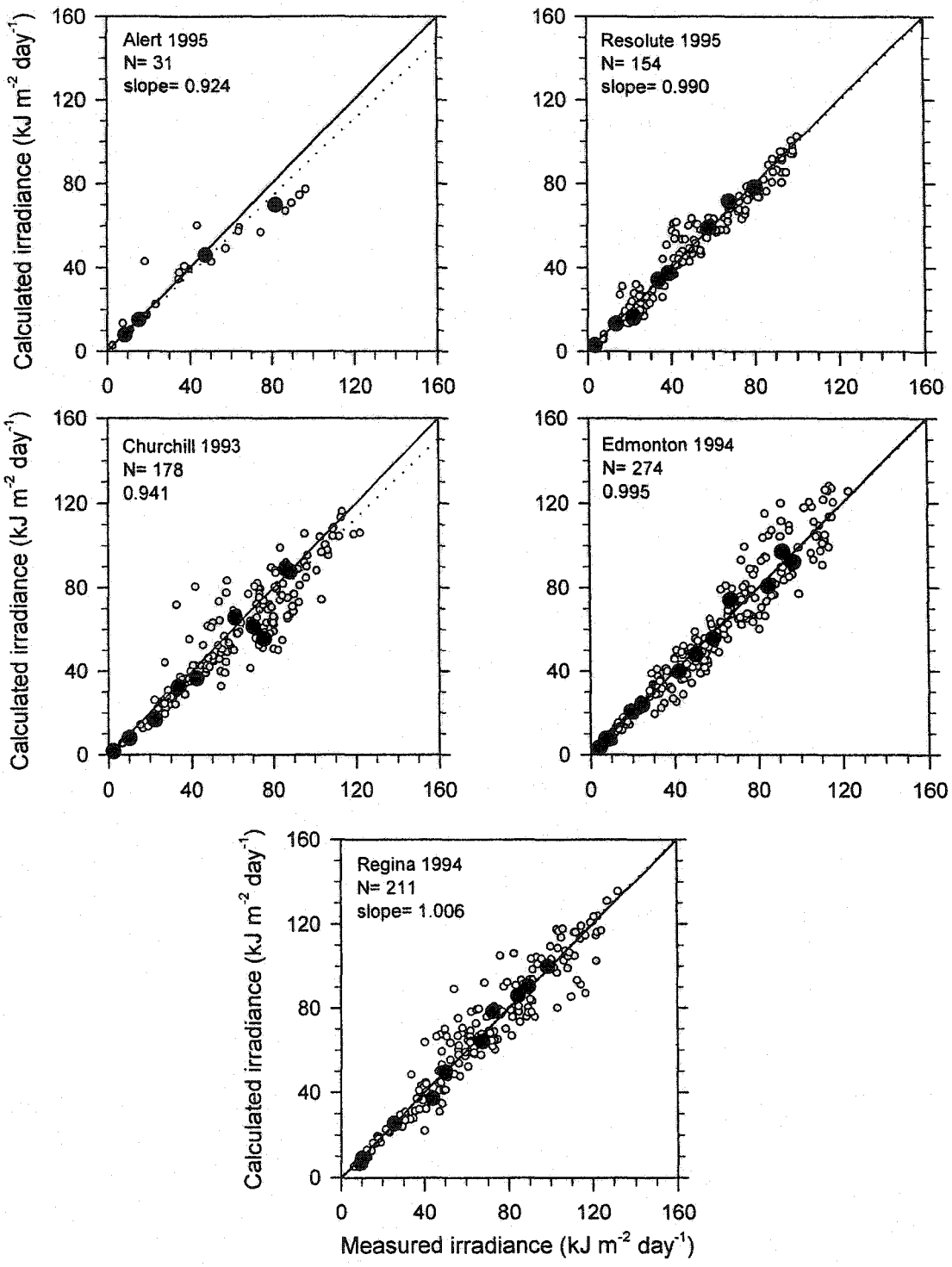

Figure 4.16a. Comparison of measured and calculated (DISORT) daily totals (white circles) and monthly averaged (black circles) irradiances at Alert, Resolute, Churchill, Edmonton and Regina, using annual values of cloud optical depth for each station. N is the number of days. The dotted lines represent linear regressions constrained to pass through the origin.

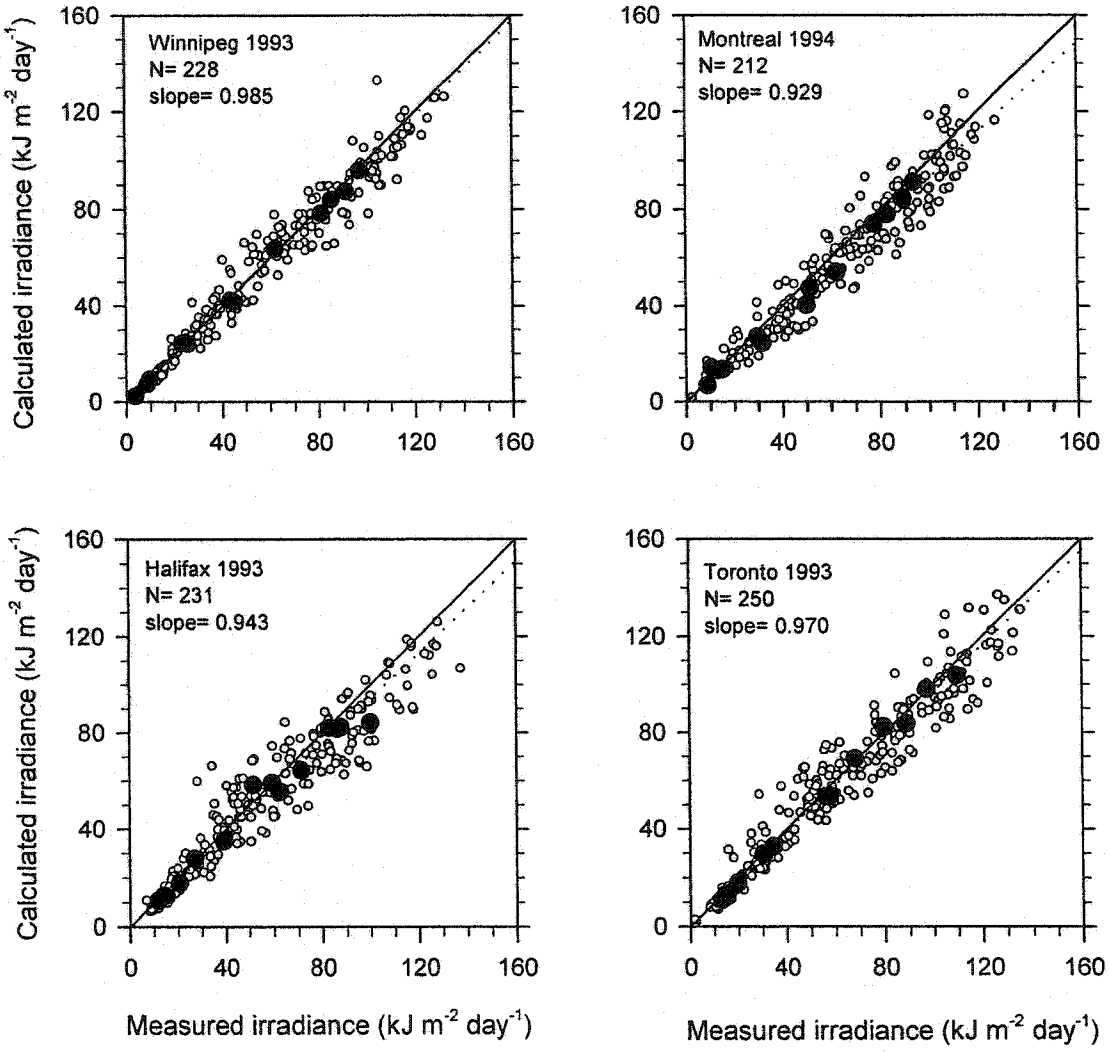

Figure 4.16b. same as Figure 4.16a but for Winnipeg, Montreal, Halifax and Toronto.

Table 4.5. Summary of delta-Eddington (DE) and DISORT 8 (D8) performance measures against measurements for daily total irradiances for the period indicated for each station. N is the number of data points and $\bar{M}$ is the mean annual measured daily total irradiance ($KJ\,m^{-2}day^{-1}$). Values of MBE and RMSE are given as percentages (italic) of $\bar{M}$. Positive MBE values indicate model overestimation.

Wavelength	Alert 1995	Resolute 1995	Churchill 1993	Edmonton 1994	Regina 1994	Winnipeg 1993	Montreal 1994	Halifax 1993	Toronto 1993
Daily total									
N	31	154	178	274	211	228	212	231	250
$\bar{M}$	38.26	51.28	60.32	49.66	63.23	54.14	62.66	54.80	60.15
%MBE (DE)	*-0.45*	*3.13*	*-0.47*	*5.55*	*6.30*	*3.73*	*-1.19*	*-1.10*	*1.92*
%MBE (D8)	*-7.59*	*-0.98*	*-5.95*	*-0.50*	*0.57*	*-1.52*	*-7.07*	*-5.75*	*-2.96*
%RMSE (DE)	*23.24*	*11.37*	*18.09*	*19.21*	*16.58*	*13.34*	*14.33*	*17.76*	*14.78*
%RMSE (D8)	*25.67*	*11.30*	*18.78*	*15.88*	*14.25*	*12.60*	*15.18*	*18.94*	*14.61*
Monthly average									
N	4	8	10	12	10	12	12	12	12
$\bar{M}$	38.27	39.76	49.09	46.33	55.02	47.79	50.17	52.18	55.81
%MBE (DE)	*-2.18*	*2.80*	*-1.85*	*5.10*	*5.30*	*3.25*	*-1.50*	*-1.20*	*1.77*
%MBE (D8)	*-9.02*	*-1.51*	*-7.31*	*0.91*	*-0.49*	*-2.00*	*-7.53*	*-5.88*	*-3.21*
%RMSE (DE)	*10.64*	*8.13*	*14.15*	*10.41*	*9.37*	*5.34*	*6.79*	*9.28*	*4.88*
%RMSE (D8)	*15.14*	*6.55*	*15.23*	*7.49*	*5.86*	*3.79*	*10.00*	*11.59*	*5.35*

values are slightly better than the DISORT values with relative MBE up to 9% and RMSE values about 26%.

The above comparisons show that the delta-Eddington algorithm is adequate for estimating surface broadband UV-B irradiance under all sky conditions from mid-latitudes to the arctic. The method has the important advantage of being approximately 1000 times computationally faster than the DISORT algorithm. Since cloudy sky irradiances are not very sensitive to uncertainty in τ_c three sets of irradiances were calculated and compared. There are daily total and monthly averaged broadband irradiances estimated from annual τ_c for each station, estimates using one τ_c for each station and estimates using one τ_c for all (or most) stations. This is done only for delta-Eddington algorithm. Model irradiances produced from the three different sets of τ_c values are discussed below.

4.4.2.1.1 Model calculations using station τ_c values for each year

In Figures 4.17, measured and calculated (delta-Eddington) daily and monthly mean daily broadband irradiances for all years of available data were compared using annual τ_c values determined for each station (Table 3.4). Agreement is good. Relative MBE is less than 1% at Alert, Resolute, Halifax and Toronto (Table 4.6). At Churchill, Edmonton, Regina, Winnipeg, and Montreal the relative MBE range from 1 to 6%. The model overestimates the surface irradiance at Alert, Churchill, Edmonton, Regina, Winnipeg and Halifax by 0.1-6% and underestimates by less than 1% at Resolute, Montreal and Toronto. RMSE values are between 13 and 24% of the mean daily

measured irradiance, decreasing to between 2% and 14% for monthly averages depending on the averaging period at each station (Table 4.6). The MBE and RMSE values for daily total UV-B irradiance are similar to those obtained by Davies *et al.* (2000) at Edmonton, Winnipeg, Halifax and Toronto. Appendix E contains all comparisons between measured and calculated daily total and monthly averages broadband irradiances for individual years for each station.

An example of the daily variation of measured and calculated irradiances is shown in Figure 4.18 for Halifax (1993-1996). This station was chosen because there were no missing months for the period. Model irradiances follow the variation of measurements well with little bias. The calculated irradiances are between ±15% of measurements. Variation between measured and calculated surface irradiances possibly reflect daily variation in τ_c. Also, measurements are affected by changing cloud amounts over periods of minutes to hours and generally the highest irradiance is measured during partly cloudy conditions due to scattering from cloud sides when the sun is not obscured (Mims and Frederick, 1994; Estupinan *et al.*, 1996; Schafer *et al.*, 1996). This could increase measurements on some days and would not be captured by the model.

4.4.2.1.2 Model calculations using pooled τ_c values for each station

Calculations based on station τ_c also show good agreement with the surface measurements as shown in Figures 4.19. The results are very similar to the calculations with annual τ_c. The surface flux is slightly underestimated (by 0.9 to 3%) at Resolute Bay, Montreal and Toronto and overestimated (by 0.8 to 6%) at other stations (Table 4.6). RMSE is between 15-19% for the daily irradiances and between 2-13% for the

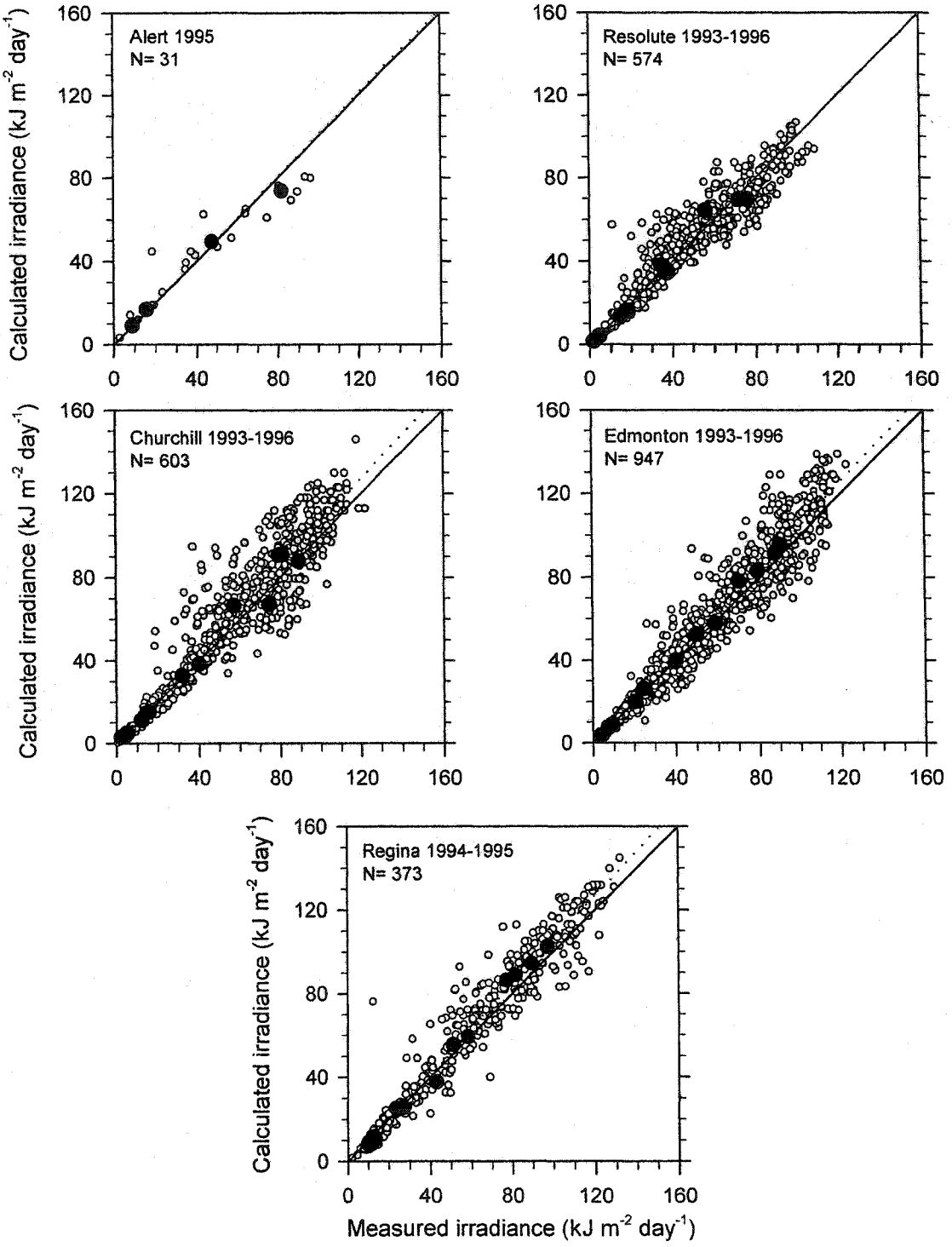

Figure 4.17a. Comparison of measured and calculated (delta-Eddington) daily totals (white circles) and monthly averaged (black circles) irradiances at Alert, Resolute, Churchill, Edmonton and Regina, using annual values of cloud optical depth for each station. N is the number of days. The dotted lines represent linear regressions constrained to pass through the origin.

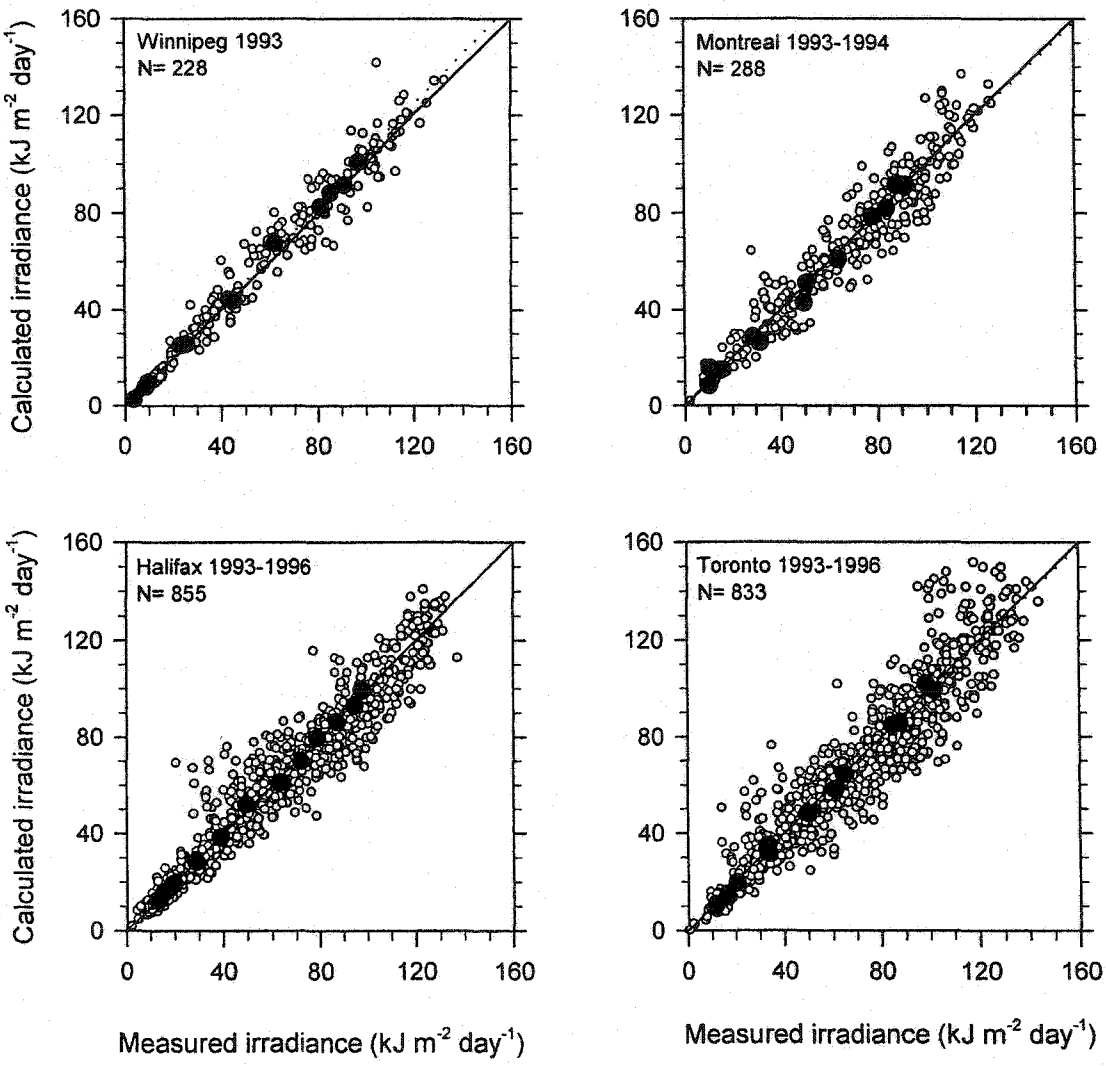

Figure 4.17b. same as Figure 4.17a but for Winnipeg, Montreal, Halifax and Toronto.

Table 4.6. Summary of delta-Eddington performance measures for daily total and monthly average irradiances using annual τ_c, station τ_c and pooled τ_c. N is the number of data points and $\bar{M}$ is the mean daily measured broadband irradiance ($kJm^{-2}day^{-1}$). Values of MBE and RMSE are given both in $kJm^{-2}day^{-1}$ and in percentages (italic) of $\bar{M}$. Positive MBE values indicate model overestimation.

Cloud optical depth τ_c	Alert	Resolute	Churchill	Edmonton	Regina	Winnipeg	Montreal	Halifax	Toronto
Annual τ_c									
Daily total									
N	31	574	603	947	373	228	288	855	833
$\bar{M}$	36.33	47.67	60.28	51.50	58.87	54.35	66.08	57.62	66.05
MBE	0.36	- 0.10	3.48	2.43	3.29	2.02	- 0.67	0.06	- 0.59
%MBE	*0.99*	*- 0.21*	*5.78*	*4.73*	*5.59*	*3.72*	*- 1.02*	*0.10*	*- 0.89*
RMSE	8.54	8.71	12.02	9.43	10.41	7.24	9.55	9.04	11.54
%RMSE	*23.52*	*18.27*	*19.95*	*18.31*	*17.69*	*13.32*	*14.45*	*15.69*	*17.47*
Slope	1.010	0.998	1.058	1.047	1.056	1.037	0.990	1.001	0.991
Monthly average									
N	4	9	12	12	12	12	12	12	12
$\bar{M}$	38.27	34.92	40.85	44.99	48.63	47.79	50.16	54.68	55.17
MBE	- 0.83	- 0.29	1.86	1.99	1.86	1.55	- 0.75	0.05	- 0.73
%MBE	*- 2.18*	*- 0.82*	*4.57*	*4.42*	*3.82*	*3.25*	*- 1.49*	*0.08*	*- 1.33*
RMSE	4.07	3.91	5.72	3.41	4.59	2.55	3.21	1.34	1.93
%RMSE	*10.64*	*11.19*	*13.99*	*7.57*	*9.44*	*5.34*	*6.40*	*2.46*	*2.60*
Slope	0.978	0.992	1.046	1.044	1.038	1.032	0.985	1.001	0.987
Station τ_c									
Daily total									
MBE		- 0.90	2.92	2.64	3.26		- 0.59	0.45	- 1.90
%MBE		- 1.89	4.84	5.12	5.54		- 0.89	0.78	- 2.88
RMSE		9.08	11.69	9.48	10.39		9.59	8.98	11.15
%RMSE		19.00	19.37	18.40	17.66		14.51	15.60	16.88
Slope		0.981	0.954	1.051	1.055		0.991	1.008	0.971

Table 4.6 (Contd).

Cloud optical depth τ_c	Alert	Resolute	Churchill	Edmonton	Regina	Winnipeg	Montreal	Halifax	Toronto
Station τ_c									
Monthly average									
MBE		- 0.88	1.49	2.16	1.83		- 0.71	0.42	- 1.84
%MBE		- 2.52	3.63	4.81	3.77		- 1.41	0.76	- 3.33
RMSE		3.87	5.39	3.56	4.56		3.23	1.36	2.35
%RMSE		11.06	13.18	7.92	9.38		6.44	2.48	4.25
Slope		0.975	1.036	1.048	1.038		0.986	1.008	0.967
Pooled τ_c									
Daily total									
MBE			0.96	3.06	2.59	1.23	0.57	- 0.75	0.36
%MBE			1.59	5.94	4.41	2.27	0.86	- 1.30	0.55
RMSE			11.38	9.55	10.21	7.12	9.56	9.05	10.93
%RMSE			18.85	18.54	17.34	13.11	14.46	15.70	16.09
Slope			1.016	1.059	1.044	1.023	1.009	0.987	1.006
Monthly average									
MBE			0.17	2.53	1.30	0.85	0.15	- 0.72	0.05
%MBE			0.41	5.62	2.66	1.78	0.30	- 1.32	0.08
RMSE			4.64	3.97	4.13	2.09	3.28	1.57	1.81
%RMSE			11.34	8.83	8.48	4.36	6.55	2.87	3.28
Slope			1.004	1.056	1.027	1.018	1.003	0.987	1.001

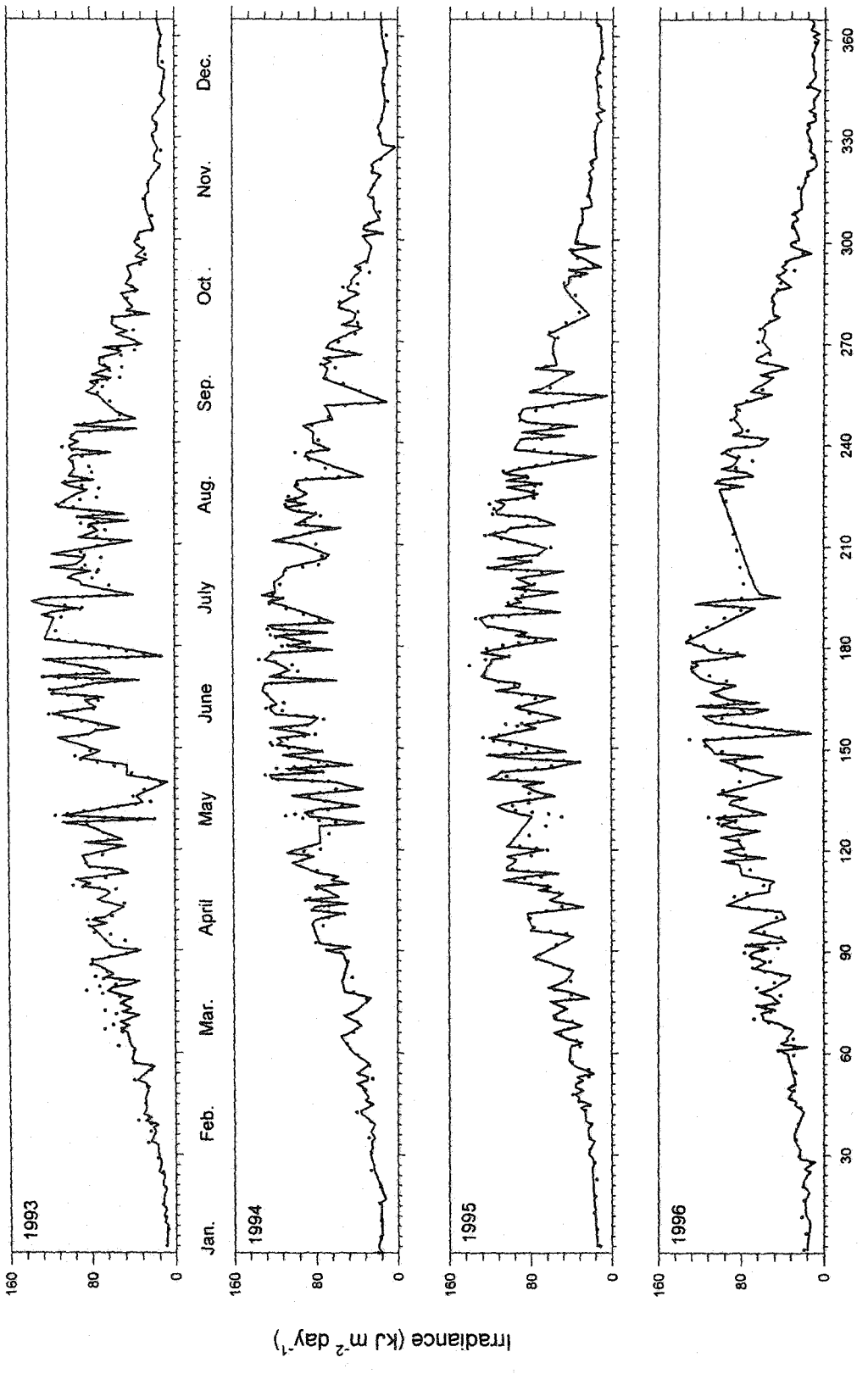

Figure 4.18. Daily total measured (solid lines) and calculated (dotted lines) broadband irradiances for Halifax (1993-1996).

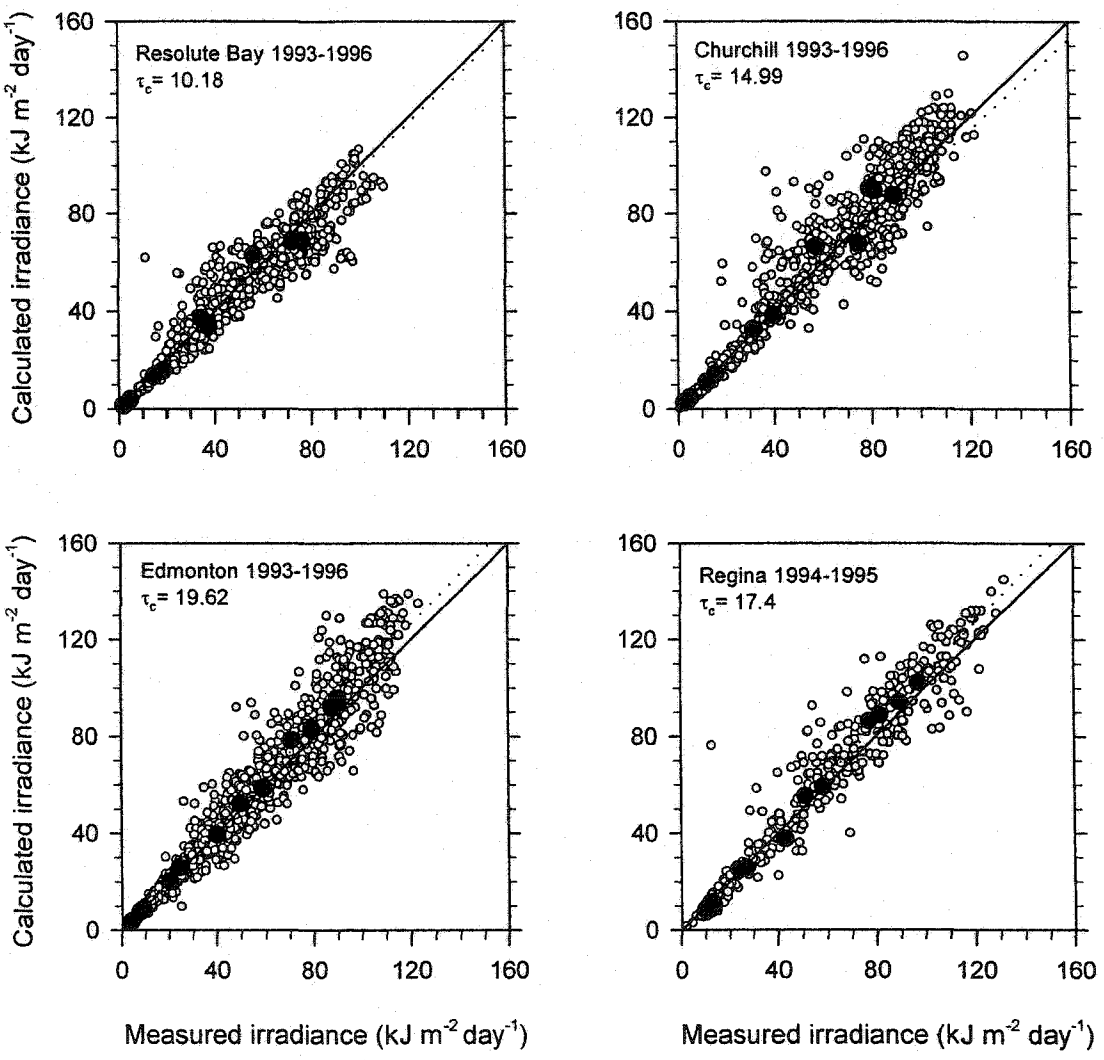

Figure 4.19a. Comparison of measured and calculated (delta-Eddington) daily totals (white circles) and monthly averaged (black circles) irradiances at Resolute Bay, Churchill, Edmonton and Regina using station cloud optical values. N is the number of days. The dotted lines represent linear regression constrained to pass through the origin.

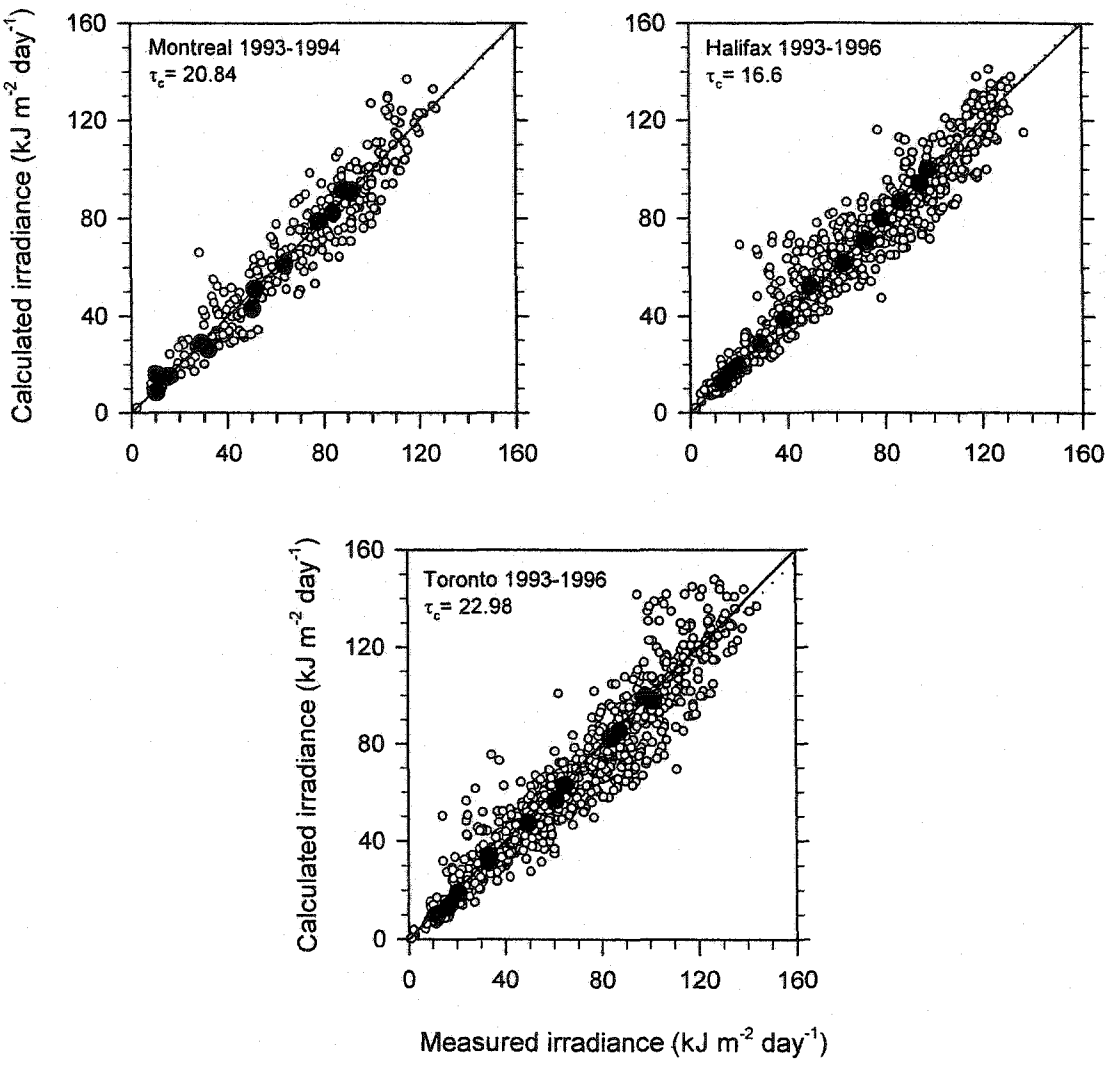

Figure 4.19b. same as Figure 4.19a but for Montreal, Halifax and Toronto.

monthly averages results. The agreement between model and measurements using station τ_c for individual years at each station is shown in Appendix F.

4.4.2.1.3 Model calculations using a pooled τ_c value

Values of τ_c for all stations were combined to produce one median τ_c, which was then used to calculate irradiances at each station. Alert was excluded because it had a much smaller τ_c (4.98) and little data (31 days only for four summer months). The effective median τ_c (17.07) was found to be too large for Resolute Bay and attenuated the model surface irradiances too much.

On the basis of this poor agreement between measured and calculated irradiances when using the effective median τ_c to generate fluxes for the arctic stations (not shown), a median τ_c of 18.7 was calculated for the pooled subarctic and midlatitudes stations. The use of this fixed τ_c to generate fluxes did not degrade the irradiance amount at all stations (subarctic and midlatitudes) as shown in Figures 4.20 and the scatter plots are similar to those of Figures 4.17 and 4.19 with MBE less than 6% and RMSE between 13-19%. The average difference in irradiance is less than 0.2% when comparing to irradiance calculations using station τ_c values for each year. Appendix G has all the comparisons between model and measured irradiances for individual years for subarctic and all midlatitudes stations using the fixed median τ_c.

The results of Figures 4.20 suggest that a τ_c value of 18.7 is adequate for subarctic and midlatitudes stations. This obviates the need for extensive computation to retrieve τ_c for each station and year.

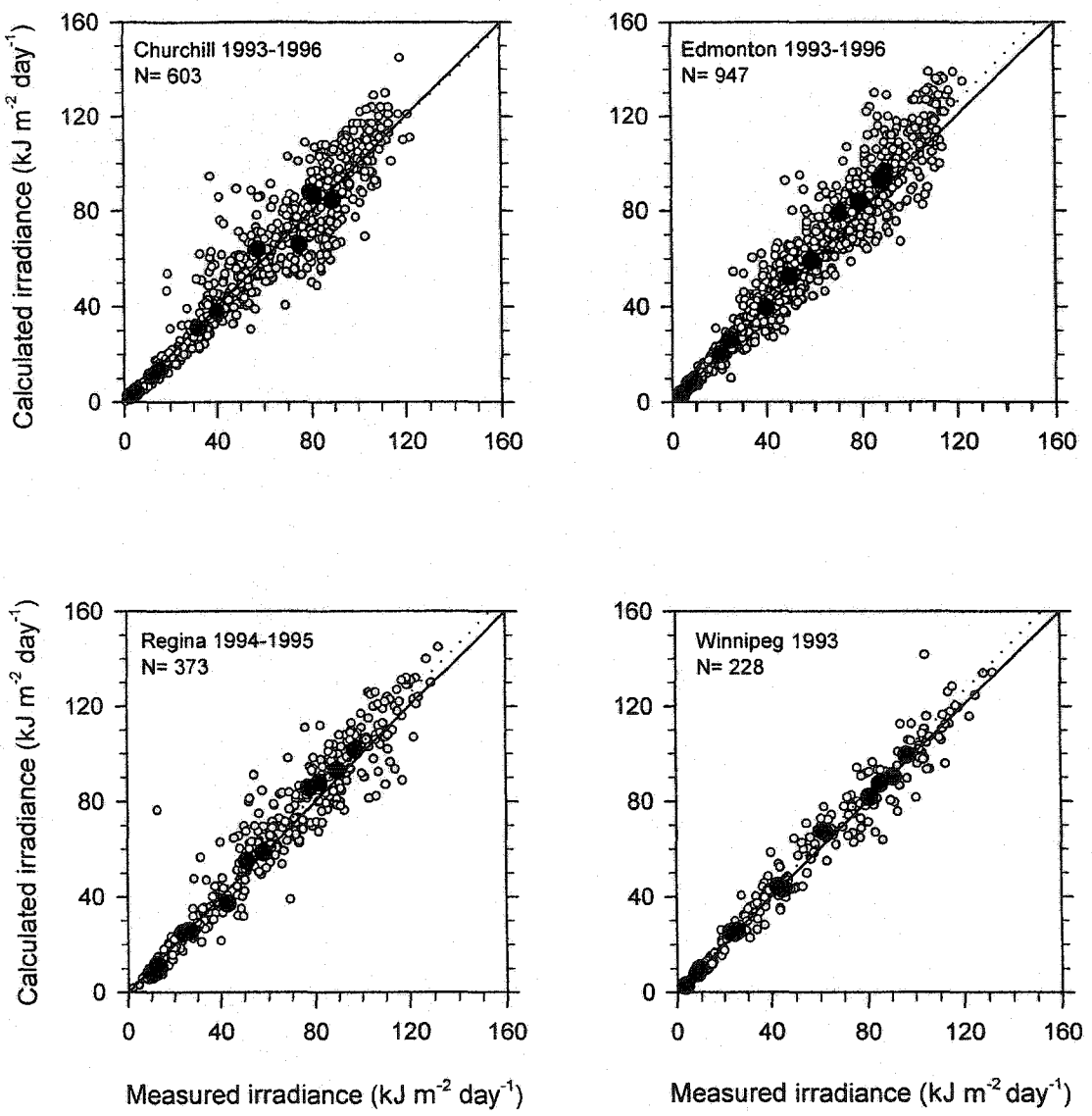

Figure 4.20a. Comparison of measured and delta-Eddington calculated daily (white circles) and monthly (black circles) irradiances at Churchill, Edmonton, Regina and Winnipeg, using a pooled cloud optical depth (18.69). N is the number of days. The dotted lines represent linear regression constrained to pass through the origin.

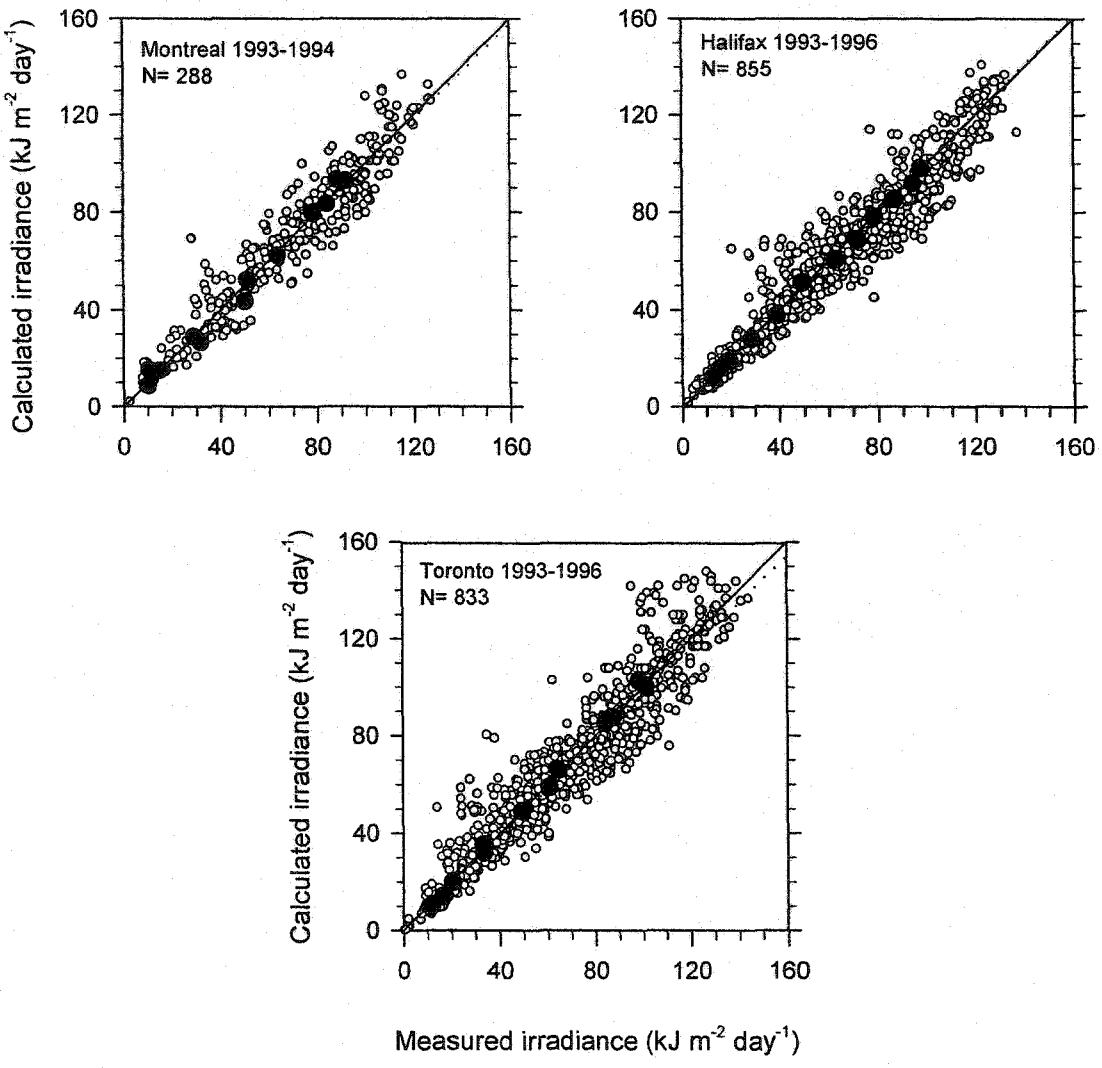

Figure 4.20b. same as Figure 4.20a but for Montreal, Halifax and Toronto.

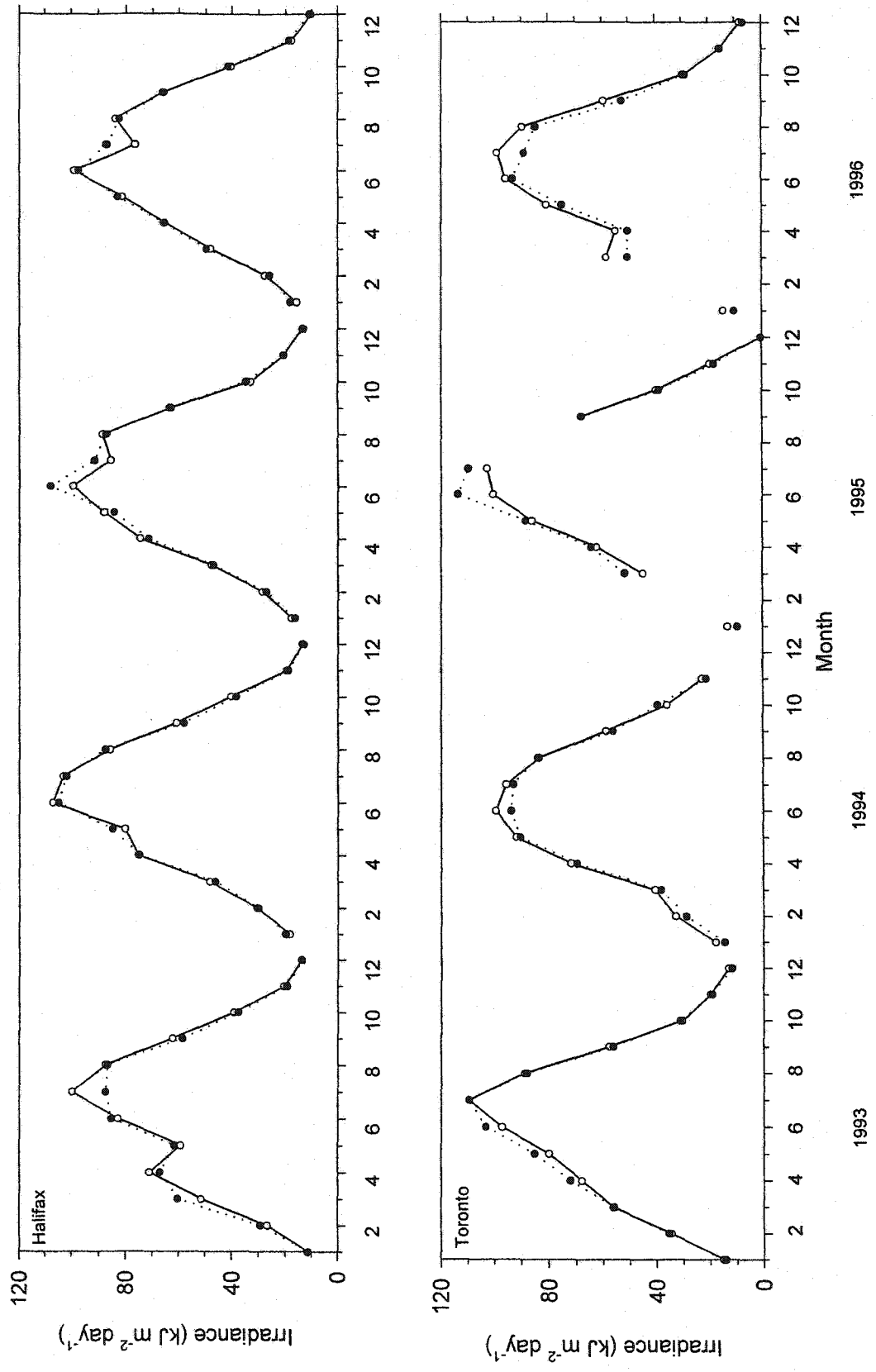

Figure 4.21. Monthly averaged broadband irradiances measured (line and white circles) and calculated by delta-Eddington model (dotted and black circles) for Halifax and Toronto for years 1993-1996.

4.4.2.2 Monthly averaged irradiance

The model performance of monthly averaged irradiance is shown in Figure 4.21 for Toronto and Halifax for 1993-1996 using annual τ_c values for each station. Similar plots for all other stations are shown in Appendix H. Agreement between calculations and measurements are generally very good at all seasons. Irradiances compare mainly to within 15%. Largest differences occur in a few summer months but they are small and change in sign from year to year.

4.5 Comparisons of two different aerosol loadings

Two urban aerosols loading are used in chapter 3 to calculate τ_c for Montreal (1993 and 1994) and Toronto (1993 and 1995), for a 50-km visibility aerosol model (light aerosol) and a 36.5 km (average of 50 km and 23 km models) model (heavier aerosol). Fluxes from the two urban aerosol loadings are compared with measurements at both stations. For Montreal there is better agreement between the light aerosol model and measurements with MBE less than 2.5% for both daily total and monthly average broadband irradiances (Table 4.7). For Toronto, the heavier aerosol model shows better agreement with MBE less than 1% and less than 2% for the daily total and monthly average, respectively. Table 4.6 shows that heavy aerosol reduces the daily surface irradiance by 2-7%. This agrees well with the findings of Chertock *et al.* (1992) who found that aerosols could reduce daily solar irradiance up to 5%.

Table 4.7. Comparisons between measured and calculated (delta-Eddington) daily total and monthly average broadband irradiances for two aerosols loading. N is the number of data points and $\bar{M}$ is the mean measured irradiance ($kJ\,m^{-2}\,day^{-1}$). Values of MBE and RMSE are given both in ($kJ\,m^{-2}\,day^{-1}$) and in percentages (italic) of $\bar{M}$. Positive MBE values indicate model overestimation.

Aerosol loading	Montreal 1993	Montreal 1994	Toronto 1993	Toronto 1995
Light aerosol				
Daily total				
N	76	212	250	153
$\bar{M}$	75.72	62.92	60.34	75.20
MBE	- 0.47	- 0.76	1.17	4.72
%MBE	*- 0.63*	*- 1.20*	*1.94*	*6.28*
RMSE	11.04	9.00	8.91	13.90
%RMSE	*14.58*	*14.31*	*14.76*	*18.48*
Slope	0.994	0.998	1.019	1.063
Monthly average				
N	8	12	12	10
$\bar{M}$	58.15	53.78	59.53	58.16
MBE	0.79	- 1.27	1.14	3.18
%MBE	*1.35*	*- 2.36*	*1.92*	*5.47*
RMSE	4.35	3.22	2.84	5.59
%RMSE	*7.49*	*6.00*	*4.77*	*9.61*
Slope	1.014	0.976	1.019	1.055
Heavy aerosol				
Daily total				
MBE	- 1.77	- 2.01	0.05	- 0.65
%MBE	*- 2.34*	*- 3.20*	*0.08*	*- 0.86*
RMSE	11.15	8.80	8.62	11.50
%RMSE	*14.72*	*13.99*	*14.28*	*15.29*
Slope	0.977	0.968	1.001	0.991

Table 4.7 (Contd).

Aerosol loading	Montreal 1993	Montreal 1994	Toronto 1993	Toronto 1995
Heavy aerosol				
Monthly average				
MBE	- 0.40	- 2.39	- 0.01	- 0.99
%MBE	*- 0.70*	*- 4.45*	*- 0.01*	*- 1.70*
RMSE	4.24	3.73	2.57	3.26
%RMSE	*7.30*	*6.93*	*4.31*	*5.61*
Slope	0.993	0.956	0.999	0.983

CHAPTER 5

Comparisons with the CCRS satellite model results

5.1 Introduction

UV-B irradiance can be estimated from surface meteorological data, as in the present study, or from satellite measurements. The performance of the McMaster model is further assessed by comparing model broadband irradiances (290-320 nm) with those from the Canada Centre for Remote Sensing (CCRS) Meteor-3/TOMS satellite based-model (Li *et al.*, 2000).

5.2 The CCRS satellite based method

The TOMS instrument on board the Meteor 3 satellite between 1991 and 1994 measured the incoming solar irradiance and bidirectional reflected radiance[13] at the TOA at three ozone-sensitive (312.35, 317.40, and 331.13 nm) and three insensitive wavelengths (339.73, 360, and 380.16 nm), all measured with a 1 nm resolution. Since atmospheric absorption at these longer wavelengths is weak, the reflected radiance represents the Rayleigh scattering, Mie scattering (aerosol and cloud particles) and surface reflection.

The CCRS satellite algorithm for retrieving surface net UV-B irradiance was developed by Li *et al.* (2000) using a simplified radiative transfer model and validated

[13] Bidirectional reflected radiance is the backscattered solar flux in a particular direction which depends on both the solar and the satellite angles where the radiation takes two-way path through the atmosphere.

against the DISORT model of Wang and Lenoble (1994). The algorithm was also tested against broadband (290-320 nm) Brewer measurements at Edmonton, Regina, Winnipeg, Saturna Island, Halifax and Toronto between 1992 and 1994 (Wang *et al.*, 2000).

The algorithm is based on a linear relationship between TOA albedo at 360 nm and surface net (absorbed) UV-B irradiance. TOA albedos were calculated from Meteor-3 TOMS reflected radiance measurements at 360 nm following spectral and angular corrections. Bidirectional reflectance and albedo are defined respectively as:

$$a(\theta_0,\theta,\phi) = \frac{\pi L(\theta_0,\theta,\phi)}{S_0 \cos\theta_0}, \tag{5.1}$$

$$\alpha(\theta_0) = \frac{F\uparrow(\theta_0)}{S_0 \cos\theta_0}, \tag{5.2}$$

where S_0 is the extraterrestrial solar irradiance at an incident angle θ_0, L is the reflected radiance measured by the satellite at a satellite angle θ, and ϕ is the azimuth angle between the sun and satellite, and $F\uparrow(\theta_0)$ is the reflected flux. The angular dependence model (ADM) is used to derive albedos from radiances (Li, 1996) and ADM is defined by:

$$R(\theta_0,\theta,\phi) = \frac{\pi L(\theta_0,\theta,\phi)}{F\uparrow(\theta_0)}. \tag{5.3}$$

Using Eqs. (5.1) and (5.3), Eq. (5.2) can be rewritten as:

$$\alpha(\theta_0) = \frac{a(\theta_0,\theta,\phi)}{R(\theta_0,\theta,\phi)}. \tag{5.4}$$

There are 12 ERBE ADMs corresponding to 12 scene types with four cloud classes over different surface types. Cloud classification required to apply the ERBE ADMs are part

of the TOMS data. These are determined by cloud cover percentages (clear, 0-5%; partly cloudy 5-50%; mostly cloudy, 50-95%; and overcast, >95%) (Li, 1996; Wang *et al.*, 2000).

The algorithm is mainly used to provide broadband estimates of surface UV-B irradiance (Wang *et al.*, 2000). The atmosphere is divided into three layers: the top layer is mainly ozone, the middle layer contains air molecules, cloud, and aerosol particles and the third layer is the surface. The surface net UV-B irradiance is given by:

$$UVB_{net} = (1 - 0.196 - 0.798\alpha_{360} - A_2)CT_{03}S_0 \cos\theta, \tag{5.5}$$

$$C = \frac{(1-\alpha_s)}{(1-\alpha_s) + A_2^*\alpha_s}, \tag{5.6}$$

where α_{360} is the TOA albedo for the earth-atmosphere system at 360 nm, C accounts for multiple reflection and aerosol absorption, α_s is surface albedo, A_2 and A_2^* represent aerosol absorption for the downwelling and upwelling UV-B irradiance, respectively, and they are parameterized following the Beer's law. T_{03} is the band-mean transmittance due to ozone absorption and is calculated by adding a series of exponential functions with constant ozone coefficients and weights shown in Table 1 of Li *et al.* (2000).

Eq. (5.5) requires the extraterrestrial solar irradiance, total ozone amount, TOA albedo, aerosol optical depth and single scattering albedo, and surface albedo. Therefore, surface UV-B irradiance can be estimated without the knowledge of cloud optical depth. The extraterrestrial irradiance was taken from Fröhlich and London (1986). Total ozone amount was taken from the TOMS data set. Surface albedo was assumed to be 0.04 for Toronto and 0.03 for other stations. Aerosol optical depth τ_a measurements were

available for Toronto (Wang *et al.*, 2000) and a value of 0.31 was substituted for missing days. For Winnipeg and Edmonton τ_a was assumed to be 0.2, and 0.1 for the remaining stations. Aerosol single scattering albedo was assumed to be 0.95 for all stations.

The transmitted surface UV-B irradiance is given by $UVB_{net}/(1-\alpha_s)$. These calculated transmitted spot values were compared with Brewer measurements for the same satellite measurement time. In the comparison three criteria were taken under consideration. Firstly, days with snow cover were neglected since the differentiation between cloud cover and snow surfaces is often difficult to detect in a satellite image. This is due to the similarity of their spectral reflectance in the solar and UV channels (Gautier *et al.*, 1993). Secondly, satellite and Brewer measurements were matched in time, zenith angle and space. Time difference between satellite and Brewer measurement was constrained to less than 7 min, and difference in their zenith angles should be less than 1°. Also the location of the ground station should be within the center of the satellite pixel with the distance less than 30 and 50 km for cloudy and clear sky conditions, respectively.

5.3 Comparison of the McMaster model and CCRS model results

The Meteor 3 reflectance measurements were made at various local times with different solar angles with mostly one value per day, up to a maximum of two values per day that matched the Brewer time (P. Tsering, personal communication, 2001). Each CCRS model estimate is compared with a simultaneous Brewer measurement and a calculation from the McMaster model using both the delta-Eddington and DISORT methods. There is a small difference in the spectral integration range used by CCRS and

the present study. CCRS presents irradiances integrated over the 290-320.5 nm waveband in 0.5 nm steps while the present study results were integrated in 1 nm steps over the 290-320 nm range. In this chapter, both models are compared with Brewer measurements integrated to the upper wavelength limit appropriate to the model.

Comparison of the McMaster model broadband irradiances and the simultaneous satellite-based results with Brewer measurements made at six stations (Edmonton in 1993 and 1994, Regina in 1994, Winnipeg in 1993, Montreal in 1993 and 1994, Halifax in 1993 and 1994, Toronto in 1993 and 1994) are presented in Figure 5.1. They represent 10 station years of data mainly between May and September, with 605 data points in total. Generally, the agreement between the three is visually good.

Table 5.2 provides performance statistics for both individual stations and pooled data. For the pooled data, the McMaster model with the delta-Eddington and DISORT methods and the CCRS model underestimate Brewer measurements by 0.3%, 6% and 3% of the mean measured irradiance. For the individual stations the relative MBE values range between ±6% for the delta-Eddington method, between –10% and 0.2% for the DISORT method and between –11% and 0.3% for the satellite-based method. These irradiance differences are smaller than differences between near simultaneous measurements made with different ground instruments (±10%) (McKenzie *et al.*, 1993; Bais *et al.*, 2001). However, the relative RMSE for the pooled data is similar (26% and 29%) for the two methods. For the individual stations, relative RMSE range from 24 to 34% and from 20 to 40% for the McMaster model and satellite-based method, respectively.

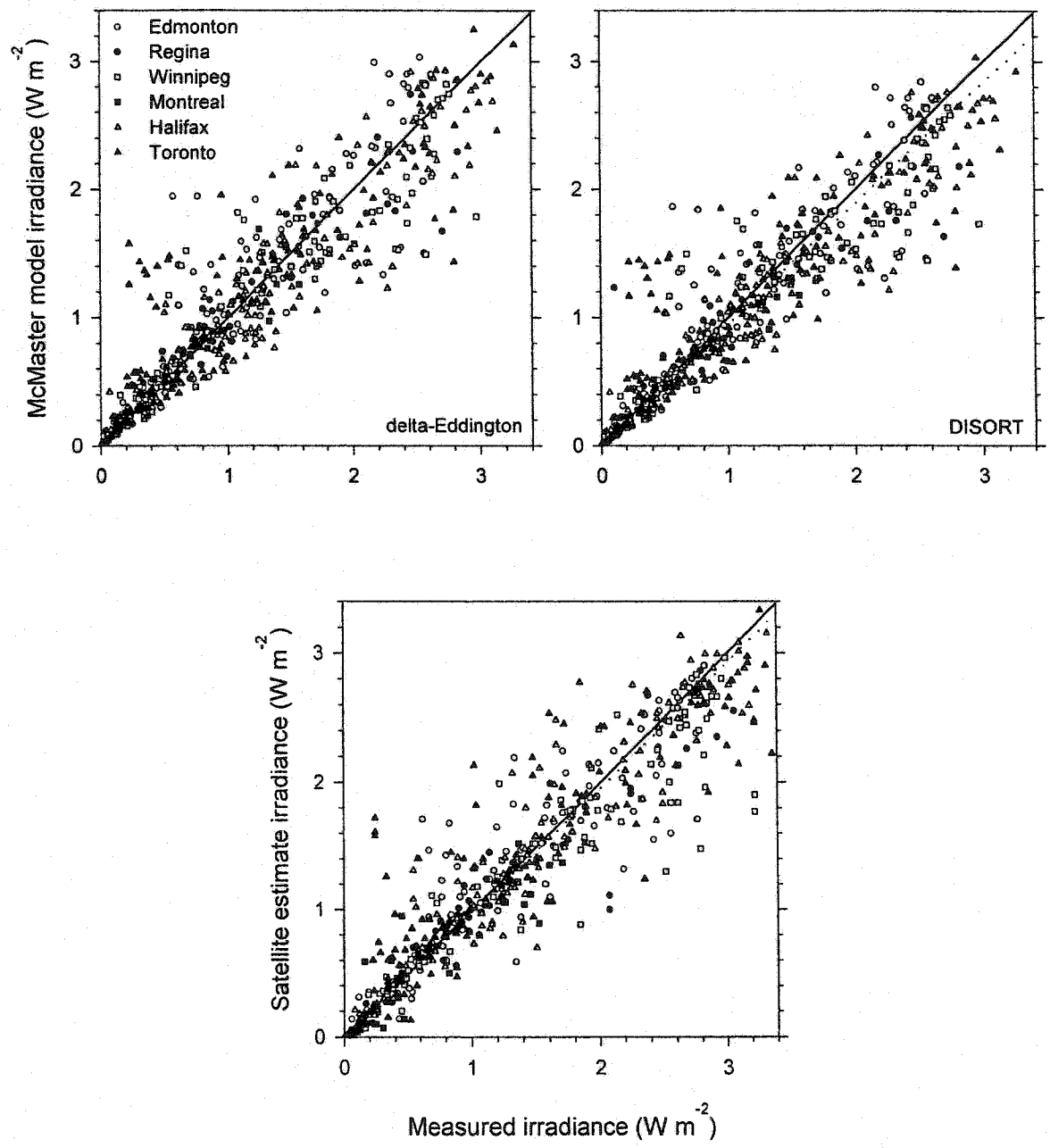

Figure 5.1. Comparison between McMaster model calculations, CCRS satellite-based model calculations and measured UV-B irradiances for all sky conditions for Edmonton, Regina, Winnipeg, Montreal, Halifax and Toronto. The dotted lines represent linear regressions constrained to pass through the oigin. A different symbol represents data for each station.

Table 5.1. Summary of the McMaster model and satellite-based method performance measures against Brewer measurements for broadband irradiances (290-320 nm) for each satellite time for the period indicated for each station. N is the number of data points and $\bar{M}$ is the mean annual measured daily irradiance ($W\ m^{-2}$). Values of MBE and RMSE are given both in $W\ m^{-2}$ and in percentages (italic) of $\bar{M}$. Positive MBE values indicate present model or satellite method overestimation.

Irradiance results	Edmonton 1993-1994	Regina 1994	Winnipeg 1993	Montreal 1993-1994	Halifax 1993-1994	Toronto 1993-1994	Pooled data
McMaster model using delta-Eddington method							
N	115	48	88	20	159	175	605
$\bar{M}$	1.16	1.20	1.54	0.66	1.19	1.13	1.21
MBE	0.07	- 0.01	- 0.08	0.01	- 0.07	0.04	- 0.0035
%MBE	*6.22*	*- 0.79*	*- 4.97*	*2.13*	*- 5.66*	*3.64*	*- 0.29*
RMSE	0.37	0.30	0.37	0.17	0.29	0.38	0.34
%RMSE	*31.73*	*25.05*	*24.25*	*26.53*	*24.50*	*33.46*	*28.59*
Slope	1.062	0.992	0.950	1.021	0.943	1.036	0.997
McMaster model using DISORT method							
MBE	0.002	- 0.08	- 0.16	- 0.04	- 0.12	- 0.03	- 0.07
%MBE	*0.15*	*- 6.62*	*- 10.06*	*- 5.78*	*- 10.28*	*- 2.38*	*- 5.80*
RMSE	0.34	0.31	0.40	0.19	0.31	0.34	0.35
%RMSE	*28.94*	*25.72*	*25.88*	*27.76*	*25.93*	*33.85*	*28.91*
Slope	1.002	0.934	0.899	0.942	0.897	0.976	0.942
Satellite method							
$\bar{M}$	1.26	1.31	1.68	0.72	1.30	1.23	1.31
MBE	0.003	- 0.07	- 0.16	- 0.08	- 0.02	0.001	- 0.04
%MBE	*0.26*	*- 5.14*	*- 9.75*	*- 10.86*	*- 1.40*	*0.06*	*- 2.73*
RMSE	0.32	0.29	0.40	0.29	0.27	0.38	0.34
%RMSE	*25.49*	*22.30*	*24.11*	*40.05*	*20.45*	*31.03*	*25.76*
Slope	1.003	0.949	0.903	0.891	0.986	1.001	0.973

The differences in McMaster model and satellite estimates of UV-B irradiance are well within the uncertainties in the model input data and Brewer measurements. These small differences cannot be explained because it could be due to uncertainties in both the surface measurements and the input parameters of the two methods. The satellite method is different because the TOMS instrument field of view is 50×50 km^2 in the nadir direction, increasing to 150×200 km^2 in the extreme off-nadir direction, while the Brewer instrument and the McMaster model are representing irradiance for a much smaller area. Therefore the values of clouds, aerosols and surface albedo detected by satellite may not represent the conditions at a station because these values are averaged over the larger area. However, the differences between surface UV-B irradiances retrieved from the visible channel of NOAA/AVHRR satellite acquired in Canada in 1994 and the Brewer measurements at the same Canadian stations were insignificant due to the smaller AVHRR pixel size which changes from a circle of 1.1 km diameter at nadir to an ellipse (2.5 km × 6.8 km) at larger scanning angle (Wang *et al.*, 2000).

This is the first study comparing satellite-based model results of UV-B irradiance with ground based model results. Although the two model forms have little in common, surprisingly, they perform almost identically which further support the accuracy of McMaster model. Since the satellite-based model cannot produce calculations throughout the day, the true usefulness of the McMaster model is apparent. The delta-Eddington method is especially appealing since it is computationally efficient compared with DISORT 8, it gives a complete temporal record and it is cheap and easy to use relative to Brewer measurements.

CHAPTER 6

Summary and Conclusions

The objectives of this study were 1) to provide a numerical model for estimating spectral and broadband UV-B irradiances for Canadian conditions; 2) to determine cloud optical depth which is essential to radiative transfer calculations; 3) to examine the relative performance of the delta-Eddington and DISORT 8 algorithms and validate model results with Brewer spectrophotometer measurements; and 4) to compare model irradiance results with simultaneous results from a satellite-based method.

In the first part of the thesis, a numerical model to estimate spectral and broadband UV-B irradiances at the surface is presented. Irradiances for all sky conditions were obtained by linearly weighting calculated clear and overcast sky irradiances with cloud amount. Irradiances were calculated from either the delta-Eddington or the DISORT 8 solutions of the radiative transfer equation at 1 nm spectral intervals. The model is physically based can be employed to calculate irradiances anywhere given daily measurements of total ozone and snow depth, and hourly cloud cover observations.

In the second part, methods for determining cloud optical properties were presented. Mie theory shows that cloud droplets scatter UV-B irradiance uniformly over the UV-B spectral range. Broadband values of cloud single scattering albedo ω_c and

asymmetry factor g_c were calculated from Mie theory for two equivalent radii; $7\mu m$ for arctic stations and $10\mu m$ for midlatitude and subarctic stations. Broadband cloud optical depths τ_c were then calculated iteratively from overcast irradiance measurements for snow free cases. τ_c values calculated by the delta-Eddington and DISORT methods are similar. This implies the broadband fluxes from the two methods must also be close. Mean τ_c values are similar to those obtained by other researchers for the global solar radiation waveband. Median τ_c was chosen as the best measure of central tendency. Values were between 5-15 for arctic and subarctic stations and increased to between 17-28 for the midlatitude stations.

Sensitivity analyses were made with model calculations for a single cloudy layer of various τ_c values to examine the accuracy of delta-Eddington in calculating the transmitted broadband UV-B irradiances under overcast conditions and to investigate the effect of using two different drop sizes ($r_e = 7\mu m$ and $r_e = 10\mu m$) on the transmitted flux.

The significant contributions from Chapter 3 are as follows:

- The retrieved values of τ_c did not show geographic variations except for smaller values in the arctic.
- Frequency distributions of τ_c are well fitted by the gamma distributions as found by Barker et al. (1998) for retrieved τ_c values for the whole solar spectrum.
- Changing the cloud altitude did not have effect in the retrieved τ_c values.

- Through comparisons with DISORT 8 results, the delta-Eddington method is unsuitable for calculating direct and diffuse irradiance components but is often satisfactory for global (direct +diffuse) broadband irradiances. Therefore, it is also suitable for estimating τ_c.
- Transmitted UV-B irradiances decrease with increasing r_e.

In the third part of the thesis, three comparisons were performed. First, model calculations of spectral and broadband irradiances from the delta-Eddington and DISORT 8 methods were compared for both daily totals and monthly averages for all sky conditions at four stations (Resolute, Churchill, Winnipeg and Toronto). Second, model calculations from both methods were validated with Brewer measurements for one year of data for all nine stations. The most important findings are:

- The delta-Eddington method produces daily total spectral irradiances for all sky conditions, which are generally 2-11% larger than those from the DISORT 8 method. The fractional overestimation by the delta-Eddington method decreases as wavelength increases. Therefore, the delta-Eddington irradiances are acceptable for wavelengths ≥ 305 nm.
- The delta-Eddington method is unsuitable for instantaneous spectral values for different times in the day below 305 nm where ozone absorption is high. At longer wavelengths its performance varies significantly with solar zenith angle and cloudiness. For clear skies, the delta-Eddington method always overestimates irradiances at all sun angles

with the error increasing, as the solar zenith angle increases. For cloudy skies the errors are much smaller.

- The delta-Eddington method performs very well for broadband calculations for both daily total and monthly averaged irradiances.
- Comparison of the delta-Eddington and DISORT spectral estimates with measurements indicate uncertainties in the Brewer measurements at wavelengths < 305 nm.
- At wavelengths ≥ 305 nm better agreement between the delta-Eddington-Brewer comparison than the DISORT 8-Brewer comparison suggests systematic overestimation by the Brewer spectrophotometers. This might indicate that the 6% increase due to cosine error is too large.
- Model estimates for broadband irradiances for both daily totals and monthly averages are good with the relative mean bias error (MBE) < 5% and relative root mean square error (RMSE) < 26% of the mean measured daily irradiance.
- A fixed τ_c value of 18.7 is adequate for all stations except the arctic. This is important because it suggests that further estimation of τ_c is not necessary.

Third, the effect of using two different urban aerosol loadings (light and heavy aerosol) were examined at Montreal and Toronto for two years of data for each station. It was shown that a light aerosol model was suitable for Montreal and a heavy aerosol model for Toronto.

The last part of the thesis further validated the model's performance by comparing its values with those obtained from a satellite-based model for times of measurements made by satellite mostly 1 per day at different local times. The two independent methods produced similar results. However, the model used here has an important advantage over the satellite model. It can be used to estimate irradiances throughout the day and thus produces daily totals. This is not possible with the satellite-based model.

This research has made significant contributions to the understanding and evaluation of UV-B irradiance models for all sky conditions. It is the first to provide extensive evaluation for spectral and broadband irradiances for a large data set, using nine stations and 26 years of data. The spectral information presented here are of importance to biologists in that it can be multiplied by an action spectrum of interest to determine potential biological exposure at each wavelength and integrated over the UV-B wavelength range to derive total exposure.

Because the model is physically based it should be applicable anywhere. Refinements to the extraterrestrial solar spectrum, Rayleigh scattering cross sections and ozone absorption coefficients are unlikely to be large and the model's linear combination of a cloudless and overcast components has been shown to work in a wide range of Canadian conditions. The greatest restriction to its use is the availability of cloud cover information.

The following recommendations are made for future research. First, the model's future application in Canada is limited by the availability of cloud data because of the cessation of cloud observations at most Canadian stations (L. J. B. McArthur, personal

communication, 2001). Alternative cloud data must be obtained. There are many possibilities: (1) digital all-sky camera photographs (2) Total Sky Imager (TSI) model 880 manufactured by Yankee environmental systems (3) sunshine duration from sunshine recorders (4) broadband radiometer measurements (5) ceilometer algorithms (6) satellite imaging from International Satellite Cloud Climatology Project (ISCCP). The first ISCCP cloud products (C dataset) had some problems, but the new version of cloud products (DX dataset) are superior to those of C dataset products due to the use of modified satellite calibration and cloud microphysical models (Trishchenko *et al.*, 2001). These ISCCP DX data are archived at NASA/Langley Research Center. They provide cloud information every 3 hours for each 30-km grid cell over the globe for the period from July 1983 through December 1999 (Rossow and Schiffer, 1999). In the United States cloud amount is also observed every 3 hours. Davies and McKay (1989) showed that good results could be obtained with a solar radiation model by linearly interpolating cloud amount for missing hours. Ceilometer algorithms use the time series of ceilometer data to calculate the cloud amount and heights of different cloud layers (Karkkainen *et al.*, 1997). The radiometer technique for estimating cloud cover is based on the irradiance difference between clear and cloudy skies (Coombes and Harrison, 1985; Long *et al.*, 1999). Sunshine duration has been recorded at many sites around the world including Canada. Cloud sensor TSI-880 has not been used in Canada. Digital all-sky camera measurements are largely experimental. There is a need to evaluate model performance with cloud data from these methods.

Second, the Brewer instrument data sets have not been corrected for the cosine error of the diffuser, temperature errors, as well as absolute radiometric calibration errors. In fact, the 6% increase made to the Brewer data in this study was an approximate correction to remove the systematic cosine error but the actual correction should be made depending on the solar zenith angle and sky illumination conditions (Wardle and Kerr, 1999).

REFERENCES

Ackerman, S.A. and G.L. Stephens (1987): The absorption of solar radiation by cloud droplets: An application of anomalous diffraction theory. *J. Atmos. Sci.*, 44, 1574-1588.

Atmospheric Environment Service (AES) (1999): *Canada's National Environmental Indicator Series: Stratospheric ozone depletion.* SOE Bulletin No. 99-2. Environment Canada, Downsview, Ontario, Canada.

Bais, A.F., C.S. Zerefos, C. Meleti, I.C. Ziomas, and K. Tourpali (1993): Spectral measurements of solar UVB radiation and its relations to total ozone, SO_2 and clouds. *J. Geophys. Res.*, 98, 5199-5204.

Bais, A.F., C.S. Zerefos, and C.T. McElory (1996): Solar UVB measurements with the double and single-monochromator Brewer ozone spectrophotometers. *Geophys. Res. Lett.*, 23, 833-836.

Bais, A.F., S. Kazadzis, D. Balis, C.S. Zerefos, and M. Blumthaler (1998): Correcting global solar ultraviolet spectra recorded by a Brewer spectroradiometer for its angular response error. *Appl. Opt.*, 37, 6339-6344.

Bais, A.F., B.G. Gardiner, H. Slaper, M. Blumthaler, G. Bernhard, R. McKenize, A.R. Wedd, G. Seckmeyer, B. Kjeldstad, T. Koskela, P.J. Kirsch, J. Gröbner, J.B. Kerr, S. Kazadzis, K. Leszczynski, D. Wardle, W. Josefsson, C. Brogniez, D. Gillotay, H. Reinen, P. Weihs, T. Svenoe, P. Eriksen, F. Kuik, and A. Redondas (2001): SUSPEN intercomparison of ultraviolet spectroradiometers. *J. Geophys. Res.*, 106, 12509-12525.

Barker, H.W., T. J. Curtis, E. Leontieva, and K. Stamnes (1998): Optical depth of overcast cloud across Canada: Estimates based on surface Pyranometer and Satellite measurements. *J. Climate*, 11, 2980-2994.

Bartlett, L.M. and A.R. Webb (2000): Changes in ultraviolet radiation in the 1990s: Spectral measurements from Reading, England. *J. Geophys. Res.*, 105, 4889-4893.

Berger, D.S. (1976): The sunburning ultraviolet meter: Design and performance. *Photochem. Photobiol.*, 24, 587-593.

Biggs R.H. and M.E.B. Joyner (1994): *Stratospheric ozone depletion/UV-B radiation in the biosphere*. NATO ASI series. Series 1: Global Environmental Change, vol 18. Springer-Verlag Berlin Heidelberg. 348pp.

Bodeker, G.E. and McKenzie, R.L. (1996) Unpublished.

Bojkov, R.D., L. Bishop, and V. Fioletov (1995a): Total ozone trends from quality controlled ground-based data (1964-1994). *J. Geophys. Res.*, 100, 25867-25876.

Bojkov, R.D., V.E. Fioletov, D.S. Balis, C.S. Zerefos, T.V. Kadygrova, and A.M. Shalamjansky (1995b): Further ozone decline during the northern hemisphere winter spring of 1994-1995 and the new record low ozone over Siberia. *Geophys. Res. Lett.*, 22, 2729-2732.

Bowker, D.E., R.E. Davis, D.I. Myrick, K. Stacy, and W.T. Jones (1985): *Spectral reflectance of natural targets for use in remote sensing studies*. NASA reference publication 1139, NASA, Langley Research Center, Hampton, Virginia.

Browman H.I., C. A. Rodriguez, F. Beland, J. J. Cullen, R.F. Davis, J.H.M. Kouwenberg, P.S. Kuhn, B. McArthur, J.A. Runge, J-F St-Pierre, and R.D. Vetter (2000): Impact of ultraviolet radiation on marine crustacean zooplankton and ichthyoplankton: a synthesis of results from the estuary and Gulf of St. Lawrence, Canada. *Marine Ecology Progress Series*, 199, 293-311.

Caldwell, M.M. and S. D. Flint (1994): Stratospheric ozone reduction, solar UV-B radiation and terrestrial ecosystems. *Climate Change*, 28, 375-394.

Cappellani, F. and C. Kochler (1999): temperature effects correction in a Brewer MKIV spectrophtometer for solar UV measurements. *J. Geophys. Res.*, 105, 4829-4831.

Chandra, S., C. Varotsos, and L.E. Flynn (1996): The mid-latitude total ozone trends in the northern hemisphere. *Geophys. Res. Lett.*, 23, 555-558.

Chandrasekhar, S. (1960): *Radiative transfer*, Dover Publications, New York, 393p.

Charache, D.H, V.J. Abreu, W.R. Kuhn and W.R. Skinner (1994): Incorporation of multiple cloud layers for ultraviolet radiation modeling studies. *J. Geophys. Res.*, 99, 23031-23039.

Chertock, B., R. Frouin, and C. Gautier (1992): A technique for global monitoring of net solar irradiance at the ocean surface. Part II: Validation. *J. Appl. Meteor.*, 31, 1067-1083.

Chubarova, N. Ye. (1991): Modeling of cirrus effect on total ultraviolet attenuation. *Atmos. Oceanic Physics*, 27, 740-744.

Coombes, C.A. and A.W. Harrison (1985): radiometric estimation of cloud cover. *J. Atmos. Ocean. Technol.*, 2, 482-490.

Curtis, T.J. (1996): Optical depth of overcast cloud in Canada inferred from surface and satellite measurements. *M.Sc.Thesis*, McMaster University, Hamilton, Ontario, 84p.

Dave, J.V. (1968): Subroutines for computing the parameters of the electromagnetic radiation scattered by a sphere. *IBM Scientific Center*, Rep. No. 320-3237, Palo Alto, Calif.

Davies, J.A. (1996): Correcting for stray light in Brewer spectroradiometers. *Environ. Technol.*, 17, 421- 426.

Davies, J.A. and D.C. McKay (1982): Estimating solar irradiance and components. *Solar Energy*, 29, 55-64.

Davies, J.A. and D.C. McKay (1989): Evaluation of selected models for estimating solar radiation on a horizontal surfaces. *Solar Energy*, 43, 153-168.

Davies, J.A. and K. Runnalls (1993): A numerical model for UV-B irradiance. *Report to the Atmospheric Environment Services (AES)*, 34p

Davies, J., P. Kuhn, G. Duhamel, J. Binyamin, and K. Runnalls (2000): An ultraviolet (290-325 nm) irradiation model for southern Canadian conditions. *Physical. Geography*, 21, 4, 327-344.

Eck, T.F., P.K. Bhartia, and J.B. Kerr (1995): Satellite estimation of spectral UVB irradiance using TOMS derived total ozone and UV reflectivity. *Geophys. Res. Lett.*, 22, 611-614.

Elterman, L. (1968): *UV, visible and IR attenuation for altitudes to 50 km.* Air Force Cambridge Research Laboratories, Environmental Research Paper No. 285, 59p.

Erlick, C. and J. E. Frederick (1998): Effects of aerosols on the wavelength dependence of atmospheric transmission in the ultraviolet and visible: 1. A "single-scattering-separate" delta-Eddington model. *J. Geophys. Res.*, 103, 11465-11472.

Essenwanger, O. (1976): *Applied statistics in atmospheric science. Part A. Frequencies and curve fitting.* Elsvier Scientific Publishing Company Jan Van Galenstraat 335, Amesterdam.

Estupinan, J. G., S. Raman, G.H. Crescenti, J.J. Streicher, and W.F. Barnard (1996): Effects of clouds and haze on UV-B radiation. *J. Geophys. Res.*, 101, 16807-16816.

Farman, J.C., B.G. Gardiner, and J.D. Shanklin (1985): Large losses of total ozone in Antarctica reveal seasonal ClO_x/NO_x interaction. *Nature*, 315, 207-210.

Feister, U., R. Grewe, and K. Gericke (1997): A method for correction of cosine errors in measurements of spectral UV irradiance. *Solar Energy*, 60, 313-332.

Forster, P.M. de F. (1995): Modeling ultraviolet radiation at the earth's surface. Part I: The sensitivity of ultraviolet irradiances to atmospheric changes. *J. Appl. Meteor.*, 34, 2412-2425.

Forster, P.M. de F. and K.H. Shine (1995): A comparison of two radiation schemes for calculating ultraviolet radiation. *Quart. J. Roy. Meteor. Soc.*, 121, 1113-1131.

Forster, P.M. de F., K.H. Shine and A.R. Webb (1995): Modeling ultraviolet radiation at the earth's surface. Part II: Model and instrument comparison. *J. Appl. Meteor.*, 34, 2426-2439.

Frederick, J.E. and D. Lubin (1988): The budget of biologically active ultraviolet radiation in the earth-atmosphere system. *J. Geophys. Res.*, 93, 3825-3832.

Frederick, J.E. and H.E. Snell (1990): Tropospheric influence on solar ultraviolet radiation: The role of clouds. *J. Climate*, 3, 373-381.

Frederick, J.E., H.E. Snell, and E.K. Haywood (1989): Solar ultraviolet radiation at the earth's surface. *Phtochem. Phtobiol.*, 50, 443-450.

Frederick, J.E., P.F. Soulen, S.B. Diaz, I. Smolskaia, C.R. Booth, T. Lucas, and D. Neuschuler (1993): Solar ultraviolet irradiance observed from southern Argentina: September 1990 to March 1991. *J. Geophys. Res.*, 98, 8891-8897.

Fröhlich C. and J. London (1986): *Revised instruction manual on radiation instruments and measurements*. WMO Tech. Note 149, World Meteorol. Organ., Geneva.

Gardiner, B.G., A.R. Webb, A.F. Bais, M. Blumthaler, I. Dirmhirn, P. Forster, D. Gillotay, K. Henriksen, M. Huber, P.J. Kirsch, P.C. Simon, T. Svenoe, P. Weihs, and C. S. Zerfos (1993): European intercomparison of ultraviolet spectroradiometers. *Environm. Technol.*, 14, 25-43.

Gautier, C., P. Ricchiazzi, and D. Lubin (1993): Mapping of surface UV over Antarctica using satellite observations. In: "*Atmospheric Radiation*". K. H. Stamnes, ed., Proc. SPIE, 2049, 199-214.

Gleason, J.F., P.K. Bhartia, J.R. Herman, R. McPeters, P. Newman, R.S. Stolarski, L. P.Flynn, G. Labow, D. Larko, C. Seftor, C. Wellemeyer, W.D. Komhyr, A.J. Miller, and W. Planet (1993): Record low global ozone in 1992. *Science*, 260, 523-526.

Green, A.E.S., T. Sawada, and E.P. Shettle (1974): The middle ultraviolet reaching the ground. *Phtochem. Phtobiol.*, 19, 251-259.

Hale, G. M. and M. R. Querry (1973): Optical constants of water in the 200-nm to 200-μm wavelength region. *Appl. Opt.*, 12, 555-562.

Han, Q., W.B. Rossow, and A.A. Lacis (1994): Near-global survey of effective droplet radii in liquid water clouds using ISCCP data. *J. Climate*, 7, 465-497.

Hansen, J. E (1971): Multiple scattering of polarized light in planetary atmospheres. Part II. Sunlight reflected by terrestrial water clouds. *J. Atmos. Sci*, 28, 1400-1426.

Hansen, J. E. and L.D. Travis (1974): Light scattering in planetary atmospheres. *Space. Sci. Rev.*, 16, 527-610.

Harris, N. R.P., G. Ancellet, L. Bishop, D.J. Hofmann, J.B. Kerr, R.D. McPeters, M. Prendez, W.J. Randel, J. Staehelin, B.H. Subbaraya, A. Volz-Thomas, J. Zawodny, and C.S. Zerefos (1997): Trends in stratospheric and free tropospheric ozone. *J. Geophys. Res.*, 102, 1571-1590.

Harrison, H (1970): Stratospheric ozone with added water vapor: Influence of high-altitude aircraft. *Science*, 170, 734-736.

Harshvardhan and M. D. King (1993): comparative accuracy of diffuse radiative properties computed using selected multiple scattering approximations. *J. Atmos. Sci.*, 50, 247-259.

Hay, J.E. and D. I. Wardle (1982): An assessment of the uncertainty in measurements of solar radiation. *Solar Energy*, 29, 271- 278.

Henderson, G.S., J.C. McConnell, S.R. Beagley, and W.F.J. Evans (1991): Polar ozone depletion: Current status. *Can. J. Phys.*, 69, 1110-1122.

Herman, G.F. and J.A. Curry (1984): Observational and theoretical studies of solar radiation in arctic stratus clouds. *J. Clim. Appli. Meteor.*, 23, 5-24.

Herman, J.R., P.K. Bahartia, J. Ziemke, Z. Ahmad, and D. Larko (1996): UV-B increases (1979-1992) from decreases in total ozone. *Geophys. Res. Lett.*, 23, 2117-2120.

Herman, J.R., N. Krotkov, E. Celarier, D. Larko, and G. Labow (1999): Distribution of UV radiation at the Earth's surface from TOMS-measured UV-backscattered radiances. *J. Geophys. Res.*, 104, 12059-12076.

Hofmann, D.J., T.L. Deshler, P. Aimedieu, W.A. Mattews, P.V. Johnston, Y. Kondo, W.R. Sheldon, G.J. Byrne, and J.R. Benbrook (1989): Stratospheric clouds and ozone depletion in the Arctic during January 1989. *Nature*, 340, 117-121.

Hu, Y.X. and K. Stamnes (1993): An accurate parameterization of the radiative properties of water clouds suitable for use in climate models. *J. Climate*, 6, 728-742.

Hughes, N.A. (1984): Global cloud climatologies: A historical review. *J. Appl. Meteor.*, 23, 724-750.

Ilyas, M. (1987): Effect of cloudiness on solar ultraviolet radiation reaching the surface. *Atmos. Environ.*, 21, 1483-1484.

Johnston, H. (19971): Reduction of stratospheric ozone by nitrogen oxide catalysts from supersonic transport exhaust. *Science*, 173, 517-522.

Jones, A.E. and J.D. Shanklin (1995): Continued decline of total ozone over Halley Antarctica, since 1985. *Nature*, 367, 409-411.

Joseph, J.H., W.J. Wiscombe, and J.A. Weinman (1976): The delta-Eddington approximation for radiative flux transfer. *J. Atmos. Sci.*, 33, 2452-2459.

Karkkainen, A-M, M. Pietarinen, J. Lonnqvist (1997): Cloud amount: Relative performance of five ceilometer algorithms vs. observer. *Amer. Meteor. Soc.*, First symposium on Integrated Observing Systems. February 2-7, Long Beach, California.

Kelfkens, G., F.R. DeGruijl, and J. C. Van der Leun (1990): Ozone depletion and increase in annual carcinogenic ultraviolet dose. *Photochem. Photobiolo.*, 52, 819-823.

Kerr, J.B. (1991): Trends in total ozone at Toronto between 1960- 1991. *J. Geophys. Res.*, 96 (D11), 20703-20709.

Kerr, J.B. (1998): Ozone loss, greenhouse gases linked. *Science*, 280, 202.

Kerr, J.B. and C.T. McElory (1993): Evidence for large upward trends of ultraviolet-B radiation linked to ozone depletion. *Science*, 262, 1032- 1035.

Kerr, J.B., C.T. McElroy, D.I. Wardle, R.A. Olafson, and W.F.J. Evans (1985): The automated Brewer spectrophotometer, In: "*Atmospheric Ozone*". Proceedings of Quadrennial Ozone Symposium, edited by C. S. Zerefos and A. Ghazi, pp. 396-401, D. Reidel, Hingham, Maas.

King, M.D. and Harshvardhan (1986): Comparative accuracy of selected multiple scattering approximations. *J. Atmos. Sci.*, 43, 784-801.

Klein, M. and R. Furrer (1994): UVB radiation changes in Berlin between 1967 and 1990 following alterations in the ozone layering. *J. Atmos. Terrest. Phy.*, 56, 363-367.

Kneizys, F.X., E.P. Shettle, L.W. Abreu, J.H.Chetwynd, G.P.Anderson, W.O.Gallery, J.E.A. Selby, and S.A. Clough (1988): *Users guide to LOWTRAN 7*, Technical Report 88-0177, Air Force Geophysics Laboratory, Bedford. Massachusetts.

Koskela, T., P. Tallas, and E. Kyrö (1993): Measured and modeled UV-B spectrum compared with some atmospheric parameters. In: "*Atmospheric Radiation*", K.H. Stamnes, ed., Proc. SPIE., 2049, 296-306.

Krotkov. N.A., P.K. Bhartia, J.R. Herman, V. Fioletov, and J. Kerr (1998): Satellite estimation of spectral surface UV irradiance in the presence of tropospheric aerosols: 1. Cloud-free case. *J. Geophys. Res.*, 103, 8779-8793.

Kuhn, P.S. (1996): Further testing of an ultraviolet-B irradiance model and the stray light problem. *M.Sc. Thesis*, McMaster University, Hamilton, Ontario, 112p.

Lenoble, J. (1993): *Atmospheric radiative transfer*, A. Deepak Pub., Hampton, Va., USA.

Leontyeva, E. and K. Stamnes (1994): Estimations of cloud optical thickness from ground-based measurements of incoming solar radiation in the Arctic. *J. Climate*, 7, 566-578.

Leontieva, E., K. Stamnes, and J.A. Olseth (1994): Cloud optical properties at Bergen (Norway) based on the analysis of long-term solar irradiance records. *Theor. Appl. Climtol.*, 50, 73-82.

Leontieva, E. and K. Stamnes (1996): Remote sensing of cloud optical properties from ground-based measurements of Transmittance: A feasibility study. *J. Appl. Meteor.*, 35, 2011-2022.

Li, Z. (1996): On the angular correction of satellite radiation measurements: the performance of ERBE angular dependence model in the Arctic. *Theor. Appl. Climtol.*, 54, 235-248.

Li, Z., P. Wang, and J. Cihlar (2000): A simple and efficient method for retrieving surface UV radiation dose rate from satellite. *J. Geophys. Res.*, 105, 5027-5036.

Liou, K.N. (1973): A numerical experiment on Chanrasekhar's discrete-ordinate method for radiative transfer: Applications to cloudy and hazy atmospheres. *J. Atmos. Sci.*, 30, 1303-1326.

Liou, K.N. (1992): *Radiation and cloud processes in the atmosphere: Theory, observation, and modeling.* Oxford University Press, New York, Oxford, 487p.

Liu, S.C., S.A. McKeen, and S. Madronich (1991): Effect of anthropogenic aerosols on biologically active ultraviolet radiation. *Geophys. Res. Lett.*, 18, 2265-2268.

Long, C.N., T.P. Ackerman, J.A. Augustine, and J.J Deluisi (1999): estimation of fractional sky cover from broadband SW Radiometer measurements. *Proc. 10th Conf. On Atmos. Rad.*, June 28-July 2, Madison, Wisconsin.

Lubin, D. and J.E. Frederick (1991): The ultraviolet radiation environment of the Antarctic Peninsula: The roles of ozone and cloud cover. *J. Appl. Meteor.*, 30, 478-492.

Lubin, D., J.E. Frederick, and A.J. Krueger (1989): The ultraviolet radiation environment of the Antarctica: McMurdo station during September-October 1987. *J. Geophys. Res.*, 94, 8491-8496.

Lubin, D., B.G. Mitchell, J.E. Frederick, A.D. Albert's, C.R. Booth, T. Lucas, and D. Neuschuler (1992): A contribution toward understanding the biospherical significance of Antarctic ozone depletion. *J. Geophys. Res.* 97, 7817-7827.

Lubin, D., E.H. Jensen, and H.P. Gies (1998): Global surface ultraviolet radiation climatology from TOMS and ERBE data. *J. Geophys. Res.*, 103, 26061-26091.

Madronich, S. (1992): Implication of recent total atmospheric ozone measurements for biologically active ultraviolet radiation reaching the Earth's surface. *Geophys. Res. Lett.*, 19, 37-40.

Madronich, S. (1993): UV radiation in natural and perturbed atmospheres. In: " *UV-B Radiation and Ozone Depletion: Effects on Humans, Animal, Plants, Microorganisms, and Materials*". M. Tevini, ed., Lewis Publishers, Boca Raton, FL, 17-69.

Madronich, S. and F.R. DeGruijl (1993): Skin cancer and ultraviolet radiation. *Nature*, 366, 23.

Mayer, B., G. Seckmeyer, and A. Kyling (1997): Systematic long-term comparison of spectral UV measurements and UVSPEC modeling results. *J. Geophys. Res.*, 102, 8755-8767.

McKenzie, R.L., W.A. Matthews, and P. V. Johnston (1991): The relationship between erythemal UV and ozone, derived from spectral irradiance measurements. *Geophys. Res. Lett.*, 12, 2269-2272.

McKenzie, R.L., M. Kotkamp, G. Seckmeyer, R. Erb, C.R. Roy, H.P. Gies, and S.T. Toomey (1993): First southern hemisphere intercomparison of measured solar UV spectra. *Geophys. Res. Lett.*, 20, 2223-2226.

McKinlay, A. F. and B. L. Diffey (1987): A reference spectrum for ultraviolet-induced erythema in human skin. *Commission internationale D'Eclairage Journal*, 6, 17-22.

Meteorological Service of Canada (MSC) (1999): *The ozone layer fact sheet.* Environment Canada Inquiry Centre. Ottawa, Ontario.

Michalsky, J.L. (1988): The astronomical almanac's algorithm for approximate solar position (1950-2050). *Solar Energy*, 40, 227-235.

Mims, F. M. and J. E. Frederick (1994): Cumulus clouds and UVB. *Nature*, 371, 291.

Min, Q-L. and L. C. Harrison (1996): Cloud properties derived from surface MFRSR measurements and comparison with GOES results at the ARM SPG site. *Geophys. Res. Lett.*, 23, 1641-1644.

Molina, L.T. and F. S. Rowland (1974): Stratospheric sink for chlorofluoromethanes: Chlorine atom-catalysed destruction of ozone. *Nature*, 249, 810-812.

Molina, L.T. and M.J. Molina (1986): Absolute absorption cross sections of ozone in the 185-350 nm wavelength range, *J. Geophys. Res.*, 91, 14501-14508.

Munro, R., R. Siddans, W. Reburn, and B.J. Keridge (1998): Direct measurement of tropospheric ozone distributions from space. *Nature*, 392, 168-171.

Pachart, E. J. Lenoble, and C. Brogniez (2000): Consistency tests on UV spectral irradiance measurements using modeling and a broadband instrument. *J. Geophys. Res.*, 105, 4851-4856.

Paur, R.J. and A.M. Bass (1985): The ultraviolet cross-sections of ozone: II. Results and temperature dependence. In: "*Atmospheric Ozone Proceedings of the Quadrennial Ozone Symposium*". Edited by C. Zerefos, and A. Ghaz, Kalkidiki, Greese, Reidel Publishing, 606-616.

Penndorf, R. (1957): Tables of the refractive index for standard air and the Rayleigh scattering coefficient for the spectral region between 0.2 and 20.0 μm and their application to atmospheric optics. *J. Opt. Soc. Amer.*, 47, 176-182.

Plass, G.N. and G.W. Kattawar (1971): Radiance and polarization of the earth's atmosphere with haze and clouds. *J. Atmos. Sci.*, 28, 1187-1198.

Press, W.H., S.A. Teukolsky, W.T. Vetterling, and B.P. Flannery (1992): *Numerical recepies in Fortran.* The Art of Scientific computing. Second ed., Cambridge Univ. Press, Cambridge, UK.

Rawlins, F. and J.S. Foot (1990): Remotely sensed measurements of stratocumulus properties during FIRE using the C130 aircraft multi-Channel radiometer. *J. Atmos. Sci.*, 47, 2488-2503.

Ricchiazzi, P. and C. Gautier (1995): Cloud scattering optical depth and local surface albedo in the Antarctic: Simultaneous retrieval using ground-based radiometry. *J. Geophys. Res.*, 100, 21091-21104.

Rossow, W.B. and R.A. Schiffer (1999): Advances in understanding clouds from ISCCP. *Bull. Amer. Meteor. Soc.*, 80, 2261-2287.

Schafer, J.S., V.K. Saxena, B.N. Wenny, W. Barnard, and J.J. DeLuisi (1996): Observed influence of clouds on ultraviolet-B radiation. *Geophys. Res. Lett.*, 23, 2625-2628.

Schippnick, P.F. and A.E.S. Green (1982): Analytical characterization of spectral actinc flux and spectral irradiance in the middle ultraviolet. *Phtochem. Phtobiol* ., 35, 89-101.

Schweiger, A.J. and J.R. Key (1992): Arctic cloudiness: Comparison of ISCCP-C2 and Nimbus-7 satellite-derived cloud products with a surface-based cloud climatology. *J. Climate*, 5, 1514-1527.

Seckmeyer, G., S. Thiel, M. Blumthaler, P. Fabian, S-Gerber, A. Gugg-Helminger, D.P. Häder, M. Huber, C. Kettner, U. Köhler, P. Köpke, H. Maier, J. Schäfer, P. Suppan, E. Tamm, and E. Thomalla (1994): Intercomparion of spectral-UV-radiation measurement systems. *Appl. Opt.*, 33, 7805-7811.

Shettle, E.P. and J.A. Weinmann (1970): The transfer of solar irradiance through inhomogeneous turbid atmospheres evaluated by Eddington's approximation. *J. Atmos. Sci.*, 27, 1048-1055.

Shettle, E.P. and R.W. Fenn (1979): *Models for the aerosols of the lower atmosphere and the effects of humidity variations on their optical properties*. AFGL Technical Report 79-0214, Air Force Geophysics Laboratory, Environmental Research Papers, No. 676, Bedford. Massachusetts.

Shindell, D.T., D. Rind, and P. Lonergan (1998): Increased polar stratospheric ozone losses and delayed eventual recovery owing to increasing greenhouse-gas concentrations. *Nature*, 392, %89-592.

Slingo, A. (1989): A GCM parameterization for the shortwave radiative properties of water clouds. *J. Atmos. Sci.*, 46, 1419-1427.

Slingo, A. and H.M. Schrecker (1982): On the shortwave radiative properties of stratiform water clouds. *Quart. J. Roy. Meteor. Soc.*, 108, 407-426.

Solomon, S. (1999): stratospheric ozone depletion: A review of concepts and history. *Rev. Geophys.*, 37, 275-306.

Staehelin, J., A. Renaud, J. Bader, R. McPeters, P. Viatte, B. Hoegger, V. Bugnion, M. Giround, and H. Schill (1998a): Total ozone series at Arosa (Switzerland): Homogeization and data comparison. *J. Geophys. Res.*, 103, 5827-5841.

Staehelin, J., R. Kegel, and N.R.P. Harris (1998b): Trend analysis of the homogenized ozone series at Arosa (Switzerland), 1926-1996. *J. Geophys. Res.*, 103, 8389-8399.

Stamnes, K. and H. Dale (1981): A new look at the discrete ordinate method for radiative transfer calculations in anisotropically computations. *J. Atmos. Sci.*, 38, 2696-2706.

Stamnes, K. and R.A. Swanson (1981): A new look at the discrete ordinate for radiative transfer calculations in anisotropically scattering atmospheres. *J. Atmos. Sci.*, 38, 387-399.

Stamnes, K. and P. Conklin (1984): A new multi-layer discrete ordinate approach to radiative transfer in vertically inhomogeneous atmospheres. *J. Quant. Spectrosc. Radiat. Transfer*, 31, 273-282.

Stamnes, K., S-C. Tsay, W.J. Wiscombe, and K. Jayawerra (1988): Numerically stable algorithm for discrete ordinate method radiative transfer in multiple scattering and emitting layered media. *Appl. Opt.*, 27, 2503-2509.

Stamnes, K., J. Slusser, and M. Bowen (1990): Biologically effective ultraviolet radiation, total ozone abundance and cloud optical depth at McMurdo station, Antarctica Sep. 15 1988 through April 15 1989. *Geophys. Res. Lett.*, 17, 2181-2184.

Stamnes, K., J. Slusser, and M. Bowen (1991): Derivation of total ozone abundance and cloud effects from spectral irradiance measurements. *Appl. Opt.*, 30, 4418-4426.

Stamnes, K., Z. Jin, J. Slusser, C. Booth, and T. Lucus (1992): Several-fold enhancement of biologically effective ultraviolet radiation levels at McMurdo station Antarctica During the 1990 ozone "HOLE". *Geophys. Res. Lett.*, 19, 1013-1016.

Stephens, G. L. (1984): The parameterization of radiation for numerical weather prediction and climate models. *Mon. Wea. Rev.*, 112, 826-867.

Stolarski, R. S. (1992): Observed of global stratospheric ozone change. *Ber. Bunsenges. Phys. Chem.*, 96, 257-263.

Stolarski, R. S., A.J. Krueger, M.R. Schoeberl, R.D. McPeters, P.A. Newman, and J.C. Alpert (1986): Nimbus 7 satellite measurements of the springtime Antarctic ozone decrease. *Nature*, 322, 808-811.

Stolarski, R.S., P. Bloomfield, R.D. McPeters, and J.R. Herman (1991): Total ozone trends deduced from Nimbus 7 TOMS data. *Geophys. Res. Lett.*,18,1015-1018.

Stolarski, R.S., R. Bojkov, L. Biship, C. Zerefos, J. Staehelin, and J. Zawodny (1992): Measured trends in stratospheric ozone. *Science*, 256, 342-349.

Tevini, M. (Ed.) (1993): *UV-B radiation and Ozone Depletion: Effects on Humans, Plants, Microorganisms and Materials*. Lewis Publishers, Boca Raton, FL.

Toon, O.B. and R.P. Turco (1991): Polar stratospheric clouds and ozone depletion. *Scient. Amer.*, June, 68-74.

Trishchenko, A.P., Z. Li, and F-L Chang (2001): Cloud optical depths and TOA fluxes: Comparison between satellite and surface retrievals from multiple platforms. *Geophys. Res. Lett.*, 28, 979-982.

Tsay, S-C., K. Jayaweera, and K. Stamnes (1983): Dependence of radiative properties of Arctic stratus clouds on cloud microstructure. *Geophys. Res. Lett.*, 10, 1188-1191.

Tsay, S-C. and K. Stamnes (1992): Ultraviolet radiation in the Arctic: The impact of potential ozone depletions and cloud effects. *J. Geophys. Res.*, 97, 7829-7840.

United Nations Environmental Programme (UNEP) (1994*): Environmental effects of stratospheric ozone depletion*. Edited by J. C. Van der Leun, A. H. Teramura, and M. Tevini, Nairobi, Kenya.

Van de Hulst, H.C. (1980): *Multiple light scattering Table, formulas and application.* Volume 1. Academic Press, INC. London LTD., 299p.

Wang, P., and J. Lenoble (1994): Comparison between measurements and modeling of UV-B irradiance for clear sky: a case study. *Appl. Opt.*, 33, 3964-3971.

Wang, P., Z. Li, J. Cihlar, D.I. Wardle, and J. Kerr (2000): Validation of an UV inversion algorithm using satellite and surface measurements. *J. Geophys. Res.*, 105. 5037-5048.

Wardle, D.L. and J.B. Kerr (1999): *Scientific sponsorship statement for Brewer spectral data from Canadian stations*. WUDC documents.

Warren, S.G. and W.J. Wicombe (1980): A model for spectral albedo of snow. II: Snow containing atmospheric aerosols. *J. Atmos. Sci.*, 37, 2734-2745.

Webb, A.R. (1992): Spectral measurements of solar ultraviolet-B in southeast England. *J. Appl. Meteor.*, 31, 212-216.

Wiscombe, W.J. (1976): On the initialization, error, and flux conservation in the doubling method. *J. Quant. Spectros. Radiat. Transfer*, 16, 637-658.

Wiscombe, W.J. (1977): *The delta-Eddington approximation for a vertically inhomogeneous atmosphere*. NCAR Technical Note-121+STR, Boulder, Colorado. 66p.

Wiscombe, W.J. and J.H. Joseph (1977): The range of validity of the Eddington approximation. *Icarus*, 32, 262-377.

Wiscombe, W.J. and S.G. Warren (1980): A model for the spectral albedo of snow. I: Pure snow. *J. Atmos. Sci.*, 37, 2712-2733.

Zeng, J., R. McKenzie, K. Stamnes, M. Wineland, and J. Rosen (1994): Measured UV spectra compared with discrete ordinate method simulations. *J. Geophys. Res.*, 99, 23019-23030.

Appendix A

Frequency distributions of cloud optical depths calculated by the delta-Eddington method for Resolute, Churchill, Edmonton, Regina, Montreal, Halifax and Toronto.

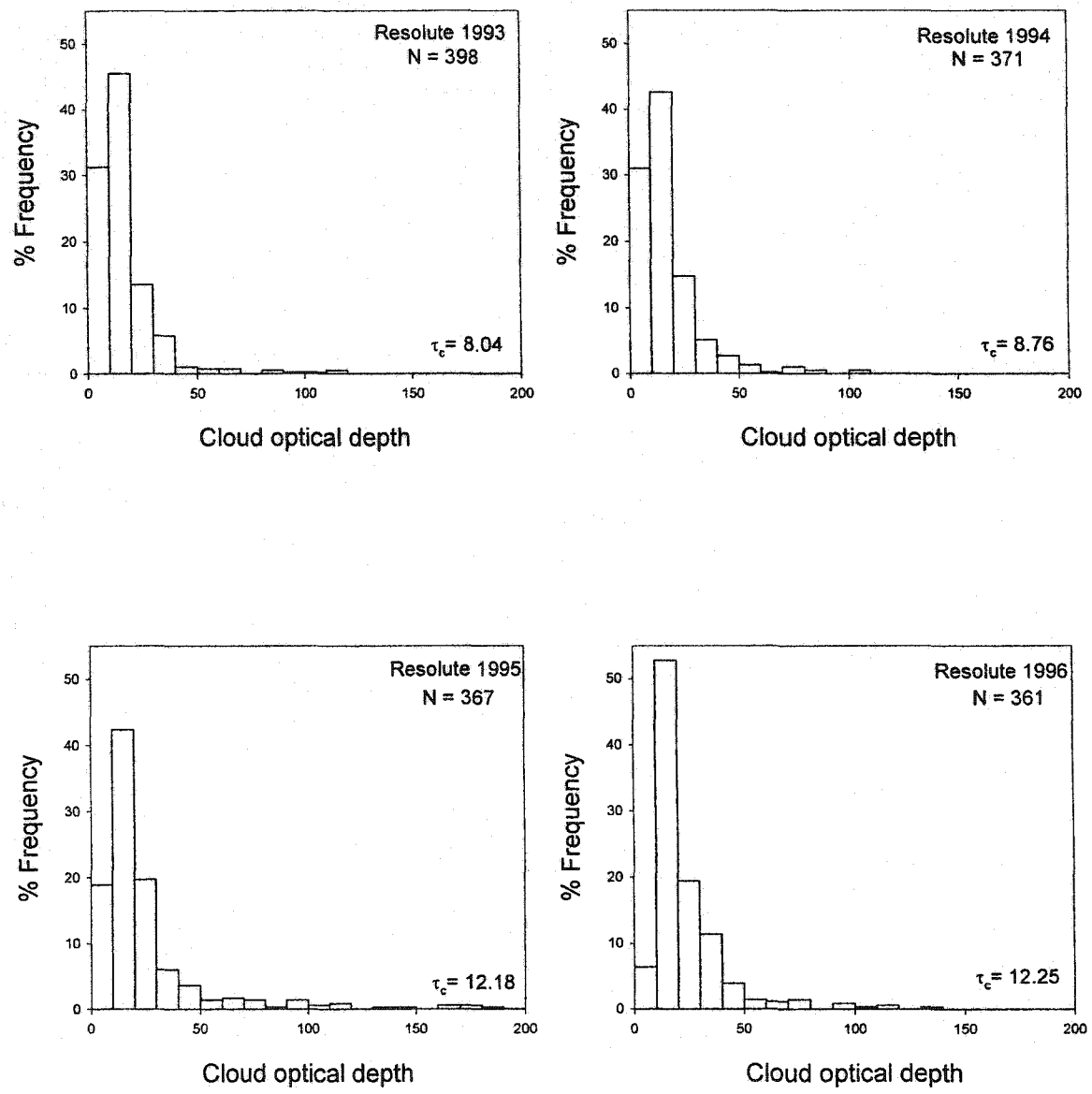

Figure A1. Frequency distributions of cloud optical depths calculated by the delta-Eddington method for Resolute Bay.

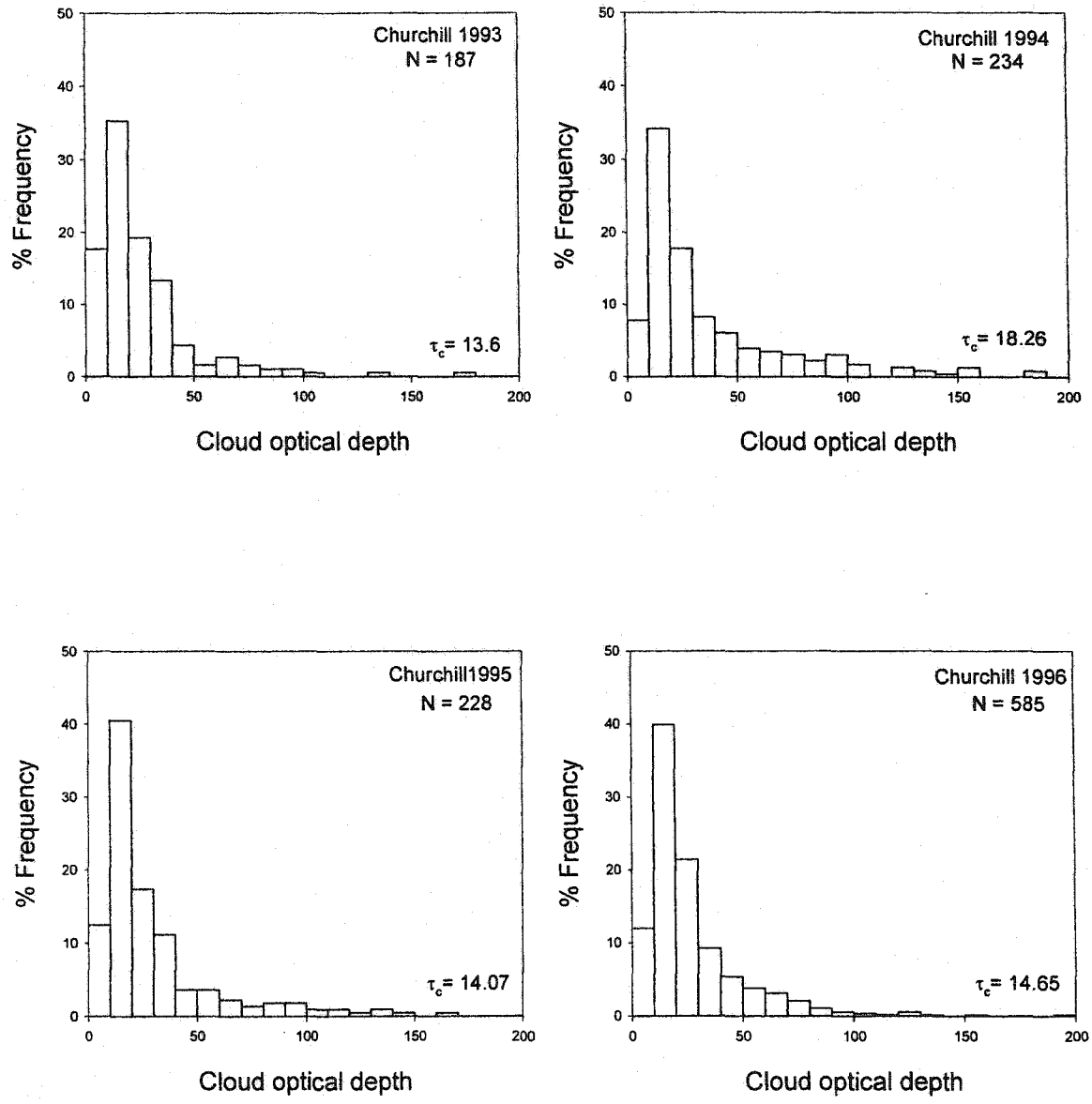

Figure A2. same as Figure A1 but for Churchill.

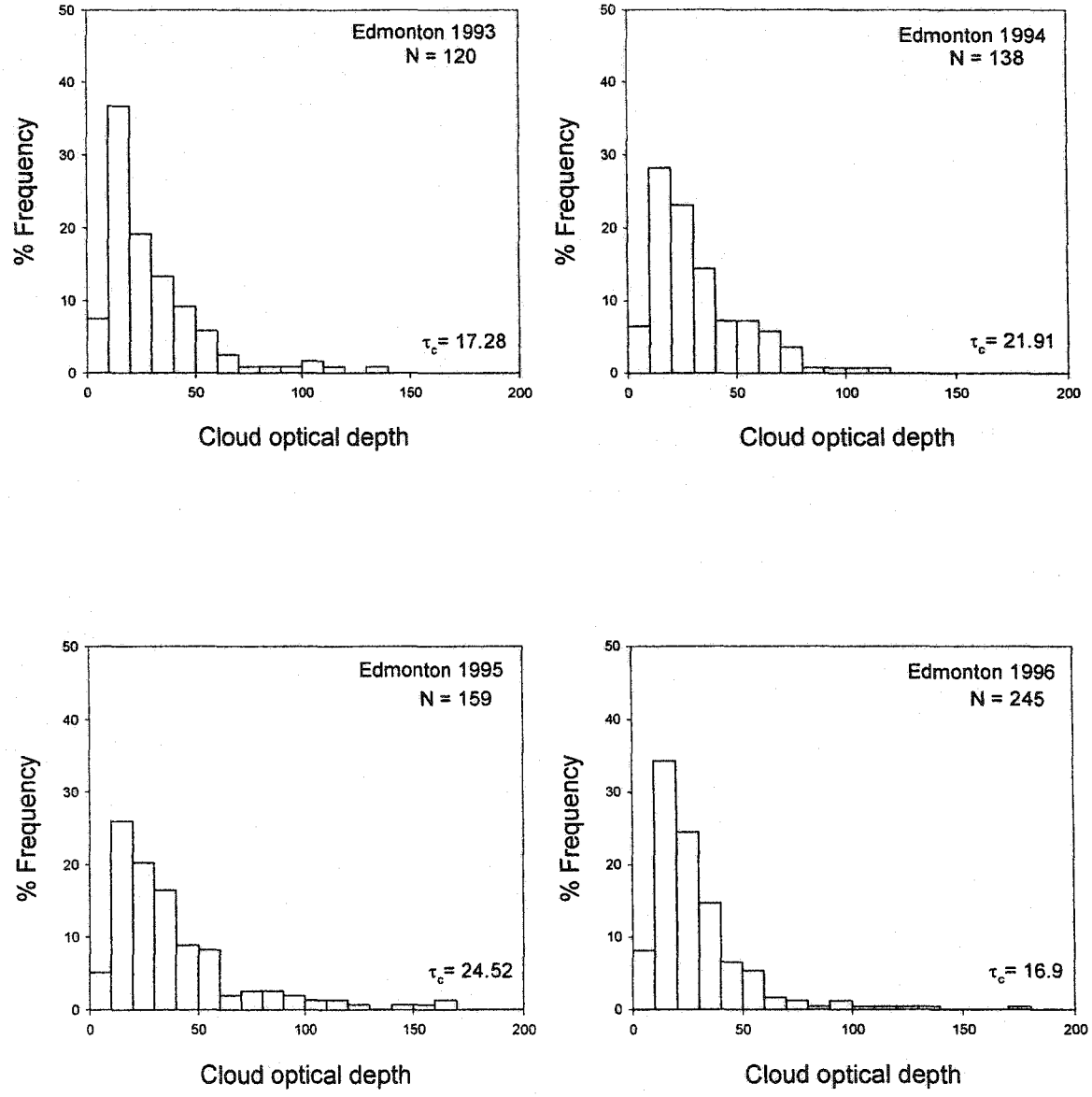

Figure A3. same as Figure A1 but for Edmonton.

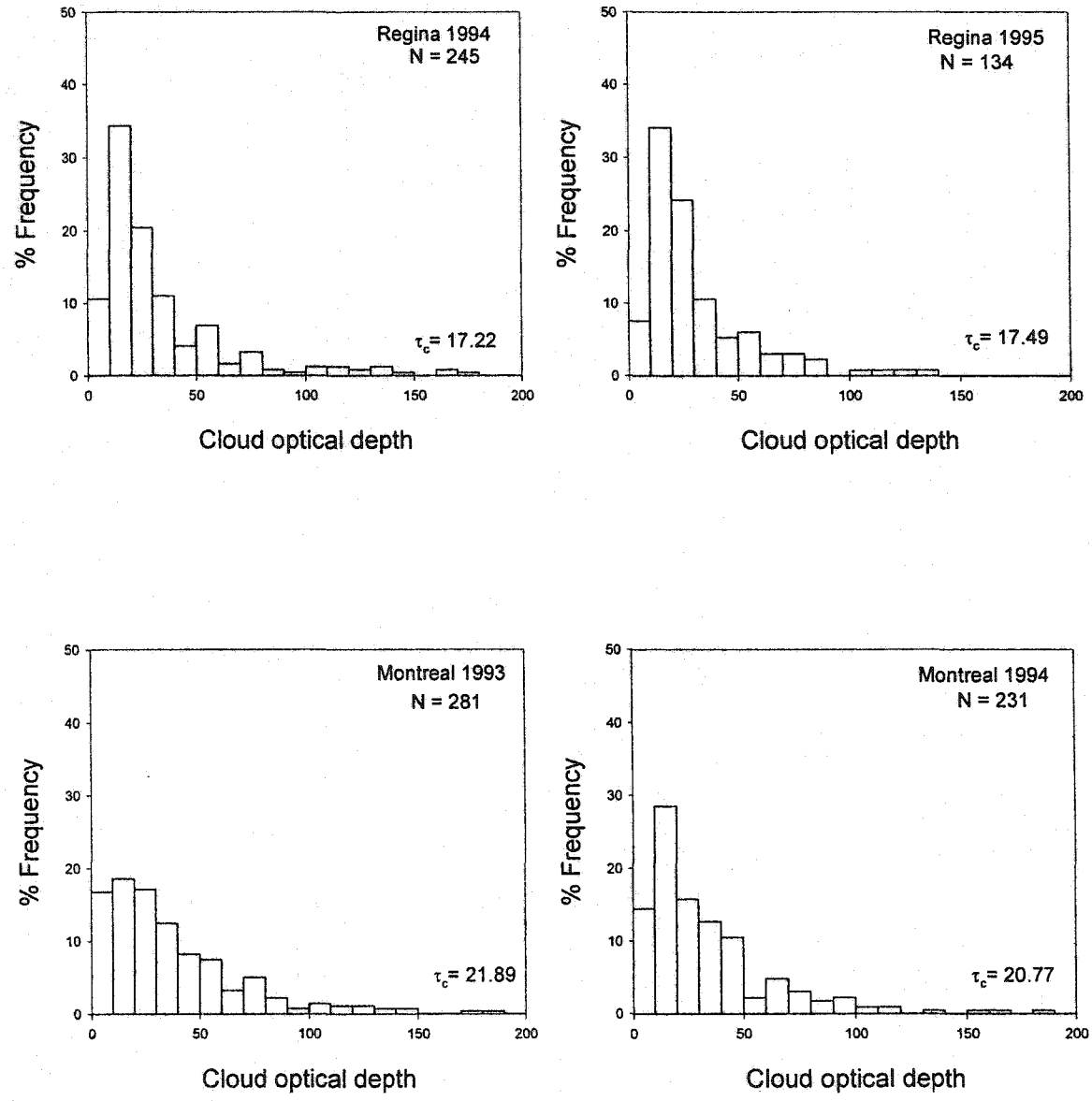

Figure A4. same as Figure A1 but for Regina and Montreal.

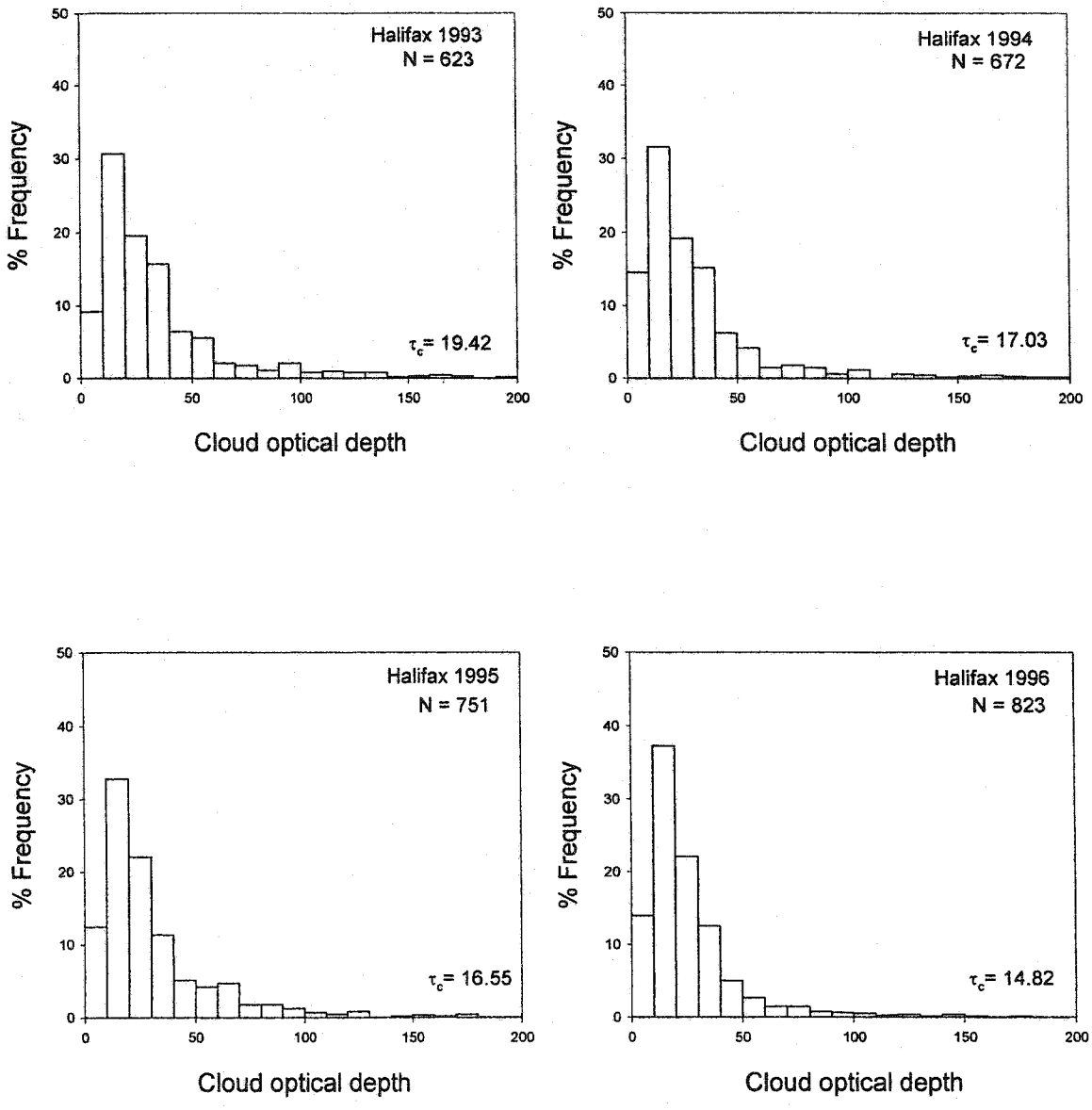

Figure A5. same as Figure A1 but for Halifax.

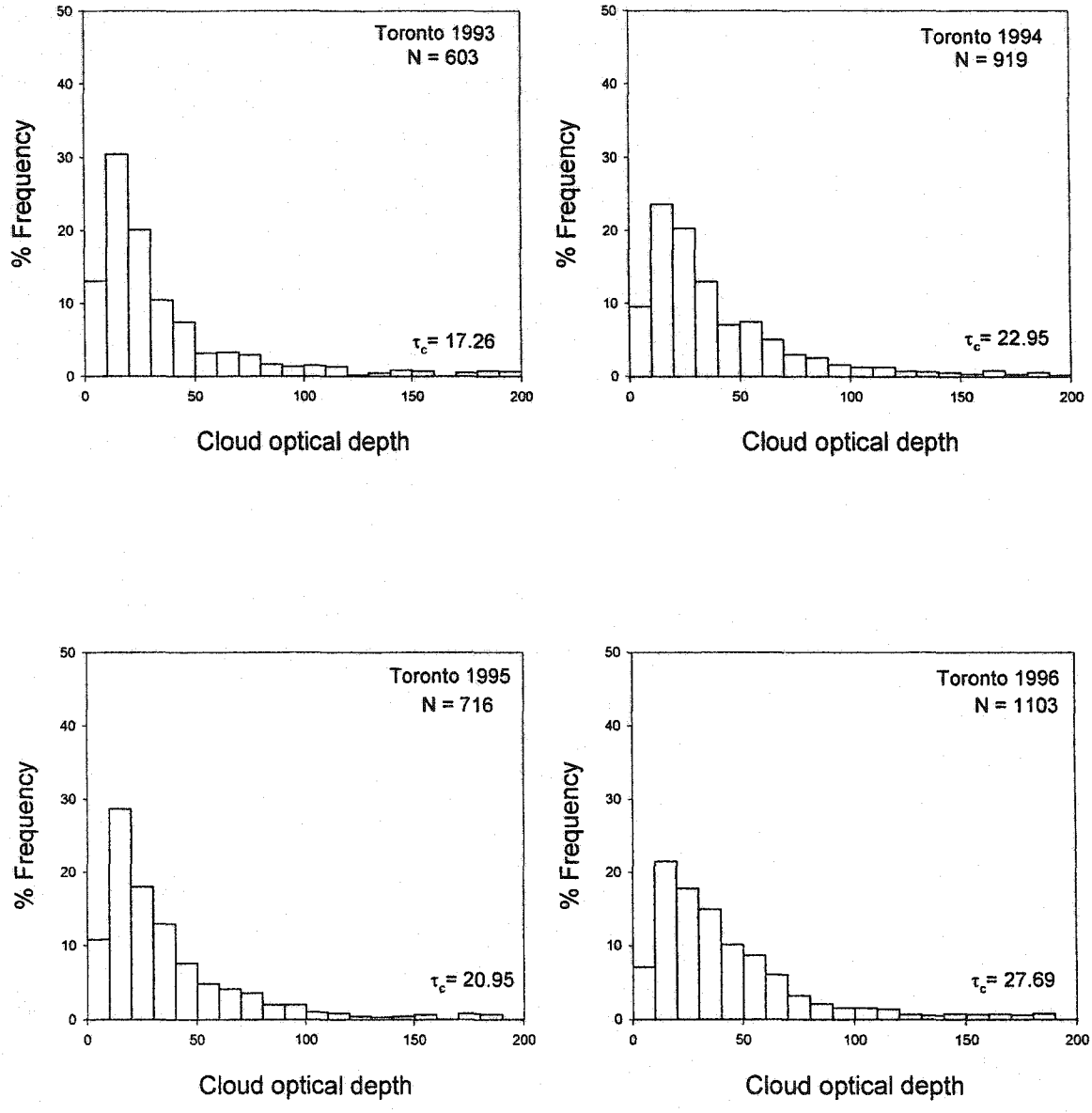

Figure A6. same as Figure A1 but for Toronto.

Appendix B

Comparison of DISORT and delta-Eddington daily total spectral irradiances calculated using annual values of cloud optical depth for each station (Table 3.4) for five wavelengths: 300, 310, 315, 320 and 325 nm.

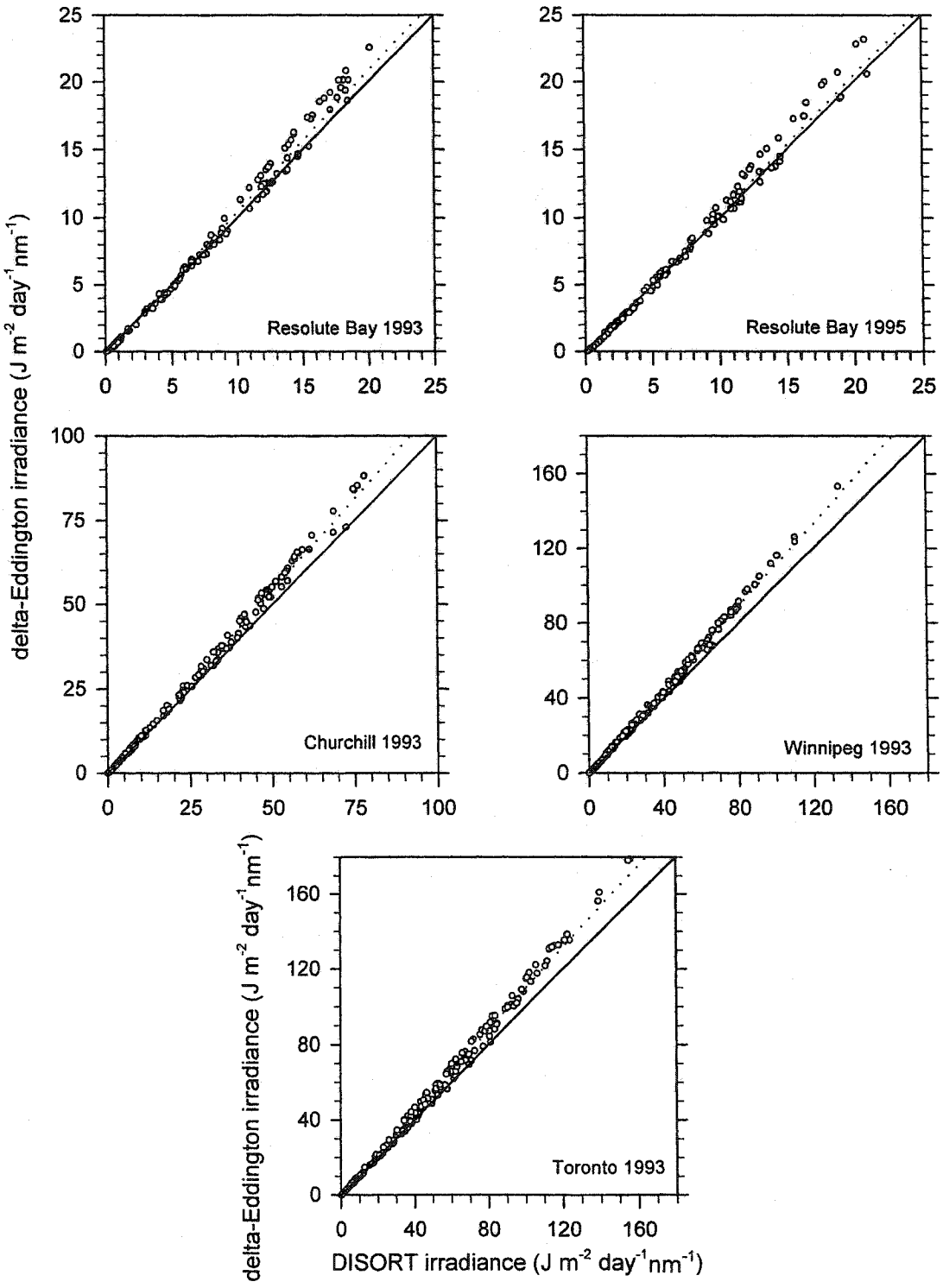

Figure B1. Comparison of DISORT and delta-Eddington daily total spectral irradiances calculated using annual values of cloud optical depth for each station (Table 3.4) for 300 nm. The dotted lines represent linear regressions constrained to pass through the origin.

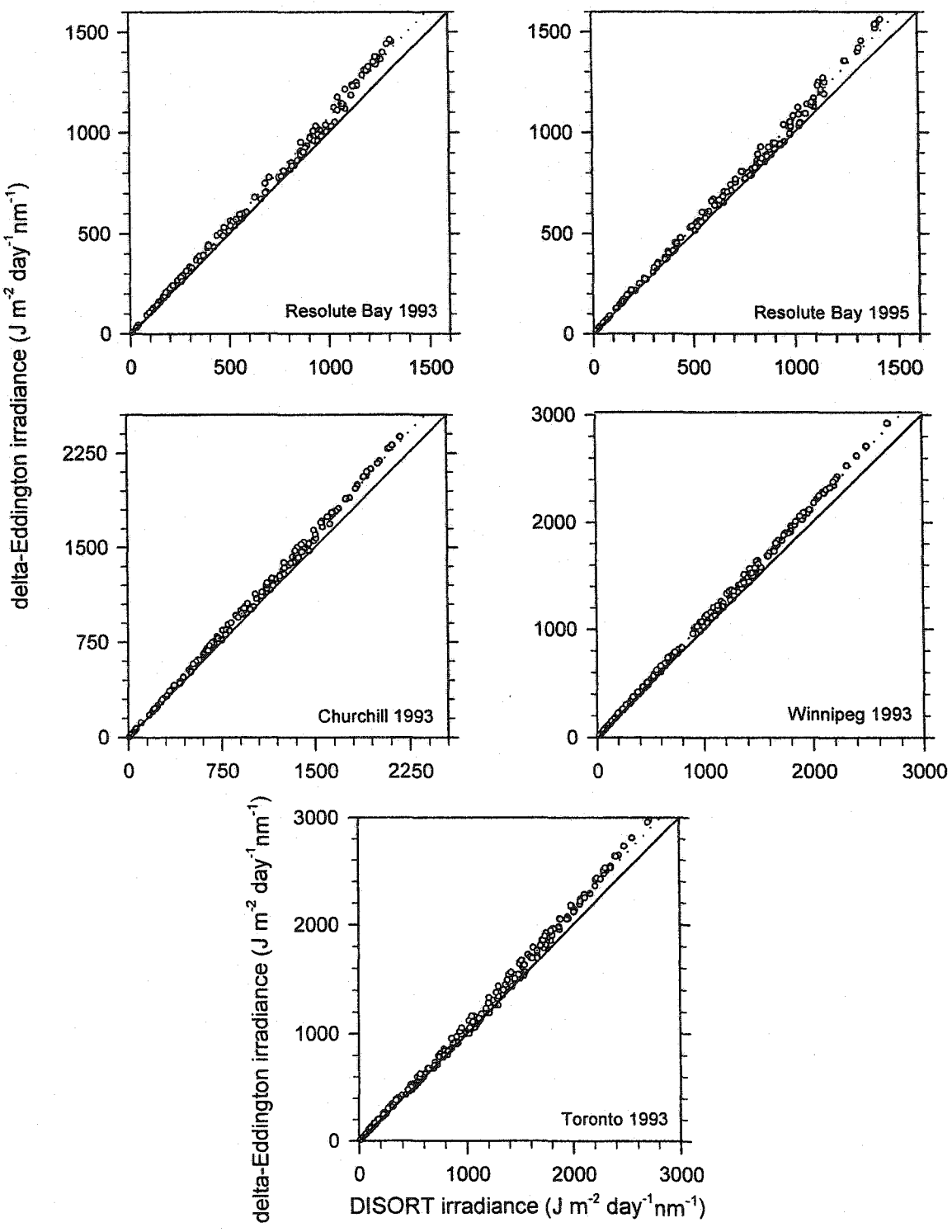

Figure B2. same as Figure B1 but for 310 nm.

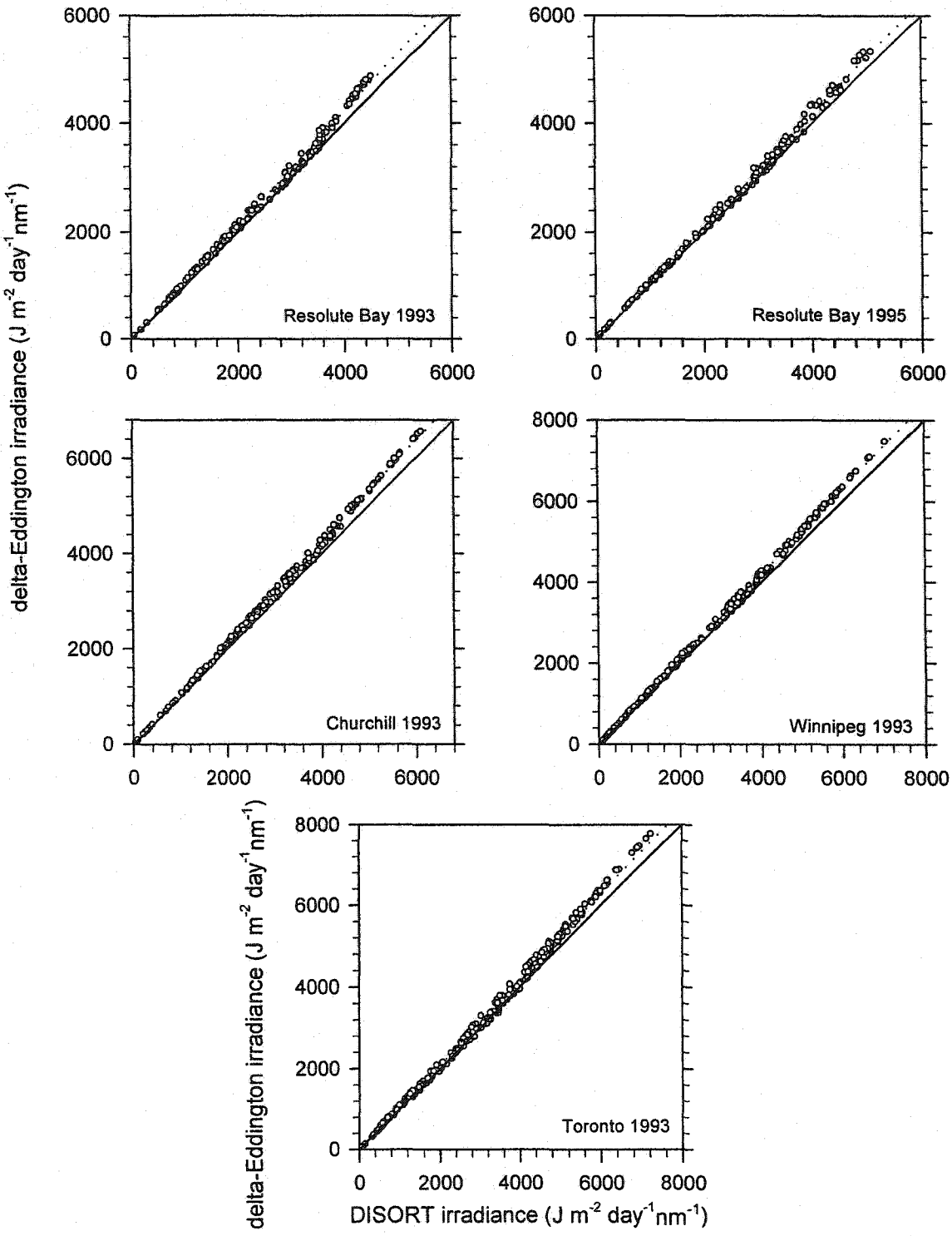

Figure B3. same as Figure B1 but for 315 nm.

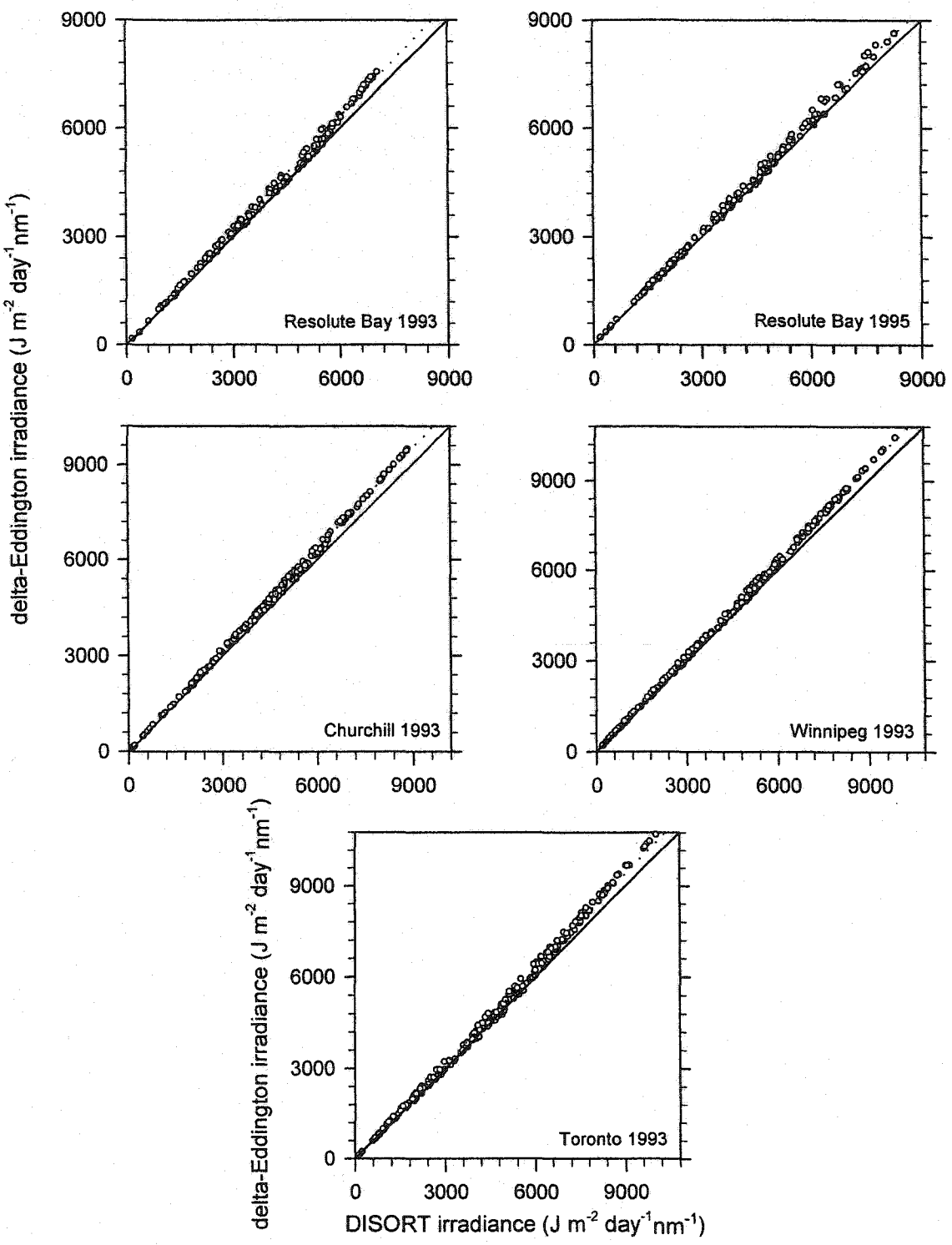

Figure B4. same as Figure B1 but for 320 nm.

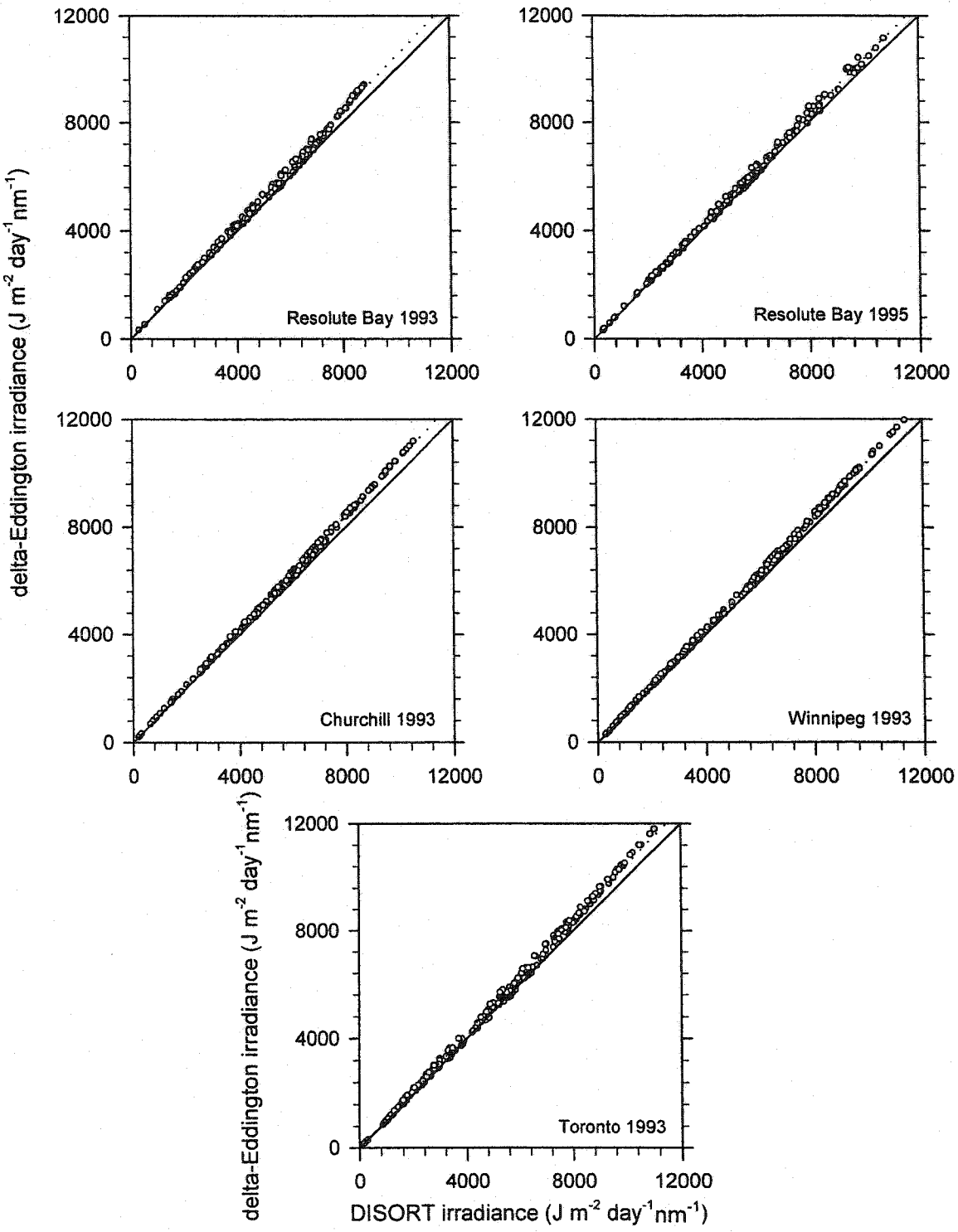

Figure B5. same as Figure B1 but for 325 nm.

Appendix C

Comparison of measured and calculated (delta-Eddington) daily total spectral irradiances using annual values of cloud optical depth for each station (Table 3.4) for 300, 310, 315, 320 and 325 nm.

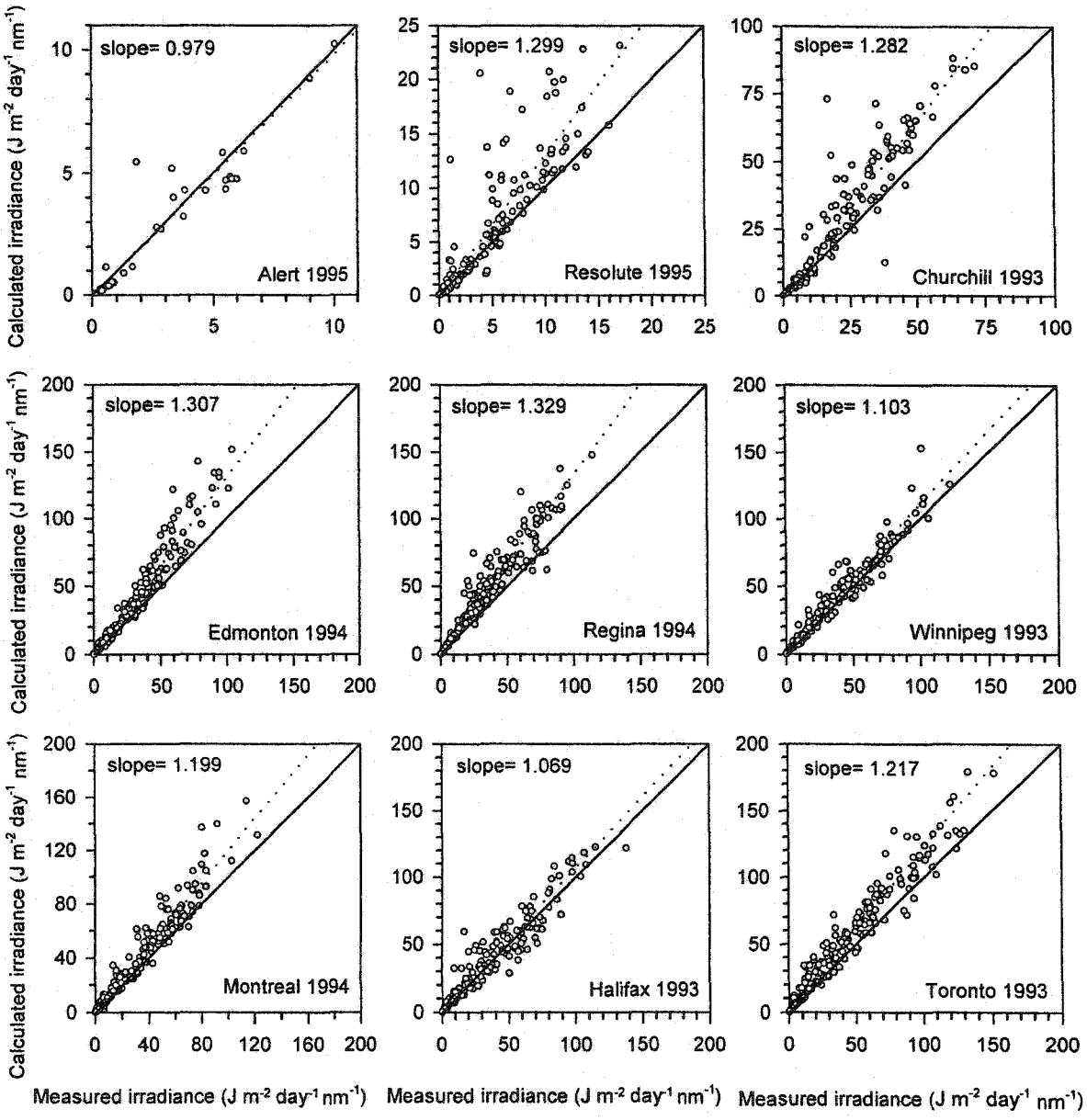

Figure C1. Comparison of measured and calculated (delta-Eddington) daily total spectral irradiances using annual values of cloud optical depth for each station (Table 3.4) for 300 nm. The dotted lines represent linear regressions constrained to pass through the origin.

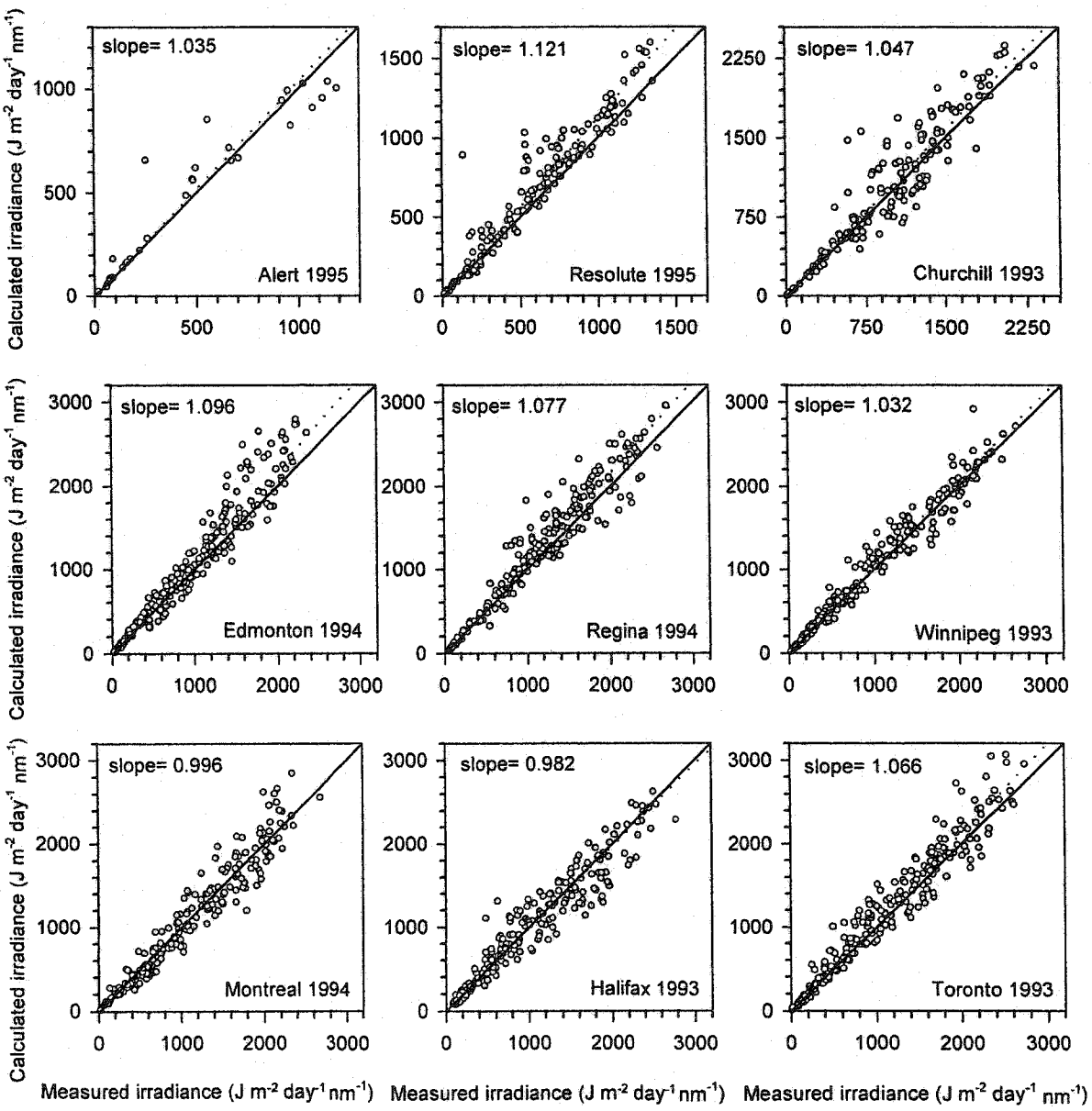

Figure C2. same as Figure C1 but for 310 nm.

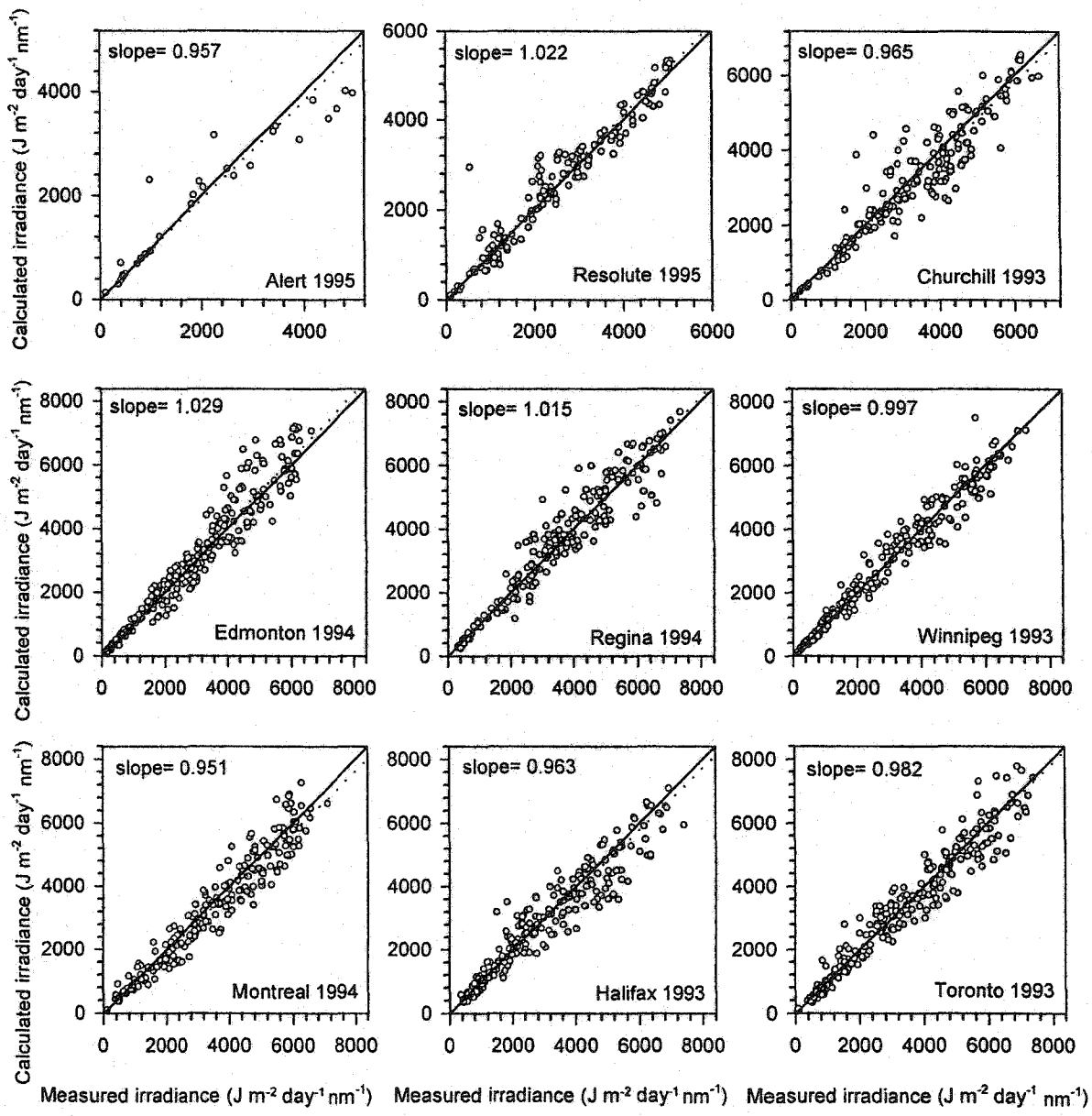

Figure C3. same as Figure C1 but for 315 nm.

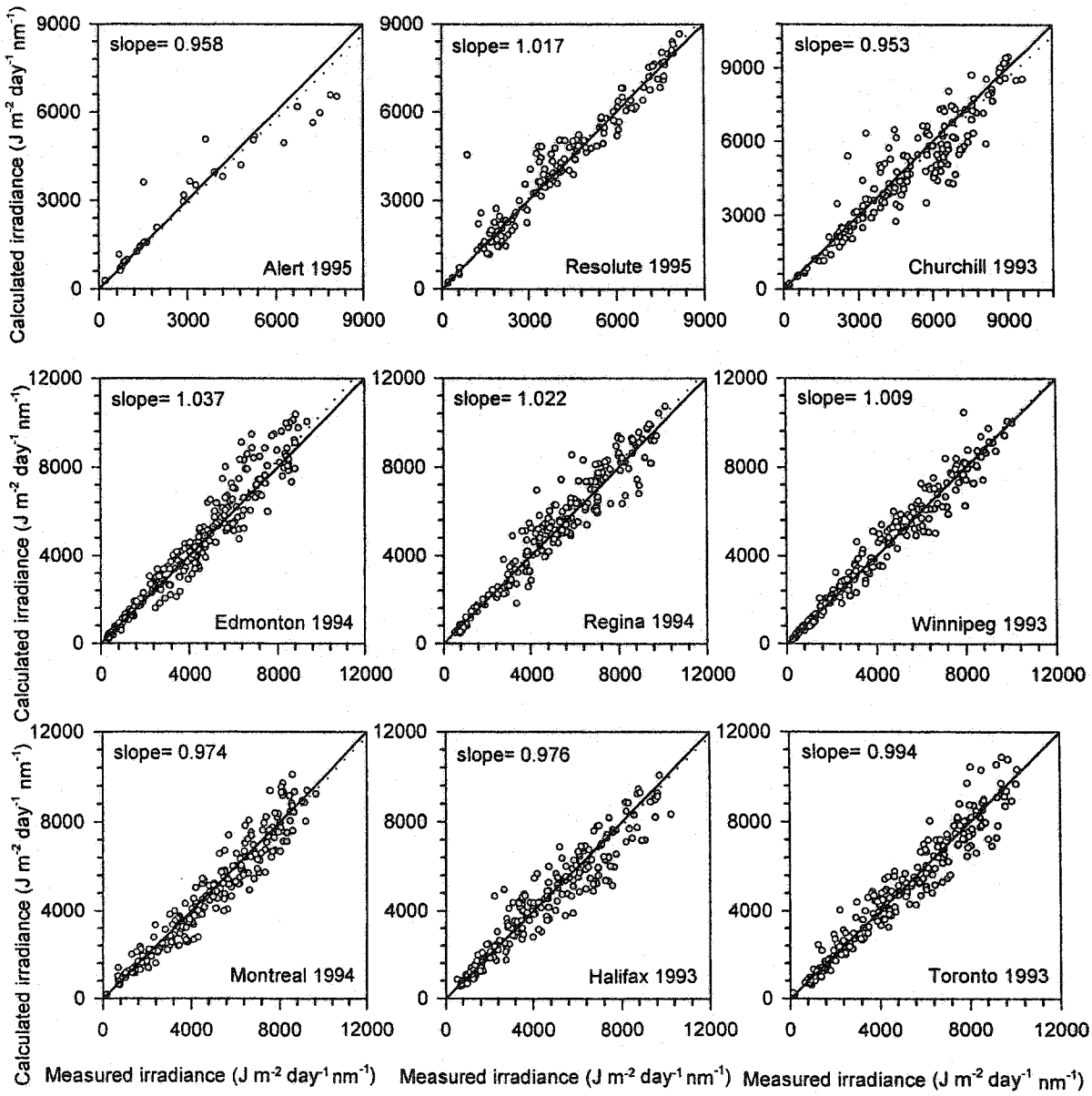

Figure C4. same as Figure C1 but for 320 nm.

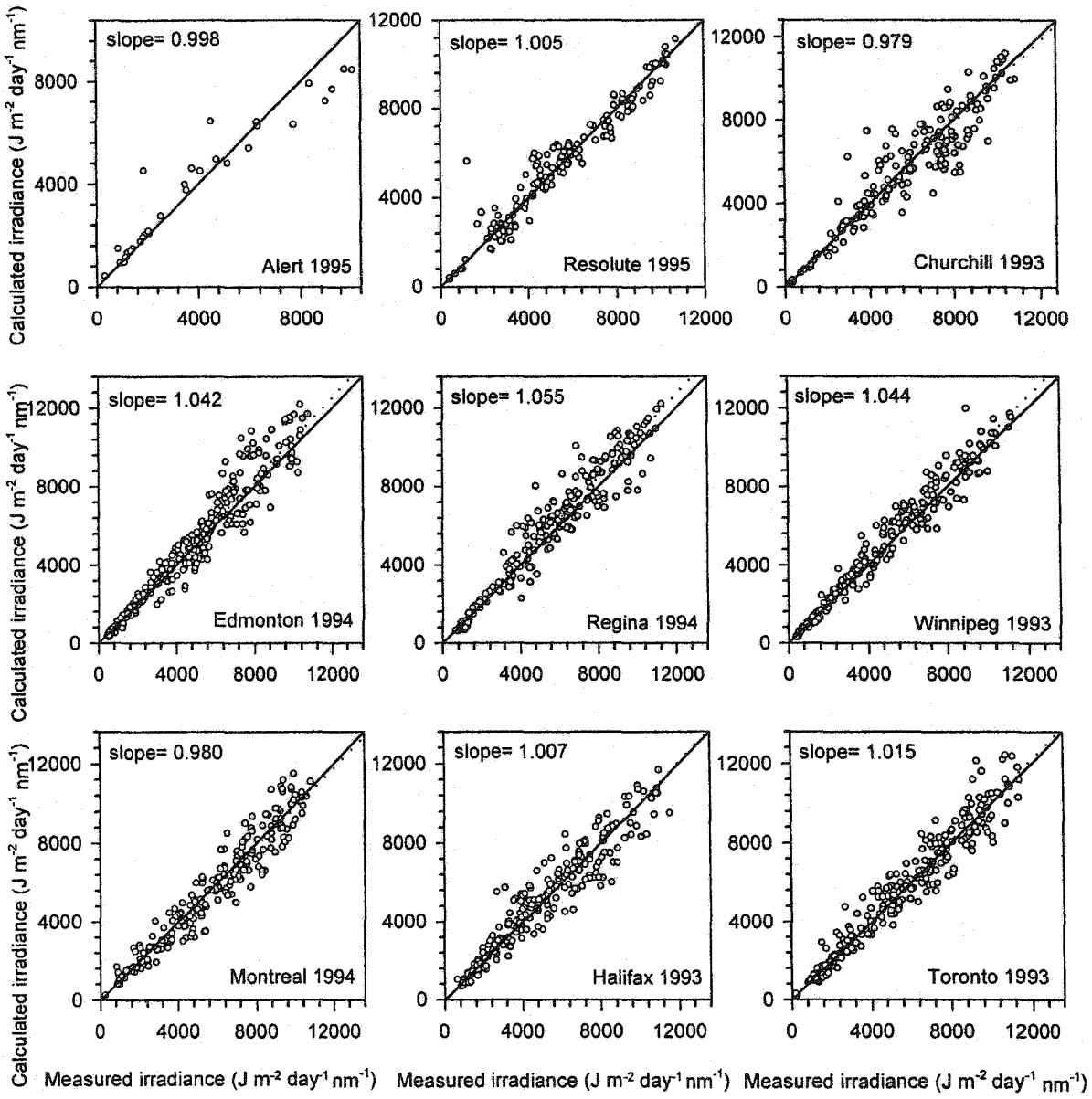

Figure C5. same as Figure C1 but for 325 nm.

Appendix D

Comparison of measured and calculated (DISORT) daily total spectral irradiances using annual values of cloud optical depth for each station (Table 3.4) for 300, 310, 315, 320 and 325 nm.

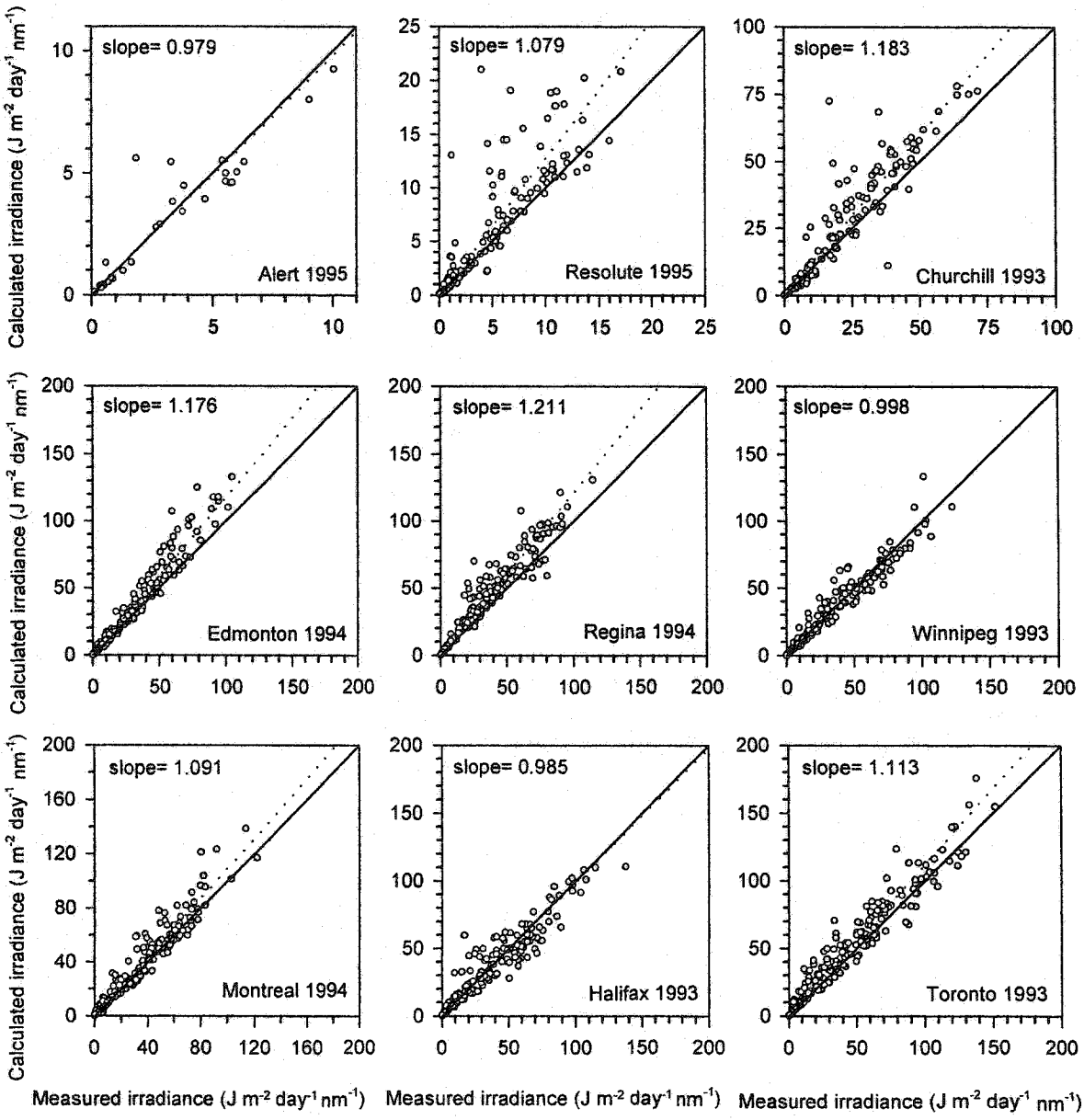

Figure D1. Comparison of measured and calculated (DISORT) daily total spectral irradiances using annual values of cloud optical depth for each station (Table 3.4) for 300 nm. The dotted lines represent linear regressions constrained to pass through the origin.

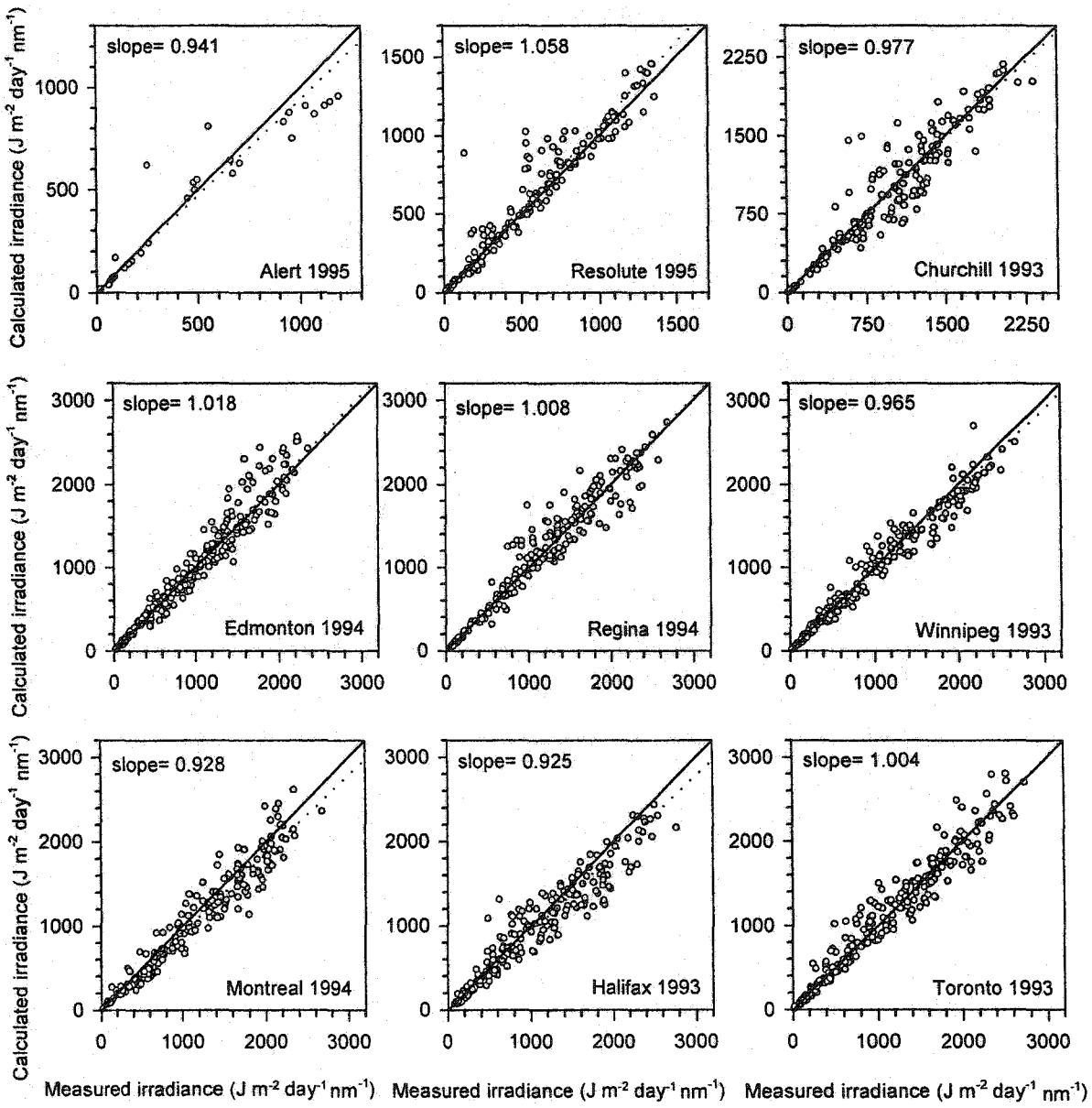

Figure D2. same as Figure D1 but for 310 nm.

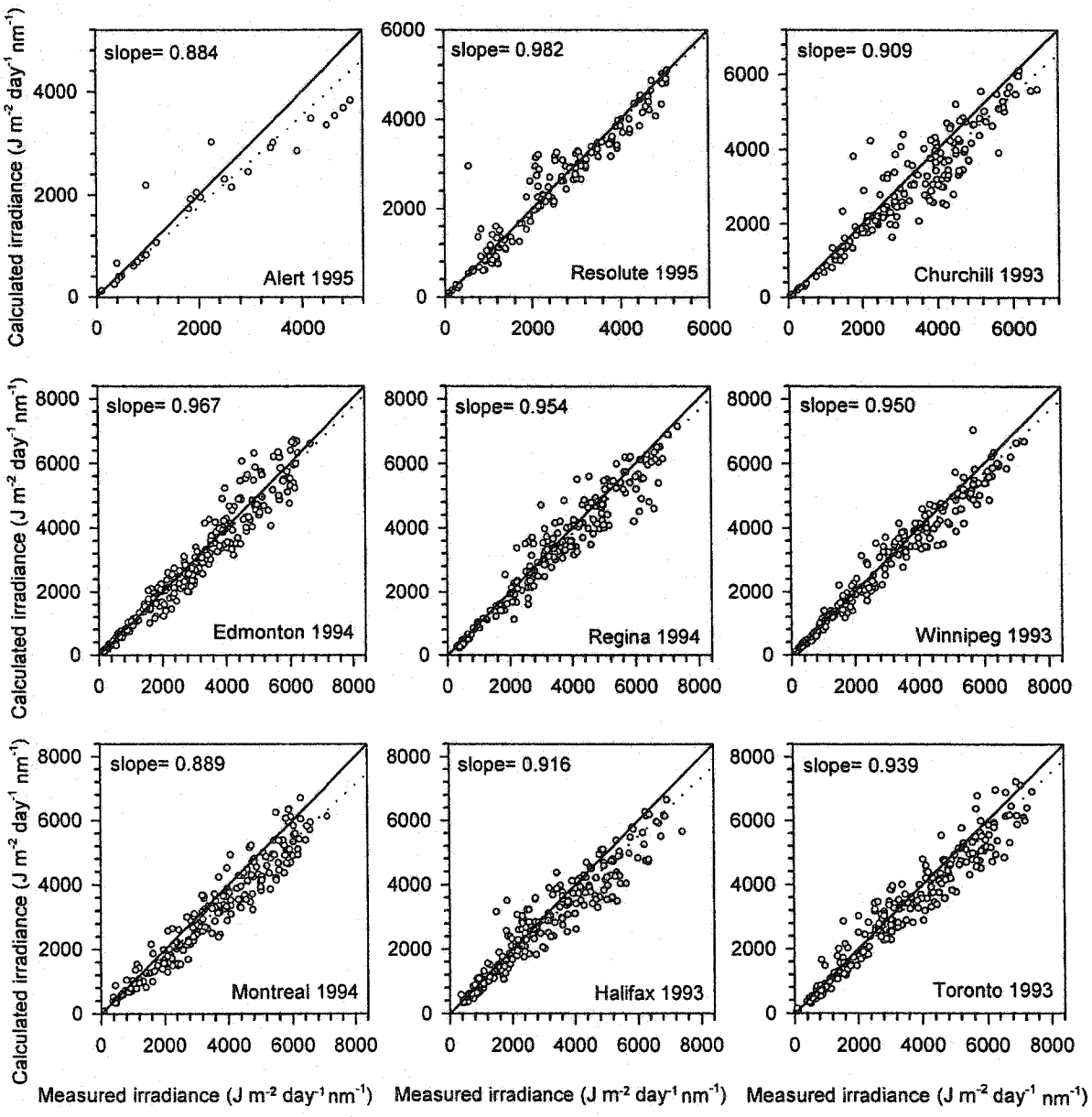

Figure D3. same as Figure D1 but for 315 nm.

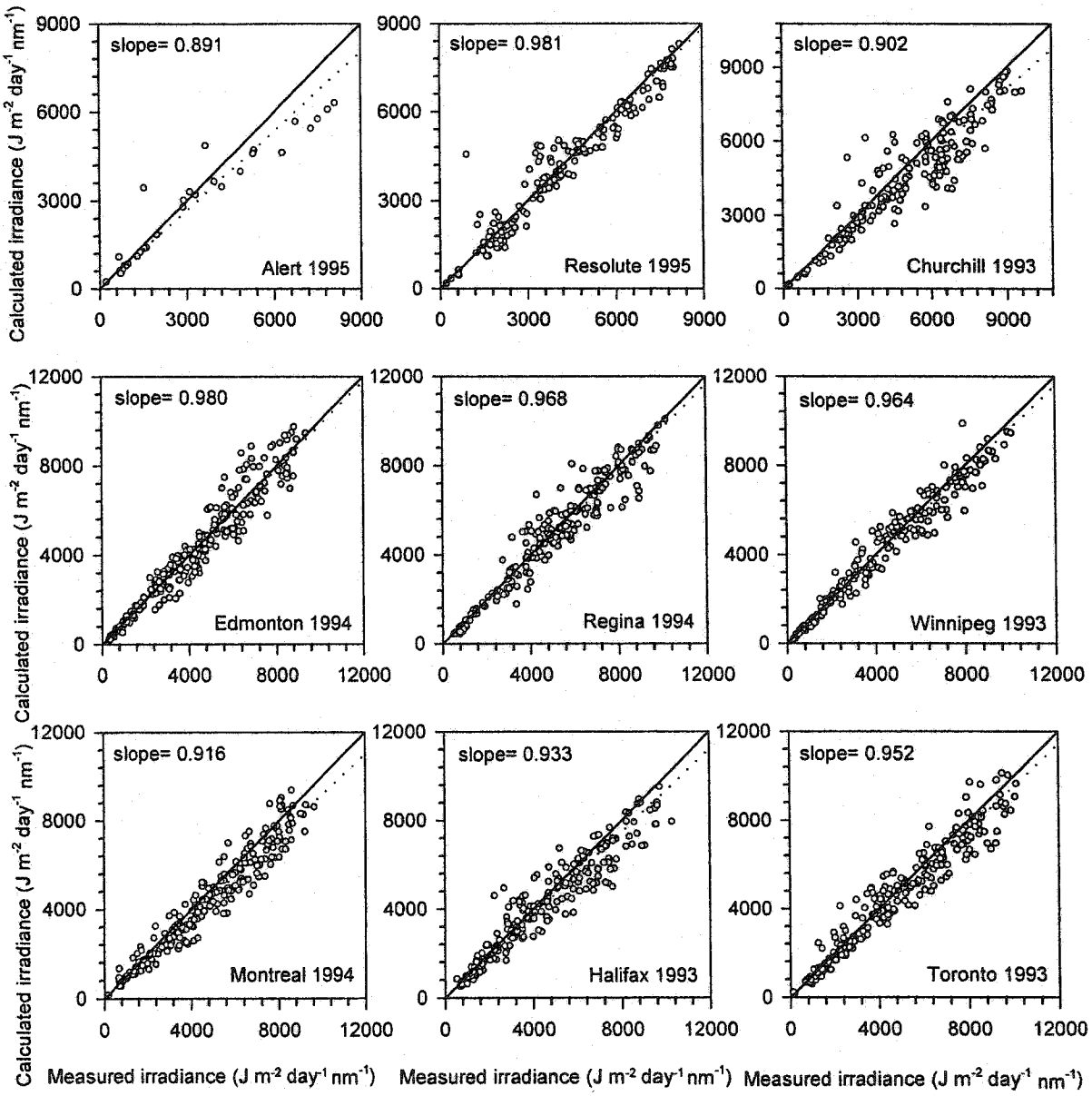

Figure D4. same as Figure D1 but for 320 nm.

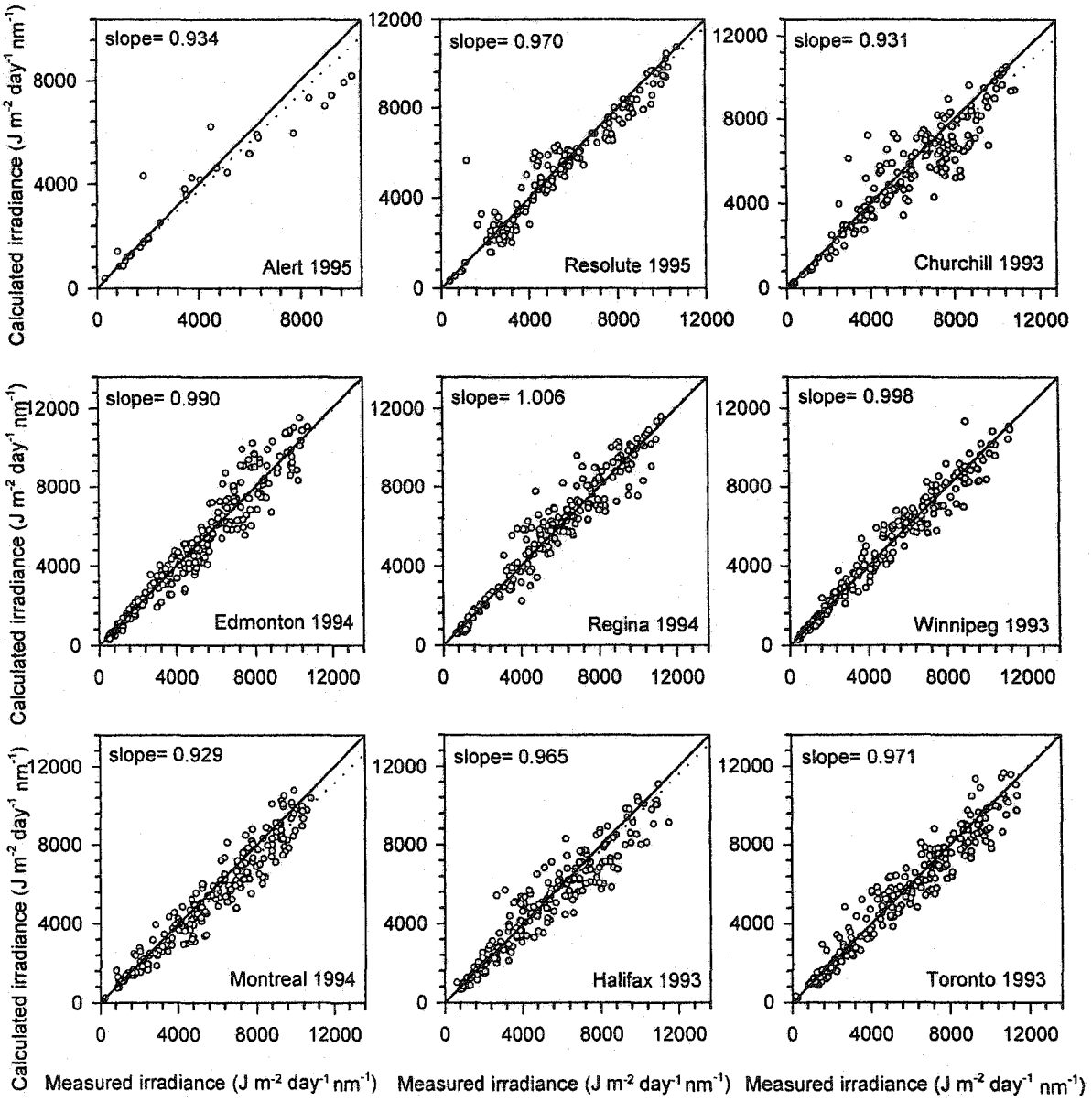

Figure D5. same as Figure D1 but for 325 nm.

Appendix E

Comparison of measured and calculated (delta-Eddington) daily totals and monthly averages irradiances For Resolute, Churchill, Edmonton, Regina, Montreal, Halifax and Toronto using annual cloud optical depth.

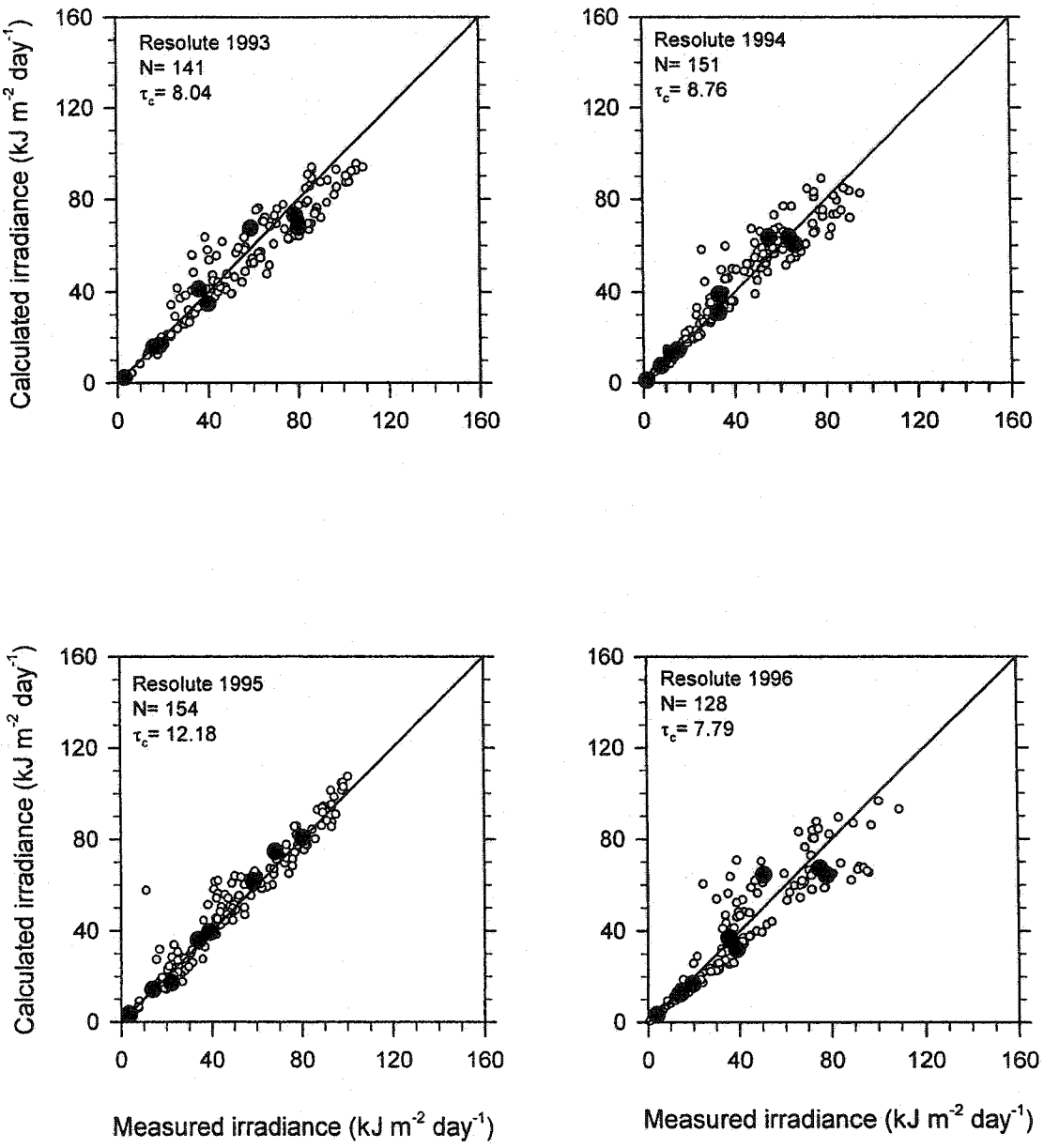

Figure E1. Comparison of measured and calculated (delta-Eddington) daily totals (white circles) and monthly averages (black circles) irradiances for Resolute Bay using annual cloud optical depth. N is the number of days.

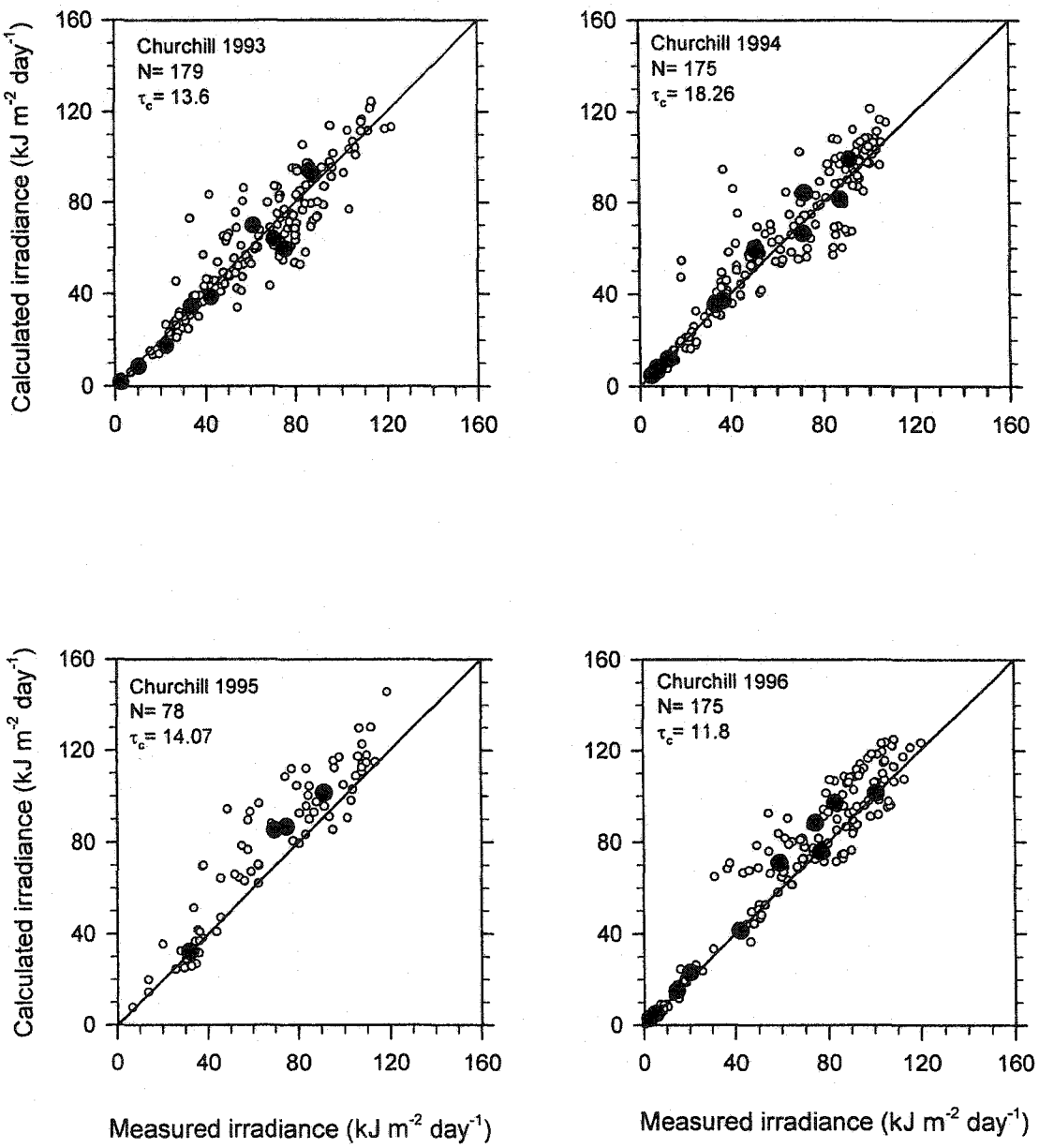

Figure E2. same as Figure E1 but for Churchill.

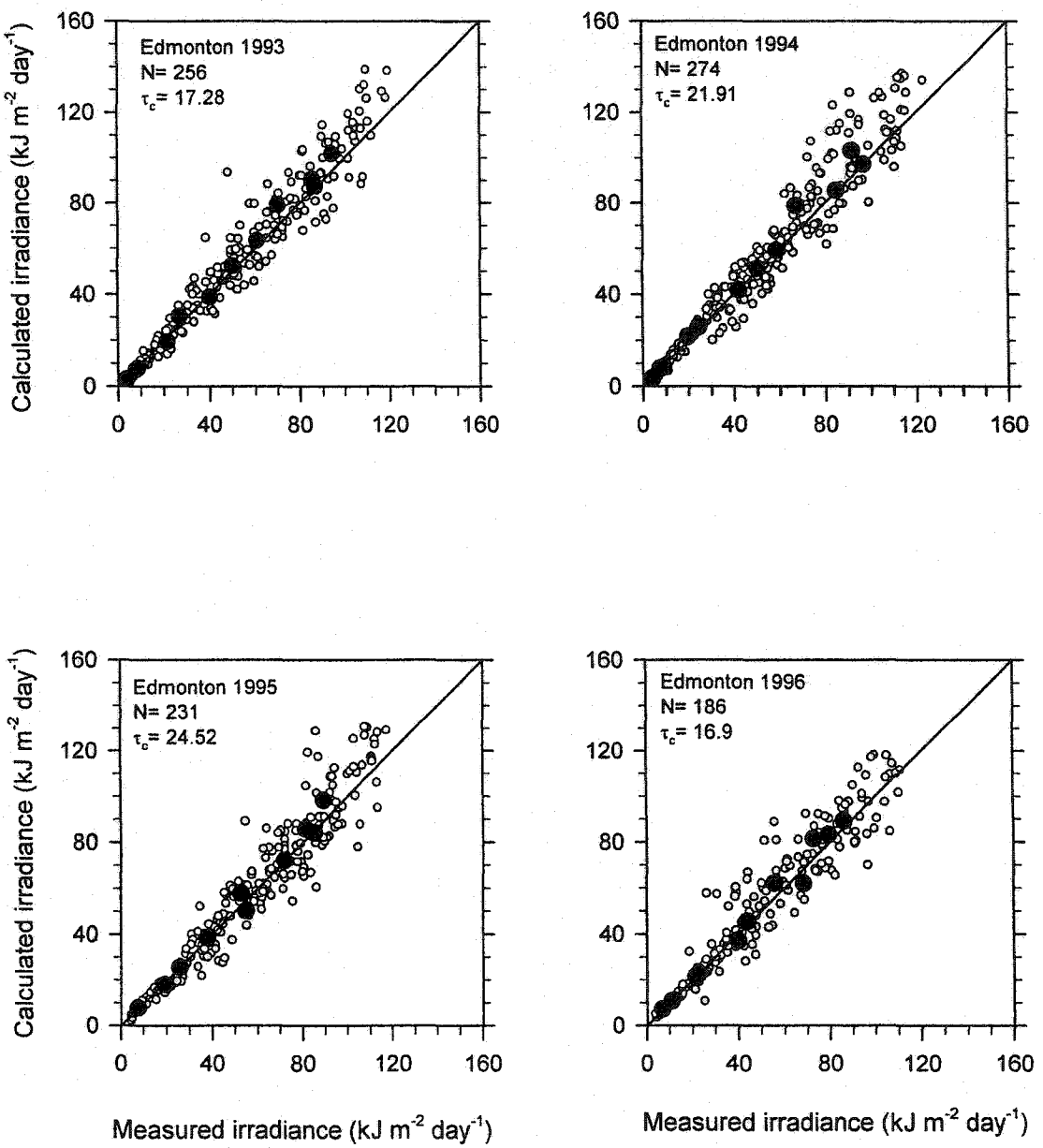

Figure E3. same as Figure E1 but for Edmonton.

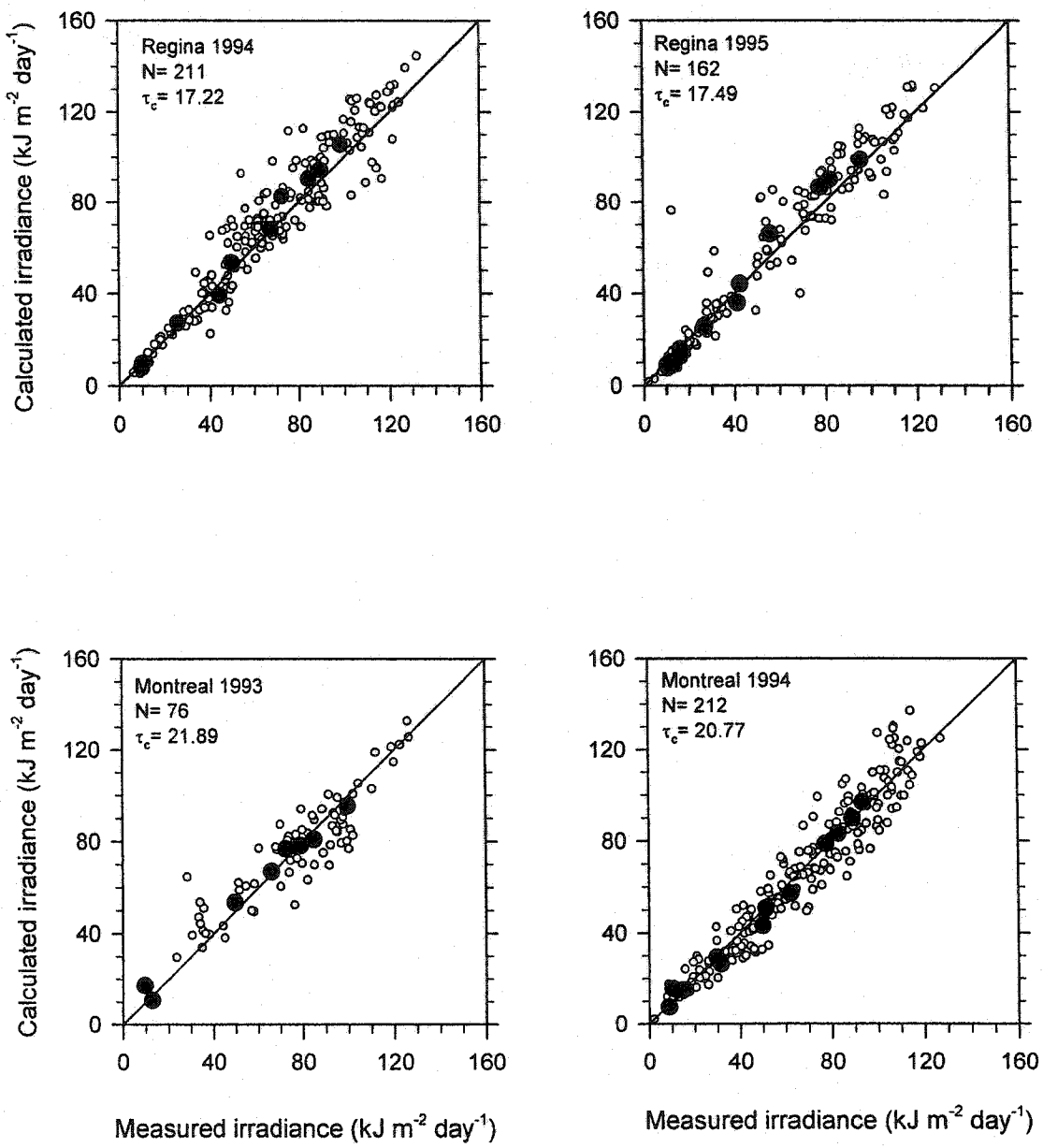

Figure E4. same as Figure E1 but for Regina and Montreal.

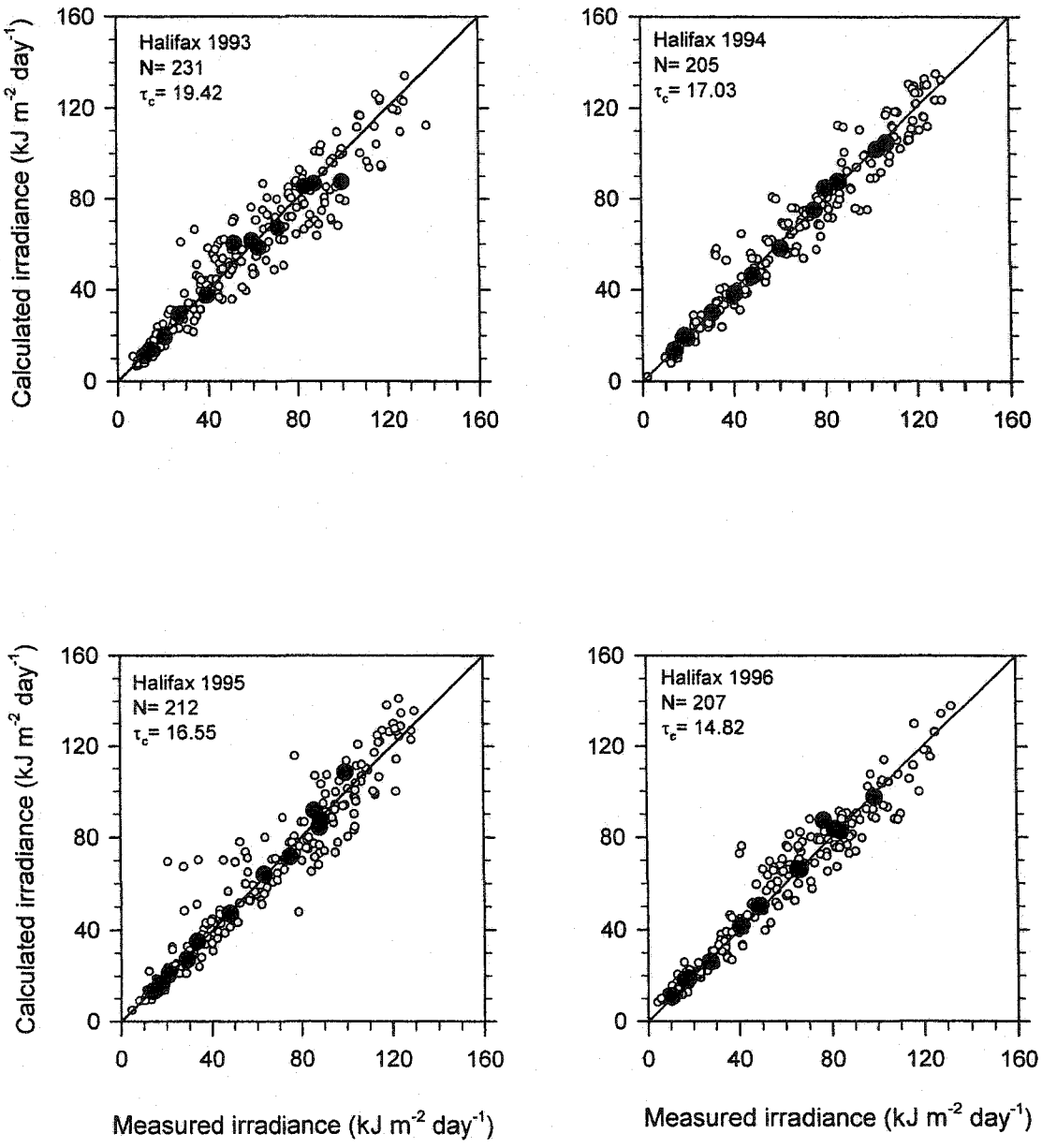

Figure E5. same as Figure E1 but for Halifax.

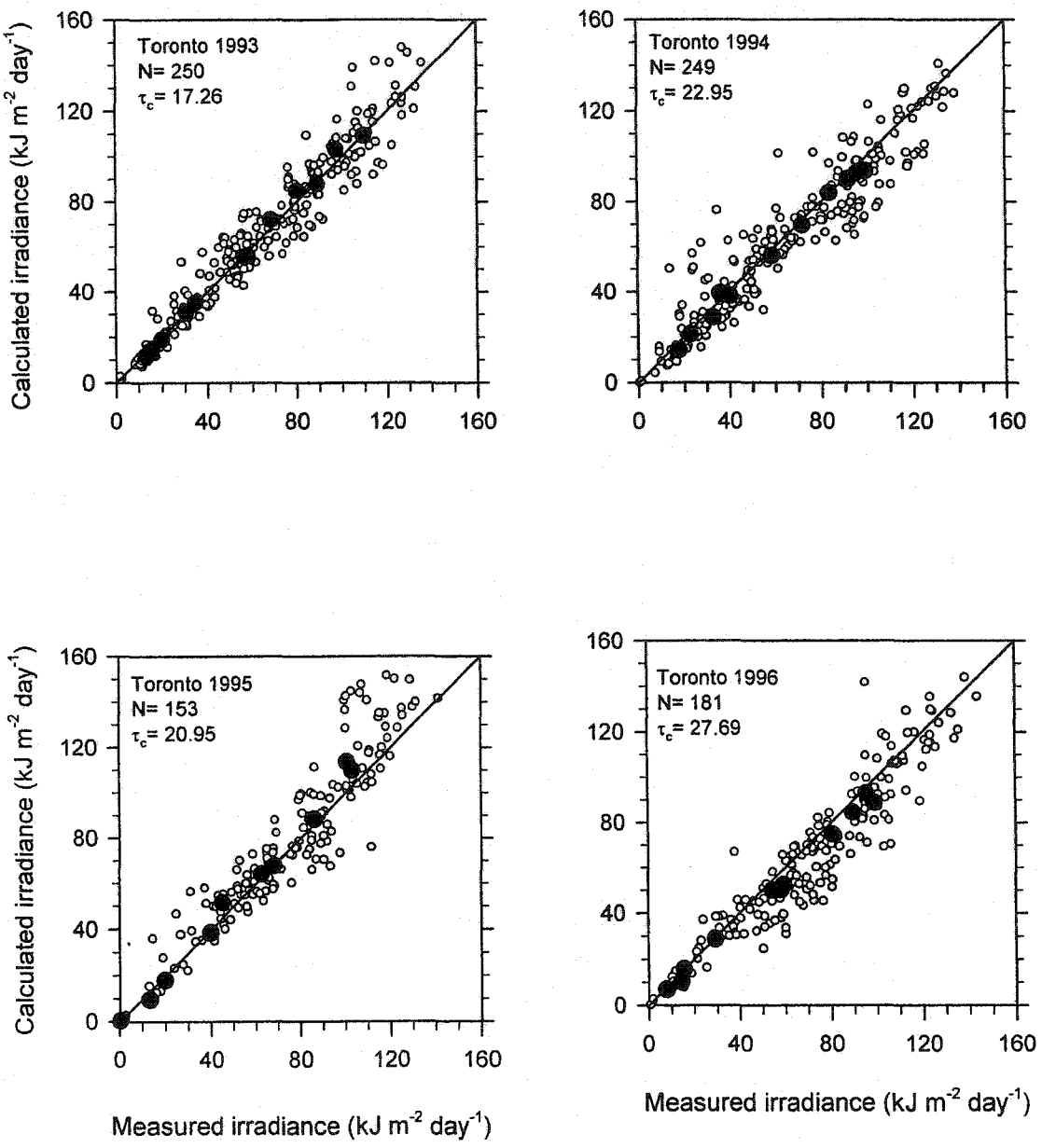

Figure E6. same as Figure E1 but for Toronto.

Appendix F

Comparison of measured and calculated (delta-Eddington) daily totals and monthly averages irradiances For Resolute, Churchill, Edmonton, Regina, Montreal, Halifax and Toronto using pooled cloud optical depth values for each station.

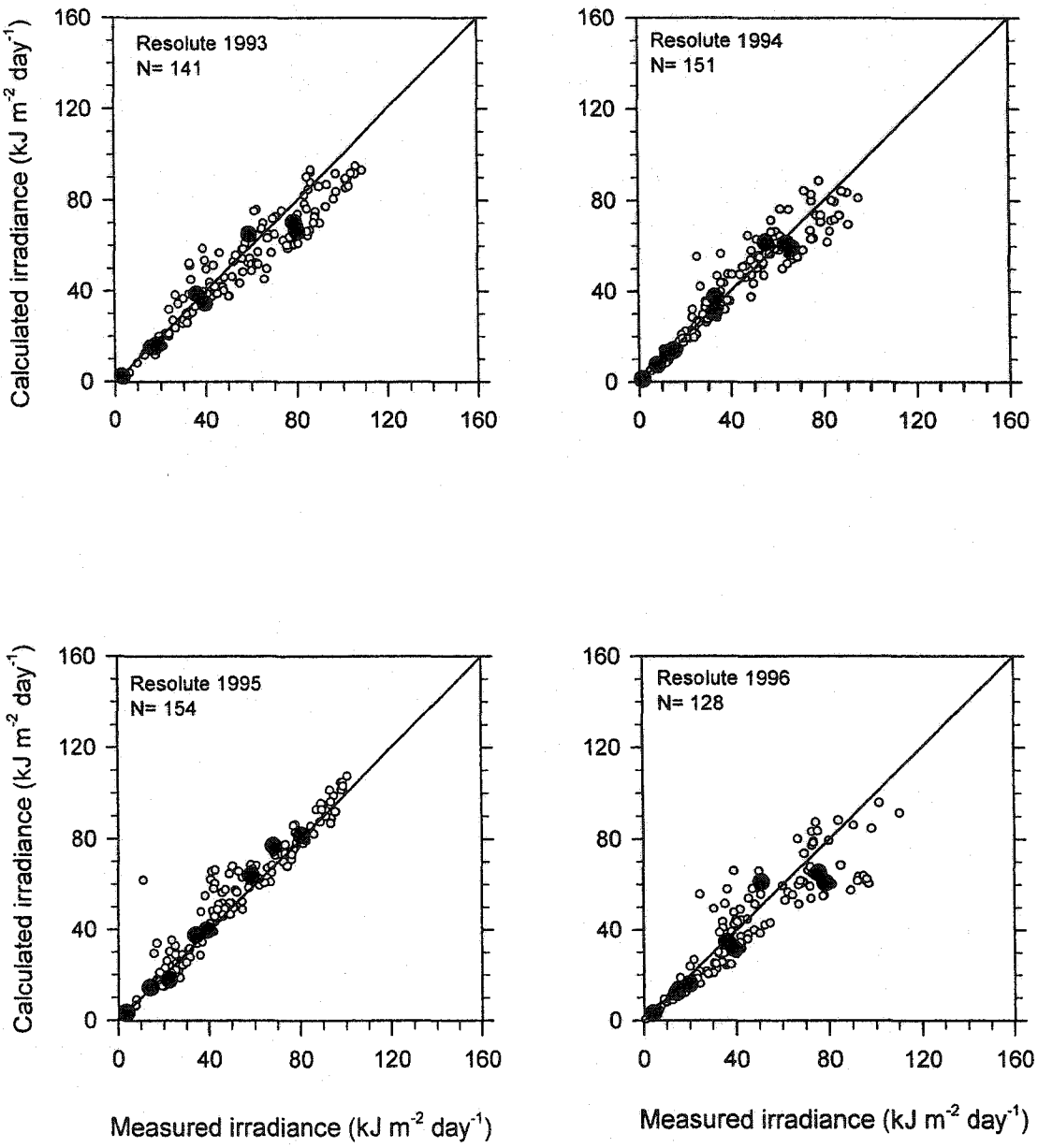

Figure F1. Comparison of measured and calculated (delta-Eddington) daily (white circles) and monthly (black circles) irradiances for Resolute Bay, cloud optical depth= 10.18. N is the number of days.

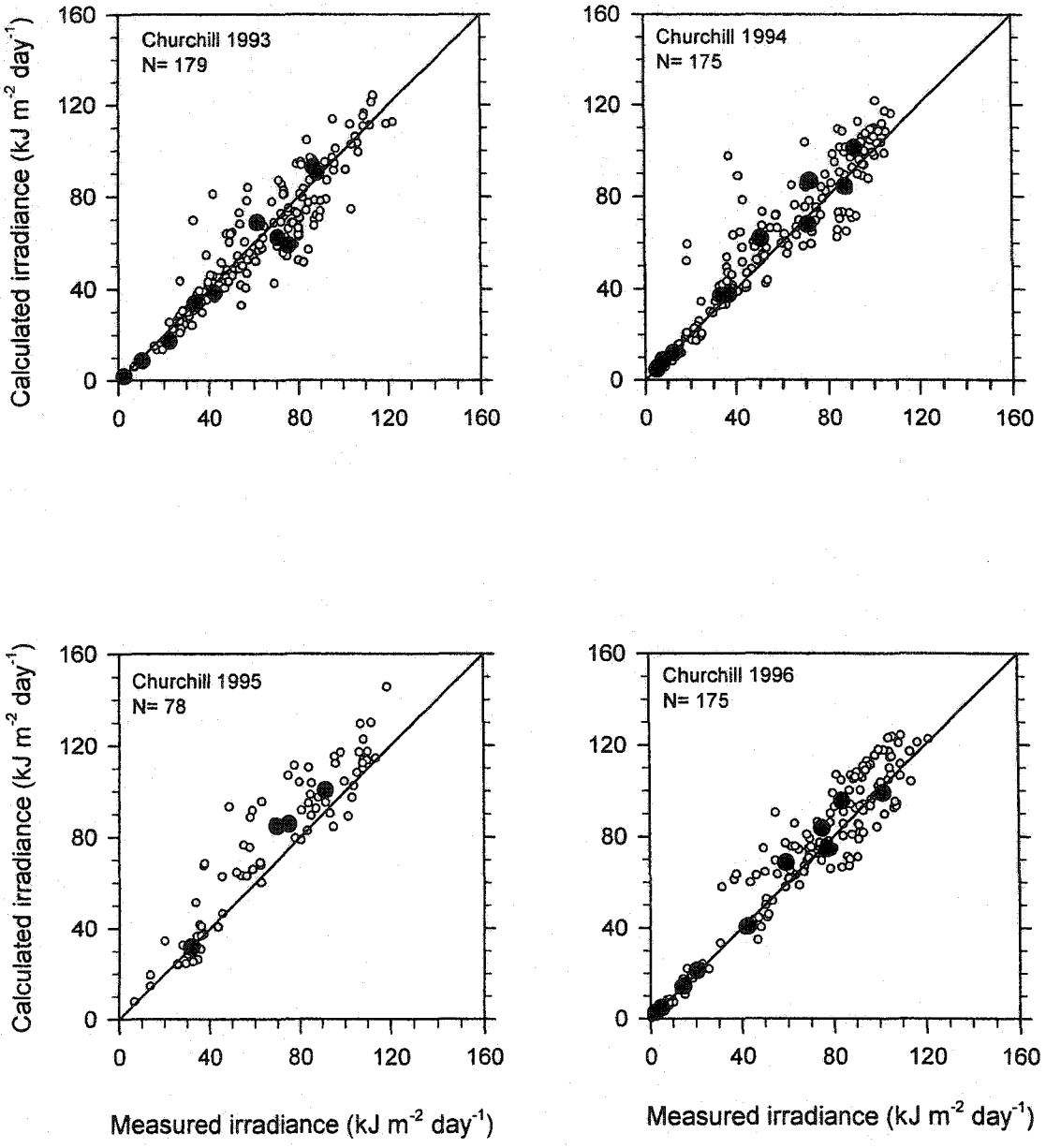

Figure F2. same as Figure F1 but for Churchill, cloud optical depth= 14.99.

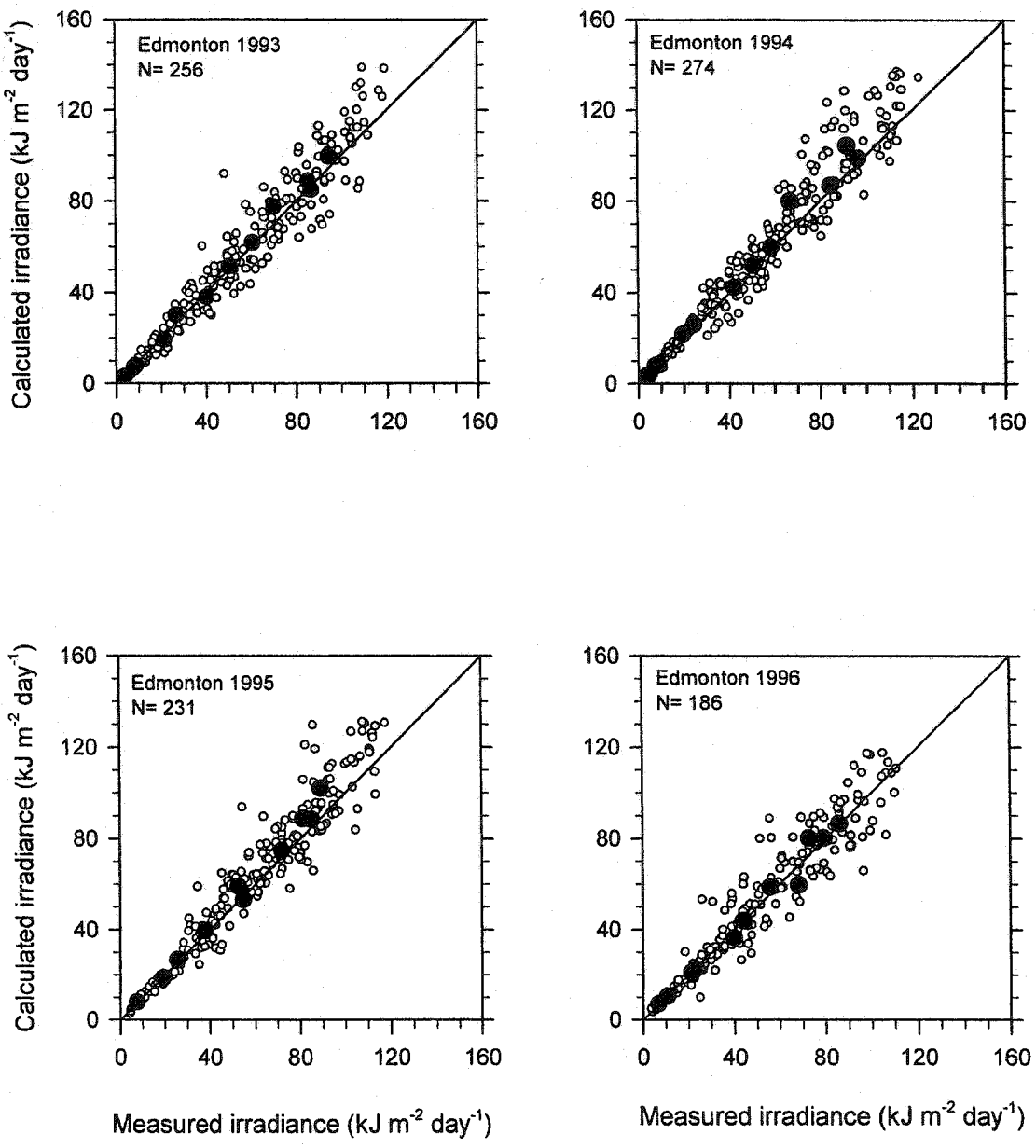

Figure F3. same as Figure F1 but for Edmonton, cloud optical depth= 19.62.

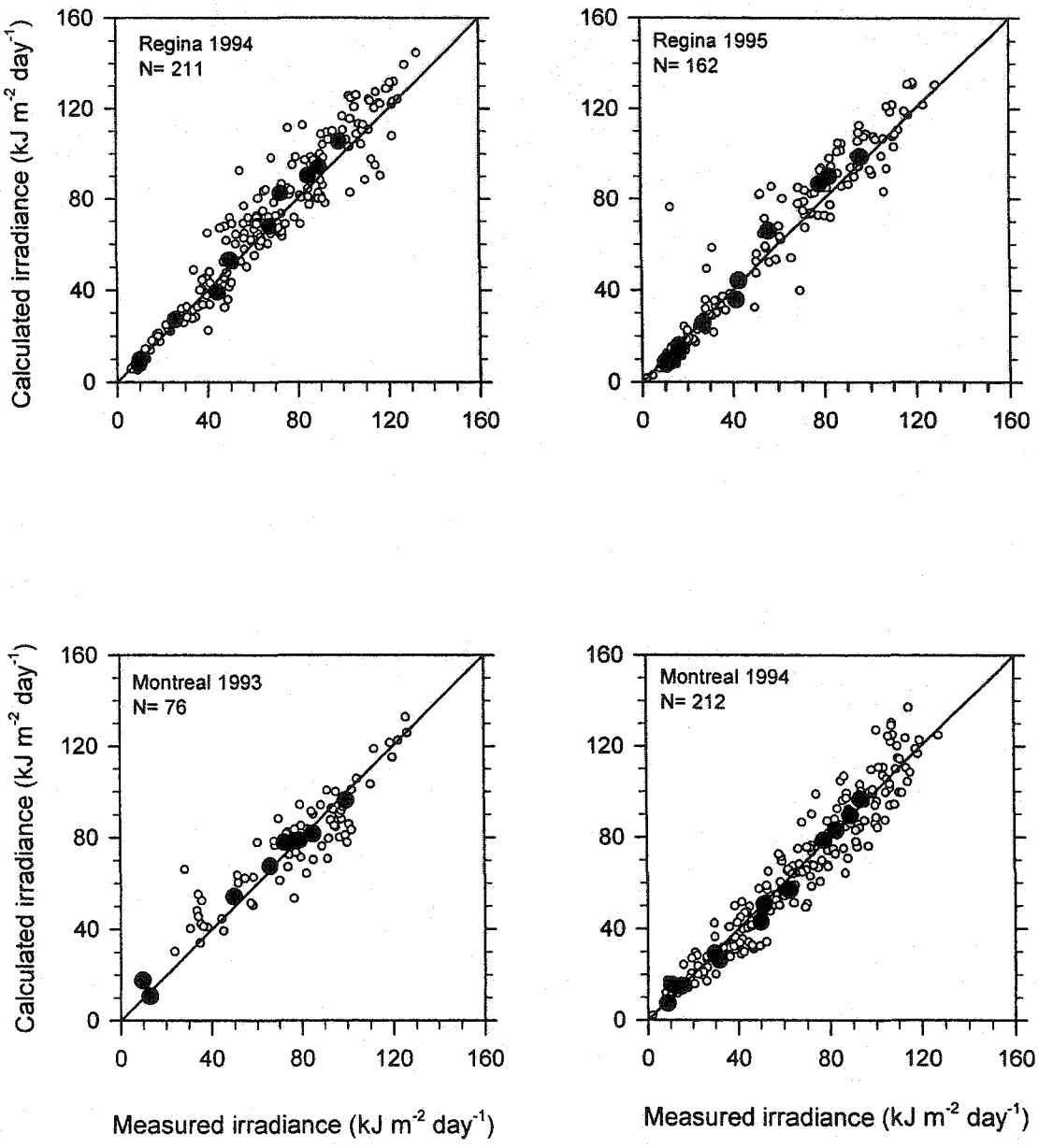

Figure F4. same as Figure F1 but for Regind (cloud optical depth= 17.4) and Montreal (cloud optical depth= 20.84).

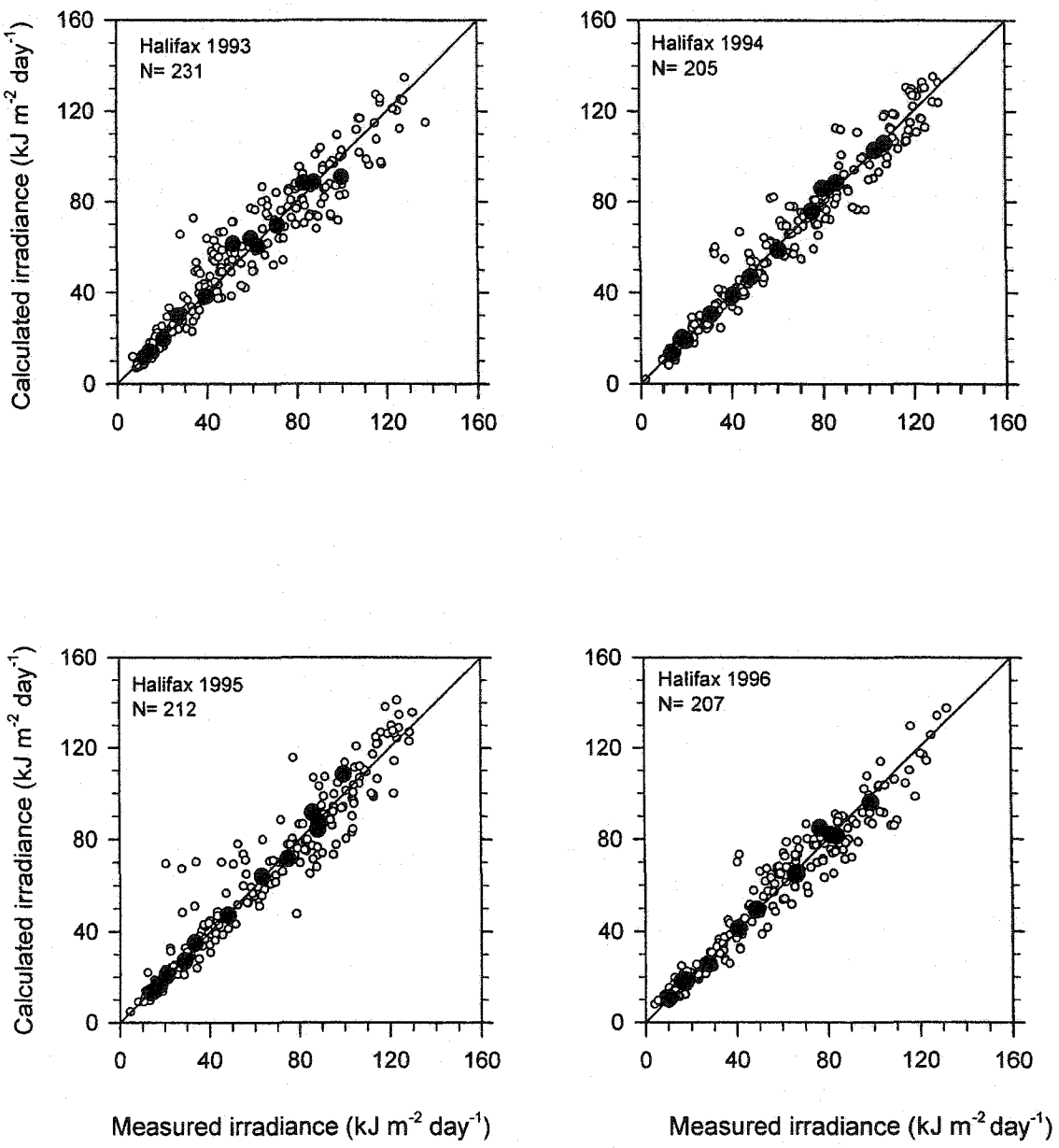

Figure F5. same as Figure F1 but for Halifax, cloud optical depth= 16.6.

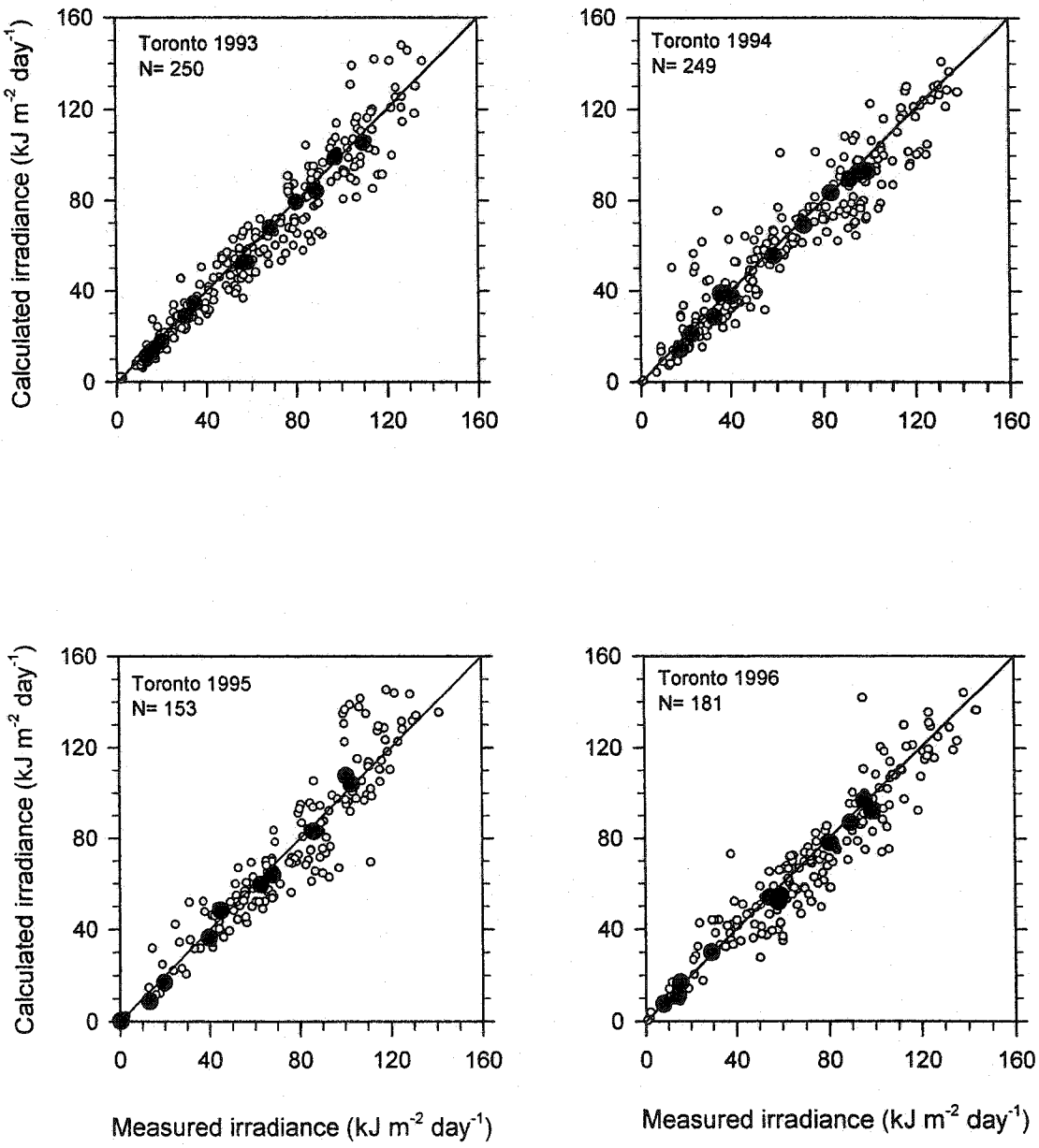

Figure F6. same as Figure F1 but for Toronto, cloud optical depth= 22.98.

Appendix G

Comparison of measured and calculated (delta-Eddington) daily totals and monthly averages irradiances For Churchill, Edmonton, Regina, Montreal, Halifax and Toronto using a pooled cloud optical depth value of 18.7.

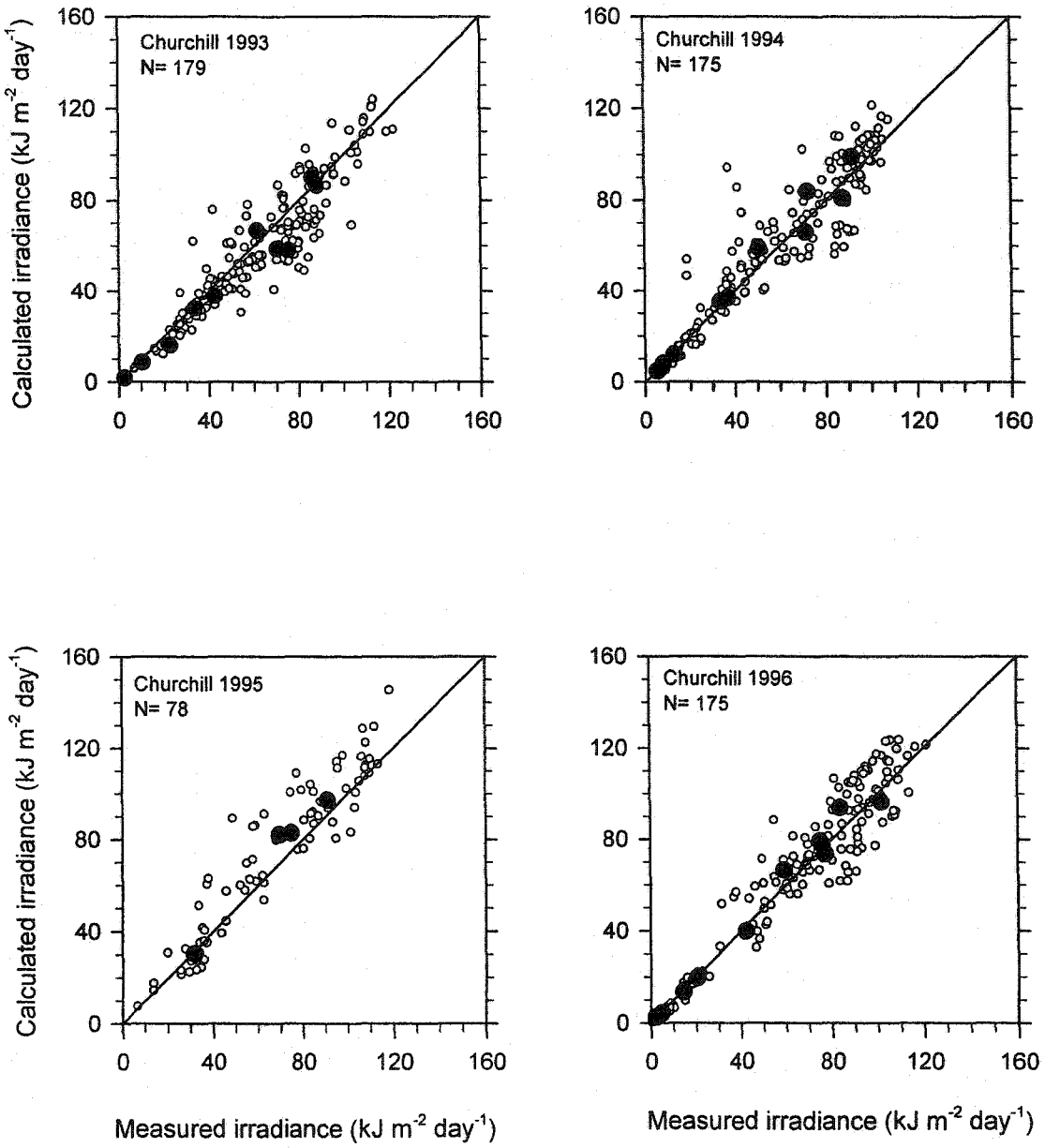

Figure G1. Comparison of measured and calculated (delta-Eddington) daily (white circles) and monthly (black circles) irradiances for Churchill, cloud optical depth= 18.7.

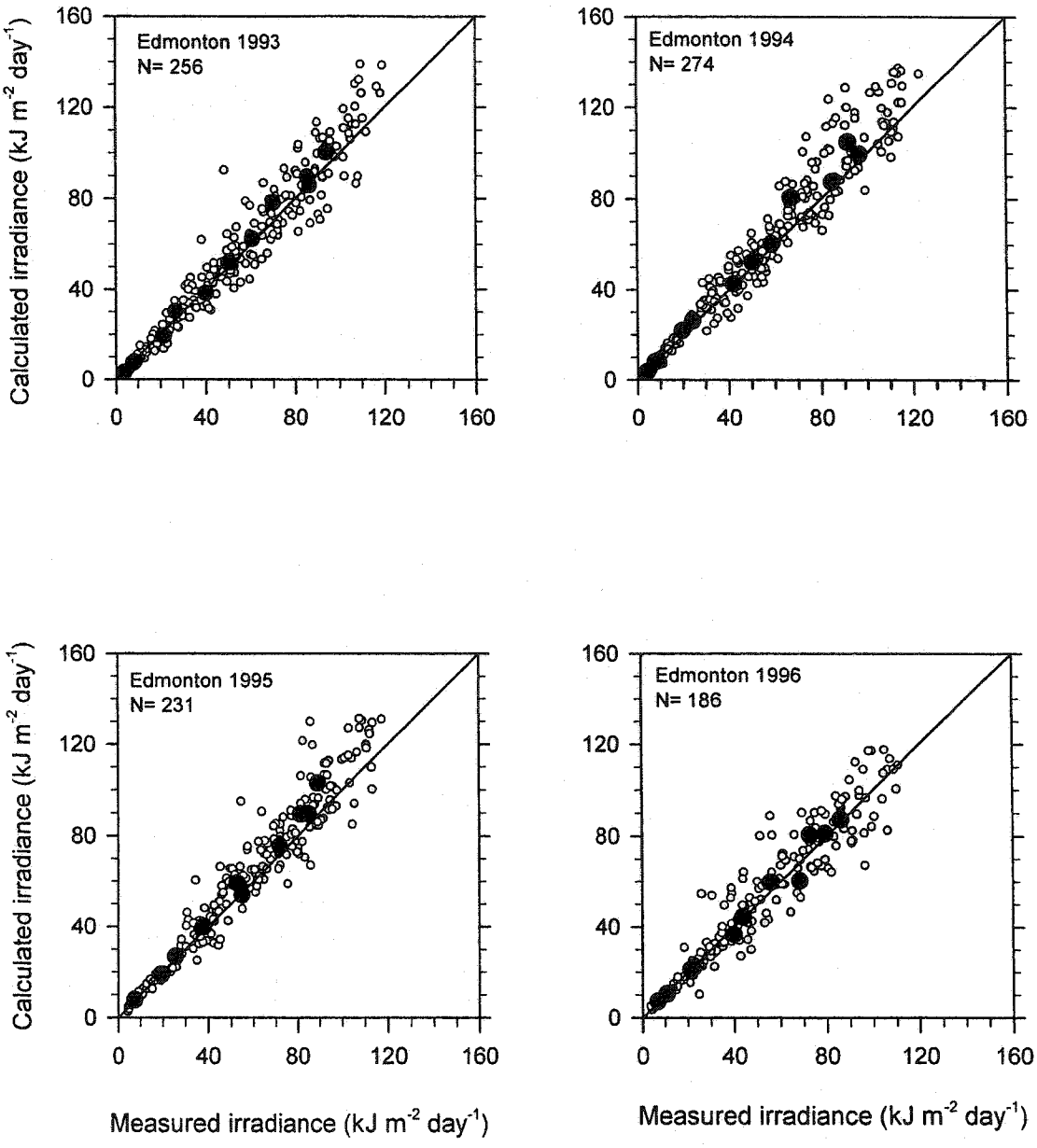

Figure G2. same as Figure G1 but for Edmonton.

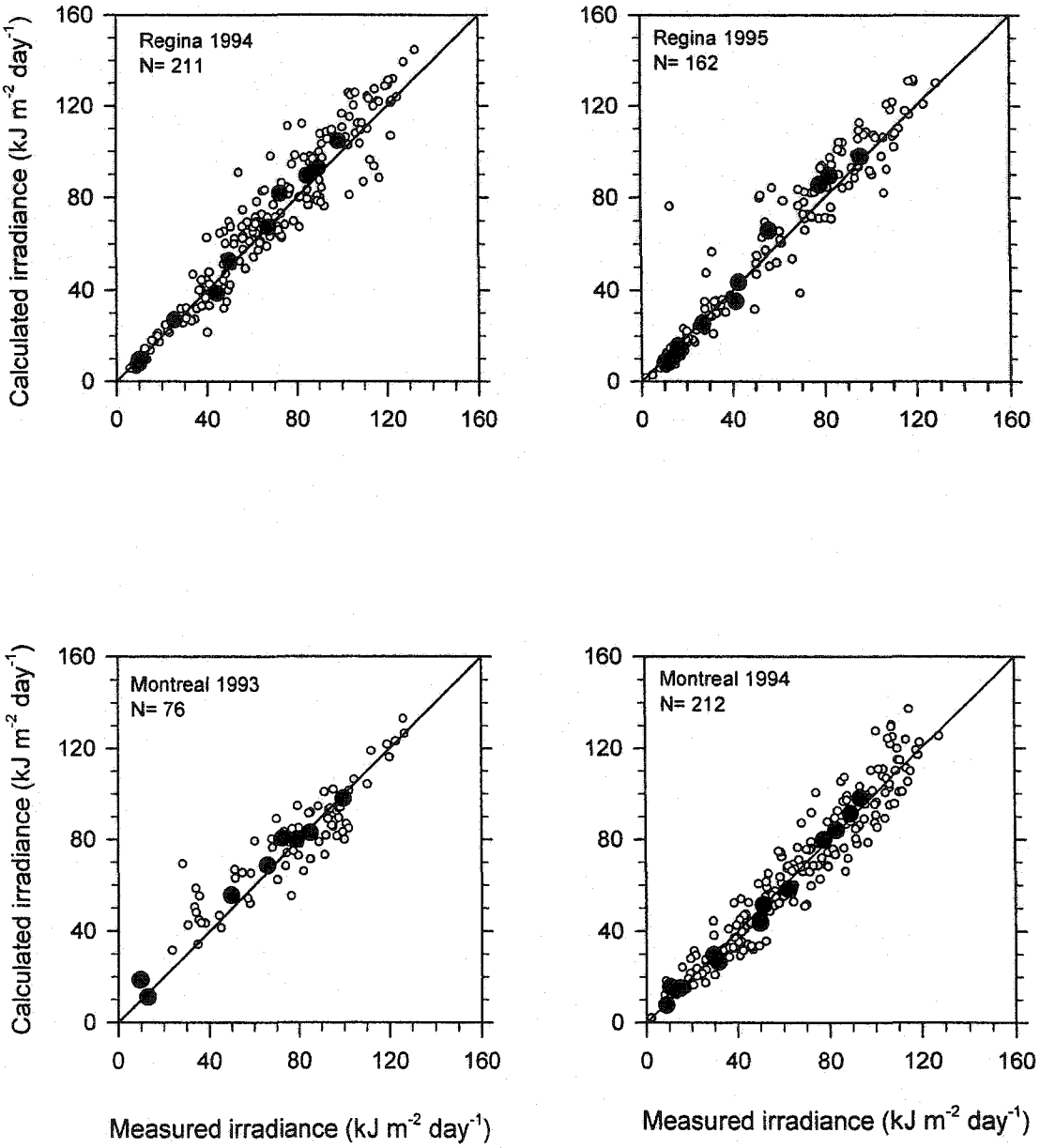

Figure G3. same as Figure G1 but for Regina and Montreal.

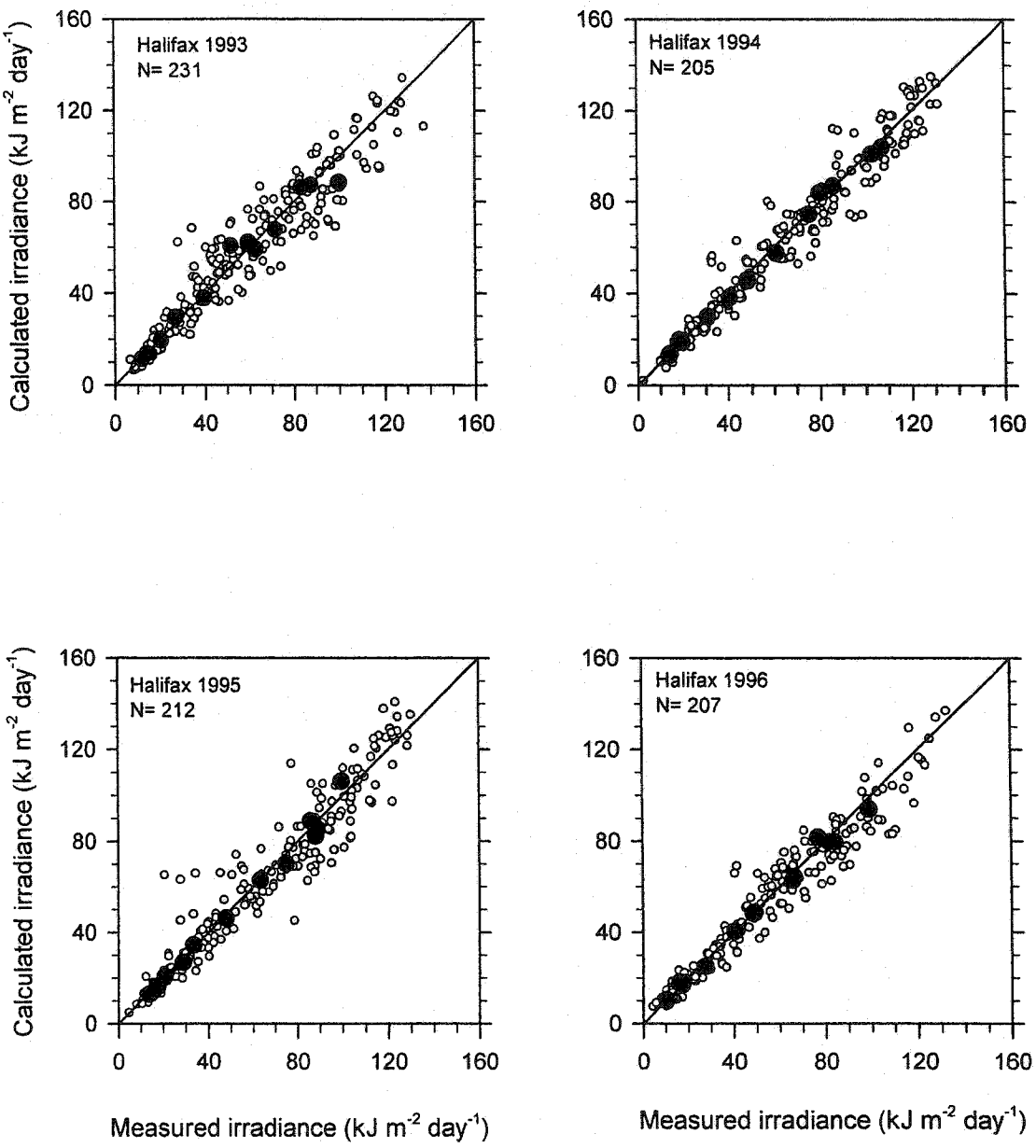

Figure G4. same as Figure G1 but for Halifax.

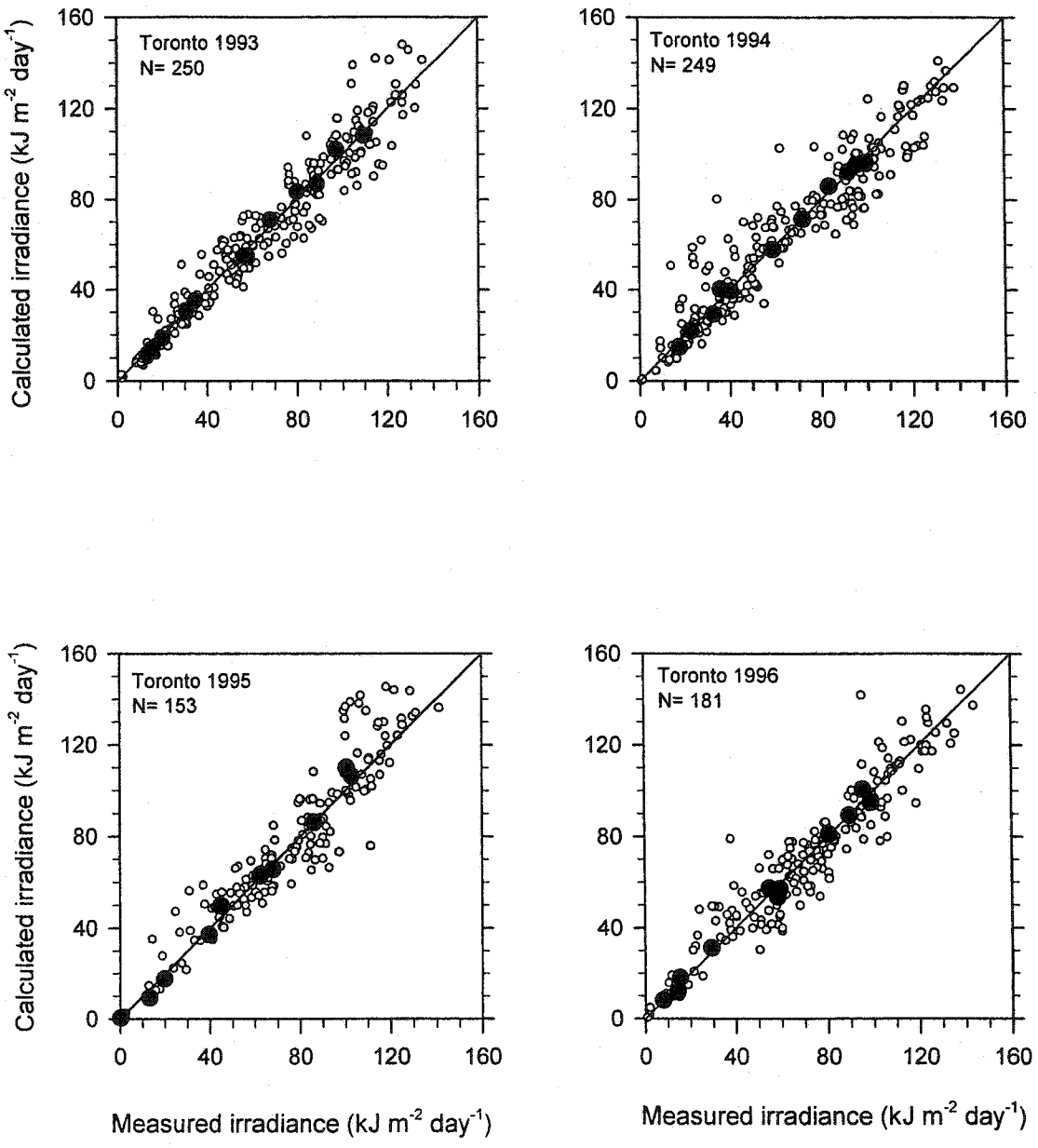

Figure G5. same as Figure G1 but for Toronto.

Appendix H

Monthly averaged measured and calculated broadband irradiances for Resolute Bay, Churchill, Regina, Montreal, Winnipeg, Alert and Edmonton for the available years.

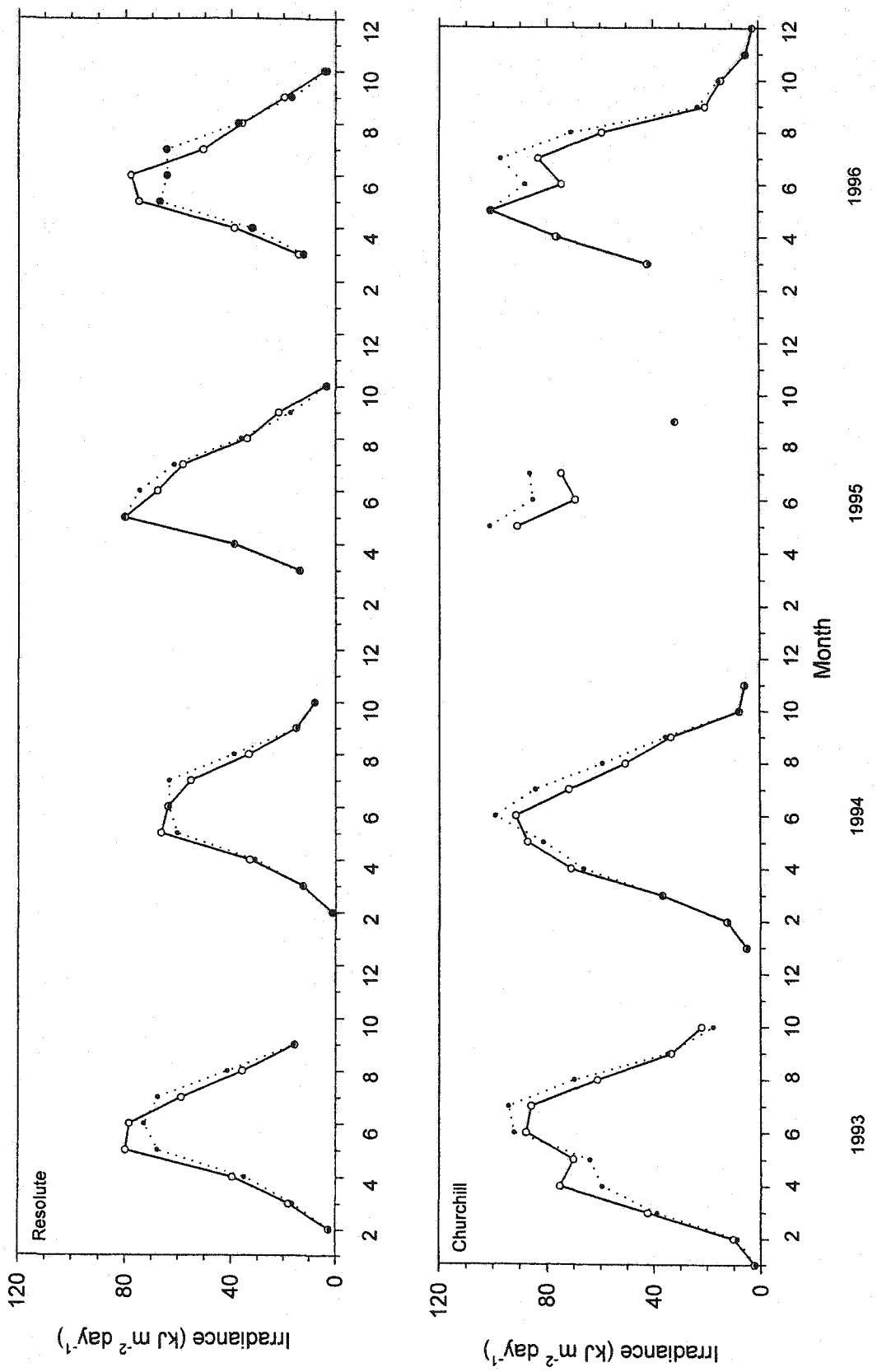

Figure H1. Monthly averaged broadband irradiances measured (solid line and white circles) and calculated (delta-Eddington) model (dotted line and black circles) for Resolute Bay and Churchill for years 1993-1996.

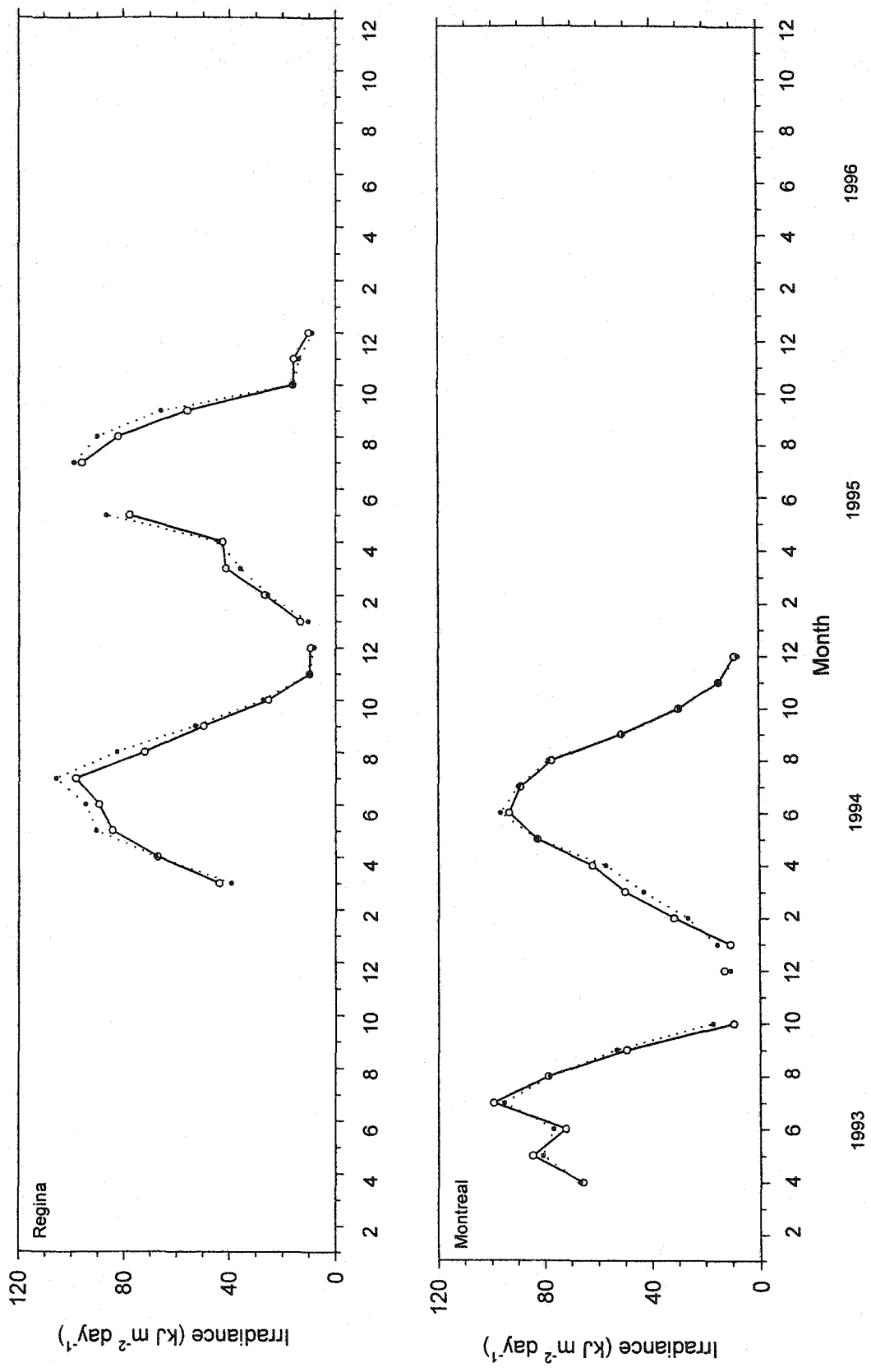

Figure H2. same as Figure H1 but for Regina and Montreal.

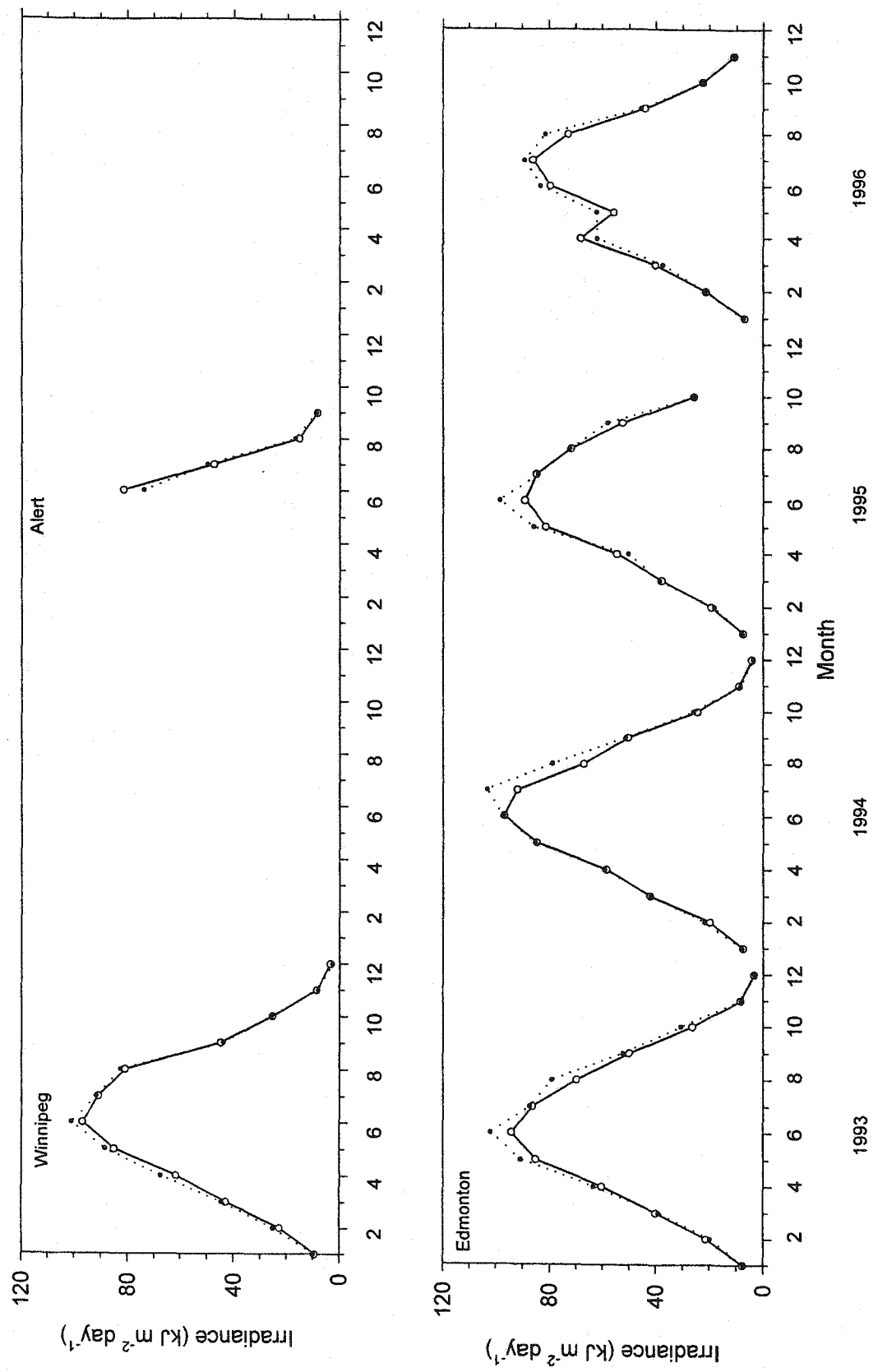

Figure H3. same as Figure H1 but for Winnipeg, Alert and Edmonton.